ACADEMY OF SCIENCES USSR

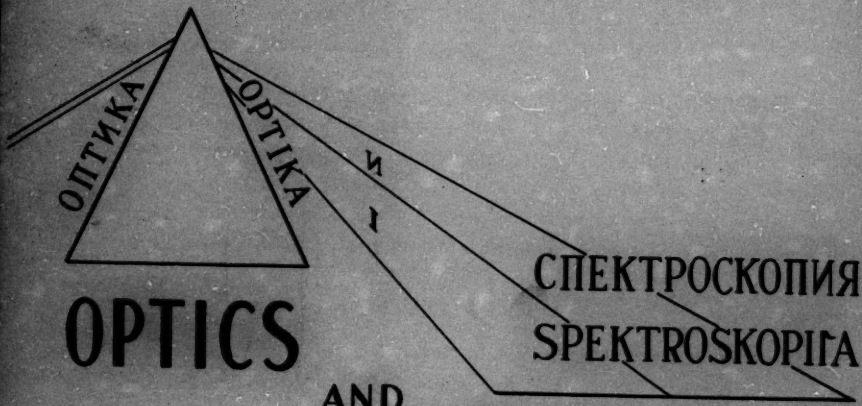

OPTICS AND SPECTROSCOPY

СПЕКТРОСКОПИЯ SPEKTROSKOPIYA

SEPTEMBER 1959 · VOL. VII · NO. 3

Translated on the Initiative of
THE OPTICAL SOCIETY OF AMERICA, INC.

With a Grant-in-Aid from
THE NATIONAL SCIENCE FOUNDATION
by MORRIS D. FRIEDMAN, INC.

RUSSIAN EDITORIAL STAFF

Editor: S. E. FRISH

Assistant Editor: P. P. FEOFILOV

Corresponding Secretary: L. S. SAZONOV

Associate Editors:

M. M. GUREVICH M. A. EL'IASHEVICH A. A. LEBEDEV V. P. LINNIK
S. L. MANDEL'SHTAM I. V. OBREIMOV V. K. PROKOF'EV
N. N. SOBOLEV A. N. TERENIN A. I. TUDOROVSKII

Translation Editorial Staff

MORRIS D. FRIEDMAN

DR. JAMES R. ARONSON, *Arthur D. Little, Inc.*
FRED W. BEHNKE, *Perkin-Elmer Corp.*
DR. RICHARD DALVEN, *Raytheon Company, Research Division,*
DR. SUMNER P. DAVIS, *University of California*
CYRUS FELDMAN, *Oak Ridge National Laboratory*
DR. CARL GARLAND, *Massachusetts Institute of Technology*
DR. D. W. MAYO, *Massachusetts Institute of Technology*
DR. CONRAD J. RAUCH, *Massachusetts Institute of Technology — Lincoln Laboratory*
DR. JOHN S. WAUGH, *Massachusetts Institute of Technology*

Published monthly by the Optical Society of America, Inc. Executive office: 1155 Sixteenth Street, N.W., Washington, D.C. Subscriptions for one year to members of the Society: Associates $13.00; Regular members and Fellows $17.00. Subscriptions for non-members of the Society: One year U. S. and Possessions, $25.00; Foreign $28.00. Back numbers: $3.00 per copy. Subscriptions, changes of address and undeliverable copies should be referred to the Executive offices in Washington, D.C. The office of publication is 2500 South State Street, Ann Arbor, Michigan. Second class postage paid at Ann Arbor, Michigan.

Printed in the U.S.A. by Edwards Brothers, Inc., Ann Arbor, Michigan.

TOM VII, Vyp. 3 OPTIKA I SPEKTROSKOPIIA Sentiabr', 1959
VOL. VII, No. 3 OPTICS AND SPECTROSCOPY September, 1959

Spectral Method of Isotopic Analysis of Lithium

F. F. GAVRILOV

Abstract: A photographic method is worked out for spectral analysis of the isotopic content of lithium using the line Li I 6707.86 Å when there is no light reabsorption. The absolute error of analysis in determining Li^6 in the concentration range from 7.5% to 90% equals 0.2%. The weight of the sample was 3×10^{-6} g. Ten analyses could be made in 8 hours.

The relative abundance of lithium isotopes $\frac{Li^7}{Li^6}$ found by this method equals 12.2 ± 0.3.

In determining the isotope content of lithium many authors [1, 2] used spectral methods of analysis based on the existence of a significant isotopic shift in its optical spectra. Not only arc [1], but molecular and spark spectra of lithium [2] were used for this purpose. In the present article we will give, on the basis of the results of the experimental work we carried out from 1953-1955, a description of a non-standard spectral method of isotopic analysis of lithium carried out using the lithium line Li I 6707.86 Å when there is no light reabsorption.

EXPERIMENTAL APPARATUS AND THE PHOTOMETRIC METHOD

A Fabry-Perot etalon crossed with a DS-1 grating spectrograph was used to resolve the isotopic structure of the resonance line of lithium.

The source of light excitation was a water-cooled, hollow-cathode gas discharge tube (Fig.1). The discharge takes place in a stream of helium at 2 mm Hg pressure and a current of 300 ma. The sample to be be studied is a thin metal film of lithium precipitated by electrolysis onto the polished face of the rod which acts as the bottom of the hollow cathode. The electrolyte is a solution of LiCl in acetone; the concentration of LiCl equals 2.4×10^{-6} g/cm^3.

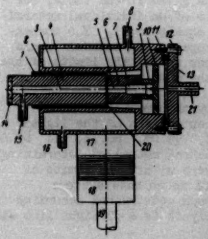

Figure 1. Gas Discharge Tube.
1- ceramic tube, 2- casing, 3- anode housing, 4- anode, 5- cathode housing, 6- cathode, 7- cathode rod, 8- water outlet, 9- cathode sleeve, 10- nut, 11- rubber gasket, 12- bolts, 13- end plate, 14- window, 15- helium inlet, 16- water inlet, 17- 18- 19- base of the tube, 20- space between the anode and cathode (1.5 mm) 21- helium outlet.

The best results, when light reabsorption is negligibly small, are obtained with a precipitate of 3×10^{-6} g lithium. Electrolysis is carried out for 5 minutes with a current of 1.5 ma. at 200 V. The lithium films prepared are very stable and practically do not burn out during the time of exposure.

The spectra are photographed on a "panchromatic" film of sensitivity 1800 KhD sensitized with a type 103a dye. The slit width of the spectrograph is 1 mm, the photographic exposure, 10 min.

The isotopic structure of the analyzed lithium line Li I 6707.86 Å is shown in figure 2. The theoretical ratio of the line intensities of the doublet $\frac{I_a}{I_b}$ and $\frac{I_c}{I_d}$ equals two.

When equality is fulfilled between the ratio of the intensities of the isotope components and the concentrations of the corresponding isotopes, the concentration of lithium isotopes may be determined by comparing the intensities of the outer components a and d (case I) or the components a, b + c (case II) and b + c, d (case III). The expediency of using one of these cases depends on the analyzed interval of the isotope concentrations; it is useful to use all the cases for cross-checking.

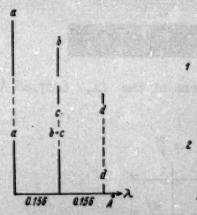

Figure 2. Isotopic structure of the Li I 6707.86 Å line.
a,b- Li^7 isotope lines,
c,d- Li^6 isotope lines.

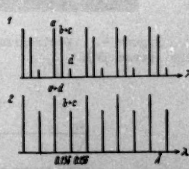

Figure 3. Isotopic structure of the Li I 6707.86 Å line using a Fabry-Perot etalon.
1- normal case,
2- case with superposed orders.

In order to simplify the structure of the analytic line and make analysis possible within a wider interval of isotopic concentrations, we used case IV with superposed orders. With an etalon 0.721 cm thick, corresponding to the free spectral range between the orders of 0.312 Å, components d and a are superposed, which results in the line structure being represented as a system of equidistant lines (Fig. 3) whose relative intensities are also linked to the relative isotopic concentrations.

Figure 4 is a photograph of the spectrogram of a sample with natural isotopic composition obtained by the method of superposed orders. For analysis using this case we used a Fabry-Perot etalon of 0.706 cm. A systematic error of the analysis, caused by inexact superposition of the orders when using this etalon thickness, is considered separately.

In order to decrease the error of analysis due to the error in determining the contrast factor

γ of the photographic emulsion, we used a special double-section multi-step weakener. The step-weakener is placed at the slit of the spectrograph where its steps are made parallel to the interference fringes. The step-weakener has two sections, each of which is made from platinum. The number of steps can be reduced to two. The magnification of the objective in front of the spectrograph slit and the height of the steps are selected so that the isotopic line pair (case IV) is placed fully within the limits of one step.

The principle of using a double-section step-weakener is as follows. If the transmissions of the steps are designated as q_n, q_{n-1}, q_{n-2}, ...%, then the connection between the blackening v_1, v_2, v_3, v_4, (Fig. 5), and the corresponding intensities is expressed by the equations

$$(1)\qquad \left(\frac{v_4 - v_1}{\gamma}\right)_i - \lg\frac{I_3}{I_1} = \left(-\lg\frac{100}{q}\right)_i, \ldots$$

$$(2)\qquad \left(\frac{v_3 - v_2}{\gamma}\right)_i - \lg\frac{I_3}{I_1} = \left(+\lg\frac{100}{q}\right)_i, \ldots,$$

where i is the number of the step.

Figure 4. Spectrogram of the Li I 6707.86 Å line (case IV).

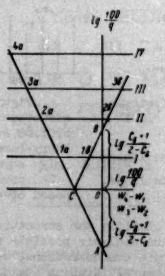

Figure 5. Theoretical Graph for the Calculation of γ.

$$\text{I} - \lg\frac{100}{q_1}; \qquad \text{II} - \lg\frac{100}{q_2};$$

$$\text{III} - \lg\frac{100}{q_3}; \qquad \text{IV} - \lg\frac{100}{q_4}.$$

Equations (1) and (2) in the coordinates $\left[\lg\frac{100}{q},\ v_4 - v_1\right]$ and $\left[\lg\frac{100}{q},\ v_3 - v_2\right]$ describe two straight lines intersecting at a point $\left[-\gamma\cdot\lg\frac{I_3}{I_1},\ 0\right]$ (Fig. 5). The slope of these straight lines obviously characterizes the value γ. As seen from figure 5, the ratio sought for the intensities $\frac{I_3}{I_1}$, which is essential for determining the relative isotopic concentrations of lithium, is found by measuring the length of the segments OA or OB.

Use of the double-section step-weakener decreases the photometric errors due to heterogeneity of the photographic emulsion and the nonuniformity in illuminating the length of the slit (uniformity of illumination is necessary only within the limits of one step).

RESULTS

In order to check the method and determine its accuracy, repeated analyses were carried out on a lithium sample with natural isotopic content.

A large number of articles have been devoted to study of the isotopic content of natural lithium. The considerable diversity in determining the relative abundance of lithium isotopes is explained primarily by the large role of the isotopic effects associated with analysis of this element. The extremely carefully carried out mass spectrometer measurements of Hoff Lu, Hintenberger and Hibbs [3] show the mean percentage of the lighter isotope of lithium as 7.5 ± 0.1%. Optical methods give an appreciably different value for Li^6. Thus, the data of Brody and co-workers give 6.9% [1], of Artaud and co-workers 7.5% [1], of Hutchinson 7.97% [4], of Schuler 8.7% [2], of Ornstein 11.0%, [5], of Nakamura 1.1% [2], and of van Wijk 12.2% [2].

The analysis was carried out without using calibration graphs. Correction for mutual superposing of lines was made by the calculation method after a preliminary careful study of the shape of the spectral line. Isotopic effects [6] were not taken into consideration here.

The results obtained are given in the table.

According to the data given in the table, the mean square absolute error of an individual determination was computed. It equals 0.2%. The concentration of the Li^6 isotope in the natural sample, which we determined, agrees within the limits of the error of analysis with the data from mass spectrometer measurements.

Analyses were made by this method of other lithium samples with concentrations of the lighter isotope of 33.3%, 35.1%, 59.0%, 66.7%, and 89.6%. The deviations of the spectral method of determining the Li^6 concentration were within the limits of error whose absolute value in no case exceeds 0.2%. The calibration graph constructed according to data from spectral analysis is a straight line with a slope of 45°.

In order to resolve the question of the influence of impurities on the results of the analysis, certain of the analyzed samples were artificially contaminated. The analyses then conducted showed that the presence of a small percentage of impurities in the sample does not hamper spectral analysis and does not decrease the accuracy of the method.

In conclusion the author considers it his agreeable duty to express thanks to A. R. Striganov and V. I. Malyshev for valuable discussions and also to Iu. P. Nazarov and M. I. Fedorovskaia for aid in completing the experiments.

Table

Sample Number	Result of Direct Measurements of Li^6 (in %)	Final Result for Li^6 (in %)	Deviation from the Mean (in %)
1	12.0	7.6	0.0
2	12.0	7.6	0.0
3	12.3	7.9	-0.3
4	11.7	7.3	+0.3
5	12.0	7.6	0.0
6	11.9	7.5	+0.1
7	12.2	7.8	-0.2
8	12.6	8.2	-0.6
9	11.6	7.2	+0.4
10	12.0	7.6	0.0
11	12.0	7.6	0.0
12	11.9	7.5	+0.1
13	12.0	7.6	0.0
14	12.3	7.9	-0.3
15	12.2	7.8	-0.2
16	12.0	7.6	0.0
17	11.8	7.4	+0.2
18	12.0	7.6	0.0
19	12.6	8.2	-0.6
20	11.8	7.4	+0.2
21	12.0	7.6	0.0
22	12.0	7.6	0.0
23	11.9	7.5	+0.1
24	11.9	7.5	+0.1
25	11.8	7.4	+0.2
Mean		7.6	±0.2 %

Note: Overall correction (superposition + inaccuracy) was for all samples equal to -4.4 %.

December 4, 1958

References

1. G. L. STUKENBROEKER, D. D. SMITH, G. K. WERNER, J. R. MCNALLY: JOSA, 41, 870, (1951); 42, 383, (1952); G. K. WERNER, D.D.SMITH, J. R. MCNALLY: JOSA, 42, 870, (1952); G. K. WERNER, D. D. SMITH, S. J. OVENSHINE, O. B. RUDOLPH, J. R. MCNALLY: JOSA, 45, 202, (1955); J. K. BRODY, M. FRED, F. S. TOMKINS: JOSA, 42, 870, (1952); Spectrochim. Acta, 6, 383, (1954); J. ARNAUD, T. BLAISE, S. GERSTENKORN: Spectrochim., Acta, 10, 110, (1957).
2. G. NAKAMURA: Nature, 128, 759, (1931); W. R. VAN WIJK, A. J. VAN KOEVERINGE: Proc. Roy. Soc., A 132, 98, (1931); H. SCHULER: Z. Phys., 66, 431, (1930); V. A. FASSEL, H. J. HEITTEL: Spectrochim. Acta, 7, 175, (1955).
3. HOFF LU: Phys. Rev., 53, 845, (1938); H. HINTENBERGER: Naturwiss., 34, 52, (1947); R. F. HIBBS: NBS, Circ., 499, Suppl. 1, (1951).
4. D. A. HUTCHISON: JACS, 76, 967, (1954).
5. L. ORNSTEIN, J. VREESWIJK, G. WOLFSOHN: Physica, 1, 53, (1934).
6. A. R. STRIGANOV, UFN, 58, 365, (1956); ZL,(12) 1476, (1955).

TOM VII, Vyp. 3 OPTIKA I SPEKTROSKOPIIA Sentiabr', 1959
VOL. VII, No. 3 OPTICS AND SPECTROSCOPY September, 1959

Partial Frequencies of Triatomic Hydrides and Deuterides of C_{2v} Symmetry

V. P. MOROZOV

Abstract: The method of partial frequencies is used to solve some problems in molecular vibration theory: a) the construction of zero approximations to the fundamental frequencies; b) the establishment of zero approximations to the force constants and interaction coefficients; c) the construction of approximate relations between the frequencies of isotopic modifications. Triatomic nonlinear symmetric hydrides and deuterides are the subjects of this study.

The investigation of zero approximations to the vibrational frequencies of polyatomic molecules was begun by El'iashevich and Stepanov [1]. Interesting possibilities in this direction and in the solution of other vibrational problems are opened up by the application of the method of partial frequencies. The partial frequency concept was defined by Mandel'shtam [2] (see [3] also) and can be formulated as follows: Let a system have n vibrational degrees of freedom described by the generalized coordinates $q_1, q_2, \ldots, q_n$. Then the partial frequency $\tilde{\omega}_i$ will be the frequency of vibrations executed by the system when $q_1 = \ldots = q_{i-1} = q_{i+1} = q_n = 0$ and $q_i \neq 0$, which is equivalent to the imposition of restraints on all the degrees of freedom except the i-th.

Let us consider the simplest two-dimensional problem of symmetric vibrations of triatomic molecules of C_{2v} symmetry.

We write the kinetic and potential energies as:

$$T = \frac{1}{2} I_1 \dot{\xi}_1^2 + I_2 \dot{\xi}_1 \dot{\xi}_2 + \frac{1}{2} I_3 \dot{\xi}_2^2 , \tag{1}$$

$$U = \frac{1}{2} V_1 \xi_1^2 + V_2 \xi_1 \xi_2 + \frac{1}{2} V_3 \xi_2^2 , \tag{2}$$

where ξ_1 and ξ_2 are symmetry coordinates characterizing the change in the length of the bonds (stretching) and the deformation of the angle, (bending) respectively, I_i are the reduced moments of inertia, V_i the reduced force constants.

Now, by definition, let us put $\xi_2 = 0$. Then the kinetic and potential energies of the system become:

$$T = \frac{1}{2} I_1 \dot{\xi}_1^2 ,$$

$$U = \frac{1}{2} V_1 \xi_1^2 .$$

As a result of integrating the appropriate Lagrangian equation of motion, we obtain an expression for the square of the partial frequency of the symmetric stretching vibration:

$$\tilde{\lambda}_1 = \tilde{\omega}_1^2 = \frac{V_1}{I_1} . \tag{3}$$

In exactly the same way, we will have for the bending vibration

$$\tilde{\lambda}_2 = \tilde{\omega}_2^2 = \frac{V_3}{I_3} . \tag{4}$$

We have shown [4], by using the method described by Strelkov [3], that the partial frequencies ω_1 and ω_2 will be near the appropriate normal frequencies as long as the eigenfrequencies of the molecules under consideration differ significantly from one another and the mass of the central atom is sufficiently large compared to the mass of the outer atoms.

An interesting form for the partial frequencies, is obtained when the kinetic and potential energies are written thus:

$$T = \frac{1}{2} B_1 \psi_1^2 + B_2 \psi_1 \psi_2 + \frac{1}{2} B_3 \psi_2^2 , \tag{5}$$

$$U = \frac{1}{2} U_1 \varphi_1^2 + U_2 \varphi_1 \varphi_2 + \frac{1}{2} U_3 \varphi_2^2 , \tag{6}$$

where ψ_i and φ_i are the symmetrized generalized momenta and generalized forces corresponding to the coordinates ξ_i; B_i are the reduced dynamic coefficients; U_i are the reduced interaction coefficients.

On the basis of the definition and integration of the appropriate equations of motion (see [5]), we obtain an expression for the squares of the partial frequencies of the symmetric stretching vibration

$$\tilde{\lambda}_1 = \tilde{\omega}_1^2 = \frac{B_1}{U_1} \tag{7}$$

and the bending vibration

$$\tilde{\lambda}_2 = \tilde{\omega}_2^2 = \frac{B_3}{U_3} . \tag{8}$$

Expressions (7) and (8) are of special interest because of the invariance of the dynamic coefficients and of the interaction coefficients of subscript i with respect to the selection of the variables ψ_k and φ_k of another subscript $k \neq i$ [1, 6, 7]. In order to differentiate the two forms of $\tilde{\omega}_i$, let us designate (3) and (4) as partial frequencies in the coordinate representation ($\tilde{\omega}_{i\xi}$) and (7) and (8) as partial frequencies in the momentum representation ($\tilde{\omega}_{i\psi}$). It is seen from table 1* that the quantities $\tilde{\omega}_{i\xi}$ and $\tilde{\omega}_{i\psi}$ for molecules with light terminal atoms are sufficiently close to the

* The data necessary to the compilation of tables 1, 2, and 3 are taken from [8].

appropriate normal frequencies. On this basis, expressions (3), (4), (7), and (8) can be considered as the zero'th approximation to the natural frequencies. The forms of the zero approximations mentioned have the advantage that they do not require a knowledge of the complete set of dynamic coefficients for the calculation. However, as is seen from the tables, they are less exact than the "natural zero approximation" introduced by El'iashevich and Stepanov [1].

Table 1

Zero Approximation to the Vibrational Frequencies of A_1 Symmetry

Molecule	Number of Freq.	Normal Freq.	$\tilde{\omega}_{1\xi}$	$\tilde{\omega}_{1\psi}$	Natural Zero Approx.
H_2O	1	3825	3825	3792	3824
	2	1654	1668	1654	1655
D_2O	1	2758	2754	2742	2761
	2	1210	1215	1212	1203
H_2S	1	2714	2708	2655	2705
	2	1214	1204	1216	1233
D_2S	1	1944	1941	1906	1939
	2	869.6	890	874.1	880.2
H_2Se	1	2366	2363	2341	2362
	2	979.6	990	980.8	988.0
D_2Se	1	1683	1682	1666	1681
	2	697.2	704	698.1	701.9

Table 2

Zero Approximation in the Ratio of the Force Constants ($10^5 \frac{\text{dyne}}{\text{cm}}$) and the Interaction Coefficients ($10^{-5} \frac{\text{cm}}{\text{dyne}}$)

Molecule	Dyn. Coef.	Known Values	Error (in %)	Zero Approx. I	Div. (in %)	Zero Approx. II	Div. (in %)
H_2O	V_1	8.323	0.2	8.323	—	8.301	0.3
	V_2	0.357	42	0.333	6.7	0.062	82
	V_3	0.768	1.7	0.766	0.3	0.755	1.7
H_2S	V_1	4.230	0.7	4.249	0.4	4.246	0.4
	V_2	0.271	74	0.092	66	0.018	93
	V_3	0.443	7.0	0.426	3.9	0.424	4.3
H_2Se	V_1	3.274	0.9	3.282	0.2	3.281	0.2
	V_2	0.133	300	0.030	77	0.005	96
	V_3	0.287	10	0.282	1.7	0.281	2.1
H_2O	U_1	0.1226	2.0	0.1205	1.8	0.1223	0.2
	U_2	-0.057	44	-0.010	82	-0.053	6.8
	U_3	1.329	3.4	1.325	0.3	1.329	—
H_2S	U_1	0.2461	7.0	0.2356	4.3	0.2365	3.9
	U_2	-0.151	88	-0.010	93	-0.0051	66
	U_3	2.351	13	2.358	0.3	2.361	0.4
H_2Se	U_1	0.3113	13	0.3047	2.1	0.3049	2.0
	U_2	-0.144	330	-0.0054	96	0.032	78
	U_3	3.547	22	3.555	0.2	3.555	0.2

The method of partial frequencies permits the zero approximation to the dynamical coefficients to be constructed also. Actually the following system of equations can be obtained from the secular equation for vibrations of A_1 symmetry:

$$B_3U_1 + B_1U_3 + 2B_2U_2 = (B_1B_3 - B_2^2)\cdot\frac{(\lambda_1 + \lambda_2)}{\lambda_1\cdot\lambda_2}, \tag{9}$$

$$U_1U_3 - U_2^2 = \frac{B_1B_3 - B_2^2}{\lambda_1\lambda_2} \tag{10}$$

This system is not sufficient to determine the complete set of interaction coefficients. However, the following approximate equality can be used as a third equation

$$\tilde{\lambda}_{1\psi} = \frac{B_1}{U_1} \approx \lambda_1. \tag{11}$$

Now solving the set of equations (9), (10), and (11), we find

$$U_1 = \frac{B_1}{\lambda_1}, \qquad U_2 = \frac{B_2}{\lambda_1}, \qquad U_3 = \frac{(B_1B_3 - B_2^2)\lambda_1 + B_2^2\lambda_2}{B_1\lambda_1\lambda_2}. \tag{12}$$

Similarly, taking the following approximate equality as the third equation

$$\tilde{\lambda}_{2\psi} = \frac{B_3}{U_3} \approx \lambda_2, \tag{13}$$

we obtain

$$U_1 = \frac{(B_1B_3 - B_2^2)\lambda_2 + B_2^2\lambda_1}{B_3\lambda_1\lambda_2}, \qquad U_2 = \frac{B_2}{\lambda_2}, \qquad U_3 = \frac{B_3}{\lambda_2}. \tag{14}$$

The equalities (12) and (14) are approximate and can be called the zero approximations with respect to the interaction coefficients. The zero approximations to V_i were studied by Glockler and Tung [9] and Torkington [10], who found them on the basis of completely different considerations. In order to distinguish the zero approximations to the dynamic coefficients, let us agree to enumerate them I and II, in conformance with the subscript of the partial frequency whose expression was used

as the additional equation.

It is easy to see that knowledge of the spectrum of just one isotopic modification is required to determine the complete set of quantities V_1 and U_1 by the method described. Known values of the force constants and the interaction coefficients are presented in table 2 with the errors which occur for Δn_1 and 5 cm^{-1} (see [8]). The discrepancies between the I and II zero approximations and the known values of V_1 and U_1 does not exceed the error mentioned except in rare cases.

Relations between the frequencies of isotopic modifications can easily be obtained by using the method of partial frequencies. Actually, as is seen from Table 1, the partial frequency of the symmetric stretching vibration of the RD_2 molecule determined by

$$\tilde{\nu}_1 = \frac{V_1}{I_1}, \tag{15}$$

is sufficiently close to the appropriate normal frequency. Now, taking (3) into account, we obtain

$$\frac{\lambda_2'}{\lambda_2} = \frac{I_3}{I_3'} \tag{16}$$

Starting from the expressions for the partial frequencies in the momentum representation, we obtain relations such as:

$$\frac{\lambda_1'}{\lambda_1} = \frac{B_1'}{B_1}, \tag{17}$$

$$\frac{\lambda_2'}{\lambda_2} = \frac{B_3'}{B_3}. \tag{18}$$

Similar formulas have been obtained by Tatevskii [11] on the basis of a similarity theorem. A comparison is presented in Table 3 of the known values of frequencies of dideutero-substituted molecules (see [8]) with those computed by our formulas and those of Tatevskii [11].

Hence, the method of partial frequencies appears to be very useful in solving the three vibrational problems considered above.

Table 3

Calculation of the Frequencies of Dideuterosubstituted Molecules by Means of Approximate Relations

Molecule	No. of Freq.	Freq.	From (15) and (16)	From (17) and (18)	From [11]
D_2O	1	2758	2754	2766	2766
	2	1210	1207	1212	1209
D_2S	1	1944	1945	1948	1948
	2	869.6	871.1	872.3	871.5
D_2Se	1	1683	1684	1684	1684
	2	697.2	697.1	697.3	697.2

In conclusion, I am grateful to I. N. Godnev for valuable suggestions during the research and to M. A. El'iashevich for discussions of the results.

December 4, 1958

References

1. M. V. VOL'KENSHTEIN, M. A. EL'IASHEVICH, B.I.STEPANOV: Kolebaniia molekul (Vibrations of molecules) GITTL, Moscow-Leningrad, 1949
2. L. I. MANDEL'SHTAM: Polnoe sobranie trudov (Complete works), 3, Moscow, 1950
3. S. P. STRELKOV: Vvedenie v teoriiu kolebanii (Introduction to the Theory of Vibrations), GITTL, Moscow-Leningrad, 1950
4. V. P. MOROZOV: Primenenie metoda partsial'nykh-chastot k vychisleniiu silovykh postoiannykh i termodinamicheskikh svoistv trekhatomnykh nelineinykh molekul (Use of the partial frequencies method to calculate the force coefficients and thermodynamic properties of atomic nonlinear moleckles) Kand.diss., Ivanova, 1953
5. V. M. TATEVSKII: ZETF, 15, (8), 445 (1945)
6. L. S. MAIANTS: Tr. FIAN, 5, 63 (1950)
7. P. G. MASLOV: Kolebaniia molekul i termodinamicheskie svoistva parov organicheskikh soedinenii (Vibrations of molecules and thermodynamic properties of organic compound vapors) Doctoral diss., Leningrad, 1953
8. V. P. MOROZOV: ZFKh, 31, 238 (1957)
9. G. GLOCKLER, JO-YON-TUNG: J.Chem.Phys., 13, 388 (1945,
10. P. TORKINGTON: J. Chem. Phys., 17, 357 (1949)
11. V. M. TATEVSKII: ZFKh., 25, 274 (1951)

TOM VII, Vyp. 3 OPTIKA I SPEKTROSKOPIIA Sentiabr', 1959
VOL. VII, No. 3 OPTICS AND SPECTROSCOPY September, 1959

Theory of the Vibrational Spectra of Polymers

I. Structure of Vibrational Bands in the Spectra of Helical Polymer Chains

IU. IA. GOTLIB

Abstract: The distribution of intensities in an optical vibration band is observed for a regular helical polymer chain. The band arising from the splitting of the separate monomer vibration breaks down into two components – parallel and perpendicular. The distribution of intensities in each component is investigated. Intensity formulas follow from the derived expressions as special cases for small chains of parallel and antiparallel coupled oscillators.

1. In recent years considerable success has been achieved in the synthesis of linear polymeric macromolecules having a regular structural chain [1]. With the help of stereospecific polymerization it is possible to construct different stereoisomeric polymers from the same monomers which differ from each other in their physical properties (melting temperature, degree of crystallinity, mechanical strength, etc.).

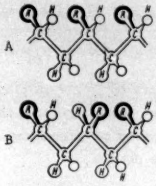

Figure 1. Structure of isotactic (A) and syndiotactic (B) polymers.

With stereospecific "head-to-tail" polymerization of vinyl polymers of the type $(CH_2 - CHR)_n$, (See figure 1), two types of regular polymers can arise depending on the conditions of polymerization: 1) isotactic polymers, in which R-groups are placed on one side of the skeletal chain, and 2) syndiotactic polymers, in which alternating R-groups are placed on the opposite side of the straightened skeletal chain.

If we take into account that in any reaction there exist certain probabilities of both syndio- and iso- connection of each monomer to the preceding one, then it is possible to represent any polymer as a succession of iso- and syndio- tactic sections. Polymers not belonging to a stereoregular structure are called atactic.

Regular iso- and syndiotactic polymers are crystallizable. In this case their structure can be investigated by means of the method of X-ray diffraction analysis, permitting one to determine the lattice parameters of the crystals formed by various chains and the nature of the periodicity along each chain.

Irregular atactic polymers with large R-groups cannot crystallize. The presence of internal rotation in chains leads to a variety of chain conformations and therefore spatial periodicity along the chain is lacking in amorphous iso- and syndiotactic and in atactic polymers.

The examination of regularities of the spectra of isolated macromolecules which are regular either in the stereoisomer or in the rotational isomer sense is a natural first approximation in solving the problem of the influence of the structure of polymers on their optical properties and, in particular, on their spectra. Then we may consider the different types of irregularity and also the interaction of chains.

As X-ray diffraction analysis shows, regular crystalline iso-tactic chains take on a helical form, whereas syndiotactic polymers usually crystallize in the form of planar or almost planar trans-chains. Therefore the study of general regularities in the spectra of helical chains is of considerable interest. In addition to the polymers of the form $(CH_2 - CHR -)_n$, obtained by means of stereospecific catalysis, macromolecules of albumin and nucleic acid are helical, as are macromolecules of some polymers with symmetric side groups: polytetrafluoroethylene, polyisobutylene, and others.

Higgs [2] examined the selection rules and polarizations in infra-red and Raman spectra for infinite helical chains. However, the question of the distribution of band intensities has not been examined up to this time. A theory of electronic spectra and optical activity for spiral polymers was proposed by Moffit, Kirkwood, and others [3,4].

Syndiotactic polymers having the trans-form can be considered to be helical with two monomers per coil, and therefore our results refer to the syndiotactic polymers as well. In this case the theoretical expressions correspond to the results obtained by Stepanov and Vidro [5] for simple models of antiparallel oscillators. The intensities, polarizations and frequencies for the trans- chains (of the polyethylene type) have been examined by Vol'kenstein and Vidro [6], Kellner [7], Theimer [8], Higgs [9], Mizushima and Shimanuchi [10], and others.

2. Our problem is to study the structure of an optical band in the vibrational spectrum of a helical chain, arising from the response of an "uncoupled" line to the oscillation of a different group, due to the existence of bonds between different groups in a polymer chain. Our derivation will rest upon the assumption of definite phase relations between vibrations in neighboring groups. These are not connected with the specific nature of the groups or the type of vibrations, but are stipulated by the periodic helical structure of the chain.

We will examine an isolated regular helical chain constructed from N identical repeating groups. Let the number of repeating groups be ν^* in the period of identity of the helix in which s coils are contained in one period, so that on one coil there are $\nu = \frac{\nu^*}{s}$ repeating groups (ν can be either integral or fractional). We introduce a Cartesian system or coordinates X, Y, Z based on the equilibrium configuration of the helix so that the Z axis is parallel to the axis of the helix; moreover, we introduce local systems of coordinates $\xi^{(n)}$, $\eta^{(n)}$, $\zeta^{(n)}$, referred to the repeating groups in the helical chain. The $\zeta^{(n)}$ axes are parallel to the

Z axis; the axes $\xi^{(n)}$ and $\eta^{(n)}$ are rotated through the angle $2\pi \frac{S}{\nu^*} = \frac{2\pi}{\nu}$ in relation to the axes $\xi^{(n-1)}$, $\eta^{(n-1)}$, of the preceding local system; there is an identical placing of all corresponding atoms of repeating groups in their own local systems.

With the introduction of the normal vibration Q in the chain there arises a corresponding dipole moment $\delta\vec{p}(Q) = \sum_{n=1}^{N} \delta\vec{p}^{(n)}(Q)$, where $\delta\vec{p}^{(n)}(Q)$ is the contribution of the nth repeating group. If the vibration is basically determined by interactions inside repeating groups, while the interaction between groups for a given type of vibration is weak, then for vibrations of similar type the orientations of the vectors $\delta\vec{p}^{(n)}$ in their local coordinate systems will be identical, and the values of the amplitudes of $\delta\vec{p}^{(n)}$ will change depending upon the form of the vibrations.

The assumed theory is inapplicable, for example, to the examination of O-Si-O stretching vibrations in linear silicone chains for which the orientations of the dipole moment of the repeating group of $O\text{-}Si(CH_3)_2\text{-}O$ in the local coordinate systems depends on the difference in phase between vibrations of neighboring O-Si and Si-O bonds and is determined by the position of the repeating groups in the chain.

Our calculations refer basically to normal vibrations connected principally with such changes of the natural coordinates as the stretching CH_2-vibrations, the symmetric bending vibration of CH_2, the stretching vibrations of CR, and so forth, for which the bond between nuclei is a perturbation and the orientations of the vectors $\delta\vec{p}^{(n)}$ are identical in their "own" coordinate systems.

If the chain is sufficiently long ($N \gg 1$), so that the influence of the terminal groups is insignificant, then $\delta\vec{p}^{(n)}(Q_k)$ can be represented in the form (cf. [6,8,9,12,13])

$$\delta\vec{p}^{(n)}(k,\theta) = \delta\vec{p}_0(k,\theta)\sin(n\theta + \delta_k), \tag{1}$$

where k is the number of the band corresponding to the "parent" vibration of the repeating groups producing the band, θ is the phase shift between neighboring repeating groups, and $\delta\vec{p}_0(k,\theta)$ is the vector amplitude. We shall assume the phase δ_k equal to zero and the possible values of θ for a chain of N groups will be determined from the condition

$$\theta_l = \frac{\pi l}{N+1}, \tag{2}$$

where $l = 1,2,\ldots N$ (see [12, 13]).

3. Let us examine the distribution of intensities in the kth band. The intensities of radiation with electric vector polarized along X, Y, or Z, respectively, will be designated by I_X, I_Y, and I_Z for the normal vibration $Q(k, l)$. As is well known (see [11]),

$$I_{X_i} = C\left(\frac{\delta p_{X_i}}{\delta Q(k,l)}\right)^2, \quad X_i = X, Y, Z, \tag{3}$$

where the quantity C depends slightly on the frequency of vibration, which in every case is within the limits of the given band.

It is possible to decompose the dipole moments $\delta\vec{p}_0^{(n)}(k, l)$ into vectors $\delta\vec{p}_{0\zeta}^{(n)}(k, l)$ parallel to the Z axis and $\delta\vec{p}_{0\xi\eta}^{(n)}$ in the planes $\xi^{(n)}$, $\eta^{(n)}$.

Correspondingly, we designate

$$\frac{\delta\vec{p}_{0\zeta}}{\delta Q_{kl}} = \frac{\mu_\zeta(k)}{\sqrt{(N+1)/2}}; \quad \frac{\delta p_{0\xi\eta}}{\delta Q_{kl}} = \frac{\mu_{\xi\eta}(k)}{\sqrt{(N+1)/2}}, \tag{4}$$

where $\sqrt{(N+1)/2}$ is a normalizing factor (see [5]), $\mu_\zeta(k)$ and $\mu_{\xi\eta}(k)$ do not depend on N. The proportionality of the amplitudes of vibrating atoms to $(N+1)^{-\frac{1}{2}}$ for a long regular chain is discussed in [8]. It is possible to show that $\mu_{\xi,\eta\zeta}$ is practically independent of l for the considered type of vibrations.

Let the angle $\delta\vec{p}_0^{(n)}\vec{z} = \alpha$, then

$$\mu\zeta = \mu\cos\alpha; \quad \mu_{\xi\eta} = \mu\sin\alpha. \tag{5}$$

The vectors $\delta\vec{p}_{0\xi\eta}^{(n)}$ lie in planes parallel to the XY plane and each is rotated through the angle $\left(\frac{2\pi}{\nu}\right)$, relative to the preceding. From (1), (2), (4) and (5), we obtain

$$\begin{aligned}
\frac{\delta p_X}{\delta Q_{kl}} &= \frac{\mu(k)\sin\alpha}{\sqrt{[(N+1)/2]}} \sum_{n=1}^{N} \sin\frac{\pi n l}{N+1}\cos\frac{2\pi n}{\nu}, \\
\frac{\delta p_Y}{\delta Q_{kl}} &= \frac{\mu(k)\sin\alpha}{\sqrt{[(N+1)/2]}} \sum_{n=1}^{N} \sin\frac{\pi n l}{N+1}\sin\frac{2\pi n}{\nu}, \\
\frac{\delta p_Z}{\delta Q_{kl}} &= \frac{\mu(k)\cos\alpha}{\sqrt{[(N+1)/2]}} \sum_{n=1}^{N} \sin\frac{\pi n l}{N+1}.
\end{aligned} \tag{6}$$

In the derivation (6) we made use of the fact that for a suitable rotation of the X and Y axes

$$\begin{aligned}
\cos(\delta\vec{p}_{0\xi\eta}^{(n)}, \vec{X}) &= \cos(2\pi n/\nu), \\
\cos(\delta\vec{p}_0^{(n)}, \vec{Y}) &= \sin(2\pi n/\nu).
\end{aligned} \tag{7}$$

The results of the summation in (6) depend on the evenness or oddness of l and on the relation between N and ν. We introduce the number τ from the condition:

$$\tau = (N/\nu) - G,$$

where G is the maximum integer smaller than N/ν. The computation of the sums gives:

l odd

$$\frac{\delta p_X}{\delta Q_{kl}} = \frac{\mu(k)\sin\alpha}{\sqrt{[(N+1)/2]}} \cos^2\pi\left(\tau + \frac{1}{\nu}\right) F(l, N, \nu),$$

$$\frac{\delta p_Y}{\delta Q_{kl}} = \frac{\mu(k)\sin\alpha}{\sqrt{[(N+1)/2]}} \sin\pi\left(\tau+\frac{1}{\nu}\right)\cos\pi\left(\tau+\frac{1}{\nu}\right)F(l,N,\nu),$$

(8)
$$\frac{\delta p_Z}{\delta Q_{kl}} = \frac{\mu(k)\cos\alpha}{\sqrt{[(N+1)/2]}} \operatorname{ctg}\frac{\pi l}{N+1}.$$

l even

(9)
$$\frac{\delta p_X}{\delta Q_{kl}} = \frac{\mu(k)\sin\alpha}{\sqrt{[(N+1)/2]}} \sin^2\pi\left(\tau+\frac{1}{\nu}\right)F(l,N,\nu),$$

$$\frac{\delta p_Y}{\delta Q_{kl}} = -\frac{\mu(k)\sin\alpha}{\sqrt{[(N+1)/2]}} \sin\pi\left(\tau+\frac{1}{\nu}\right)\cos\pi\left(\tau+\frac{1}{\nu}\right)F(l,N,\nu),$$

$$\frac{\delta p_Z}{\delta Q_{kl}} = 0;$$

$$F(l,N,\nu) = \frac{\sin\frac{\pi l}{2(N+1)}\cos\frac{\pi l}{2(N+1)}}{\sin\left[\frac{\pi l}{2(N+1)}+\frac{\pi}{\nu}\right]\sin\left[\frac{\pi l}{2(N+1)}-\frac{\pi}{\nu}\right]}$$

4. Now let us examine the intensities of radiation polarized along the long axis of the helical chain (parallel band I_Z) and polarized in the XY plane (perpendicular band $I_{XY} = I_X + I_Y$):

l odd

$$I_Z(k,l) = C\left(\frac{\delta p_Z}{\delta Q_{kl}}\right)^2 = \frac{2C}{N+1}\mu^2(k)\cos^2\alpha\operatorname{ctg}^2\frac{\pi l}{N+1}$$

(10)
$$I_{XY}(k,l) = C\left[\left(\frac{\delta p_X}{\delta Q_{kl}}\right)^2+\left(\frac{\delta p_Y}{\delta Q_{kl}}\right)^2\right] =$$

$$= \frac{2C}{N+1}\mu^2(k)\sin^2\alpha\cos^2\pi\left(\frac{1}{\nu}+\tau\right)F^2(l,N,\nu).$$

l even

(11)
$$I_Z(k,l) = 0;$$

$$I_{XY}(k,l) = \frac{2C}{N+1}\mu^2(k)\sin^2\alpha\sin^2\pi\left(\frac{1}{\nu}+\tau\right)F^2(l,N,\nu),$$

where C depends slightly on frequency within the given band.

The basic dependence of the intensity I_{XY} on l in a given band is determined by the function F^2 [see (9)]. The maximum of F^2 is attained at the minimum value of the difference

$$[\pi l/2(N+1)] - (\pi/\nu).$$

If $N \gg 1$, then the condition for a minimum gives us approximately

$$l_{extr.} \approx [2(N+1)/\nu] \approx [2N/\nu],$$

which corresponds to a phase shift of $\frac{2\pi}{\nu}$ between vibrations in neighboring repeating groups. On both sides of the line $\omega(l_{extr.})$ there are lines with rapidly diminishing intensity (see figure 2). The function $I_Z(k, l)$ attains a maximum at $l = 1$ which for large N corresponds to neighboring cells vibrating in phase.

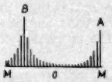

Figure 2. Distribution of intensities in the band corresponding to a helical polymer for a component polarized parallel (A) and perpendicular (B) to the axis of the chain.

Therefore, the most intense vibrations in the infrared spectrum of helical chains are the two for which neighboring rotating units vibrate either in phase (vibrations polarized along the long axis of the chain) or out of phase by $2\pi/\nu$. If we examine the phase shift in one spatial period of identity of the helix, then it appears to equal to $2\pi(\nu^*/\nu) = 2\pi s$ (s is a whole number equal to the number of coils in one period); that is, the neighboring spatial groups vibrate in phase. The results indicated correspond to the selection rules for infinite chains derived by Higgs [2].

The presence of parallel and perpendicular subbands connected with the symmetry properties of the helical chain is germane for electronic transitions as well (see [3,4]).

We write the expression for the full intensity of the kth band, since intensities of separate lines are conveniently compared with the full intensity of the band. In the calculation of the full intensity, it is simpler not to sum the complicated expressions (10, 11), but to represent the full intensity I_k at once as

$$I_k = C\sum_{l=1}^{N}\left[\sum_{n=1}^{N}\frac{\delta\vec{p}^{(n)}}{\delta Q_{kl}}\right]^2 =$$

(12)
$$= C\sum_{l=1}^{N}\left\{\sum_{n=1}^{N}\left(\frac{\delta\vec{p}^{(n)}}{\delta Q_{kl}}\right)^2 + 2\sum_{n'=1}^{n-1}\sum_{n=2}^{N}\left(\frac{\delta\vec{p}^{(n)}}{\delta Q_{kl}}\cdot\frac{\delta\vec{p}^{(n')}}{\delta Q_{kl}}\right)\right\}.$$

After a simple summation, using the fact that

$$\sum_l \sin\frac{\pi n l}{N+1}\sin\frac{\pi n' l}{N+1} = [(N+1)/2]\,\delta_{nn'},$$

we obtain the following expression for I_k:

(13)
$$I_k = C\,N\mu^2(k).$$

We conclude from (13) that the full intensity of the band is the same for regular chains with identical amplitudes of transition moments in one repeating group, even if the stereoisomeric structure of these polymers is different (helices with a different screw pitch, iso- and syndiotactic polymers, etc.). We note that C depends slightly on the structure of the chain. Such bands with a constant amplitude of the dipole moment may be bands

corresponding to the characteristic stretching vibrations of CH_2. These vibrations interact with other vibrations comparatively weakly, and their absolute amplitudes in different stereoisomers can be close to one another. Then the full intensity of such bands will be the same in different stereoisomers, although the form of the splitting, the distribution of intensities in the band and the polarization of the components will be materially different.

The computation of the full intensity I_{kZ} is performed by means of direct summation

$$\left(\sum_{l = 1, 3, 5 \ldots \leq N} \operatorname{ctg}(\pi l/(N+1)) = (N+1)/2 \right)$$

and gives

(14) $I_{kZ} = NC \cos^2\alpha_l^2(k)$ and $I_{k,\ XY} = NC \sin^2\alpha_l^2(k)$

We notice that I_{kZ} and I_{kXY} separately do not depend on the helix parameters, with the exception of the angle α between the direction of the dipole moment $\delta\vec{p}_0(k)$ and the axis of the chain.

5. Let us examine in more detail the distribution of intensities for different lines of the band. For example, let us take a chain with three repeating groups on one coil of the helix ($\nu = 3$). In this case, there is one residue per turn of the helical chain.

Let $\tau = (N/3) - G$ where G is the largest whole number which is smaller than $(N/\nu) \equiv (N/3)$, i. e. $\tau > 0$. Investigation of the three possible cases $\tau = 0$, $1/3$ and $2/3$ shows that the distribution of intensities is practically independent of τ (or of N). At $\tau = 0$ and $1/3$ the most intense pairs are lines in the perpendicular band c.

$l^* = 2G + 1$ and $l^* = 2G$ (for $\tau = 0$) and $l^* = 2G + 2$ and $2G + 1$ (for $\tau = 1/3$).

The intensity of these pairs of lines is 0.83 of the full intensity of the perpendicular band. For $\tau = 2/3$, most intense in the perpendicular band are the three components with $l^* = 2G + 1$, $2G + 2$ and $2G + 3$, in which must be 0.91 of the total intensity of the band. On both sides of the main component the intensities of the lines fall off as $1/(l - l^*)^2$.

For lines of the parallel band, the most intense is the line with $l = 1$, independently of N (cf. [5, 6]), where 0.83 of the intensity of the entire band occurs. The general character of the dependence is represented in figure 2.

Hence, we assume that the frequency $\omega_k(\theta)$ is a monotonic function of θ (and l), for example, $\omega(\theta) = \omega_0 + M \cos\theta$ (cf. with [2], eq. 27). In this case the width of the entire band $\Delta\omega = 2M$, while the maximum of the perpendicular band lies at

$$\omega(2\pi/3) = \omega_0 - \tfrac{1}{2} M,$$

i. e., a distance 0.5M from the edge of the band. Therefore the perpendicular band, speaking generally, remains asymmetrical. The maximum of the parallel band in this case lies at $\omega(\theta) = \omega_0 + M$. The distance between maxima of the parallel and perpendicular bands (1.5M) in our example may be of the same order as the natural width of the bands. Therefore no splitting will be observed with unpolarized light.

The magnitude of the splitting depends, of course, on the nature of the interaction. Thus for CH_2 stretching vibrations, the interaction between vibrations in neighboring groups is evidently not large, inasmuch as the eigen frequencies of angles and bonds, across which the interaction of the two nearest CH_2 groups is accomplished, differ strongly from the frequencies of the CH_2 stretching vibrations (much less than the last).

In the case of rocking and twisting vibrations of the CH_2 groups, their interaction will be stronger with the skeleton of the chain and through the skeleton with each other and the splitting of the band into two (Z- and XY- bands) may be significant.

The syndiotactic polymer with repeating units $(CH_2 - CHR - CH_2 - CRH -)$ can be examined if we put $\nu = 1$. In this case we obtain formulas from (8)-(11) defining intensity of radiation for a system of parallel coupled oscillators, where by $\delta\vec{p}_0$, we mean the moment of all repeating units. The case of a system of successive antisymmetrical oscillators (CH_2 groups in polyethylene) corresponds to the "helix" with $\nu = 2$ (see also [5]).

The splitting of lines and the band structure arising in helical polymers from the interaction of vibrations in monomeric groups connected to the chain has been investigated. The band splits into two components I_Z and I_{XY} (parallel and perpendicular), polarized respectively along the axis of the helix and in the perpendicular plane. In the band I_{XY} the main part of the intensity of the band occurs in 2 – 3 internal lines; on both sides of these lines the intensity falls off as $1/(l - l^*)^2$. In the band I_Z the most intense line is the edge line of the band. The distribution of intensities for very long chains corresponds to the selection rules proposed earlier by Higgs.

The transition to the cases $\nu = 1$ and $\nu = 2$ leads to previously known formulas for a system of parallel or antiparallel coupled oscillators.

In conclusion I consider it my pleasant duty to express sincere thanks to M. V. Vol'kenshtein for the interest he showed in this work and for valuable discussion.

December 29, 1958

References

1. E. S. KRONGAUZ, A. P. SUPRUN: Usp Khim., 27, 1056 (1958)
2. P. W. HIGGS: Proc. Roy. Soc., 220, 472, (1953)
3. W. MOFFIT: J.Chem.Phys. 25, 467 (1958)
4. W. MOFFIT, D. FITTS, J. G. KIRKWOOD: Proc.Nat. Acad. Sci., 43, 723, (1957)
5. L. I. VIDRO, B.I. STEPANOV: DAN USSR, 82, 557, (1952)
6. L. I. VIDRO, M. V. VOL'KENSHTEIN: DAN, USSR, 85, 1243 (1952)
7. L. KELLNER: Proc.Phys. Soc. A64, 521 (1951)
8. O. THEIMER: J. Chem. Phys., 27, 408, 1041, (1957)
9. P. W. HIGGS: J.Chem. Phys., 23, 1450, (1955)
10. S. MIZUSHIMA: Structure of molecules and Internal Rotation, (IL, 1957)
11. M. V. VOL'KENSHTEIN, M. A. EL'IASHEVICH, B. I. STEPANOV: Kolebaniia molekul (Vibrations of molecules). GITTL, 1949
12. J.G.KIRKWOOD: J.Chem.Phys., 7, 506, (1939)
13. K. S. PITZER: J.Chem.Phys., 8, 711 (1940)

TOM VII, Vyp. 3 OPTIKA I SPEKTROSKOPIIA Sentiabr', 1959
VOL. VII, No. 3 OPTICS AND SPECTROSCOPY September, 1959

Investigation of Infrared Absorption Spectra of Hydrocarbons at Various Temperatures in the Liquid and Solid Phases

K. H. KESLER, IU. A. PENTIN, E. G. TRESHCHOVA
AND V. M. TATEVSKII

Abstract: The infrared absorption spectra of a series of hydrocarbons were studied at room temperature in the liquid phase and at low temperatures (down to -172°C) in the solid phase in order to ascertain the changes which take place in the spectra in the transition from the liquid to the solid. From a study of these changes conclusions could be reached concerning the presence or absence of rotational isomers in each of the phases and concerning the change of concentration of the rotational isomers with temperature.

Few investigations have been concerned with the study of the infrared absorption spectra of the hydrocarbons, especially the branched-chain types, as a function of temperature (cf. ref. [1]). The accumulation of further experimental data in this field appears therefore to be not without interest. In the present investigation we have studied normal (n-heptane, n-octane), branched-chain alkanes (3-methylheptane, 2,3-dimethyl-heptane, 2,4-dimethylpentane, 2, 5-dimethylhexane, 2,2,5,5-tetramethylhexane) and branched-chain alkenes (2-methylheptene-2 and 3,3-dimethylheptene-1). The normal alkanes were studied in order to compare the results of the present investigation with the results of earlier workers [2-4]; in general there was found to be good agreement. Of the branched-chain alkanes only 3-methylheptane and 2, 5-dimethylhexane in the liquid phase had been previously investigated [5]. The remaining branched-chain alkanes and alkenes were studied for the first time in the liquid as well as in the solid phase.

All the hydrocarbons investigated were obtained from other laboratories where their physical constants or degree of purity had been determined *. These data are given in Table 1.

APPARATUS AND METHODS OF MEASUREMENT

The infrared spectra were investigated in the region from 700 to 1800 cm^{-1} using an IKS-2 double-beam infrared spectrometer with an NaCl prism. The spectral slit-width in the region studied was 7-10cm^{-1}. Narrow bands with sharply defined maxima were measured by means of a calibration curve with an accuracy of 2-3 cm^{-1} and of 5-7 cm^{-1} in the frequency regions 700-1200 cm^{-1} and 1200-1800 cm^{-1}, respectively. For wide bands with poorly defined maxima the accuracy was lower and depended on the shape of the band.

Various liquid cells were used with path-lengths of 0.03 to 0.48 mm, depending on the substance and the experimental conditions. To investigate the spectra at low temperatures a special cell was built; the design assured a practically constant path length between the windows when the substance was in the liquid state and also after it had crystallized. It was thus possible to compare the absorption spectra of a substance in the liquid and solid phases with a single absorption path length.

The thermocouple used was calibrated at the following fixed points: melting snow (0°C), a freezing mixture of 33 parts of rocksalt and 100 parts of snow (-20°C), sublimation of solid CO_2 (-78°C) and boiling nitrogen (-196° C). The potential difference of the thermocouple junctions was measured with a millivoltmeter with an accuracy in the temperature determination of ± 2° C. Measurements were carried out at temperatures from 20° to -172°C.

To prevent the outer windows of the cell from becoming clouded over the housing of the cell was heated by hot water flowing in a coil.

The order of the experiment was as follows. The cell was filled with the liquid hydrocarbon, mounted and encased in the metal housing; the whole system was then flushed with dry nitrogen gas for 10-15

*The authors express their deep gratitude to Professor R.IA.Levina and A.V.Iogansen who furnished the hydrocarbon samples for this investigation.

Table 1

Hydrocarbon	Degree of purity (in mole %)	Boiling pt.(°C)		n_D^{20}		Temp. of Crystallization in °C
		Our preparation	From data in the literature [7]	Our preparation	From data in the literature [7]	From data in the literature[7]
n-Heptane	99.0	—	98.43	—	1.38764	-90.6
n-Octane	—	125	125.6	—	1.39743	from -52.8 to -56.9
2,4-Dimethylpentane	98.6	—	80.5	—	1.38145	-119.9
2,5-Dimethylhexane	96.3	—	109.1	—	1.39246	-91.4
2,2,5,5-Tetramethylhexane	97.6	135	137.5	1.4064	1.40550	-12.6
2,3-Dimethylheptane	—	140(760mm)	140.65	1.4087	1.4085	—
3-Methylheptane	—	117.5(721mm)	118.92	1.3983	1.39848	-120.6
2-Methylheptene-2	—	121.5(750mm)	122.6	1.4180	1.4172	—
3,3-Dimethylheptene-1	—	128(741mm)	128.8[8]	1.4150	1.4135[8]	—

Table 2
Infrared Spectra of n-Heptane and n-Octane in the Liquid and Crystalline Phases

n-Heptane				n-Octane			
This Investigation		Data in the literature		This Investigation		Data in the literature [3]	
Liquid	Crystal	Liquid [9]	Crystal [2]	Liquid	Crystal	Liquid	Crystal
1465	+	1470	+	1465	+	1465	+
1375	+	1377	+	1386	+	1378	+
						1355	-
1330	+	1342	+	1339	-	1341	-
1295	+	1300	+	1303	+	1301	+
	1276	1278	-		1226	1270	+
					1200	1225	+
1229	+	1232	+			1200	+
1177	+	1176	+				
1154	+	1166	-				
1137	-	1137	+	1139	+	1136	-
1077	+	1074	+	1080	+	1078	+
	1058		1055	1032	1022	1036	-1020
1017	-	1020	-	1001	-	1005	+
954	-	965	-	967	-	967	-
		945	-				
932	+	930	+				
	912			915	-	915	-
900		908	+	900	-	896	-
		900	-	887	+	889	+
878	+	875	+	878	+	878	+
865	-	863	-				
				843	-	844	-
827	-	833	-				
				806	-	794	-
773	+	773	+	764	-	765	-
740	-	739	-	753	+	751	+
724	-	723	+	723	+	722	+

Note: The presence or absence of an absorption band in the solid phase is indicated by + or - respectively.

Table 3
Infrared Spectra of Hydrocarbons at Room Temperature and at Low Temperature

3-Methyl-heptane		2,3-Dimethyl-heptane		3,3-Dimethyl-heptene-1		2-Methyl-heptene-2	
Liquid 20°C	Solid -160°C	Liquid 20°C	Solid -84°C	Liquid 20°C	Solid -120°C	Liquid 20°C	Solid -172°C
				1794 w	+		
				1685 w	+		
						1664 m	+
						1645 m	+
				1630 s	+		
				1560 w	+	1553 w	+
1470 vs	+			1475 vs	+		
		1466 vs	+			1467 vs	+
						1453 vs	+
						1432 m	+
				1420 s	+		
1384 vs	+	1381 vs	+	1385 vs	+	1385 vs	+
1350 w	+			1375 s	+		
				1342 w	+		
						1323 w	+
1314 w	+			1319 w	+	1311 w	+

Note: The relative intensities are designated: vs - very strong, s - strong, m - medium, w - weak, vw - very weak.

minutes to remove moisture and carbon dioxide. Cooling was carried out by adding liquid nitrogen or a mixture of solid carbon dioxide and acetone to the glass reservoir. At the same time continuous and repeated recordings of the spectrum were begun. Prior to obtaining low temperatures close to the freezing point of the hydrocarbon, the space inside the housing contained an atmosphere of dry nitrogen. When temperatures close to the freezing point of the substance were reached, a vacuum pump was connected to the system and the pressure maintained at 1-3 mm Hg. When the experiment was conducted under these conditions there was practically no evaporation of the substance in the cell. In order to obtain good crystals and to prevent the formation of a glassy solid, the cooling was carried out slowly, especially in the neighborhood of the freezing point.

The spectrum of each hydrocarbon was recorded several times with repeated cooling and heating of the sample. Altogether, 200 recordings of the spectra of the hydrocarbons at various temperatures were obtained; in figures 1-3 reduced absorption curves of the substances are presented.

DISCUSSION OF THE RESULTS

Normal Paraffins. The spectra obtained for n-heptane and n-octane in the liquid and crystalline states are in good agreement with data given in the literature [3, 4]. Our observations for these substances in the liquid phase at room temperature and in the solid phase at low temperatures are summarized in Table 2. As can be seen from the table the spectra become simpler in the transition to the crystalline state.

Branched-Chain Hydrocarbons. The spectra of the branched-chain alkanes and alkenes investigated are presented in figures 1-3. By comparing the spectra obtained at low temperatures it is possible to divide the substances tentatively into three different groups: group I, (Table 3), consisting of 3-methylheptane, 2,3-dimethyl-heptane and 3,3-dimethylpentene-1; group II (Table 4) consisting of 2, 4-dimethylpentane, 2, 5-dimethylhexane and 2,2,5,5-tetramethylhexane; group III (Table 3), 2-methylheptene-2.

In the absorption spectra of the hydrocarbons of group I, no substantial changes are observed at low temperatures. No marked simplification of the spectra and no marked change in the relative intensities of the bands are found on solidification. On lowering the temperature an increase in the peak intensities and an improved resolution of the bands are observed. This was also noted by Axford and Rank and others [2,10] for 2-methylbutane and 2, 3-dimethylbutane on solidification. The substances of

Table 3 (continued)

3-Methyl-heptane		2,3-Dimethyl-heptane		3,3-Dimethyl-heptene-1		2-Methyl-heptene-2	
Liquid 20°C	Solid -160°C	Liquid 20°C	Solid -84°C	Liquid 20°C	Solid -120°C	Liquid 20°C	Solid -172°C
1302 w	+	1304 w	+				
1274 w	+						
				1268 w	+		
						1257 w	+
		1245 w	+				
						1232 w	+
1212 w	+	1214 vw	+				
				1206 m	+		
1190 w	+			1197 m	+	1196 w	+
		1176 w	+				
				1169 m	+	1149 w	+
1154 m	+	1150 w	+				
1145 m	+						
1124 w	+	1123 s	+	1128 w	+	1120 m	+
				1102 m	+	1102 m	+
1086 w	+			1088 w	+	1083 m	increases
		1077 w	+	1075 w	+		
1059 w	+					1052 w	+
1044 w	+	1039 w	+	1036 m	+		
				1024 m	+		
1014 w	+	1018 m	+			1012 w	+
1000 m	+	1002 w		1003 vs	+		
						986 m	+
		974 w	+			974	decreases
						970 m	+
961 m	+			958 w	+		
				935 w	+	938 w	+
928 w	+					928	increases
		918 w	+			920 w	+
				910 vs	+		
906 m	+					904 w	increases
894 m	+	894 w	+				
				887 m	+	881 w	+
873 w	+	869 m	+			864 w	+
		855 w	+				
						837 s	+
818 w	+	819 w	+			825 s	+
		798 w	+				
		783 m	+	784 m	+		
772 m	+					776 w	+
762 m	+	763 w	+	767 w	+	766 w	+
				752 w	+		
		746 w	+			742 m	+
				731 m	+		
728 s	+	728 s	+			728 m	increases
				690 s	+		

Note: The relative intensities are designated: vs - very strong, s - strong, m - medium, w - weak, vw - very weak.

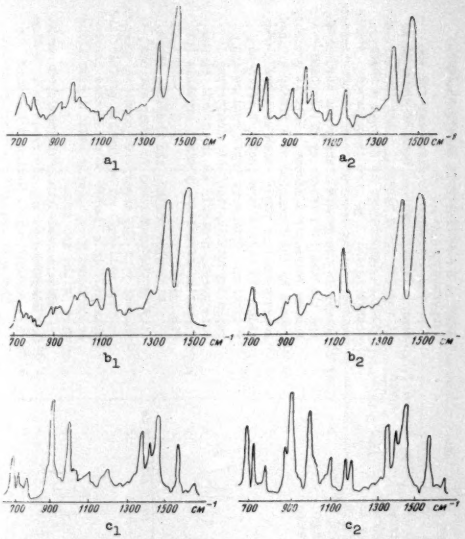

Figure 1. Absorption spectra (path-length 0.03 mm)
a_1 - 3-methylheptane in the liquid phase at 20°C, a_2 - the same at -160°C; b_1 - 2,3-dimethylheptane in the liquid phase at 20°C, b_2 - the same at -84°C; c_1 - 3,3-dimethylheptene-1 in the liquid phase at 20°C, c_2 - the same at -120°C.

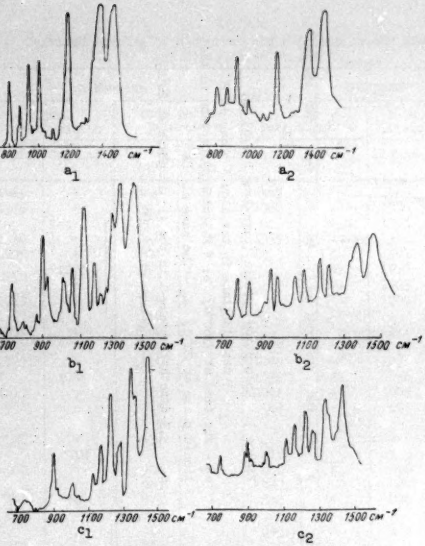

Figure 2. Absorption spectra:
a_1 - 2,4-dimethylpentane in the liquid phase at 20°C,
a_2 - the same in the solid phase at -150°C (path-length 0.1mm);
b_1 - 2,5-dimethylhexane in the liquid phase at 20°C,
b_2 - the same in the solid phase at -160°C (path-length 0.1mm);
c_1 - 2,2,5,5-tetramethylhexane (dineopentyl) in the liquid phase at 20°C, c_2 - the same in the solid phase at -19 to -36°C (path-length 0.03 mm).

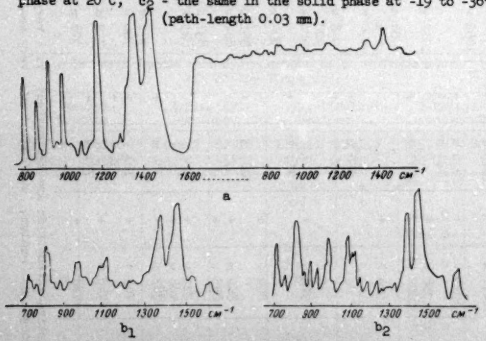

Figure 3. Absorption spectra:
a - 2,4-dimethylpentane immediately before crystallization (supercooled liquid) on the left hand side of the diagram, and after rapid crystallization (finely-divided crystalline phase) on the right side; b_1 - 2-methylheptene-2 in the liquid phase at 20°C, b_2 - the same after cooling to -172°C (path-length 0.03 mm).

group I probably become glassy at low temperatures.

The situation is different for the branched-chain hydrocarbons of group II as it was for the n-alkanes. When the crystallization temperature is reached a sharp change in their spectra is observed. At the solidification temperature an abrupt increase occurs in the general background absorption, and the absolute intensity of the band maxima decreases somewhat. This is probably caused by the formation of a finely divided polycrystalline phase which scatters a considerable part of the incident infrared radiation. With very rapid cooling and rapid crystallization this scattering is very great, probably as the result of the formation of extremely small crystals [cf. Fig. 3(a)].

With slow cooling the absolute intensity of the background is lower and the intensity of the absorption bands is greater, so that well-defined absorption profiles are obtained; in a number of cases this is accompanied by a clearly evident simplification of the spectrum.

Considerable change in the spectrum at low temperatures was observed for 2, 4-dimethyl pentane and 2, 5-dimethylhexane.

The spectrum of 2, 4-dimethylpentane [Fig. 2(a)] at low temperatures shows a decrease in the intensities of the 1164, 983, and 805 cm^{-1} bands relative to the other bands.

In the spectrum of 2, 5-dimethylhexane [Fig. 2(b)] there is a large decrease in the intensities of the bands at 917 and 1165 cm^{-1}; the bands at 859 and 833 cm^{-1} disappear, along with one of those at 750 and 757 cm^{-1} and one of those at 1034 and 1048 cm^{-1}; the band at 1252 cm^{-1} decreases and the band at 809 increases considerably in intensity.

The spectrum of 2, 2, 5, 5-tetramethylhexane [Fig. 2(c)] shows clear evidence of crystallization at low temperatures; however, no simplification of the spectrum in the solid phase as compared with the liquid and no change of the relative intensities were observed.

The essential difference between the substances of groups I and II consists in the different symmetry of the geometrical configuration of the possible rotational isomers. The possible rotational isomers of all the compounds of group I do not possess any elements of symmetry, except perhaps 3, 3-dimethylheptene-1, for which the existence of an isomer with a single plane of symmetry can be presumed. This means that among the several possible rotational isomers which can be present for these substances there is none which possesses outstanding advantages over the others with respect to the formation of a regular molecular crystalline lattice. The rotational isomers of the hydrocarbons of group I are unsymmetrical and the formation of a crystalline lattice is difficult. These substances therefore have no tendency to form a definite crystal structure; and they

Table 4

Infrared Spectra of Hydrocarbons at Room Temperature and at Low Temperatures

2,4-Dimethyl-pentane		2,5-Dimethyl-hexane		2,2,5,5-Tetramethyl-hexane	
Liquid 20°C	Crystal -150°C	Liquid 20°C	Crystal -160°C	Liquid 20°C	Crystal -36°C
1469 vs	+	1470 vs	+	1469 vs	+
1448 vs	+	1451 vs	+		
		1431 s	+		
				1420 m	+
1383 vs	+	1384 vs	+	1385 s	+
		1371 s	+		
1363 vs	+			1363 vs	+
1342 s	+				
		1325 s	+		
1318 m	-				
		1292 w	+	1287 m	+
1277 w	+				
		1265 w	+		
1247 w	+	1252 w	decreases		
				1237 vs	+
1225 vw	+	1227 w	-		
		1212 m	+		
1202 w	+				
		1190 w	-		
				1172 m	+
1164 vs	decreases	1165 vs	decreases strongly	1146 w	+
1123 w	+			1128 m	+
		1101 w	+		
		1086 m	+	1080 w	+
1072 w	+				
		1062 w	-		
				1052 w	+
1049 w	+	1048 w	-		
		1034 m	+		
1029 w	-			1028 w	+
1010 w	+	1011 w	+	1006 m	+
		992 w	+		
983 s	decreases strongly			978 w	+
		974 w	+	971 w	+
		963 w	-		
956 w	+	954 m	+		
				948 w	+
938 w	-	931 w	-		
				926 m	+
917 s	+	917 vs	decreases strongly		
				907 s	+
892 w	-			890 m	+
		884 m	+		
		871 w	+	873 w	+
865 m	+				
851 w	-	859 w	-		
840 w	-			840 w	+
		833 w	-		
828 w	+				
805 s	decreases strongly	809 m	increases	805 vw	+
		791 w	+	793 w	+
785 w	+				
		775 w	+	773 w	+
767 w	+				
		757 s	-	757 w	+
		750 s	+		
				743 w	+
		729 w	+	730 vw	+
		706 w	+		
		696 w	+	686 w	+

Note: The intensity designations are the same as in table 3.

become glassy at low temperatures.

Some of the possible rotational isomers of the hydrocarbons of group II possess fairly high symmetry. It is possible to visualize rotational isomers of 2, 5-dimethylhexane and dineopentyl (2, 2, 5, 5-tetramethylhexane) which have, besides a plane of symmetry, also a center of symmetry; 2,4-dimethylpentane has a possible isomer with a plane of symmetry. In addition, the isomers of all three compounds have axes of symmetry (Fig. 4).

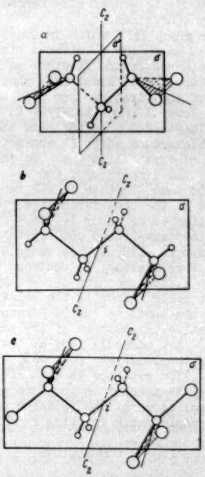

Figure 4. Isomers of high symmetry: (a) 2,4-dimethylpentane; (b) 2,5-dimethylhexane; (c) 2, 2, 5, 5-tetramethylhexane.

The rotational isomer with the highest symmetry should have an advantage over all the others with respect to the possibility of forming a crystal lattice; there exists therefore a highly organized crystalline structure formed from molecules of this particular highly-symmetrical isomer. From these considerations one can assume that 2, 4-dimethylpentane and 2, 5-dimethylhexane exist in the crystalline phase as a single highly organized symmetrical rotational isomer.

All other possible rotational isomers of the substances in question have lower symmetry and hence 'freeze out' during the formation of the crystalline lattice. Consequently, absorption bands which disappear or decrease in relative intensity on crystallization must belong completely or in part (in the case of superposition of bands) to the rotational isomers which are least organized

in the crystal lattice.

In the case of 2, 2, 5, 5-tetramethylhexane (dineopentyl) it is possible to imagine two rotational isomers of symmetry C_{2h} (trans-isomer) and C_{2v} (gauche-isomer) if one considers the tert-butyl radicals as units. However, the spectrum shows practically no change on crystallization. There is thus reason to believe that dineopentyl exists in the gaseous and crystalline phases in the form of the trans-isomer alone. Because of steric hindrance resulting from the presence of the two tert-butyl groups, the existence of the gauche-isomer would be practically impossible under ordinary conditions.

For group III, which includes only 2-methylheptene-2 among the substances studied, the picture of the changes in the spectrum on lowering the temperature is different from that for the substance of the first two groups. When the temperature is lowered (down to -172° C) the spectrum of 2-methylheptene-2 does not show the sharp increase in the background which is characteristic of the process of crystallization. On the other hand, upon lowering the temperature, the spectral changes reduce to some decrease in the band width and an increase in the peak intensities in the same way as the substances of group I. Thus one can assume that 2-methylheptene-2 does not crystallize at temperatures down to -172° C, the range used in our experiments. Nevertheless, in contrast to the substances of group I, the spectrum of 2-methylheptene-2 showed a considerable change in the relative intensity of some of the bands at low temperatures [Fig. 3(b)]. The relative intensities of the bands at 938 and 974 cm^{-1} are markedly less at low temperatures and those of the bands at 904, 928, 986, 1083 cm^{-1} are greater. The evidence is that liquid 2-methylheptene-2 is present in the form of at least two rotational isomers, the relative amounts of which change considerably in going from 20° to -172° C.

CONCLUSIONS

1. Infrared absorption spectra were obtained in the region ~700-1800 cm^{-1} at room temperature and at low temperatures (down to -172° C) for n-heptane, n-octane, 3-methylheptane, 2,3-dimethylheptane, 2-methylheptene-2, 3,3-dimethylheptene-1, 2,2,5,5-tetramethylhexane, 2,4-dimethylpentane, 2,5-dimethylhexane; the spectra of five of these were observed for the first time.

2. It was found that for 2,4-dimethylpentane and 2,5-dimethylhexane changes take place in the spectrum of the crystalline phase, which indicate that in this phase there is a smaller number of rotational isomers present than in the liquid phase; probably only the single isomer with the highest symmetry is present.

3. The different behaviour of the hydrocarbons on solidification is discussed from the point of view of the possible rotational isomers. The suggestion is made that crystallization is possible for those substances for which, among the possible rotational isomers, there is one with an adequately high degree of symmetry; this isomer possesses an advantage over the others in the sense that it is able to form a regular molecular crystalline lattice.

November 26, 1958

References

1. A. V. IOGANSEN: Fiziko-khimicheskie svoistva individual'nikh uglevodorodov (Physical-chemical Properties of Individual Hydrocarbons) Vol. 6, Gostoptekhizdat, 1957
2. D. W. E. AXFORD, D. H. RANK: J. Chem. Phys., 18, 51 (1950)
3. J. K. BROWN, N. SHEPPARD, D. M. SIMPSON: Disc. Faraday. Soc. No. 9, 261 (1950)
4. J. K. BROWN, N. SHEPPARD, D. M. SIMPSON: Phil. Trans. Roy. Soc. Lond. A247, 35, (1954)
5. R. A. OETJEN, H. M. RANDALL, W. E. ANDERSON: Rev. Mod. Phys., 16, 260, (1944)
6. N. SHEPPARD, D. M. SIMPSON: Quart. Reviews, Lond. Chem. Soc., 7, 19, (1953)
7. M. D. TILICHEEV: Fiziko-khimicheskie svoistva individual'nikh uglevodorodov (Physical chemical Properties of Individual Hydrocarbons) Vol. 5, Gostoptekhizdat, 1954.
8. R. D. OBOLENTSEV: Fizicheskie konstanty komponentov legkikh motornykh topliv (Physical Constants of the Components of Light Motor Fuels). Gostoptekhizdat (1943).
9. American Petroleum Institute Research Project No. 44. Catalogue of Infrared Absorption Spectral Data. Carnegie Institute of Technology, Pittsburgh
10. J. K. BROWN, N. SHEPPARD: J. Chem. Phys., 19, 976 (1951)

TOM VII, Vyp. 3 OPTIKA I SPEKTROSKOPIIA Sentiabr', 1959
VOL. VII, No. 3 OPTICS AND SPECTROSCOPY September, 1959

Optical Characteristics of Water and Ice in the Infrared and Radiowave Regions of the Spectrum

L. D. KISLOVSKII

Abstract: Values of the optical constants of water and ice have been calculated on the basis of a method proposed by the author for a broad range of the infrared and radiofrequency spectrum. Certain earlier well-known data and our own experimental data were employed for the calculations. The values of the optical constants which have been found are in satisfactory agreement with the experimental data available in the literature.

CHARACTERISTICS OF WATER IN THE INFRARED PART OF THE SPECTRUM

Water is a classical example of a substance in which the relation between the refractive index in the visible region and the dielectric permeability ($n^2 = \varepsilon_r$) is not fulfilled. As is well known, this discrepancy is connected with the existence, in the region between the visible spectrum and the radio frequency band, of a number of strong absorption bands connected with the permanent dipole moment of the water molecule. The most prominent of these bands are located around 3, 6, 16, and 60 μ, but the most powerful - the Debye absorption band - is at approximately 1 cm. In the last decade a series of original papers and reviews, among which we may mention [1-14]* have been devoted to investigation of the individual absorption bands and discussion of their nature. Even the values of the optical constants of water have not been reliably determined up to the present time — the data available in the literature are not complete and in a number of cases are contradictory. The present work contains a calculation of the optical constants of water, carried out on the basis of a conceptual model [15]. The calculations employ well-known data from the literature for separate characteristic points in the spectrum and results of special measurements we carried out. A summary of the experimental values of the optical characteristics of water in the infrared region of the spectrum which were used for the calculation is given in Table 1.

Table 1

Characteristic	λ(in μ)	Value of Characteristic	Source
Maximum reflection at fluorite-water interface	2.83	$R' = 0.017$	Our measurements
Maximum absorption	2.92	—	[16]
Limiting value of n	—	$n_0 = 1.327$	[17]
Maximum reflection at fluorite-water interface	6.0	$R' = 0.0042$	Our measurements
Minimum reflection at fluorite-water interface	6.55	$R' = 0.0012$	"
Minimum reflection at air-water interface	11.0	—	[1]
Maximum absorption	15.8	$k \approx 0.5$	[9]
Maximum reflection at air-water interface	20	—	[1]
Maximum absorption	60	$R^0 = 0.11$	[1]
Value of short-wave dielectric permeability	300	$\varepsilon = 4.2$	[13]

Note: R' is the reflection coefficient at a fluorite-water interface; R^0 the reflection coefficient at an air-water interface; n_0 the refractive index; ε the dielectric permeability; k the absorption coefficient.

Data in the table make it possible to determine the values of the optical constants of water from 2.2 to 100 μ and to find the dispersion formula in the near infrared.** Beyond 100 μ the influence of the microwave band makes itself felt — the calculation for this region of the spectrum is presented below.

Values of the absorption coefficient of liquid distilled water between 0.250 and 1.4 μ are presented in the book by Kleshnin [18]; values in the range 0.7 - 2.5 μ, in the work of Curcio and Petty [19]. By comparing the data of [18] with the data of [19, 20], we may conclude that in the curve of Curcio and Petty the absorption coefficient is plotted on a decimal basis.

The basic valence band of water, corresponding to vibration of the O = H bond, lies at 2.92 μ. Because of the marked polarization of the bond under consideration the absorption in this band is strong, and measurement of its intensity is difficult. The numerous attempts at quantitative measurement in the region of peak absorption [9,10,21,22] do not give a reliable estimate of the absorption coefficient; they agree poorly among themselves and with data concerning anomalous dispersion in this region [23].

Strong absorption bands, as is well known, show up well in the reflection spectrum; this makes it possible to find the optical constants [15, 24, 25]. The reflection spectrum of water has been investigated repeatedly; a good reflection band has been obtained in the 3.0 - 3.2 μ region [2, 26, 27, 28]. Results of measurements of the first three authors are given in the table by Gehrts [27], whose data appear to us to be most reliable in addition to the data of Brieger [28]. The data of each of these authors is sufficient for determination of the optical constants by (our) method [15] in the region of the band under consideration, but the significant differences among them*** compelled us to carry out supplementary measurements.

The reflection spectrum at a fluorite-water boundary in the range 2.1 - 3.4 μ was obtained on an IKS-11 instrument with a lithium fluoride prism, employing a special cell with a wedge-shaped fluorite window which made it possible to distinguish between the reflection from the air-fluorite boundary

* Monograph [1] contains a detailed critical review of all published data up to 1938.

**In the region $\lambda < 2.2$ μ there are a series of weak overtone absorption bands, not appearing in the reflection spectra and not significantly influencing the dispersion. These bands have been thoroughly studied by transmission.

***Thus, the minimum value of the reflection coefficient near 2.7 μ is 0.76% according to [27], and 1.41% according to [28].

and that from the fluorite-water boundary. The ratio of the reflection coefficients of these boundaries was measured at each wavelength. In Figure 1, A represents the spectrum of the absolute values of the reflection coefficient R', obtained by a calculation employing well-known values of the refractive index of fluorite.

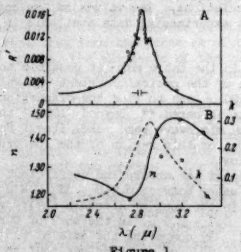

Figure 1

The figure shows a double maximum, which is well known in absorption [10, 14], but has not been observed up to the present time in reflection. In view of the hypotheses of certain authors concerning the complex structure of this band, we carried out supplementary measurements employing a high resolution diffraction apparatus constructed in our laboratory [29]. This work indicated the absence of any additional structure in accordance with the ideas of Bulanin [14].

The data of the first three lines of table 1 were used to construct the "resonance circle" shown in Figure 2, This is used to determine the values of the optical constants in the range 2.2 - 3.4 μ (Figure 1-B)*. Figure 2 also shows maximum and minimum reflection values in the region of the given band at an air-water boundary (they are designated R^0 and are in satisfactory agreement with the data of other authors [1, 27].

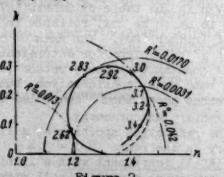

Figure 2

The minimum value of the index of refraction (λ = 2.74 μ) agrees with the maximum transmission of water vapor recorded by Malyshev [30]. The maximum absorption is characterized by the value k ≃ 0.3. In agreement with well-known experimental data, the half-width of the absorption band is equal to 410 cm-1. Using data of table 1, it is possible to extrapolate Schultz's [17] dispersion formula for the ultraviolet and visible to the near infrared, adding a term [15] due to the absorption band at 2.92 μ. For 20° C the formula then takes the form:

$$(1)\quad n^2 = 1.29 + \frac{0.47\cdot\lambda^2}{\lambda^2 - (0.119)^2} - \frac{0.08\cdot\lambda^2}{(2.92)^2 - \lambda^2} (\lambda \text{ in } \mu)\ldots$$

Formula (1) agrees fairly well with experimental data between 0.1829 and 2.0 μ. A comparison of the calculated values for the near infrared with well-known experimental data [1] is presented in table 2.

Table 2

λ(in μ)	n	
	Experiment[1]	Calculation
0.768	1.3289	1.3287
1.028	1.3245	1.3245
1.256	1.3210	1.3210
1.500	1.316	1.3157
2.0	1.300	1.2996

The strong absorption bands lying on the long wavelength side of the 2.92 μ band overlap so much that it is possible to consider them only as a group. The weak band at 4.74 μ cannot lead to a significant change in the trend of the optical constants. The absorption in this band, according to [9], is a factor of 10 weaker than in the band at 6 μ. (See curve k, Fig. 6B).

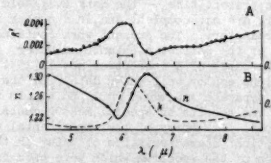

Figure 3

In figure 3, A represents our measurements of the reflection spectrum at a fluorite-water interface in the 4.5 - 8.5 μ range, referred to the absolute value of the reflection coefficient. Figure 4 presents the corresponding "resonance circle"**, and figure 3B the optical constants found with the aid of figure 4. The data obtained agree well with the data of Malyshev [30] on the transmission maximum of water vapor at 5.9 μ and with well-known works on transmission in this region [9, 22], but give considerably lower values for the refractive index than those used in the literature [1, 13]. These values therefore require additional careful verification.

Figure 5 presents the resulting "resonance curve" for all the bands of water in the infrared region of the spectrum. Figure 6 gives the reflection spectrum of an air-water boundary (A)

*For simplicity we assume the band to be isolated, and the angle of incidence normal. We introduce thereby an error which is less than the uncertainty in the original data.

** In constructing the "resonance circle" (Fig. 4) it is necessary to take into account the disturbing influence of the complex band near 15.8 μ. The calculation was carried out, as in [15], by combining the corresponding vectors.

constructed from figure 5 and the spectral variation of the optical constants (B). Well-known values from the literature [1] are represented by points on the curves.

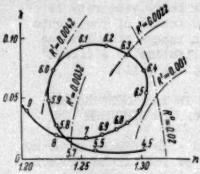

Figure 4

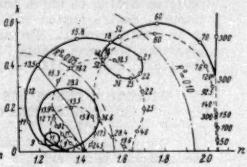

Figure 5

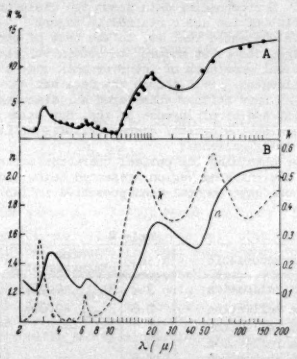

Figure 6

Table 3 contains a summary of the characteristics of the different bands we obtained; λ_k is the wavelength of the absorption maximum, n_o is the value of the index of refraction, which is affected by all bands of shorter wavelength than the given one, F(Q) is the quality factor of the given oscillation, regarded as a classical oscillator with friction [15]. The 15.8 μ band had to be represented as the superposition of two bands, in view of the impossibility of obtaining agreement with the well-known experimental data of Table 1 in any other way. It is possible to try to treat this splitting as a short-range phenomenon in liquid water [31], taking into consideration that the short wavelength component is close to the absorption band of ice [32].

CHARACTERISTICS OF WATER IN THE RADIO BAND

The absorption of radio waves by liquid water has been thoroughly studied [33-35]; it results from a broad Debye relaxation band. Recent investigations [35] have shown that it is sufficient to consider one relaxation time; that is the classical Debye formula is fully applicable:

$$(2)\quad \varepsilon'_\omega = \varepsilon_o + \frac{\varepsilon_c - \varepsilon_o}{1+\left(\frac{\omega}{\omega_s}\right)^2}; \quad \varepsilon''_\omega = \frac{\varepsilon_c - \varepsilon_o}{1+\left(\frac{\omega}{\omega_s}\right)^2}\cdot\frac{\omega}{\omega_s} + \frac{\sigma_o}{\omega},$$

Table 3

λ_k	n_o	n_∞	F(Q)	Nature of band
2.92	1.327	1.355	7.5	Stretching vibration
6.15	1.355	1.360	8.0	Bending vibration
13.5	1.360	1.415	3.2	
18	1.415	1.655	1.6	Intermolecular vibration
60	1.655	2.05	1.1	Vibration of quasi-crystalline structure
10650*	2.05	9.0	–	Molecule-dipole relaxation

* λ_s = 1.74 mm corresponds with this value [12] (see formula (4) below).

where $\varepsilon_\omega = \varepsilon'_\omega - i\,\varepsilon''_\omega$ is the complex dielectric permeability; ω_s is the frequency corresponding to the maximum of ε''_ω; ε_c is the dielectric permeability at zero frequency; σ_o is the electrical conductivity for direct current [36]. The term σ_o/ω, which takes account of the effect of electrical conductivity resulting from free charge carriers, does not begin to become important for fairly pure water until some distance from the Debye band.

Combining the Debye formula with the Maxwell relations between the complex values of the dielectric permeability and the index of refraction, it is easy to obtain formulas [12] expressing n and k through transformed Debye formulae:

$$(3)\quad \begin{cases} n = \sqrt{\frac{\varepsilon_o}{2}}\cdot\sqrt{\left(\frac{a^2+\omega_{rel.}^2}{1+\omega_{rel.}^2}\right)^{\frac{1}{2}} + \frac{a+\omega_{rel.}^2}{1+\omega_{rel.}^2}} \\ k = \sqrt{\frac{\varepsilon_o}{2}}\cdot\sqrt{\left(\frac{a^2+\omega_{rel.}^2}{1+\omega_{rel.}^2}\right)^{\frac{1}{2}} - \frac{a+\omega_{rel.}^2}{1+\omega_{rel.}^2}}, \end{cases}$$

where $\omega_{rel} = \frac{\omega}{\omega_s}$ and $a = \frac{\varepsilon_c}{\varepsilon_o}$. Using (3), it is possible to obtain an expression for the maximum value of k in the given band and for the corresponding wavelength:

$$(4)\quad \begin{cases} k_m = \sqrt{\frac{\varepsilon_c}{8}}\cdot\frac{1-\frac{\varepsilon_o}{\varepsilon_c}}{\sqrt{1+\frac{\varepsilon_o}{\varepsilon_c}}} \\ \lambda_k = \lambda_s\cdot\sqrt{\frac{(1+a)^2-4}{4a^2-(1+a)^2}} \end{cases}$$

and also to plot the spectral variation of the optical constants in the radio region (Fig. 7).

For $a \to \infty$, we have $k_m \to \sqrt{\frac{\epsilon_c}{6}}$ and $\lambda_k \to \lambda_s \frac{1}{\sqrt{3}}$. On the other hand, for $\lambda \ll \lambda_s \frac{\epsilon_0}{\epsilon_c}$

$$\begin{cases} n = n_0 + \dfrac{\epsilon_c^2}{8n_0^3}\left(\dfrac{\lambda}{\lambda_s}\right)^2, \\ k = \dfrac{\epsilon_c}{2n_0} \cdot \dfrac{\lambda}{\lambda_s} \end{cases} \tag{5}$$

and for $\lambda \gg \lambda_s$

$$n = n_\infty - \frac{3}{8} n_\infty \left(\frac{\lambda_s}{\lambda}\right)^2; \quad k = \frac{n_\infty}{2} \cdot \frac{\lambda_s}{\lambda}.$$

The last expressions are correct for water if $\lambda < 30$ cm. In this region a number of authors [1, 37-39] observed weak absorption bands and the resultant variation of the refractive index, although without complete confidence that these bands were not the result of impurities. Using formula (3) and values of ϵ_0, ϵ_c and λ_s which are well-known from the literature [12, 35] for a series of temperatures, it is possible to calculate the temperature dependence of the optical constants defined by the Debye band. Figure 8 depicts the spectral variation of k for four temperatures. The well-known data on the temperature variation of the reflection coefficient at 310 μ [1] agree quantitatively with the result of such a calculation.

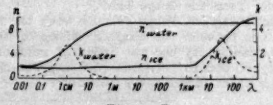

Figure 7

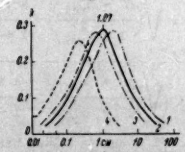

Figure 8

1 - 0°C; 2 - 20°C; 3 - 40°C; 4 - 100°C.

In reference [12] the spectral curve of k in the far infrared joins up poorly with the microwave curve. This might be explained by assuming that in the experiments of Cartwright, [4, 6], who investigated absorption in the far infrared, the absorbing layer of water was heated to 40° C by the radiation (Fig. 8). From formula (5) it follows that on the short wavelength side of the Debye band, for $\lambda \ll \lambda_s \cdot \frac{\epsilon_0}{\epsilon_d}$, the absorption produced for a given layer thickness does not depend on wavelength but depends sharply on the temperature. According to this formula, a layer of water 1 mm thick should transmit no more than 0.2% of the visible radiation incident upon it, which contradicts everyday experience. This apparent contradiction is of course completely resolved if one proceeds from the theory of the liquid state as developed by Frenkel' [40], according to which the Debye viscosity is an integral manifestation of "defects" of the liquid as an ideal crystal. For an interaction lasting less than the mean stable "lifetime of a defect" the liquid behaves like an ideal solid.

CHARACTERISTICS OF ICE IN THE INFRARED AND RADIOWAVE REGIONS OF THE SPECTRUM

The proposed method can also be used to obtain the optical characteristics of ice, although much less data has been published for it than for water. A discussion of the nature of the different bands, a review of experimental data on transmission and a copious bibliography may be found in references [32, 41-43]. Corresponding data about the dielectric properties of ice are contained in papers [44-46]. Below is presented what is, to the best of our knowledge, the first attempt to obtain values of the optical constants of ice over this wide a range of wavelengths. Even though the data are quite adequate, we have neither considered nor discussed dichroism and birefringence of ice, nor attempted to determine the optical characteristics of its different modifications.

For obtaining the optical characteristics of ice in the infrared region presented below, only the well-known experimental data presented in Table 4 were used.

Table 4

Characteristic	λ(in μ)	Value of characteristic	Ref.
Maximum reflection	3.2	$R_{0\ max}$=0.051	[47]
Minimum reflection	2.8	R_{min}=0.006	[47]
Maximum reflection	13	—	[48]
Minimum reflection	10	—	[48]
Maximum absorption	12.5	—	[32]
Maximum absorption	62	k ≃0.3	[5]
Value of short-wave dielectric permeability	—	ε =3.17	[49]

Remark: Data in the table pertain to a temperature of -10°C.

The calculation is conducted according to the following approximate formulas easily obtained from the ideas developed earlier [15]:

$$\rho_0^2 = \rho_{0\,ice} \cdot \rho_{\infty\,ice}; F(Q) = \frac{\dfrac{\rho_0}{\rho_{0\,ice}} \cdot \left(\dfrac{\lambda_{0\,ice}}{\lambda_{min}}\right)^2 + \dfrac{\rho_{\infty\,ice}}{\rho_0}}{\left(\dfrac{\lambda_{0\,ice}}{\lambda_{min}}\right)^2 - 1}; \tag{6}$$

$$\lambda_k = \lambda_{0\,ice} \cdot \sqrt{\frac{F(Q) - \dfrac{\rho_0}{\rho_{0\,ice}}}{F(Q) - \dfrac{\rho_{0\,ice}\,\rho_{min}}{1 - \rho_0}}}; \quad k_m = \frac{2(\rho_{0\,ice} - \rho_{min})}{(1 - \rho_0)^2};$$

(6)-cont'd

(6)cont'd

$$n_e = n_o \pm \frac{k_m}{2};\ k_e = \frac{k_m}{2};\ \lambda_{n\,min} = \lambda_{o\,ice} \cdot \sqrt{\frac{F(Q) - \frac{\rho_o}{\rho_{o\,ice}}}{F(Q)+1+\frac{\rho_{o\,ice}-\rho_{min}}{1-\rho_o}}};$$

$$\rho_\infty = \rho_o + \frac{\rho_{o\,ice} - \rho_{min}}{\sqrt{F^2(Q)+1}},$$

From the result of the calculation we constructed spectral plots of the optical characteristics of ice (Fig. 9). The most important calculated values are given in Table 5.

Table 5

Band	Characteristic
Near 3μ	n_o=1.302; F(Q)=8.8; λ_k=3.1; k_m=0.39; n_o=1.342
Near 12μ	n_o=1.33<1.342, since dispersion caused by the band near 62μ is of influence, R_{min}=0.006; $R_{o\,ice}$=0.07; F(Q)=4; k_m=0.5; n_∞=1.46; $n = 1.33 - \frac{0.13\lambda^2}{(12.5)^2-\lambda^2}$
Near 62μ	n_o=1.46; n_∞=1.76; k_m=0.46 $n = 1.46 - \frac{0.3\lambda^2}{(62)^2-\lambda^2}$

The value n_o = 1.302, found for the reflection band of ice near 3.2 μ, agrees well with the value n_o = 1.3015, obtained for that same temperature by Eringhaus' [1] measurement of the dispersion of ice in the visible. Using his data in conjunction with our own, (Table 5) it is possible to obtain [15] a formula for the dispersion of polycrystalline ice in the visible and near infrared regions (t^0 = -10°C):

$$(7) \qquad n = 1 + \frac{0.3015 \cdot \lambda^2}{\lambda^2 - (0.096)^2} - \frac{0.04 \cdot \lambda^2}{(3.1)^2 - \lambda^2}.$$

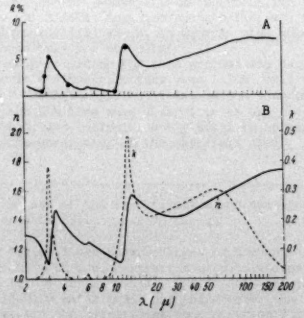

Figure 9

Recent data [32, 41, 42] allow one, using formulas (6), to determine the characteristics of ice at low temperatures — down to the temperature of liquid nitrogen. Upon cooling, the band near 3 μ increases significantly in intensity. (The reflection attains a maximum of 12%). The weak reflection band near 6 μ becomes even weaker. The band near 12.5 μ shifts toward the short wavelength side.

The dielectric characteristics of ice were determined some time ago [50], but for some unknown reason did not become widely known. Thus, various articles and even reference books [51] quote the limiting value ϵ_c = 3.1 instead of 100. Some authors explain this by saying that the Debye band of ice owes its origin to "defects" [52]. On the other hand, as was shown above, the Debye band of water is also connected with them — "defects" are equally intrinsic to the nature of real crystals and liquids. The optical constants in the Debye absorption band of ice were determined by us according to formula (3) of the present article, using experimental values of ϵ_o, ϵ_∞, and ω_s given [44,50]. The results of the calculation for a temperature of -10° C are shown in figure 7. From the figure it is evident that, in contrast with water, ice has a broad transparent "window" in the wavelength region from half a millimeter to several meters. The long-wavelength boundary shifts rapidly with change of temperature. In the even lower frequency range λ>1 km. [cf. formula (2)] the optical characteristics of water and ice, as is well known, are extremely sensitive to impurities since in this region electrical conductivity and small dielectric losses start to become important. To process the materials in this case it is convenient to use a graphical method recently developed for semiconductors [53].

Thus, the data obtained here, while laying claim to high precision, make it possible to show the applicability of the method [15] to the analysis of the complex strong absorption spectra, by using the spectra of water and ice as an example. For greater accuracy, new experimental data are necessary, especially in the 10 to 2500 μ region.

In conclusion, I take this opportunity to express profound thanks to B. S. Neporent for his interest and encouragement, and to all those colleagues who took part in discussion of the present work.

December 25, 1958

References

1. N. E. DORSEY: Properties of Ordinary Water-substance, New York, 1940
2. H. RUBENS, E. LADENBURG: Verh. D. Phys. Ges., 11, 16, (1909)
3. H. RUBENS: Verh. D. Phys. Ges., 17, 315, (1915)
4. C. H. CARTWRIGHT: Nature, 135, 872, (1935)
5. C. H. CARTWRIGHT: Nature, 136, 181,(1935)
6. C. H. CARTWRIGHT, J. ERRERA: Proc. Roy. Soc., A154, 138, (1936)
7. J. BERNAL: IG. TAMM, Nature, 135, 229, (1935)
8. E. K. PLYLER, C. J. GRAVEN: J. Chem. Phys., 2, 303, (1934)
9. E. K. PLYLER, N. ACQUISTA: JOSA, 44, 505, (1954)
10. E. GREINARCHER, W. LUTTKE, K. MECKE: Zs. Electrochim. 59, 23, (1955)
11. M. SOHM: Zs. f. Phys., 116, 34, (1940)

12. M. MAGAT: J. Chim. Phys., 45, 91, (1948)
13. K. S. SHIFRIN: Scattering of Light in Cloudy Atmosphere, M.-L., 1951
14. M. O. BULANIN: Dissertation, Leningrad Univ. 1958
15. L. D. KISLOVSKII: OiS, 1, 672, (1956); 2, 186, (1957)
16. V. M. CHULANOVSKII: DAN USSR, 93, 25, (1953)
17. D. SCHULZ, Z. WISS: Pädagog. Hochschule Potsdam. Math.-naturwiss. Reihe No. 1-2, 45, 1955-56
18. A. F. KLESHNIN: Plants and Light, M., 1954
19. A. CURCIO, C.C.PETTY: JOSA, 41, 302, (1951)
20. V. BRÜGEL: Physik und Technik UR Strahlung, 1951
21. U. LIDDEL: J. Chem. Phys., 45, 82, (1948)
22. R. M. ADAMS, J. J. KATZ: JOSA, 46, 895, (1956)
23. V. M. CENTANO: JOSA, 31, 244, (1941)
24. T. H. HAVELOCK: Proc. Roy. Soc., A105, 488, (1924)
25. T. S. ROBINSON: Proc. Phys. Soc., B65, 910, (1952)
26. A. K. ANSTRÖM: Phys. Rev., 3, 47, (1914)
27. F. GEHRTS: Ann. d. Phys., 47, 1095, (1915)
28. K. BRIEGER: Ann. d. Phys., 57, 287, (1918)
29. B. S. NEPORENT, et al.: OiS, 3, 289, (1957)
30. V. I. MALYSHEV: Phys. sb. L'vov Univ., 3(8), 121, 1957
31. G. H. HAGGIS, J. B. HASTED, T. J. BUCHANAN: J. Chem. Phys., 20, 1452, (1952)
32. P. A. GIGUERE, K. B. HARVEY: Can. J. Chem., 34, 798, (1956)
33. J. A. SAXTON: Proc. Roy. Soc., A213, 473, (1952)
34. J. A. LANE, J. A. SAXTON: Proc. Roy. Soc., A213, 400, (1952)
35. E. H. GRANT, T. J. BUCHANAN, H. F. COOK: J. Chem. Phys., 26, 156, (1957)
36. L. D. KISLOVSKII: OiS, 5, 66, (1958)
37. A. R. KILLI: Invest.Disper. in Elect. Spectrum of Liquids, Odessa, 1908
38. H. RUKOP: Ann. d. Phys., 42, 489, 532, (1913)
39. M. ALIMOWA: Ann d. Phys., 9, 176, (1931)
40. IA. I. FRENKEL': Theory of the Liquid State, Acad. Sciences Press, USSR, 1945
41. N. OAKMAN: Advances in Phys., 7,(26), 199, (1958)
42. D. F. HORNIG, H. F. WHITE, F. P. REDING: Spectrochim. Acta, 12, 338 (1958)
43. N. OCKMAN, G. B. B. M. SUTHERLAND: Proc. Roy. A247, 434, (1958)
44. A. STEINEMAN, H. GRANICHER: Helv. Phys. Acta, 30, 553, (1957)
45. H. GRANICHER: Proc. Roy. Soc., A247, 453, (1958)
46. A. STEINEMAN: Helv. Phys. Acta, 30., 581, (1957)
47. G. BODE: Ann. d. Phys., 30, 326, (1909)
48. M. L. VEINGEROV: Zs. f. Phys., 70, 104, (1931)
49. J. LAMB, A. TURNEY: Proc. Phys. Soc., B62, 272, (1949)
50. C. P. SMYTH, C. S. HITCHCOCK: J. Amer. Chem. Soc., 54, 4631, (1932)
51. Short Handbook of Chemistry, 3rd ed., Goskhimizdat, 1954
52. M. FREYMANN, R. FREIMAN: J. Phys. Rad., 15, 165, (1954)
53. F. A. GRANT: J. Appl. Phys., 29, 76, (1958)

TOM VII, Vyp. 3 OPTIKA I SPEKTROSKOPIIA Sentiabr', 1959
VOL. VII, No. 3 OPTICS AND SPECTROSCOPY September, 1959

The Influence of p-Toluidine on the Quantum Yields of Photooxidation and Photodimerization of Some Anthracene Derivatives

A. S. CHERKASOV AND T. M. VEMBER

Abstract: The influence of p-toluidine on the quantum yields of fluorescence and photochemical transformations of 9-methylanthracene (II) and 9-methyl-10-methoxymethylanthracene (I) has been investigated. A kinetic scheme has been proposed which describes the experimental results.

Investigation of the photochemical transformations of a series of anthracene derivatives (whose ultimate products were photo-oxides and photodimers) has shown [1, 2] that the experimental results may be described satisfactorily by the following kinetic scheme:

	Relative rate constants
$A + h\nu \rightarrow A^* \rightarrow {}^1A,$	
${}^1A \rightarrow {}^3A,$	t,
${}^1A \rightarrow A + h\nu_f,$	f,
${}^1A + A \rightarrow A_2,$	d,
${}^1A + A \rightarrow {}^3A + A,$	p,
${}^1A + O_2 \rightarrow {}^3A + O_2,$	q,
${}^3A + S \rightarrow A + S,$	k_1,
${}^3A + O_2 \rightarrow AOO,$	k_2,
$AOO \rightarrow A + O_2,$	k_3,
$AOO + A \rightarrow A + AO_2,$	k_4,

where A, A*, ${}^1A$, ${}^3A$ are molecules of the material, respectively in the unexcited, first excited, singlet excited and triplet excited states. S is the solvent molecule, O_2 is the oxygen molecule, A_2 is the photodimer, AOO is the intermediate photo-oxide and AO_2 the photo-oxide molecule.

We were interested in determining whether this scheme could also be used in those cases where photochemical conversions occur in the presence of known fluorescence suppressors. A positive answer to this question ought to be evidence of the fact that the scheme, on the whole, correctly reflects the transformations which actually proceed during the absorption of light energy by a material.

For this purpose we have investigated the influence of p-toluidine on the quantum yield of fluorescence and the quantum yield of photochemical transformations* of 9-methyl-10-methoxymethylanthracene (I), which forms only the photo-oxide, and 9-methylanthracene (II) which, in deoxygenated solutions, forms only the photodimer [2].

Use of p-toluidine for this purpose was shown to be possible since solutions were illuminated by light of wavelength ~365 mμ, which is not absorbed by them, and the long wave absorption of the products formed, was insignificantly small in comparison with the absorption of the materials used (Fig. 1).**

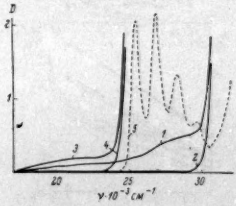

Figure 1. Absorption spectra of alcohol solutions.

Ordinate axis-optical density D of the solution for a 10 mm thick layer.

1.—p-Toluidine at a concentration of 10^{-1} mole/l after irradiation. 2.—The same solution before irradiation. 3.—A mixture of p-Toluidine (10^{-1} mole/l concentration) and 9-methyl-10-methoxy-anthracene (I) (concentration 6.10^{-3} mole/l) after irradiation. 4.—The same solution before irradiation. 5.—Solution 3 diluted 25 times.

The values of the experimentally determined quantum yields of fluorescence, photo-oxidation and photodimerization of materials I and II under conditions of differing concentrations of p-Toluidine are presented in figures 2 and 3.

As is evident from figures 2a, 2b, and 3, p-toluidine strongly suppresses the fluorescence of alcohol solutions of these materials, while for the concentration region investigated the reciprocal of the quantum yield of fluorescence is linearly dependent on the concentration of p-toluidine. The quantum yields for the formation of photoproducts in the presence of p-toluidine also diminish, with a particularly strong influence being apparent on photo-oxidation. Thus, the quantum yield of formation of the photodimer of material II (Fig. 3)(concentration of the starting material in the deoxygenated solution is 6.10^{-3} m/l) is equal to 0.12 in the absence of p-toluidine and 0.05 when it is present in a 3.10^{-2} m/l concentration. The quantum yield of the photo-oxidation reaction of material I in 6.10^{-3} m/l concentration in air-saturated ethanol drops from 0.16 in the absence of p-toluidine to 0.015 in a 3.10^{-2} m/l concentration.

From examination of the scheme presented above it follows that reduction of the quantum yield of photodimerization, in the presence of deactivation of the excited molecule by a foreign suppressor, ought to be proportional to the decrease of the fluorescence yield. As is evident from figure 3, the experimental data obtained are in good agreement with this conclusion. The experimental dependence of the quantum yield of photodimerization of II on the concentration of p-toluidine almost coincides with the curve calculated in accordance with

*The method of the investigation was analogous to that used in [3].

**In figure 1 are shown changes of absorption of solutions with a concentration of p-toluidine equal to 10^{-1} mole/l. Usually the duration of the photo-oxidation experiments was not greater than two hours, and the p-toluidine concentration did not exceed 4.10^{-2} mole/l.

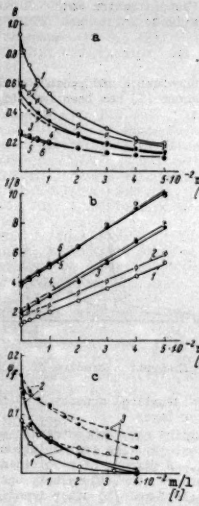

Figure 2. Dependence of quantum yields of fluorescence B and photo-oxidation φ_f of alcohol solutions of 9-methyl-10-methoxy-anthracene (I) on concentration of p-toluidine [T].

a and b: Suppression of fluorescence by p-toluidine with the following concentrations of I in moles/l. : 1 – 10^{-5} (O_2 free medium). 2 – 10^{-5}. 3 – 3.10^{-3}. 4 – 6.10^{-3}. (solutions saturated with air) 5 – 10^{-5} and 3.10^{-3} (solutions saturated with oxygen).

c. Experimental (solid lines) and calculated (according to the suppression of fluorescence; dashed lines) quantum yields of photo-oxidation of material I in the following concentrations in moles/l. : 1 – 3.10^{-3}. 2 – 6.10^{-3} (solutions saturated with air) 3 – 3.10^{-3} (solution saturated with oxygen).

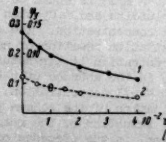

Figure 3. Dependence of quantum yields of fluorescence and dimerization of 9-methylanthracene (II) on the concentration of p-toluidine [T] for a deoxygenated alcohol solution.

1. Yield of fluorescence. 2. Yield of dimerization (experimental points and curve calculated according to the suppression of fluorescence by p-toluidine). Concentration of material II is equal to 6.10^{-3} mole/l.

suppression of the fluorescence.

However such a relationship is not found for photo-oxidation, and the experimental values of the quantum yields of photo-oxidation of material I turn out to be less than calculated under the assumption that they are proportional to the decrease of fluorescence (Fig. 2, c).

Thus, the influence of a suppressor on photo-oxidation is found to be more complicated than on photo-dimerization, and in order to explain the experimental results it is necessary to assume that other processes besides deactivation of the singlet molecules take place, leading to a reduction of the quantum yield of photo-oxide formation. These should be processes of interaction of the suppressor with other intermediate products of photo-oxidation, i.e., with ^3A or AOO. We must also consider that the result of the interaction of the suppressor with the singlet excited molecule need not lead only to its deactivation, but perhaps also to its transition to the triplet state [4], whereupon it can form the photo-oxide by interaction with oxygen.

Assuming the possibility of the following processes taking place with participation of the suppressor (T):

		Relative rate constants
(1)	$^1A + T \rightarrow A + T$,	m,
(2)	$^1A + T \rightarrow {}^3A + T$,	m,
(a)	$^3A + T \rightarrow A + T$,	m_1,
(b)	$AOO + T \rightarrow A + TOO$,	m_2,

we carried out a comparison with experiment of the quantum yields of photo-oxide (φ_{AO_2}) as a function of the concentration of p-toluidine (T).

Introducing processes (1) and (a), (1) and (b), (2) and (a) or (2) and (b) into the general scheme of photochemical transformations, we obtain the following expressions for φ_{AO_2}:

(1,a)
$$\varphi_{AO_2} = \frac{\frac{t}{f+t} + \frac{p}{f+t}[A] + \frac{q}{f+t}[O_2]}{1 + \frac{p}{f+t}[A] + \frac{q}{f+t}[O_2] + \frac{m}{f+t}[T]} \times \frac{\frac{k_2}{k_1}[O_2]}{1 + \frac{k_2}{k_1}[O_2] + \frac{m_1}{k_1}[T]} \cdot \frac{\frac{k_4}{k_3}[A]}{1 + \frac{k_4}{k_3}[A]},$$

(2,a)
$$\varphi_{AO_2} = \frac{\frac{t}{f+t} + \frac{p}{f+t}[A] + \frac{q}{f+t}[O_2] + \frac{m}{f+t}[T]}{1 + \frac{p}{f+t}[A] + \frac{q}{f+t}[O_2] + \frac{m}{f+t}[T]} \times \frac{\frac{k_2}{k_1}[O_2]}{1 + \frac{k_2}{k_1}[O_2] + \frac{m_1}{k_1}[T]} \cdot \frac{\frac{k_4}{k_3}[A]}{1 + \frac{k_4}{k_3}[A]},$$

(1,b)
$$\varphi_{AO_2} = \frac{\frac{t}{f+t} + \frac{p}{f+t}[A] + \frac{q}{f+t}[O_2]}{1 + \frac{p}{f+t}[A] + \frac{q}{f+t}[O_2] + \frac{m}{f+t}[T]} \times$$

$$\times \frac{\frac{k_2}{k_1}[O_2]}{1+\frac{k_2}{k_1}[O_2]} \cdot \frac{\frac{k_4}{k_3}[A]}{1+\frac{k_4}{k_3}[A]+\frac{m_2}{k_3}[T]},$$

$$\varphi_{AO_2} = \frac{\frac{t}{f+t}+\frac{p}{f+t}[A]+\frac{q}{f+t}[O_2]+\frac{m}{f+t}[T]}{1+\frac{p}{f+t}[A]+\frac{q}{f+t}[O_2]+\frac{m}{f+t}[T]} \times$$

$$(2,b) \quad \times \frac{\frac{k_2}{k_1}[O_2]}{1+\frac{k_2}{k_1}[O_2]} \cdot \frac{\frac{k_4}{k_3}[A]}{1+\frac{k_4}{k_3}[A]+\frac{m_2}{k_3}[T]} \cdot$$

The constants introduced into these expressions, except the constants $\frac{m}{f+t}$, $\frac{m_1}{k_1}$ and $\frac{m_2}{k_3}$ for I, have been defined earlier [2]. The constant for the suppression of fluorescence by p-toluidine $\frac{m}{f+t}$ was calculated from data on the suppression of fluorescence of deoxygenated solutions in the absence of concentration suppression, while constants $\frac{m_1}{k_1}$ and $\frac{m_2}{k_3}$ were found from corresponding expressions for φ_{AO_2} by using experimental values of photo-oxidation yields of I in 3×10^{-3} M solution saturated with air in the presence of p-toluidine.

The values of all the constants needed for the calculation of the quantum yields of the photo-oxidation reaction of material I in ethyl alcohol in the presence of p-toluidine are the following:

$\frac{t^*}{f+t}$	$\frac{p^*}{f+t}$	$\frac{q^*}{f+t}$	$\frac{m}{f+t}$	$\frac{k_2}{k_1}$	$\frac{k_4}{k_3}$	m_1/k_1		m_2/k_3	
						(1a)	(2a)	(1b)	(2b)
0.07	69	236	76	11830	86.6	3126	8956	230	672

* The sum of constants f+t for I in alcohol is $7.4 \cdot 10^{-7}$ [2].

We have calculated the dependence of the quantum yields of photo-oxidation on the concentration of p-toluidine for air-saturated alcohol solutions of material I of concentration 3.10^{-3} mole/l and 6.10^{-3} mole/l, and for an oxygen saturated solution of concentration 3.10^{-3} mole/l. The above equations were used. The experimental data obtained are also presented in figure 4, from which it is seen that the dependences calculated from equations (1a), (2a) and (2b) differ considerably from experiment, and only equation (1b) describes the experimental data well. We must note that the presence of process (b) can also explain the fact that the long wavelength absorption manifest after illumination of air-saturated alcohol solutions of p-toluidine (which is apparently an absorption by products of the oxidation of p-toluidine), is increased in the presence of I. Livingston also had to assume the occurrence of an analogous process to explain the results obtained in investigating the sensitization of anthracene photo-oxidation by 9, 10-diphenyl-anthracene [5].

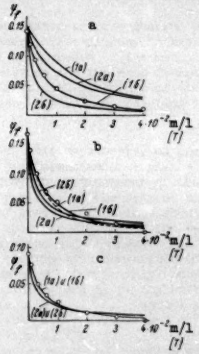

Figure 4. Dependence of the quantum yields of photo-oxidation φ_f of I on the concentration of p-toluidine [T], calculated according to equations 1a, 1b, 2a, and 2b, (see text).

a.—Concentration of I is 3.10^{-3} mole/l. (solution saturated with oxygen); b and c.—Concentration of I is 6.10^{-3} and 3.10^{-3} mole/l., respectively (solutions saturated with air). Experimental values are shown by points.

Thus, investigation of the influence of p-toluidine on the photo-dimerization of II and photo-oxidation of I has shown that p-toluidine strongly reduces the rates of these reactions (expecially the latter) and, for example, in concentrations of 3.10^{-2} or higher I is photochemically practically unchanged. Diminution of the quantum yield of photodimerization is explained without additional assumptions by the scheme proposed earlier [1, 2], for the photochemical transformations of anthracene derivatives. The quantum yields of photo-oxide observed experimentally are also well described by this scheme if it is assumed that interaction of the suppressor with a molecule excited in the singlet state leads to its complete deactivation, and that the suppressor destroys the intermediate photo-oxide (evidently being itself oxidized), by separating out starting material.* The results obtained do not allow us to assert that interaction of the suppressor with the molecule excited in the singlet state can not only deactivate it to the ground state, but can also transform it to the state which is active towards photo-oxidation (the triplet state), nor do they prove that suppression of triplet molecules is completely absent, or that some kind of other processes

*In separate experiments it was shown that p-toluidine does not react with the final stable photo-oxide of material I under conditions of the experiment, and that in deoxygenated solutions it does not undergo photo-chemical changes.

which take place with participation of the suppressor are involved. However we can say that in all probability these processes do not play important roles in the case investigated.

December 4, 1958

References

1. E. J. BOWEN, D. W. TANNER: Trans. Farad. Soc., 51, 475, (1955)
2. T. M. VEMBER, A. S. CHERKASOV: OiS, 6, 232, (1959) (See 6, p.148)
3. A. S. CHERKASOV, T. M. VEMBER: OiS, 4, 203, (1958)
4. V. V. ZELINSKII, V. P. KILOBKOV, N. I. KONDARAKI: DAN SSSR, 117, 391, (1957); V. V. ZELINSKII, V. P. KOLOBKOV: OiS, 1, 560, (1956)
5. R. LIVINGSTON: J. de chim. phys. (in press).

TOM VII, Vyp. 3
VOL. VII, No. 3

OPTIKA I SPEKTROSKOPIIA
OPTICS AND SPECTROSCOPY

Sentiabr', 1959
September, 1959

Absorption Spectra, Fluorescence Spectra and Quantum Yields of Fluorescence of Some Methyl- and Methyl-meso-arylanthracenes

A. S. CHERKASOV

Abstract: The absorption and fluorescence spectra have been investigated and the quantum yields of fluorescence determined for some α- and β-methyl derivatives of anthracene, meso-diphenylanthracene and meso-di-o-tolylanthracene. It has been demonstrated that the close spatial arrangement of the methyl and aryl groups in α-methyl-meso-arylanthracenes gives rise to an interaction between the two substituents. This interaction, which is stronger in the activated state, destroys the vibrational structure of the fluorescence spectra, shifts the bands to lower frequencies, and, in some cases, leads to a reduction in the quantum yields.

In previous investigations [1-4] of anthracene derivatives it has been established that the influence of substituents, which possess multiple bonds in conjugation with the anthracene nucleus, on the appearance and position of the absorption bands depends to an important extent on steric hindrance factors which affect the establishment of a co-planar conjugated system.

The influence of conjugation, which is most apparent in the case of compounds in which steric hindrance is absent or small (e.g. in 9-cyano-anthracene or 9-anthraldehyde), on the absorption spectra is shown by the considerable shift of the bands to lower frequencies relative to the spectra of anthracene and by the washing out of the vibrational structure of the long wavelength band.

In the meso-aryl derivatives of anthracene a planar configuration of the molecule is hindered by steric interaction of the hydrogen atoms (or of substituent groups) in the ortho positions of the benzene ring and in the α-positions of the anthracene nucleus*. Absorption spectra of these compounds differ little in structure from the spectra of unsubstituted anthracene, which is evidence for the absence of a noticeable interaction between the π-electrons of anthracene and the benzene nucleus.

We have previously demonstrated [4, 6, 7], however, that substitution in the meso position of the anthracene nucleus by aryl substituents such as phenyl, m- and p-tolyl, and p-bromophenyl groups, which have little affect on the absorption spectra, can cause significant changes in the fluorescence spectra (a loss of the vibrational structure, a reduction of the distance between the vibrational maxima, and an increase in the displacement of the fluorescence spectrum with respect to the absorption spectrum). It was suggested at that time that the fundamental cause of this phenomenon is the increased conjugation of the benzene and anthracene rings in the excited state (the non-identity of the radiating and absorbing molecules may be inferred from the fact that after absorption of a quantum of light the molecule becomes more planar **.) In accordance with this hypothesis, an increase of steric hindrance to the formation of a planar configuration brought about by the replacement of the hydrogen atom in the ortho position of the benzene nucleus by a substituent of greater dimensions should result in a fluorescence spectrum similar to the spectra of unsubstituted anthracene and its meso-alkyl derivatives. This is seen clearly by a comparison of the fluorescence spectrum of 9, 10-di-o-tolyl-anthracene with the spectra of di-m- and di-p-tolylanthracenes [4,7], and the spectrum of 9, 10-di-o-anisyl-anthracene with the spectra of 9-p-anisyl- and 9, 10-di-p-anisyl-anthracenes (Fig. 1)***.

In connection with the question of the influence of steric hindrance on the spectra of meso-arylanthracene derivatives, it seemed worthwhile to investigate those derivatives which possess substituents in the α and β- positions of the anthracene nucleus.

In this paper we present the results of a study of the absorption and fluorescence spectra**** of some methylanthracene derivatives of the type:

where one or two of the R's corresponds to $-CH_3$ (the rest to H's), while X may be either $-CH_3$ or -H. The quantum yields of fluorescence for these compounds also have been determined.

*An examination of scale models has shown that an overlapping of the spheres of action of the hydrogen atoms takes place even if it is assumed that their dimensions are determined by the covalent radii. Jones [5] has found by employing the Van der Waal's radius of the hydrogen atom that the phenyl group in mesophenylanthracenes is twisted from the plane of the anthracene nucleus by an angle of not less than 57°. We must assume, however, that these calculations are very approximate.

**An analogous assumption already has been made by Braude and co-workers [8] to explain some absorption properties of benzene derivatives containing substituents capable of conjugation.

***The synthesis of 9-p-anisylanthracene (m.p. 164-5°) employed the reaction of anthrone and $p\text{-}CH_3OC_6H_4MgBr$ and was carried out under previously described conditions [9] in ether solution. The product was purified by repeated recrystallizations and chromatography on Al_2O_3. The synthesis of 9, 10-di-p-(m. p. 280-2°) and 9, 10-di-o-anisylanthracene (m.p. 298-300°) involved the reduction of the corresponding dihydroxy-dihydroanthracenes by stannous chloride and HCl in acetic acid. The dihydroxy-dihydroanthracenes were obtained from the reaction of o- and p-anisyl magnesium bromides and anthraquinone [10]. The products were purified by chromatography and recrystallization from xylene.

**** The method of investigation was analogous to that described in [6,7].

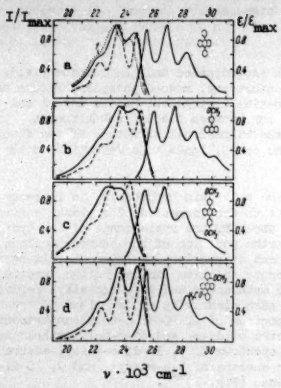

Figure 1. Fluorescence spectra (on the left) and absorption spectra (on the right) of anthracene derivatives.

a. 9, 10-diphenylanthracene. b. 9-p-anisylanthracene. c. 9, 10-di-p-anisylanthracene. d. 9, 10-di-o-anisylanthracene.

Temperature 20° (solid line) and -183° (broken line). Solvent: ethanol.

1 - Solid solution of 9, 10-diphenylanthracene in polystyrene (at 20°).

Ordinate axis: in all figures the relative quantum intensities of fluorescence are on the left and the relative values of molar coefficients of absorption are on the right.

ABSORPTION AND FLUORESCENCE SPECTRA

The presence of methyl substituents in the α- or β- positions of the anthracene nucleus are, by themselves, of little influence on the spectra. The fluorescence and absorption spectra of 1-methyl-, 2-methyl-, 1,3-dimethyl-, 2,3-dimethyl-, and 1,4-dimethylanthracenes are presented in figure 2. As may be noted, the bands have well pronounced vibrational structure and are shifted somewhat to lower frequencies relative to the corresponding bands in anthracene.*

If, however, there are aryl substituents in the meso positions of the anthracene nucleus in addition to methyl substituents, the appearance of the absorption and especially the fluorescence spectra is strongly dependent upon the position of the methyl groups. In the case, where the methyl groups are located on the β-positions of the anthracene nucleus, they exhibit practically no influence, thus, the absorption and fluorescence spectra of 2-methyl-and 2, 3-dimethyl-9, 10-diphenylanthracene are almost identical with the spectra of 9, 10-diphenylanthracene, and the spectra of 2-methyl- and 2, 3-dimethyl-9, 10-di-o-tolylanthracene coincide with the spectra of 9, 10-di-o-tolylanthracene (Fig. 3). If, on the other hand, the methyl groups are placed in the α-positions of the anthracene ring, very noticeable changes in the fluorescence spectra (and, to a lesser extent, in the absorption spectra) are observed.

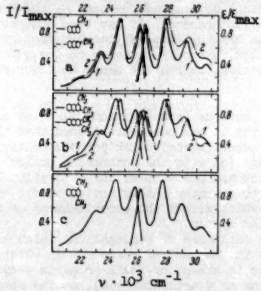

Figure 2. Fluorescence spectra (on the left and absorption spectra (on the right) of anthracene derivatives.

a. 1-methylanthracene (1) and 2-methylanthracene (2); b. 1, 3-dimethylanthracene (1) and 2, 3-dimethylanthracene (2); c. 1, 4-dimethylanthracene. Solvent: ethanol. Temperature 20°.

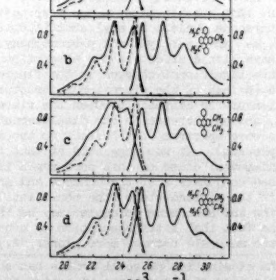

Figure 3. Fluorescence spectra (on the left) and absorption spectra (on the right) of anthracene derivatives.

a. 2-methyl-9, 10-diphenylanthracene; b. 2-methyl-9,10-di-o-tolylanthracene; c. 2,3-dimethyl-9,10-diphenylanthracene; d. 2,3-dimethyl- 9,10 di-o-tolylanthracene. Temperature 20° (solid lines) and -183° (broken lines).

There is a significantly greater shift of the bands to lower frequencies than in the case of β-methyl-meso-aryl substituents, and furthermore, the vibrational structure has been almost completely

* The positions of the individual maxima in the absorption and fluorescence spectra of these compounds are presented in reference [11], which also contains similar data for the methyl-meso-aryl-derivatives of anthracene.

washed out (Fig. 4)*. The washing out of the vibrational structure is accompanied, as is found in other anthracene derivatives [3, 6, 7], by an increase in the distance between the main maxima of the fluorescence spectra and the long wavelength absorption band. This spacing in 1, 4-dimethyl-9, 10-diphenyl- and 1, 4-dimethyl-9, 10-di-o-tolyl-anthracene is 4550 and 3825 cm^{-1} respectively, as opposed to values of 3500 cm^{-1} for 9, 10-diphenylanthracene and 3125 cm^{-1} for 9, 10-di-o-tolylanthracene. In these compounds the wavelength shift of the fluorescence spectra relative to the spectrum of anthracene is significantly greater than the values calculated by simply adding up the influence of the substituents [11].

Thus, when methyl substituents are in the α-positions and aryl substituents are in the meso positions of the anthracene nucleus simultaneously the interaction between them is clearly demonstrated in the fluorescence spectra. It seems perfectly reasonable to us to assume that this phenomenon is fundamentally due to the close spatial position of the substituents and not their mutual influence, which would be translated through the anthracene group. In the latter case, we would obviously expect the mutual influence of groups on more remote parts of the anthracene nucleus to also affect the fluorescence spectra.

It would seem, that the close spatial positioning of the methyl and aryl functions ought to cause strong repulsive forces between these groups, but if this reasoning is correct the repulsive forces would result in a weakening of the conjugation between the benzene ring and the anthracene nucleus. Thus, the α-methyl-meso-arylanthracenes should possess the spectral characteristics of anthracene, however, as we have seen, this is not the case. It is suggested, therefore, that the principal interaction between the aryl and α-methyl substituents consists of the formation of a weak bond between a methyl hydrogen atom and the π-electrons of the benzene ring (the methyl hydrogen atoms bear a partial positive charge because of hyperconjugation). This hypothesis satisfactorily explains the observed facts, but in order to decide whether it is correct further investigation will be necessary.

The fluorescence bands of the meso-aryl derivatives of anthracene have been shown to be temperature dependent. Thus, at low temperatures a sharp improvement was observed in the resolution of the vibrational structure. As is evident from figure 4, even the very broad bands of the α-methyl-meso-aryl derivatives of anthracene acquire the characteristic appearance of unsubstituted anthracenes at liquid air temperatures. In addition, the bands shift to higher frequencies** and the value of this shift is greatest in 1, 4-dimethyl-9, 10-diphenyl- and 1, 4-dimethyl-9, 10-di-o-tolylanthracene (900 and 450 cm^{-1}, respectively), i.e. in compounds in which the spectra are the most washed out at room temperature. The similarity of the fluorescence spectrum of an ethanolic solution of 9, 10-diphenylanthracene with a solid solution of this material in polystyrene (Fig. 1) may be considered as evidence for the fact that the spectral changes result from the low temperatures involved and not from an increased rigidity of the medium.

If we continue to assume that a different equilibrium configuration of these molecules exists in the excited state, i. e. that after absorption of a quantum of light a reorientation of the molecule takes place which involves a change of energy levels [12] the temperature dependence of the fluorescence spectrum may be explained by the fact that the levels are separated by an energy barrier. At low temperatures the vibrational energy of the molecule might be insufficient for overcoming this barrier***, and transitions would then take place between different levels than at higher temperatures.

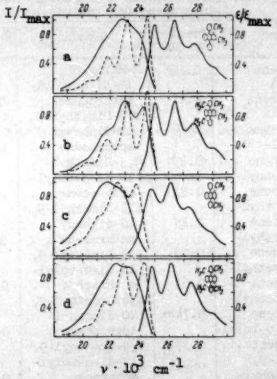

Figure 4. Fluorescence spectra (on the left) and absorption spectra (on the right) of anthracene derivatives.

a. 1, 3-dimethyl-9, 10-diphenylanthracene; b. 1, 3-dimethyl-9, 10-di-o-tolylanthracene; c. 1, 4-dimethyl-9, 10-diphenylanthracene; d. 1, 4-dimethyl-9, 10-di-o-tolylanthracene.

Temperature 20° (solid line) and -183° (broken line).

QUANTUM YIELDS OF FLUORESCENCE

Evaluation of the data with respect to the fluorescence yield of various methyl substituted anthracenes (see table) has established that the influence of a methyl group is noticeably dependent upon its position on the anthracene nucleus. The meso-methyl substituents have the highest quantum yields and the

* In this series of compounds, however, the fluorescence spectra exhibits a noticeably better resolution of the vibrational structure of the o-tolyl derivatives than in the case of the spectra of the phenyl derivatives.

** It should be pointed out that the fluorescence spectra of anthracene, mesoalkyl substituted anthracenes, and other related derivatives, which at room temperature possess structural spectra, are almost completely unchanged at low temperatures, however, the band centers may be shifted somewhat at lower frequencies.

*** It has been assumed that transition to a stable excited state electronic level takes place following the establishment of an equilibrium distribution of the molecules at a given temperature in accordance with the vibrational level.

β-methyl substituents have the lowest. Introduction of a second methyl group into the remaining meso position doubles the quantum yield, whereas the yields from α, α-, β, β-, or α, β-disubstituted anthracenes are little different from the quantum yields of the corresponding mono-substituted molecules. The observed lowering of the fluorescence yields on going from meso to α and further to β substituents may be explained by the previously discussed assumption that one of the factors which causes greater fluorescence yields in the anthracene series is, evidently, the increased delocalization of the electron cloud on the anthracene nucleus [3, 13].

The presence of methyl substituents on the side ring of the anthracene nucleus of meso-aryl derivatives has insignificant influence on the fluorescence yields. Only the α-methyl substituents of 9, 10-diphenylanthracene are exceptions to the preceding statement.

Fluorescence Quantum Yield of Ethanolic Solutions of Anthracene Derivatives

Compound	Quantum yield	Compound	Quantum yield
Anthracene	0.22*	2-Methyl-9, 10-di-o-tolyl-anthracene . .	0.65
1-Methyl-anthracene . .	0.27	2,3-Dimethyl-9, 10-diphenyl-anthracene . .	0.68
2-Methyl-anthracene . .	0.16	2,3-Dimethyl-9, 10-di-o-tolyl-anthracene . .	0.59
9-Methyl-anthracene . .	0.29	1,3-Dimethyl-9, 10-diphenyl-anthracene . .	0.27
1,3-Dimethyl-anthracene . .	0.21	1,3-Dimethyl-9, 10-di-o-tolyl-anthracene . .	0.65
1,4-Dimethyl-anthracene . .	0.25	1,4-Dimethyl-9, 10-diphenyl-anthracene . .	0.095
2,3-Dimethyl-anthracene . .	0.20	1,4-Dimethyl-9, 10-di-o-tolyl-anthracene . .	0.58
9,10-Dimethyl-anthracene . .	0.63		
9,10-Diphenyl-anthracene . .	0.74**		
9,10-Di-o-tolyl-anthracene . .	0.57		
2-Methyl-9, 10-diphenyl-anthracene . .	0.66		

*According to the data of reference [14].
**In previous publications [6,7,15] we erroneously cited the value of 0.84 as the quantum yield for 9,10-diphenylanthracene.

As is evident from the tables, methyl group substitution in one of the α-positions, and to a greater extent in both of the α-positions (of one ring), of 9, 10-diphenylanthracene results in a sharp lowering of the quantum yield (from 0.74 in 9, 10-diphenylanthracene to 0.26 in 1, 3-dimethyl-9, 10-diphenylanthracene and 0.095 in 1, 4-dimethyl-9, 10-diphenylanthracene). This fact is evidently associated with the suggestion that there is a greater interaction of the aryl and methyl groups which are sterically held close to each other.

December 4, 1958

References

1. R. N. JONES: Chem. Rev., 41, 353 (1947)
2. M. MARTYNOFF, M. CHAVIN, M. GRUMEZ, AND N. LEFEVRE: Bull. Soc. Chim. France, 167 (1958)
M. MARTYNOFF, C. r., 244, 205 (1957); 243, 2097 (1956); 240, 2425, (1955)
3. A. S. CHERKSOV, AND T. M. VEMBERG: OiS, 1, 663 (1956)
4. A. S. CHERKASOV: Phys. sb. Lvov Univ., V. 3, (8), 381 (1957)
5. R. N. JONES: J. Amer. Chem. Soc., 67, 2127 (1945)
6. A. S. CHERKASOV: ZFKh, 29, 2209 (1955)
7. A. S. CHERKASOV: IAN USSR SF, 20, 478(1956)(See CTT)
8. E. A. BRAUDE, E. R. H. JONES, H. P. KOCH, R. W. RICHARDSON, F. SONDHEIMER, AND J. B. TOOGOOD, J. Chem. Soc., 1890 (1949); E. A. BRAUDE AND F. SONDHEIMER: J. Chem. Soc., 3754 (1955); E. A. BRAUDE AND C. J. TIMMONS: J. Chem. Soc., 3766 (1955); E. A. BRAUDE AND F. SONDHEIMER: J. Chem. Soc., 3773 (1955); E. A. BRAUDE AND W. F. FORBES: J. Chem. Soc., 3776 (1955)
9. F. KROLLPFEIFFER AND F. BRANSCHELD: Ber., 56, 1617 (1923); A. SIGLITZ AND R. MARX: Ber., 56, 1619 (1923)
10. A. HALLER AND A. COMTESSE: C. R., 150, 1290 (1910); C. K. INGOLD AND P. G. MARSHALL: J. Chem. Soc., 3080, (1926)
11. A. S. CHERKASOV: OiS, 6, 496 (1959)(See 6, 315)
12. B. S. NEPORENT: ZFKh, 30, 1048 (1956); Tr. GOI, 25, V. 150, Oborongiz, 1957
13. V. V. ZELINSKII: Tr. GOI, Sessiia pamiiati C. I. VAVILOVA: Oborongiz, 1953
14. E. J. BOWEN AND A. NORTON: Trans. Farad. Soc., 35, 44 (1939)
15. A. S. CHERKASOV, V. A. MELCHANOV, T. M. VEMBERG, AND K. G. VALDAIKINA: DAN SSSR, 109, 292 (1956) (See Sov. Phys. Doklady)

TOM VII, VYP. 3
VOL. VII, NO. 3

OPTIKA I SPEKTROSKOPIA
OPTICS AND SPECTROSCOPY

Sentiabr', 1959
September, 1959

Theory of the Faraday Effect in the Region of Exciton Absorption of Light in Molecular Crystals

A. F. LUBCHENKO

Abstract: A theory of the Faraday effect in molecular crystals is developed in which excitons may exist for the case of weak coupling of the exciton excitation to the lattice vibrations and for arbitrary values of the absorption coefficient. The gyration vector which gives the rotation of the plane of polarization in an external magnetic field is calculated; formulae are derived which determine the Verdet dispersion coefficient for crystals of high and intermediate symmetry near the exciton absorption band, as well as the values of the refractive indices in this region.

POLARIZATION OF THE CRYSTAL IN THE PRESENCE OF A CONSTANT UNIFORM EXTERNAL MAGNETIC FIELD

We will consider a molecular crystal*, composed of N unit cells, each of which contains σ molecules. Due to the forces of interaction between them, the molecules are "deformed" relative to their free state and hence their wave functions differ from those of the free molecules [1]. If a constant uniform external magnetic field is applied to the crystal, the deformation of the molecules is increased because of the field, where the molecules occupying different sites in the unit cell will be deformed in differing degrees. To take account of this, we will divide the molecules in the unit cell into groups for which the cosine of the angle between the direction of the field $\vec{H}$ and the direction of the dipole moment (the average moment or the moment of a given transition) are the same; these groups of molecules will be designated by α, whereas molecules within the group are designated by $\rho_\alpha = 1, 2 \ldots \sigma_\alpha$, and where, in agreement with the above, $\sum_\alpha \sigma_\alpha = \sigma$.

The wave functions of the molecules in a crystal in an external magnetic field may be written down easily if the wave functions of the free molecules are known. Using the general methods of perturbation theory one may show [2] that

$$(1)\qquad \psi^{l_o}_{\vec{n}\rho_\alpha} = \bar{\varphi}^{l_o}_{\vec{n}\rho_\alpha} + iH \sum_l c^l_{11_o} \bar{\varphi}^l_{\vec{n}\rho_\alpha} + H^2 \sum_l c^l_{21_o} \bar{\varphi}^l_{\vec{n}\rho_\alpha}$$

and

$$(2)\qquad \psi^f_{\vec{n}\rho_\alpha} = \bar{\varphi}^f_{\vec{n}\rho_\alpha} + iH \sum_l c^l_{1f} \bar{\varphi}^l_{\vec{n}\rho_\alpha} + H^2 \sum_l c^l_{2f} \bar{\varphi}^l_{\vec{n}\rho_\alpha}.$$

Here $\psi^{l_o}_{\vec{n}\rho_\alpha}$, $\psi^f_{\vec{n}\rho_\alpha}$ are the wave functions of the molecules of the crystal in a uniform external magnetic field corresponding to the ground and excited states, l_o is a complete set of quantum numbers describing the ground state, $f = l_1, l_2 \ldots$ is a complete set of quantum numbers characterizing the excited state of the molecules, $\psi^f_{\vec{n}\rho_\alpha}$ are the solutions of the equations

$$\left[\vec{H}_{\vec{n}\rho_\alpha}\left(r\frac{\partial}{\partial r}\right) - \vec{H}M_{\vec{n}\rho_\alpha z}\right]\psi^f_{\vec{n}\rho_\alpha} = E^f_{\vec{n}\rho_\alpha}(\vec{H})\psi^f_{\vec{n}\rho_\alpha}.$$

The $c^l_{1l_o}$ and $c^l_{2l_o}$, c^l_{1f} and c^l_{2f} are constants (for a given l) of first and second order of smallness respectively, related to the matrix element of the z-component of the total magnetic moment of the crystal, $\bar{\varphi}^l_{\vec{n}\rho_\alpha}$ are the wave functions of the isolated molecules, $\vec{n}$ is the number of unit cells in the crystal, H is the z component of the magnetic field intensity (we are assuming that the field is directed along the axis Oz). To simplify the calculation we assume also that the energy levels of molecules in different groups are sufficiently far removed from one another.** Then the Schrödinger equation,

$$(\vec{T}_R + \vec{H}_o - W)\Psi = U\Psi,$$

where $\vec{T}_R$ is the energy operator of the translational and orientational vibrations of the molecule,

$$\vec{H}_o = \sum_{\vec{n}\rho_\alpha} \vec{H}_{\vec{n}\rho_\alpha}\left(r\frac{\partial}{\partial r}\right) + \frac{1}{2}\sum_{\substack{\vec{n}\rho_\alpha,\vec{m}\rho_\beta \\ (\vec{n}\rho_\alpha \neq \vec{m}\rho_\beta)}}{}' V_{\vec{n}\rho_\alpha,\vec{m}\rho_\beta} - H\sum_{\vec{n}\rho_\alpha} M_{\vec{n}\rho_\alpha z},$$

and $\vec{H}_{\vec{n}\rho_\alpha}\left(r\frac{\partial}{\partial r}\right)$ is the Hamiltonian operator for the free molecule, $V_{\vec{n}\rho_\alpha,\vec{m}\rho_\beta}$ is the energy interaction between the molecules $\vec{n}\rho_\alpha$ and $\vec{m}\rho_\beta$,

$$M_{\vec{n}\rho_\alpha z} = \sum_i \frac{e_i}{2M_i c}\left[(\vec{r}_{\vec{n}\rho_\alpha i}\vec{p}_{\vec{n}\rho_\alpha i}) + 2\vec{\sigma}_{\vec{n}\rho_\alpha i}\right]_z,$$

where z indicates the component of the total magnetic moment, $\vec{r}_{\vec{n}\rho_\alpha i}$ are the coordinates of the ith charge on the $\vec{n}\rho_\alpha$ molecule, M_i is its mass,

*In speaking of a crystal we have in mind its main part.

**If this assumption is not fulfilled and the energy levels of the molecules of the various groups do lie close together, then the problem must be solved using the perturbation theory for close-lying levels. A similar problem for the case of crystals has been considered in [3, 4].

$\vec{p}_{\vec{n}\rho_\alpha j}$ and $\vec{\sigma}_{\vec{n}\rho_\alpha j}$ are momentum and spin operators of this charge, W is the operator for the exciton-phonon interaction, has solutions for a nondegenerate stationary state in the form:

a) for the ground state:

$$\Psi^{1o}_{[n_s]} = [(S\sigma N)!]^{-\frac{1}{2}} \sum_\nu (-)^\nu P_\nu \prod_{\vec{n}\alpha\rho_\alpha} \psi^{1o}_{\vec{n}\rho_\alpha} \chi$$

$$\chi \prod_s f_{n_s}(\xi_s) \exp\left[-\frac{it}{h} U^{1o}_{[n_s]}\right], \tag{3}$$

$$U^{1o}_{[n_s]} = \sum_{\vec{n}\alpha\rho_\alpha} E^{1o}_{\vec{n}\rho_\alpha}(H) + V_o + \sum_s h\omega_s (n_s + \tfrac{1}{2});$$

b) and for an excited (one exciton) state:

$$\Psi^{f\mu}_{[n_s]} = [\sigma_\alpha N(S\sigma N)!]^{-\frac{1}{2}} \sum_{\vec{n}\alpha\rho_\alpha} B^{f\mu}_{\rho_\alpha}(\vec{k}) \chi$$

$$\chi \left(\sum_\nu (-)^\nu P_\nu \psi_{n\rho} \prod_{\vec{n}'\alpha'\rho'_{\alpha'}} \psi^{1o}_{\vec{n}'\rho'_{\alpha'}} \right) \chi \tag{4}$$

$$\chi \prod_s f_{n_s}(\xi_s) \exp[i\vec{k}\vec{n}] - \frac{it}{h} U^{f\mu}_{[n_s]}(\vec{k}),$$

$$U^{f\mu}_{[n_s]}(\vec{k}) = \sum_{\vec{n}\beta\rho_\beta} E^{1o}_{\vec{n}\rho_\beta}(H) + \Delta E^f_{\vec{n}\rho_\alpha} + V_o + D^f_{\vec{n}\rho_\alpha} +$$

$$+ \epsilon^f_{\mu\alpha}(\vec{k}) + \sum_s h\omega_s (n_s + \tfrac{1}{2}).$$

Here $f_{n_s}(\xi_s)$ are the wave functions of harmonic oscillators, ξ_s the normal coordinates, n_s the quantum numbers of the lattice vibrations, the symbol $[n_s]$ indicates the complete set of quantum numbers for the vibrational state of the crystal; V_o and $D^f_{\vec{n}\rho_\alpha}$ are, respectively, the zero order terms (in a power series of the displacements of the molecules from their equilibrium positions in the ground state) of the expansions of the matrix element of the interaction energy and the difference in the interaction energies of the unexcited and excited $\vec{n}\rho_\alpha$ molecules with the remaining molecules, $E^1_{\vec{n}\rho_\alpha}$ are the eigenvalues of the energy operator of the molecule in the field H, $\Delta E^f_{\vec{n}\rho_\alpha} = E^f_{\vec{n}\rho_\alpha}(H) - E^{1o}_{\vec{n}\rho_\alpha}$, S is the number of electrons in the molecule, P_ν is one of the $(S\sigma N)!$ possible permutations of pairs of electrons among the molecules, $\epsilon^f_{\mu\alpha}(\vec{k})$ is an addition to the excitation energy of the crystal, arising from the resonance interaction between the molecules ρ_α, $B^{f\mu}_{\rho\alpha}(\vec{k})$ are coefficients determined by equations (3.15) of reference [1] and normalized so that

$$\sum_{\rho_\alpha} B^{f\mu}_{\rho_\alpha}(\vec{k})\, B^{*\,f\mu}_{\rho_\alpha}(\vec{k}) = \sigma_\alpha \delta_{\mu\mu'},$$

$$\sum_{\mu} B^{f\mu}_{\rho_\alpha}(\vec{k})\, B^{f\mu}_{\rho_\beta}(\vec{k}) = \sigma_\alpha \delta_{\alpha\rho_\beta}$$

ω_s are the eigenfrequencies of the translational and orientational vibrations of the lattice, $\vec{k}$ is the reduced wave vector. We note that the solutions (3) and (4) differ from the solutions of the Schrödinger equation for the free crystal [1-5] only in that the functions $\psi^j_{\vec{n}\rho_\alpha}$ and $\psi^{1o}_{\vec{n}\rho_\alpha}$, defined in (1) and (2) depend on the strength of the magnetic field.

We now assume that at t=0 a plane electromagnetic wave is incident on the crystal and that the field strength of the wave in the crystal is given by the expression

$$\vec{E} = \frac{1}{2}\vec{E}_o \exp[i(\vec{Q}\vec{r} - \omega t)] + \frac{1}{2}\vec{E}^*_o \exp[-i(\vec{Q}^*\vec{r} - \omega t)] \tag{5}$$

where $\vec{Q} = \dfrac{\omega(n + i\kappa)}{c}\vec{s}$, and where $\vec{s}$ is a unit vector along the wave normal, n and κ are the indices of refraction and absorption of light in the crystal. Then the operator for the interaction of the electromagnetic wave with the crystal may be written in the form

$$\vec{H}' = -\sum_{n\rho_\alpha j} \frac{e_j}{M_j c} \chi \vec{A}_{\vec{n}\rho_\alpha} \vec{j}^{\,p}_{\vec{n}\rho_\alpha j} \tag{6}$$

Here χ is a tensor quantity which takes account of the difference between the transverse field acting on the molecule and the average macroscopic field ($\chi_{xy} = \delta_{xy} - s_x s_y$), and $\vec{A}$ is the vector potential of the latter; with the help of (5) this may be written in the form

$$\vec{A} = \frac{1}{2}\vec{A}_o \exp[i(\vec{Q}\vec{r} - \omega t)] + \frac{1}{2}\vec{A}^*_o \exp[-i(\vec{Q}^*\vec{r} - \omega t)]$$

with

$$\vec{A}_o = -\frac{ic}{\omega}\vec{E}_o, \quad \vec{A}^*_o = \frac{ic}{\omega}\vec{E}^*_o.$$

In order not to restrict the generality, we will assume from the start that $\kappa \neq 0$; then expanding the vector potential in a Fourier series and substituting it in (6), we find, if we use the Riemann-Lebesgue theorem [6] (where we have put $\vec{q}\vec{r}_{\vec{n}\rho_\alpha j} = \vec{q}\vec{n}$),

$$\vec{H}' = -\sum_{\vec{n}\rho_\alpha \vec{q} j} \left[\frac{e_j \chi \vec{A}^*_o \vec{p}_{\vec{n}\rho_\alpha j}}{2Li M_j c \beta_1 \beta_2 \beta_3} \exp[i(\vec{q}\vec{n} - \omega t)] + \right.$$

$$\left. + \frac{e_j \chi \vec{A}_o \vec{p}_{\vec{n}\rho_\alpha j}}{2Li M_j c \beta_1 \beta_2 \beta_3} \exp[i(\vec{q}\vec{n} + \omega t)] \right]. \tag{7}$$

Here $q_x = \frac{2\pi}{L}\delta_x$, $(x = 1, 2, 3)$, $\delta_x = 0, \pm 1, +2\ldots$, L_x are the dimensions of the crystal (cf. footnote 1) along the axes O_x, $L = L_x L_y L_z$, $\beta_x = q_x - q$, $\beta'_x = -q^*_x - q_x$.

Under the influence of the perturbation (7), the crystal goes over into an excited state whose wave function is determined by the equation

$$(8) \qquad ih\frac{\partial F}{\partial t} = (\vec{T}_R + \vec{H}_0 - W + \vec{H}')F.$$

We seek solutions of (8) in the form

$$F = b^{l_0}_{[n_s]}\Psi^{l_0}_{[n_s]} + \sum_{f'\mu'}\sum_{\vec{k}'[n'_s]} b^{f'\mu'}_{[n'_s]}(\vec{k}')\Psi^{f'\mu'}_{[n'_s]}(\vec{k}')\exp[-i\Gamma^{f'}_{\mu'}t] - \sum_{\lambda} c_\lambda \Psi_\lambda, \qquad (9)$$

$(f' \neq l_0)$

where Ψ_λ describes all possible excited states of the crystal, except the single exciton states, corresponding to excitation of the molecules ρ_α. Then substituting (9) into (8), it is easy to determine the probability amplitudes [2] $b^{l_0}_{[n_s]}$, if one uses the initial conditions that at $t = 0$ we have $b^{f\mu}_{[n_s]} = \delta_{l_0 f}$. From this we have immediately the wave function of the excited state of the crystal

$$F = \Psi^{l_0}_{[n_s]} + \left(\frac{N}{\sigma_\alpha}\right)^{\frac{1}{2}} \sum_{f\mu\rho_\alpha\vec{q}} \frac{B^{*f\mu}_{\rho_\alpha}(\vec{q})\Omega_{f_\mu}(\vec{q})(\chi\vec{E}_0\cdot\vec{\mathscr{P}}^{fl_0}_{\rho_\alpha})\exp\left[it(\Omega_{f_\mu}(\vec{q})-\omega)\right]}{2L i\beta_1\beta_2\beta_3 h\omega\left[\Omega_{f_\mu}(\vec{q})-\omega-i\Gamma^f_\mu\right]}\Psi^{f\mu}_{[n_s]}(\vec{q}) -$$

$$-\left(\frac{N}{\sigma_\alpha}\right)^{\frac{1}{2}}\sum_{f\mu\rho_\alpha\vec{q}}\frac{B^{*f\mu}_{\rho_\alpha}(\vec{q})\Omega_{f_\mu}(\vec{q})\ (\chi\vec{E}_0\cdot\vec{\mathscr{P}}^{fl_0}_{\rho_\alpha})\exp\left[it(\Omega_{f_\mu}(\vec{q})+\omega)\right]}{2L i\beta'_1\beta'_2\beta'_3 h\omega\left[\Omega_{f_\mu}(\vec{q})+\omega-i\Gamma^f_\mu\right]} \times$$

$$\times\ \Psi^{f\mu}_{[n_s]}(\vec{q}) + \sum_\lambda c_\lambda\Psi_\lambda.$$

Here

$$h\Omega_{f\mu}(\vec{q}) \equiv U_{f_\mu}(\vec{q}) - U^{f\mu}_{[n_s]}(\vec{q}) - U^{l_0}_{[n_s]},$$

$$\vec{\mathscr{P}}^{fl_0}_{\rho_\alpha} = \langle\Psi^f_{\vec{n}\rho_\alpha}\left|\sum_i e_i\vec{r}_{\rho_\alpha i}\right|\Psi^{l_0}_{\vec{n}\rho_\alpha}\rangle. \qquad (10)$$

Knowing the functions F we can calculate the electric moment $\vec{P}$ per unit volume of the crystal due to the electromagnetic perturbation

$$(11) \qquad \vec{P}(\vec{m}) = \int F^*\vec{p}(\vec{m})Fd\tau - \int\Psi^{l_0}_{[n_s]}\vec{p}(\vec{m})\Psi^{l_0}_{[n_s]}\,d\tau.$$

Here

$$\vec{p}(\vec{m}) = \frac{1}{\delta\Delta\nu^3}\sum_{\vec{n}\rho_{\alpha i}} e_i(\vec{r}_{\vec{n}\rho_{\alpha i}} - \vec{m})\ D(\vec{r}_{\vec{n}\rho_{\alpha i}} - \vec{m}),$$

$$D(\vec{r}_{\vec{n}\rho_{\alpha i}} - \vec{m}) = \begin{cases} 1, & \text{when } -\vec{a}_j\Lambda \leqslant (\vec{r}_{\vec{n}\rho_{\alpha i}} - \vec{m}) \leqslant \vec{a}_j\Lambda, \\ 0, & \text{in all other regions,} \end{cases}$$

the $\vec{a}_j$ are the basis vectors of the crystal lattice, $j = 1, 2, 3$, and $2\Lambda|\vec{a}_j| \ll \lambda$, where λ is the wave length of the light in the crystal, Δ is the volume of the unit cell. Putting the expression for F in (11) and carrying out the integrations, we find *

$$(12) \qquad \vec{P}(\vec{m}) = \vec{P}_1(\vec{m}) + \vec{P}^*_1(\vec{m}),$$

where

$$\vec{P}_1(\vec{m}) = \vec{P}_2(\vec{m}) +$$

$$\frac{1}{\omega\sigma_\alpha\Delta}\sum_{f\mu\rho\rho'}\frac{B^{*f\mu}_\rho(\vec{Q})B^{f\mu}_{\rho'}(\vec{Q})\Omega_{f_\mu}(\vec{Q})\ (\chi\vec{E}_1\cdot\vec{\mathscr{P}}^{fl_0}_\rho)\vec{\mathscr{P}}^{l_0f}_{\rho'}}{U_{f_\mu}(\vec{Q}) - h\omega - ih\Gamma^f_\mu(\vec{Q})} -$$

$$-\frac{1}{\omega\sigma_\alpha\Delta}\sum_{f\mu\rho\rho'}\frac{B^{*f\mu}_{\rho_\alpha}(\vec{Q}^*)B^{f\mu}_{\rho'}(\vec{Q}^*)\Omega^*_{f_\mu}(-\vec{Q}^*)(\chi\vec{E}_1\cdot\vec{\mathscr{P}}^{l_0f}_\rho)\vec{\mathscr{P}}^{fl_0}_{\rho'}}{U^*_{f\mu}(-\vec{Q}^*) + h\omega + ih\Gamma^f_\mu(-\vec{Q}^*)}.$$

$$\vec{P}_2(\vec{m}) = \int\Psi^{l_0}_{[n_s]}\vec{p}(\vec{m})\sum_\lambda c_\lambda\Psi_\lambda\,d\tau.$$

We further make more explicit the dependence of $\vec{\mathscr{P}}^{fl_0}_\rho$ and $\vec{\mathscr{P}}^{l_0f}_{\rho'}$ on the strength of the magnetic field; to do this we put (1) and (2) into (10). Then we have

$$\vec{\mathscr{P}}^{fl_0}_\rho = \vec{P}^{fl_0}_{1\rho} + i\vec{H}\vec{P}^{fl_0}_{2\rho} + \vec{H}^2\vec{P}^{fl_0}_{3\rho},$$

where

$$\vec{P}^{fl_0}_{1\rho} = \vec{P}^{l_0f}_{1\rho} = \langle\bar{\Psi}^f_{\vec{n}\rho}\left|\sum_i e_i\vec{r}_{\rho i}\right|\bar{\Psi}^{l_0}_{\vec{n}\rho}\rangle,$$

$$\vec{P}^{fl_0}_{2\rho} = \vec{P}^{l_0f}_{2\rho} = \sum_l c^l_{1l_0}\langle\bar{\Psi}^f_{\vec{n}\rho}\left|\sum_i e_i\vec{r}_{\rho i}\right| \times$$

$$\times\ \bar{\Psi}^l_{\vec{n}\rho}\rangle - \sum_l c^l_{1f}\ \langle\bar{\Psi}^l_{\vec{n}\rho}\left|\sum_i e_i\vec{r}_{\rho i}\right|\bar{\Psi}^{l_0}_{\vec{n}\rho}\rangle,$$

$$\vec{P}^{fl_0}_{3\rho} = \vec{P}^{l_0f}_{3\rho} = \sum_l c^l_{1l_0}\langle\bar{\Psi}^f_{\vec{n}\rho}\left|\sum_i e_i\vec{r}_{\rho i}\right|\bar{\Psi}^l_{\vec{n}\rho}\rangle + \sum_l c^l_{2f}\langle\bar{\Psi}^l_{\vec{n}\rho}\left|\sum_i e_i\vec{r}_{\rho i}\right|\bar{\Psi}^{l_0}_{\vec{n}\rho}\rangle -$$

$$-\sum_{ll'} c_l\ c_{ll_0}\ \bar{\Psi}_{\vec{n}\rho}\left|\sum_i e_i\vec{r}_{\rho i}\right|\bar{\Psi}^{l'}_{\vec{n}\rho}\rangle.$$

*Here we drop the subscripts α and ρ, since in the future we will consider only the dipole moments of structurally equivalent molecules.

If we further limit ourselves to the consideration of naturally non-active crystals, neglecting the dependence of $\vec{E}^{f\mu}_{\rho}(\vec{Q})$ on $\vec{Q}$, and introducing the notation

$$\frac{1}{\sqrt{\sigma_\alpha \Delta}} \sum_{\rho} \vec{E}^{f\mu}_{\rho'} \vec{P}^{f1_0}_{j\rho} = \vec{P}^{f1_0}_{j\mu},$$

$$\frac{1}{\sqrt{\sigma_\alpha \Delta}} \sum_{\rho'} \vec{E}^{f\mu}_{\rho'} \vec{P}^{f1_0}_{j\rho'} = \vec{P}^{f1_0}_{j\mu}, \quad j = 1, 2, 3;$$

$$\frac{\Omega_{\vec{s}f\mu}}{\omega} \vec{P}^{f1_0}_{1\mu} \vec{P}^{f}_{1\mu} = \vec{a}^{f}_{\vec{s}\mu},$$

$$\frac{\Omega_{\vec{s}f\mu}}{\omega} [\vec{P}^{f1_0}_{1\mu} \vec{P}^{f1_0}_{3\mu} + \vec{P}^{f1_0}_{3\mu} \vec{P}^{f1_0}_{1\mu} + \vec{P}^{f1_0}_{2\mu} \vec{P}^{f1_0}_{2\mu}] = \vec{R}^{f}_{\vec{s}\mu},$$

where $\Omega_{\vec{s}f\mu}$ is the zero order term of the expansion of $\Omega_{f\mu}(\vec{Q})$ in a series in $\vec{Q}$, then $\vec{P}_1(\vec{m})$ may be rewritten in the form

$$\vec{P}_1(\vec{m}) = \vec{P}_2(\vec{m}) + \sum_{f\mu} \frac{(\vec{a}^{f}_{\vec{s}\mu} + H^2 \vec{R}^{f}_{\vec{s}\mu})\chi \vec{E}_1}{U_{f\mu}(\vec{Q}) - h\omega - ih\Gamma^{f}_{\mu}(\vec{Q})} -$$

$$- \sum_{f\mu} \frac{(\vec{a}^{f}_{\vec{s}\mu} + H^2 \vec{R}^{f}_{\vec{s}\mu})\chi \vec{E}_1}{U_{s\mu}(\vec{Q}) + h\omega + ih\Gamma^{*f}_{\mu}(-\vec{Q}^*)} + \frac{iH}{4}[\vec{G} \cdot (\chi \vec{E}_1)]. \tag{13}$$

Here $\vec{G}$ is an axial vector with components

$$G_x = \sum_{f\mu} \alpha_{f\mu} [\vec{P}^{f1_0}_{2\mu} \cdot \vec{P}^{f1_0}_{1\mu}]_x,$$

$$G_y = -\sum_{f\mu} \alpha_{f\mu} [\vec{P}^{f1_0}_{2\mu} \cdot \vec{P}^{f1_0}_{1\mu}]_y,$$

$$G_z = \sum_{f\mu} \alpha_{f\mu} [\vec{P}^{f1_0}_{2\mu} \cdot \vec{P}^{f1_0}_{1\mu}]_z. \tag{14}$$

$$\alpha_{f\mu} = \frac{8\pi\Omega_{\vec{s}f\mu} \left[\Omega_{f\mu}(\vec{Q}) - \omega + \gamma_{2f\mu} - \frac{\gamma^2_{1f\mu}}{2\Omega_{f\mu}(\vec{Q})} \right]}{\omega [U_{f\mu}(\vec{Q}) + h\omega] [(\Omega_{f\mu}(\vec{Q}) - \omega + \gamma_{2f\mu})^2 + \gamma^2_{1f\mu}]} +$$

$$+ \frac{4\pi i \Omega_{\vec{s}f\mu} \gamma_{1f\mu}}{h\omega [(\Omega_{f\mu}(\vec{Q}) - \omega + \gamma_{2f\mu})^2 + \gamma^2_{1f\mu}]},$$

where the expression for $\alpha_{f\mu}$ is obtained under the assumption that in the ultraviolet region of the spectrum $|\Omega_{f\mu}(\vec{Q}) + \omega| \gg |\Gamma^{f}_{\mu}(\vec{Q})|$ and $\Gamma^{f}_{\mu} = \gamma_{1f\mu} + i\gamma_{2f\mu}$.

We assume also that the zone $f'\mu'$, into which the transitions which we are considering occur is located far from the remaining zones, so that virtual transitions into these zones add to the tensor dielectric susceptibility an additional term of magnitude $\epsilon + H\epsilon'$, which depends weakly on frequency. Then putting

$$\vec{P}_2(\vec{m}) + \sum_{f\mu \neq f'\mu'} \frac{(\vec{a}^{f}_{\vec{s}\mu} + H^2 \vec{R}^{f}_{\vec{s}\mu})\chi \vec{E}_1}{U_{f\mu}(\vec{Q}) - h\omega - ih\Gamma^{f}_{\mu}(\vec{Q})} =$$

$$= \frac{(\epsilon + H^2\epsilon') - 1}{4\pi} \vec{E}_1$$

and neglecting the third term in (13), we may write the vector electric displacement $\vec{D}_1$ in the form:*

$$\vec{D}_1 = (\epsilon + H^2\epsilon')\vec{E}_1 + \frac{4\pi(a_{\vec{s}} + H^2 R_{\vec{s}})\chi \vec{E}_1}{U(\vec{Q}) - h\omega - ih\Gamma(\vec{Q})} + iH[\vec{G} \cdot (\chi \vec{E}_1)].$$

Further, let us use the method of effective masses and let us put

$$U(\vec{Q}) = U + \frac{h^2\omega^2}{2M_{\vec{s}}c^2}(n + i\kappa)^2,$$

where $M_{\vec{s}}$ is the conventional effective mass of the exciton along the direction $\vec{s}$. If we now introduce the definitions

$$\frac{2M_{\vec{s}}c^2}{h\omega}\left(1 - \frac{U_{\vec{s}}}{h\omega}\right) = g_{\vec{s}}, \quad \frac{2M_{\vec{s}}c^2\gamma_2}{h\omega^2} = \theta_{\vec{s}}, \quad \frac{8\pi M_{\vec{s}}c^2}{h^2\omega^2} a = d_{\vec{s}},$$

$$\frac{8\pi M_{\vec{s}}c^2}{h^2\omega^2} R_{\vec{s}} = b_{\vec{s}}, \quad \frac{2M_{\vec{s}}c^2}{h\omega^2}\left(\gamma_1 - \frac{h\omega^2}{M_{\vec{s}}c^2} n\kappa\right) = \rho_{\vec{s}},$$

then the expression for $\vec{D}_o$ becomes

$$\vec{D}_o = (\epsilon + H^2\epsilon')\vec{E}_o + \frac{(n^2 - \kappa^2 - g_{\vec{s}} + \theta_{\vec{s}} + i\rho_{\vec{s}})(d_{\vec{s}} + H^2 b_{\vec{s}})\chi \vec{E}_o}{(n^2 - \kappa^2 - g_{\vec{s}} + \theta_{\vec{s}})^2 + \rho^2_{\vec{s}}} +$$

$$+ iH[\vec{G} \cdot (\chi \vec{E}_o)]. \tag{15}$$

This latter expression, along with Maxwell's equation for plane waves

$$\vec{D}_o = (n + i\kappa)^2[\vec{E}_o - \vec{s}(\vec{s}\vec{E}_o)] \tag{16}$$

determine the propagation of electromagnetic waves through a crystal in the presence of a constant uniform external magnetic field.

ROTATION OF THE PLANE OF POLARIZATION IN A MAGNETIC FIELD

We now consider the rotation of the plane of

*If the states of the crystal are degenerate, then in the second term of $\vec{D}_1$ there is a sum over these states (a sum over μ).

polarization (the Faraday effect) in crystals of cubic and middle symmetry in the presence of an external magnetic field, near the region of exciton absorption of light. Since in this region $\gamma_{1f\mu} = 0$, we have $\varkappa = 0$ and equations (15) and (16) take the form

$$\vec{D}_0 = (\epsilon + H^2\epsilon')\vec{E}_0 + \frac{(d_{\vec{s}} + H^2 b_{\vec{s}})\chi\vec{E}_0}{n^2 - g} + \tag{17}$$

$$+ iH[\vec{G} \cdot (\chi\vec{E}_0)]; \quad \vec{D}_0 = n^2[\vec{E}_0 - \vec{s}(\vec{s}\vec{E}_0)].$$

Crystals of Cubic Symmetry. We choose as axes the cubic axes (C_3 or C_4) and neglect in equation (17) terms proportional to H^2 as quantities of higher order. Then choosing [2], $s = (0, 0, 1)$, $d_{\vec{s}ik} = d\delta_{ik}$, $d_{\vec{s}33} = 0$, $\epsilon_{ik} = \epsilon\delta_{ik}$, $D_x = (\Xi\vec{E}_0)_x = n^2E_x$, $D_y = (\Xi\vec{E}_0)_y = n^2E_y$, $D_z = 0$, we may rewrite the system (17) in the form

$$\left.\begin{aligned} n^2D_x &= \epsilon D_x + \frac{D_x d}{n^2 - g} - iG_z D_y H \\ n^2D_y &= \epsilon D_y + \frac{D_y d}{n^2 - g} + iG_z D_x H \end{aligned}\right| \begin{matrix} 1, \\ \pm 1, \end{matrix} \tag{18}$$

since, because of the symmetry of the system crystal + magnetic field, we have $G_x = G_y = 0$. From (18) we obtain the equations

$$(n^2 - \epsilon - \frac{d}{n^2 - g} + HG_z)(D_x + iD_y) = 0,$$

$$(n^2 - \epsilon - \frac{d}{n^2 - g} - HG_z)(D_x - iD_y) = 0,$$

which will be satisfied simultaneously if we put

$$D_x = iD_y; \quad n^2 - \epsilon - \frac{d}{n^2 - g} + HG_z = 0; \tag{19}$$

$$D_x = -iD_y; \quad n^2 - \epsilon \frac{d}{n^2 - g} - HG_z = 0.$$

Neglecting the quantity HG_z, we obtain in the zero order approximation the solutions

$$n_{\pm}^2 = \frac{g + \epsilon}{2} \pm \sqrt{\frac{1}{4}(g - \epsilon)^2 + d}, \tag{20}$$

$$D_x^{\pm} \neq 0, \quad D_y^{\pm} \neq 0, \quad D_z = 0, \quad E_z = 0;$$

and in the first order approximation the solutions of (19) are of the form

$$\frac{D_y}{D_x} = i, \quad n'^2_{+} = n_+^2 + H\frac{(n_+^2 - g)^2 G_z^+}{d + (n_+^2 - g)^2},$$

$$n'^2_{-} = n_-^2 + H\frac{(n_-^2 - g)^2 G_z^-}{d + (n_-^2 - g)^2},$$

$$\frac{D_y}{D_x} = -i, \quad n''^2_{+} = n_+^2 - H\frac{(n_+^2 - g)^2 G_z}{d + (n_+^2 - g)^2},$$

$$n''^2_{-} = n_-^2 - H\frac{(n_-^2 - g)^2 G_z^-}{d + (n_-^2 - g)^2},$$

where G_z^+ and G_z^- are obtained by substituting (20) in (14). The specific rotation of the plane of polarization is given by the expression

$$\vartheta_{\pm} = \frac{\pi}{\lambda_0}(n'_{\pm} - n''_{\pm}),$$

whence, after substituting the values of $n'_{\pm}$ and $n''_{\pm}$, we obtain the following values of the Verdet constant

$$R_+ = \frac{\pi(n_+^2 - g)^2 G_z^+}{[d + (n_+^2 - g)^2]\lambda_0 n_+},$$

$$R_- = \frac{\pi(n_-^2 - g)^2 G_z^-}{[d + (n_-^2 - g)^2]\lambda_0 n_-}.$$

We note that, for positive effective mass of the exciton, there will not exist any waves in the crystal with indices of refraction n'_- and n''_- in the given frequency range (since $n'^2_- < 0$ and $n''^2_- < 0$); in this region only the value R_+ of the Verdet constant has physical meaning. Similarly, where n'^2_- and n''^2_- become positive, waves with refractive indices n'_- and n''_+ will generally be of small amplitude, and the Verdet constant R_- will have physical meaning.

For negative effective mass near the strong absorption region, the peculiarities of the spatial dispersion will not be felt, in practice [7]; here the Verde constant will be given by an expression analogous to the expression of classical optics

$$R = \frac{\pi G_z^0}{\lambda_0 n_0},$$

where n_0 is the index of refraction calculated without taking account of spatial dispersion.

Crystals of Middle Symmetry. We take the Oz axis along a fourfold (or three or six-fold) axis and consider transitions from the ground state to a state whose wave function transforms according to the same irreducible representation as the z-component of the polar vector. Then taking $\vec{s} = (0,0,1)$

$$d = d_3\begin{pmatrix} 0 & 0 & 0 \\ 0 & 0 & 0 \\ 0 & 0 & 1 \end{pmatrix}, \quad \epsilon = \begin{pmatrix} \epsilon & 0 & 0 \\ 0 & \epsilon & 0 \\ 0 & 0 & \epsilon_3 \end{pmatrix},$$

and neglecting quantities in (17) proportional to H^2 we rewrite it in the form

$$\left.\begin{aligned}(n^2 - \epsilon)\, D_x + iHG_z D_y = 0\\ (n^2 - \epsilon)\, D_y - iHG_z D_x = 0\end{aligned}\right| \quad \begin{matrix}1,\\ \pm i.\end{matrix}$$

Hence we obtain the equation

$$(n^2 - \epsilon + HG_z)(D_x + iD_y) = 0,$$

$$(n^2 - \epsilon - HG_z)(D_x - iD_y) = 0,$$

which have the solutions

$$\frac{D_y}{D_x} = i, \quad n_1 = n_0 + \frac{HG_z^0}{2n_0}; \quad \frac{D_y}{D_x} = -i, \quad n_2 = n_0 - \frac{HG_z}{2n_0},$$

where $n_0 = \sqrt{\epsilon}$, and G_z^0 is obtained by putting n_0 into (14). The specific rotation of the plane of polarization is determined in this case by the formula

$$\vartheta = \frac{\pi}{\lambda}(n_1 - n_2) = H\frac{\pi G_z^0}{\lambda_0 n_0},$$

which is analogous to the formula of classical optics, and the Verdet constant may be written in the form

$$R = \frac{\pi G_z^0}{\lambda_0 n_0}.$$

We now consider a transition from the ground state to a state whose wave function transforms according to the same irreducible representation as the x and y components of the polar vector, when $\vec{s} = (0,0,1)$. In this case [8]

$$d_{\vec{s}} = d\begin{pmatrix}1&0&0\\0&1&0\\0&0&0\end{pmatrix}, \qquad \epsilon = \begin{pmatrix}\epsilon&0&0\\0&\epsilon&0\\0&0&\epsilon_3\end{pmatrix},$$

and the system (17) takes on the form

$$\begin{aligned}&(n^2 - \epsilon - \frac{d}{n^2 - g} + HG_z)(D_x + iDy) = 0,\\ &(n^2 - \epsilon - \frac{d}{n^2 - g} - HG_z)(D_x - iDy) = 0.\end{aligned} \tag{21}$$

Equations (22) are satisfied if we put

$$D_x = -iD_y, \quad n^2 - \epsilon - \frac{d}{n^2 - g} - HG_z = 0, \tag{22}$$

$$D_x = +iD_y, \quad n^2 - \epsilon - \frac{d}{n^2 - g} + HG_z = 0.$$

The solutions (22) in zero approximation (neglecting HG_z) have the form

$$n_{\pm}^2 = \frac{g + \epsilon}{2} \pm \sqrt{\frac{1}{4}(g - \epsilon)^2 + d},$$

$$D_x^{\pm} \neq 0, \quad D_y^{\pm} \neq 0, \quad D_z = 0, \quad E_z = 0;$$

and in the first approximation we find

$$\frac{D_y}{D_x} = i, \quad n'^2_+ = n_+^2 + \frac{(n_+^2 - g)^2 HG_z^+}{d + (n_+^2 - g)^2},$$

$$n'^2_- = n_-^2 + H\frac{(n_-^2 - g)^2 G_z^-}{d + (n_-^2 - g)^2},$$

$$\frac{D_y}{D_x} = -i, \quad n''^2_+ = n_+^2 - H\frac{(n_+^2 - g)^2 G_z^+}{d + (n_+^2 - g)^2},$$

$$n''^2_- = n_-^2 - H\frac{(n_-^2 - g)^2 G_z^-}{d + (n_-^2 - g)^2}.$$

The specific rotation of the plane of polarization is determined in this case by the formula

$$\vartheta_{\pm} = H\frac{\pi(n_{\pm}^2 - g)^2 G_z^{\pm}}{[d + (n_{\pm}^2 - g)^2]\lambda_0 n_{\pm}}$$

and the Verdet constant has the form

$$R_{\pm} = \frac{\pi(n_{\pm}^2 - g)^2 G_z^{\pm}}{[d + (n_{\pm}^2 - g)^2]\lambda_0 n_{\pm}},$$

moreover all the conclusions made previously concerning the propagation of light in cubic crystals remain in force here as well.

Analogously, one may consider the propagation of light near the region of excition absorption in crystals of other symmetries, where the Oz axis is directed perpendicular to the axis of highest order; in all these cases the polarization turns out to be elliptical rather than circular. All these cases, as well as the Cotton-Muton effect, are considered in reference [2] and we will not consider them further here.

In conclusion I extend thanks to A. S. Davydov for valuable discussions and interest in this work.

December 15, 1958

References

1. A. S. DAVYDOV: The Theory of the Absorption of Light in Molecular Crystals. Akad. NAUK, UKR SSR Press, Kiev, 1951
2. A. F. LUBCHENKO: UFZh, 4, 183, (1959)
3. A. F. LUBCHENKO: OiS, 1, 867 (1956)
4. A. F. LUBCHENKO AND E. I. RASHBA: OiS, 4, 580, (1958)
5. A. F. LUBCHENKO: OiS, 5, 404, (1958)
6. E. TITCHMARSH: Theory of Functions.
7. A. S. DAVYDOV, A. F. LUBCHENKO: ZETF, 36, 1499, (1958) (See: Sov.Phys. JETP)
8. S. I. PEKAR: ZETF, 33, 1022, (1957) (See: Sov. Phys. JETP).

TOM VII, Vyp. 3
VOL. VII, No. 3

OPTIKA I SPEKTROSKOPIIA
OPTICS AND SPECTROSCOPY

Sentiabr', 1959
September, 1959

Theory of the Linear Kerr Effect in the Region of Exciton Absorption of Light by Molecular Crystals

A. F. LUBCHENKO

Abstract: A theory is developed of the linear Kerr effect for molecular crystals in which excitons are formed when there is a weak coupling between exciton excitation and lattice vibrations and an arbitrary value of the absorption coefficient. Equations have been obtained which determine the propagation of light in the region of exciton absorption in a constant uniform external electric field; the third rank tensor has been calculated which specifies the optical anisotropy, and also the value of the double refraction for crystals of cubic and medium symmetry when light propagation is along the direction of the external electric field parallel to the axis of the highest order.

CRYSTAL POLARIZATION DEPENDENT ON AN ELECTROMAGNETIC FIELD WHEN THERE IS A CONSTANT UNIFORM EXTERNAL ELECTRIC FIELD

The constant uniform electric field in which the crystal is placed causes a change in the wave functions of the molecules of this crystal. This change may be calculated by the usual methods of perturbation theory in which it is necessary to take into consideration that the cosine of the angle (ϕ_α) between the direction of the field and the direction of the transition dipole moments for the various molecules of the elementary unit cell will vary. Therefore we will separate all the molecules of the elementary unit cell into groups, for each of which cos ϕ_α has the same value. We will designate these groups by the letter $\alpha = 1,2\ldots$, while the molecules within the group we will number $\rho_\alpha = 1, 2 \ldots \sigma_\alpha$; the whole number of molecules $\sigma = \sum_\alpha \sigma_\alpha$. Now, if $\bar{\varphi}^{l}_{\vec{n}\rho_\alpha}$ designates the wave function of the isolated molecule when there is no external electric field, then when there is one, the wave function $\psi^{lf}_{\vec{n}\rho_\alpha}$ of this same molecule is written as*

$$\psi^{lf}_{\vec{n}\rho_\alpha} = \bar{\varphi}^{lf}_{\vec{n}\rho_\alpha} + \sum_{l} \left(\vec{E} c^{l}_{\vec{n}\rho_\alpha f} \right) \bar{\varphi}^{l}_{\vec{n}\rho_\alpha}. \tag{1}$$

Here l (l_o, ...) is the complete set of quantum numbers which characterize the states of the molecule (to simplify matters we will consider these states as non-degenerate), f is one of the possible values of l, $\vec{E}$ is the effective value of the intensity of the electric field, $c^{l}_{\vec{n}\rho_\alpha f}$ is the constant (for a given l and f) of the first order approximation, which determines the correction for the wave function $\bar{\varphi}^{f}_{\vec{n}\rho_\alpha}$, dependent on the field $\vec{E}$ (which is linked to the transition dipole moment in the $\vec{n}\rho_\alpha$-th molecule).

The Hamiltonian of the crystal, consisting of N unit cells, when there is an external electric field, takes the form

$$\vec{H}_o = \vec{T}_R + \sum_{\vec{n}\rho_\alpha} \vec{H}_{\vec{n}\rho_\alpha} \left(\vec{r}\, \frac{\partial}{\partial \vec{r}} \right) + \frac{1}{2} \sum_{\vec{n}\rho_\alpha, \vec{m}\rho_\beta}{}' V_{\vec{n}\rho_\alpha, \vec{m}\rho_\beta} - \sum_{\vec{n}\rho_\alpha, i} e_i (\vec{E}\vec{r}_{\vec{n}\rho_\alpha i}). \tag{2}$$

Here $\vec{T}_R = -\frac{h^2}{2M} \sum_{\vec{n}\rho_\alpha} \Delta_{\vec{n}\rho_\alpha}$ is the operator for the translation and rotation vibrations of the molecules of the crystal, $\vec{H}_{\vec{n}\rho_\alpha} \left(\vec{r}\, \frac{\partial}{\partial \vec{r}} \right)$ is the Hamiltonian for the free molecule, $V_{\vec{n}\rho_\alpha, \vec{m}\rho_\beta}$ is the operator of the interaction energy of the molecules $\vec{n}\rho_\alpha$ and $\vec{m}\rho_\beta$, e_i is the charge, $\vec{r}_{\vec{n}\rho_\alpha i}$ is the radius vector of the i-th charge, M is the mass of the molecule; the prime on the symbol for the sum (here and in the following on the symbol of the product) indicates that $\vec{n}\rho_\alpha \neq \vec{m}\rho_\beta$. Solution of the equation

$$(\vec{H}_o + W)\, \psi = U \psi,$$

where W is the exciton-phonon interaction operator, can be carried out in precisely the same way as was done in Reference [1]; here the wave functions ψ of the non-degenerate states of the crystal and the energy values corresponding to them, are written as

a) for the ground (l_o) state

$$\psi^{l_o}_{[n_s]} = [(S\sigma N)!]^{-\frac{1}{2}} \sum_{\nu} (-)^{P_\nu} \prod_{\vec{n}\rho_\alpha} \psi^{l}_{\vec{n}\rho_\alpha} \prod_{s} f_{n_s}(t_s)\, \chi \exp\left[-\frac{it}{h} U^{l_o}_{[n_s]} \right], \tag{3}$$

$$U^{l_o}_{[n_s]} = \sum_{\vec{n}\rho_\alpha} E^{l_o}_{\vec{n}\rho_\alpha}(\vec{E}) + V_o + \sum_{s} h\omega_s \left(n_s + \tfrac{1}{2} \right)$$

b) for the excited (single-exciton) state

$$\psi^{f\mu}_{[n_s]}(\vec{k}) = [\sigma_\alpha N(S\sigma N)!]^{-\frac{1}{2}} \sum_{\vec{n}\rho_\alpha} B^{f\mu}_{\vec{n}\rho_\alpha}(\vec{k})\, \chi$$

* We consider the functions $\bar{\varphi}^{l}_{\vec{n}\rho_\alpha}$ to be real.

$$\chi\Big[\sum_{\nu}^{\nu}(-)\,P_\nu \psi^{f}_{\vec{n}\rho_\alpha}\prod_{\vec{n}\rho_\beta}{}' \psi_{\vec{n}\rho_\beta}\Big]\chi$$

(4)

$$\chi\prod_s f_{n_s}(\xi_s)\exp\Big[\vec{i}\vec{k}\vec{n} - \frac{it}{\hbar}U^{f\mu}_{[n_s]}(\vec{k})\Big]$$

$$U^{f\mu}_{[n_s]}(\vec{k}) = \sum_{\vec{n}\rho_\beta} E^{1_0}_{\vec{n}\rho_\beta}(\vec{E}) + \Delta E^{f}_{\vec{n}\rho_\alpha} + V_0 + D^{f}_{\vec{n}\rho_\alpha}(0) +$$

$$+ \epsilon^{f}_{\mu}(\vec{k}) + \sum_s \hbar\omega_s\,(n_s + \tfrac{1}{2})$$

Here $f_{n_s}(\xi_s)$ are the wave functions which describe the vibrations of the crystal lattice (they are selected as functions of the harmonic oscillators, ξ_s are the normal coordinates, n_s are the quantum numbers of the lattice vibrations; the symbol $[n_s]$ designates the complete set of quantum numbers n_s which characterize the vibratory state of the crystal), ω_s are the natural frequencies of the vibrations of the crystal lattice, S is the number of electrons in the molecule, P_ν is one of the possible $(S\sigma N)!$ permutations of the electron pairs, $E^{1_0}_{\vec{n}\rho_\alpha}$, $E^{f}_{\vec{n}\rho_\alpha}$ are, respectively, the energy of the ground and the f-th excited state of the molecule*, $\Delta E^{f}_{\vec{n}\rho_\alpha} = E^{f}_{\vec{n}\rho_\alpha} - E^{1_0}_{\vec{n}\rho_\alpha}$, $D^{f}_{\vec{n}\rho_\alpha}(0)$ is the difference of the interaction energy of the excited and unexcited $\vec{n}\rho_\alpha$ molecule from all the rest, when all the molecules of the crystal are in equilibrium, $\epsilon^{f}_{\mu}(\vec{k})$ is the addition to the excitation energy of the crystal which arises as a result of resonance interaction between the molecules in a state of equilibrium, V_0 is the zero term of the power series expansion of the potential energy of the crystal in deviations of the molecules from the equilibrium position (both here and in the previous cases we have in mind equilibrium positions corresponding to an unexcited state of the crystal), μ is the number of the exciton band, $\vec{k}$ is the reduced wave vector, $B^{f\mu}_{\rho_\alpha}(\vec{k}) = B^{*f\mu}_{\rho_\alpha}(-\vec{k})$ are coefficients determined by Eq. (3.15) of Ref. [1] and are normalized so that

$$\sum_{\alpha\rho_\alpha} B^{f\mu'}_{\rho_\alpha}(\vec{k})\,B^{*f\mu}_{\rho_\alpha}(\vec{k}) = \sigma\delta_{\mu\mu'},$$

$$\sum_{\mu} B^{f\mu}_{\rho_\alpha}(\vec{k})\,B^{f\mu}_{\rho_\beta}(\vec{k}) = \sigma\delta_{\rho_\alpha\rho_\beta}.$$

*They are solutions of the equation

$$\Big[H_{\vec{n}\rho_\alpha}\Big(r\,\frac{\partial}{\partial r}\Big) - \sum_i e_i\Big(\vec{E}r_{\vec{n}\rho_\alpha i}\Big)\Big]\varphi^{f}_{\vec{n}\rho_\alpha}E^{f}_{\vec{n}\rho_\alpha}(\vec{E})\psi^{f}_{\vec{n}\rho_\alpha}.$$

We assume now that at the time $t = 0$ there falls on the crystal a plane electromagnetic wave whose field intensity in the crystal is given by the expression

$$\vec{E} = \tfrac{1}{2}\vec{E}_0\exp\,[i(\vec{Q}\vec{r} - \omega t)] + \tfrac{1}{2}\vec{E}^{*}_0\exp\,[-i(\vec{Q}^{*}\vec{r} - \omega t)] \equiv \vec{E}_1 + \vec{E}^{*}_1$$

where $\vec{Q} = \dfrac{\omega(n + i\kappa)}{c}\vec{s}$, $\vec{s}$ is the unit vector of the wave normal, n is the index of refraction, and κ is the absorption coefficient. Then the operator of the interaction energy of this wave with the crystal is written as

$$\vec{H}' = -\sum_{\vec{n}\rho_\alpha i}\frac{e_i}{M_i c}\chi\vec{A}_{\vec{n}\rho_\alpha i}\vec{P}_{\vec{n}\rho_\alpha i},$$

where $\vec{P}_{\vec{n}\rho_\alpha i}$ is the momentum of the ith charge of the $\vec{n}\rho_\alpha$-th molecule, $\vec{A}_{\vec{n}\rho_\alpha i}$ is the value of the vector potential at the location of this charge, χ is a tensor taking into consideration the difference of the transverse field acting on the molecule from the mean macroscopic field, and c is the velocity of light in a vacuum. Under the influence of the electromagnetic perturbation, the crystal makes the transition to an excited state whose wave function is given by the equation

$$i\hbar\frac{\partial F}{\partial t} = (\vec{H}_0 + W + \vec{H}')\,F \tag{5}$$

We seek a solution of the latter in the form

$$F = b^{1_0}_{[n_s]}\Psi^{1_0}_{[n_s]} + \sum_{f'\mu'k'[n'_s]\,(f'\neq 1_0)} b^{f'\mu'}_{[n'_s]}(\vec{k}')\,\chi$$

$$\chi\,\Psi^{f'\mu'}_{[n'_s]}(\vec{k}')\exp\,[-\Gamma^{f'}_{\mu'}t] + \sum_\lambda c_\lambda\Psi_\lambda. \tag{6}$$

Here $b^{f\mu}_{[n_s]}$ are time-dependent probability amplitudes, Ψ_λ are wave functions describing all possible excited states except the single-exciton state. Now, substituting (5) in (6), we multiply the expression obtained on the left by F^{*} and integrate the product obtained over all the variables of the system. Then, if we take into consideration that $b^{f\mu}_{[n_s]} = \delta_{f1_0}$ when $t = 0$, we obtain

$$b^{f\mu}_{[n_s]}(\vec{k}) = \frac{(f_\mu\vec{k}n_s|H'|000n_s)}{fh}\exp\,[+\Gamma^{f}_{\mu}t].$$

The matrix element $(f_\mu\vec{k}n_s|H'|000n_s)$ can easily be calculated if the vector potential is expanded in a Fourier series and, neglecting the optical activity, we put $\vec{Q}\vec{r}_{\vec{n}\rho_\alpha i} \simeq \vec{Q}\vec{n}$ on the basis of the Riemann-Lebesgue [2] theorem. Then we obtain the following expression for the function (6)

$$F = \Psi^{1_0}_{[n_s]} +$$

$$+\left(\frac{N}{\sigma}\right)^{\frac{1}{2}} \sum_{f_\mu \alpha \rho_\alpha \vec{q}} \frac{B^{f_\mu}_{\rho_\alpha} \Omega_{f_\mu}(\vec{q}) \left(\chi \vec{E}_0^* \cdot \vec{\mathscr{P}}^{f1_0}_{\rho_\alpha}\right) \exp\left\{it[\Omega_{f_\mu}(\vec{q})-\omega]\right\}}{2L\beta_1\beta_2\beta_3 \hbar\omega\, [\Omega_{f_\mu}(\vec{q}) - \omega - i\Gamma^{f}_{\mu}]}$$

$$\Psi^{f_\mu}_{[n_s]}(\vec{q}) - \tag{7}$$

$$-\left(\frac{N}{\sigma}\right)^{\frac{1}{2}} \sum_{f_\mu \alpha \rho_\alpha \vec{q}} \frac{B^{f_\mu}_{\rho_\alpha} \Omega_{f_\mu}(\vec{q}) \left(\chi \vec{E}_0^* \cdot \vec{\mathscr{P}}^{f1_0}_{\rho_\alpha}\right) \exp\left\{it[\Omega_{f_\mu}(\vec{q})+\omega]\right\}}{2L\beta_1\beta_2\beta_3 \hbar\omega\, [\Omega_{f_\mu}(\vec{q}) + \omega - i\Gamma^{f}_{\mu}]}$$

$$\Psi^{f_\mu}_{[n_s]}(\vec{q}) + \sum_{\lambda} c_\lambda \Psi_\lambda .$$

Here $q_j = \frac{2\pi}{L_j}\eta_j$; $\eta_j = 0, \pm 1, \pm 2\ldots$; $j = 1,2,3$; L_j are the dimensions of the primary region of the crystal along the axes ox_j; $L = L_1L_2L_3$; $\beta_j = Q_j - q_j$; $\beta'_j = -Q^*_j - q_j$; $\hbar\,\Omega_{f_\mu}(\vec{q}) \equiv U_{f_\mu}(\vec{q}) = U^{f_\mu}_{[n_s]}(\vec{q}) - U^{1_0}_{[n_s]}$; $\vec{\mathscr{P}}^{f1_0}_{\rho_\alpha} = \left\langle \Psi^{f}_{\vec{n}\rho_\alpha} \middle| \sum_i e_i \vec{r}_{\vec{n}\rho_\alpha i} \middle| \Psi^{1_0}_{\vec{n}\rho_\alpha} \right\rangle$; $B^{f_\mu}_{\rho_\alpha}$ is the zero term of the expansion of $B^{f_\mu}_{\rho_\alpha}(\vec{q})$ in a series in $\vec{q}$.

Using Eq. (7), we calculate the electrical dipole moment per unit volume of the crystal $\vec{P}$, which is induced by the electromagnetic perturbation

$$\vec{P}(\vec{m}) = \left\langle F^* \middle| \vec{\mathscr{P}}(\vec{m}) \middle| F \right\rangle - \left\langle \Psi^{1_0}_{[n_s]} \middle| \vec{\mathscr{P}}(\vec{m}) \middle| \Psi^{1_0}_{[n_s]} \right\rangle ,$$

where

$$\vec{\mathscr{P}}(\vec{m}) = \frac{1}{\delta\Lambda^3\Delta} \sum_{\vec{n}\rho_\alpha} e_i(\vec{r}_{\vec{n}\rho_\alpha i} - \vec{m})\, D(\vec{r}_{\vec{n}\rho_\alpha i} - \vec{m}),$$

(8)

$$D(\vec{r}_{\vec{n}\rho_\alpha i} - \vec{m}) = \begin{cases} 1, \text{ when } -\vec{A}_j\Lambda \leqslant (\vec{r}_{\vec{n}\rho_\alpha i} - \vec{m}) \leqslant \vec{A}_j\Lambda, \\ 0, \text{ in the whole remaining region,} \end{cases}$$

$\vec{A}_j$ are the basis vectors of the crystal lattice, $2\Lambda|\vec{A}_j| \ll \lambda$, λ is the wavelength of light in the crystal, and Δ is the volume of the elementary unit cell. On the basis of (7) we obtain from (8)

$$\vec{P}(\vec{m}) = \vec{P}_1(\vec{m}) + \vec{P}^*_1(\vec{m}),$$

where

$$\vec{P}_1(\vec{m}) = \vec{P}_2(\vec{m}) +$$

(9)

$$+\frac{1}{\hbar\omega\Delta} \sum_{f_\mu \alpha\beta\rho_\alpha\rho_\beta} \frac{B^{f_\mu}_{\rho_\alpha} B^{f_\mu}_{\rho_\beta} \Omega_{f_\mu}(\vec{q}) \left(\chi \vec{E}_1 \cdot \vec{\mathscr{P}}^{f1_0}_{\rho_\alpha}\right) \vec{\mathscr{P}}^{1_0 f}_{\rho_\beta}}{\Omega_{f_\mu}(\vec{q}) - \omega - i\Gamma^{f}_{\mu}(\vec{q})} -$$

$$-\frac{1}{\hbar\omega\Delta} \sum_{f_\mu \alpha\beta\rho_\alpha\rho_\beta} \frac{B^{f_\mu}_{\rho_\alpha} B^{f_\mu}_{\rho_\beta} \Omega^*_{f_\mu}(-\vec{q}^*) \left(\chi \vec{E}_1 \cdot \vec{\mathscr{P}}^{f1_0}_{\rho_\alpha}\right) \vec{\mathscr{P}}^{1_0 f}_{\rho_\beta}}{\Omega^*_{f_\mu}(-\vec{q}^*) + \omega + i\Gamma^{*f}_{\mu}(-\vec{q}^*)}$$

$$\vec{P}_2(\vec{m}) = \left\langle \Psi^{1_0}_{[n_s]} \middle| \vec{P}(\vec{m}) \middle| \sum_\lambda c_\lambda \Psi_\lambda \right\rangle .$$

In Eq. (9) the second sum is much smaller than the first in the neighborhood of the absorption region, therefore we will neglect it in future. The first sum, if we take into consideration that

$$\vec{\mathscr{P}}^{f1_0}_{\rho_\alpha} = \vec{P}^{f1_0}_{\rho_\alpha} + \eta^{f1_0}_{\rho_\alpha} \vec{E},$$

where

$$\vec{P}^{f1_0}_{\rho_\alpha} = \left\langle \bar{\Psi}^{f}_{\vec{n}\rho_\alpha} \middle| \sum_i e_i \vec{r}_{\vec{n}\rho_\alpha i} \middle| \bar{\Psi}^{1_0}_{\vec{n}\rho_\alpha} \right\rangle,$$

$$\vec{P}^{11_0}_{1\rho_\alpha} = \left\langle \bar{\Psi}^{1}_{\vec{n}\rho_\alpha} \middle| \sum_i e_i \vec{r}_{\vec{n}\rho_\alpha i} \middle| \bar{\Psi}^{1_0}_{\vec{n}\rho_\alpha} \right\rangle,$$

$$\vec{P}^{f1}_{2\rho_\alpha} = \left\langle \bar{\Psi}^{f}_{\vec{n}\rho_\alpha} \middle| \sum_i e_i \vec{r}_{\vec{n}\rho_\alpha i} \middle| \bar{\Psi}^{1}_{\vec{n}\rho_\alpha} \right\rangle,$$

$$\eta^{f1_0}_{\rho_\alpha} = \sum_i \left[\vec{P}^{11_0}_{1\rho_\alpha} \vec{c}^{1}_{\vec{n}\rho_\alpha i} + \vec{P}^{f1}_{2\rho_\alpha} \vec{c}^{1}_{\vec{n}\rho_\alpha 1_0} \right]$$

is a second rank tensor, can be written so that its explicit dependence on the field intensity $\vec{E}$ is apparent. Thus, the expression for $\vec{P}_1(m)$ may be rewritten as

$$\vec{P}_1(\vec{m}) = \vec{P}_2(\vec{m}) +$$

$$+\frac{1}{\hbar\omega\Delta} \sum_{f_\mu \alpha\beta\rho_\alpha\rho_\beta} \frac{B^{f_\mu}_{\rho_\alpha} B^{f_\mu}_{\rho_\beta} \Omega_{f_\mu}(\vec{q}) \left(\chi \vec{E}_1 \cdot \vec{P}^{f1_0}_{\rho_\alpha}\right) \vec{P}^{f1_0}_{\rho_\beta}}{\Omega_{f_\mu}(\vec{q}) - \omega - i\Gamma^{f}_{\mu}(\vec{q})} +$$

(10)

$$+\frac{1}{\hbar\omega\Delta} \sum_{f_\mu \alpha\beta\rho_\alpha\rho_\beta} X$$

$$\times \frac{B^{f\mu}_{\rho_\alpha} B^{f\mu}_{\rho_\beta} \eta_{f\mu}(\vec{q}) \left\{ (\chi\vec{E}_1 \cdot \eta^{f1_0}_{\rho_\alpha}\vec{e})\, \vec{P}^{f1_0}_{\rho_\beta} + (\chi\vec{E}_1 \cdot \vec{P}^{f1_0}_{\rho_\alpha})\eta^{f1_0}_{\rho_\beta}\vec{e} \right\}}{\Omega_{f\mu}(\vec{q}) - \omega - i\Gamma^{f}_{\mu}(\vec{q})}$$

We assume further

$$\frac{1}{\sqrt{\sigma\Delta}} \sum_{\alpha\rho_\alpha} B^{f\mu}_{\rho_\alpha} \vec{P}^{f1_0}_{\rho_\alpha} = \vec{P}^{f1_0}_{\mu},$$

$$\frac{1}{\sqrt{\sigma\Delta}} \sum_{\beta\rho_\beta} B^{f\mu}_{\rho_\beta} \vec{P}^{f1_0}_{\rho_\beta} = \vec{P}^{f1_0}_{\mu},$$

$$\frac{1}{\sqrt{\sigma\Delta}} \sum_{\alpha\rho_\alpha} B^{f\mu}_{\rho_\alpha} \eta^{f1_0}_{\rho_\alpha} = \eta^{f1_0}_{\mu},$$

$$\frac{1}{\sqrt{\sigma\Delta}} \sum_{\beta\rho_\beta} B^{f\mu}_{\rho_\beta} \eta^{f1_0}_{\rho_\beta} = \eta^{f1_0}_{\mu},$$

$$\frac{\Omega_{\vec{s}f\mu}}{\omega} \vec{P}^{f1_0}_{\mu} \vec{P}^{f1_0}_{\mu} = a^{f}_{\vec{s}\mu},$$

$$\frac{\Omega_{\vec{s}f\mu}}{\omega} \left[\vec{P}^{f1_0}_{\mu} \left(\eta^{f1_0}_{\mu}\vec{E} \right) + \left(\eta^{f1_0}_{\mu}\vec{e}\vec{E} \right) \vec{P}^{f1_0}_{\mu} \right] = \zeta^{f}_{\vec{s}\mu},$$

where $\Omega_{\vec{s}f\mu}$ is the zero term of the expansion of $\Omega_{f\mu}(\vec{q})$ in the power series in $\vec{q}$. Then Eq. (10) may be rewritten as

$$\vec{P}_1(\vec{m}) = \vec{P}_2(\vec{m}) + \sum_{f\mu} \frac{(a^{f}_{\vec{s}\mu} + \zeta^{f}_{\vec{s}\mu})(\chi\vec{E}_1)}{U_{f\mu}(\vec{q}) - h\omega - ih\Gamma^{f}_{\mu}(\vec{q})}.$$

It is easy to see that the second rank tensor $\zeta^{f}_{\vec{s}\mu}$, which is the sum of the two dyads constructed from the vectors $\vec{P}^{f1_0}_{\mu}$ and $\eta^{f1_0}_{\mu}\vec{E}$, is symmetric with respect to the permutations of $\vec{P}^{f1_0}_{\mu}$ and $\eta^{f1_0}_{\mu}\vec{E}$; the tensor $a^{f}_{\vec{s}\mu}$ is also symmetric; the values of the components of these tensors depend on the direction of the wave normal $\vec{s}$.

Now we propose that the band $f'\mu'$, in which we are examining the transitions, is located far from the remaining bands, so that virtual transitions in these bands introduce an additional contribution of magnitude ϵ and Ξ to the tensor of the dielectric permeability and the tensor arising from the linear Kerr effect, respectively, where ϵ and Ξ depend slightly on frequency. Then, setting

$$\vec{P}_2(\vec{m}) + 4\pi \sum_{f\mu \neq f'\mu'} \frac{(a^{f}_{\vec{s}\mu} + \zeta^{f}_{\vec{s}\mu})(\chi\vec{E}_1)}{U_{f\mu}(\vec{q}) - h\omega - ih\Gamma^{f}_{\mu}(\vec{q})} =$$

$$= \frac{\epsilon - 1}{4\pi}\vec{E}_1 + \frac{1}{4\pi}\Xi\vec{E}_1,$$

we can write the induction vector $\vec{D}_1 = \vec{E}_1 + 4\pi\vec{P}_1$ as*

$$D_i = \epsilon_{fk}E_k + \Xi_{fk}E_k + \frac{4\pi(a_{\vec{s}fk} + \zeta_{\vec{s}fk})(\chi\vec{E})_k}{U(\vec{q}) - h\omega - ih\Gamma(\vec{q})}.$$

Limiting ourselves in future to crystals of high and middle symmetry, we will consider that the external electric field is directed along one of the symmetry axes, which we will take as the axis Oz; then only the third component of the external electrical field $\mathcal{E}_3$ will be other than zero. The tensors Ξ and ζ will thus be written as

$$\Xi_{fk} = G_{fk3}\,\mathcal{E}_3,$$

$$\zeta_{fk} = \Lambda'_{fk3}\,\mathcal{E}_3 = P_f\eta_{k3}\,\mathcal{E}_3 + P_k\eta_{f3}\,\mathcal{E}_3,$$

and the components of the induction vector will be defined by the expression

$$(11) \qquad D_i = (\epsilon_{fk} + G_{fk3}\mathcal{E}_3)E_k + \frac{4\pi(a_{fk} + \Lambda'_{fk3}\mathcal{E}_3)(\chi\vec{E})_k}{U(\vec{q}) - h\omega - ih\Gamma(\vec{q})}.$$

Now, using the effective mass, and setting

$$U(\vec{q}) = U_{\vec{s}} + \frac{h^2\omega^2}{2M_{\vec{s}}c^2}(n + i\kappa)^2,$$

where $M_{\vec{s}}$ is conditionally designated the effective mass of the exciton in the direction $\vec{s}$. Then, introducing the notation

$$\frac{2M_{\vec{s}}c^2}{h\omega}\left(1 - \frac{U_{\vec{s}}}{h\omega}\right) = g_{\vec{s}};\ \frac{2M_{\vec{s}}c^2}{h^2\omega^2}a_{\vec{s}} = d^{\vec{s}};\ \Gamma = \gamma_1 + i\gamma_2,$$

$$\frac{2M_{\vec{s}}c^2}{h\omega^2}\gamma_2 = \theta_{\vec{s}};\ \frac{8\pi M_{\vec{s}}c^2}{h^2\omega^2}\Lambda'_{fk3}\,\mathcal{E}_3 = \Lambda^{\vec{s}}_{fk3}\,\mathcal{E}_3,$$

$$\frac{2M_{\vec{s}}c^2}{h\omega^2}\left(\gamma_1 - \frac{h\omega^2}{M_{\vec{s}}c^2}n\kappa\right) = \rho_{\vec{s}},$$

we rewrite (11) as

$$(12) \qquad D_i = (\epsilon_{fk} + G_{fk3}\mathcal{E}_3)E_k +$$

$$+ \frac{(n^2 - \kappa^2 - g_{\vec{s}} + \theta_{\vec{s}} + i\rho_{\vec{s}})(d^{\vec{s}}_{fk} + \Lambda^{\vec{s}}_{fk3}\mathcal{E}_3)(\chi\vec{E})_k}{(n^2 - \kappa^2 - g_{\vec{s}} + \theta_{\vec{s}})^2 + \rho^2_{\vec{s}}}.$$

The latter expression, together with the Maxwell equation for plane waves

$$(13) \qquad \vec{D} = (n + i\kappa)^2[\vec{E} - \vec{s}(\vec{s}\vec{E})]$$

determines the propagation of light in crystals when there is a constant uniform external electric field

* Here we have omitted the subscripts $f'\mu'$ and the 1, indicating that only the amplitudes $\vec{D}$ and $\vec{E}$, standing in $e^{i(\vec{q}\vec{r} - \omega t)}$, are taken.

directed along the axis Oz. We note here that the third rank tensors G_{fk3} and Λ_{fk3} are symmetrical according to the two first subscripts and have the same characteristics as the piezo-electric tensors [3]. Therefore the linear Kerr effect will exist in the same 20 classes of crystals which have piezo-electric characteristics.

THE LINEAR KERR EFFECT

We will consider the optical properties of crystals of high and middle symmetry in a constant uniform external electrical field near the region of exciton absorption of light, assuming in all cases that the unit vector of the wave normal is directed along the field $\vec{E}$. Since in this region $\kappa = 0$, Eqs. (12) and (13) may be written as

$$D_f = (\epsilon_{fk} + G_{fk3}\mathcal{E}_3)E_k + \frac{(d_{fk} + \Lambda_{fk3}\mathcal{E}_3)(\chi\vec{E})_k}{n^2 - g}$$

$$\vec{D} = n^2[\vec{E} - \vec{s}(\vec{s}\vec{E})]. \tag{14}$$

Let us examine the solution of this equation.

Crystals of Cubic Symmetry. By virtue of the characteristics of the third rank tensor it will have components other than zero only for the classes T_d and T, where [4] $G_{231} = G_{132} = G_{123}$; therefore, if we consider that in the system of coordinates, whose axes are those of a cube [7], $d_{fk} = d\delta_{fk}$ $(d_{33} = 0)$, $\epsilon_{fk} = \epsilon\delta_{fk}$, the system (14) is written as

$$\left(n^2 - \epsilon - \frac{d}{n^2 - g}\right)D_1 + \left(G_{123}\mathcal{E}_3 + \frac{\Lambda_{123}\mathcal{E}_3}{n^2 - g}\right)D_2 = 0,$$
$$\left(n^2 - \epsilon - \frac{d}{n^2 - g}\right)D_2 + \left(G_{123}\mathcal{E}_3 + \frac{\Lambda_{123}\mathcal{E}_3}{n^2 - g}\right)D_1 = 0. \tag{15}$$

Equating the determinant of (15) to zero, we obtain

$$n^2 - \epsilon - \frac{d}{n^2 - g} = \pm\left(G_{123}\mathcal{E}_3 + \frac{\Lambda_{123}\mathcal{E}_3}{n^2 - g}\right). \tag{16}$$

Far from the region of exciton absorption (where n^2 may be neglected in comparison to g), Eq. (16) has the solution*

$$n_1 = n_o + \frac{G_{123}\mathcal{E}_3}{2n_o},\ D_1^{(1)} \neq 0,\ D_2^{(1)} \neq 0,\ D_3 = 0,\ E_3 = 0,$$
$$n_2 = n_o - \frac{G_{123}\mathcal{E}_3}{2n_o},\ D_1^{(2)} \neq 0,\ D_2^{(2)} \neq 0,\ D_3 = 0,\ E_3 = 0, \tag{17}$$

where $n_o = \sqrt{\epsilon}$. If, following Born [5], we introduce a mean refractive index according to the formula

$$\bar{n} = \frac{2n_1 + n_2}{3}, \tag{18}$$

then, from (17) we obtain

$$\frac{n_2 - \bar{n}}{n_1 - \bar{n}} = -2, \tag{19a}$$

and the value for birefringence far from the absorption region will be determined by the expression

$$n_1 - n_2 = \frac{G_{123}\mathcal{E}_3}{n_o}. \tag{19b}$$

Near the region of exciton absorption, the solutions for Eq. (16) are

$$n'^2_{\pm} = \frac{g + \epsilon + G_{123}\mathcal{E}_3}{2} \pm$$
$$\pm\sqrt{\tfrac{1}{4}(g - \epsilon - G_{123}\mathcal{E}_3)^2 + (d + \Lambda_{123}\mathcal{E}_3)},\ D_1'^{\pm} \neq 0,$$
$$D_2'^{\pm} \neq 0,\ D_3 = 0,\ E_3 = 0,$$
$$n''^2_{\pm} = \frac{g + \epsilon - G_{123}\mathcal{E}_3}{2} \pm \tag{20}$$
$$\pm\sqrt{\tfrac{1}{4}(g - \epsilon + G_{123}\mathcal{E}_3)^2 + (d - \Lambda_{123}\mathcal{E}_3)},\ D_1''^{\pm} \neq 0,$$
$$D_2''^{\pm} \neq 0,\ D_3 = 0,\ E_o = 0,$$

and the value of birefringence is given by the formulas

$$\Delta n_+ = n'_+ - n''_+ =$$
$$= \frac{G_{123}\mathcal{E}_3}{2n_+} - \frac{\tfrac{1}{2}(g - \epsilon)G_{123}\mathcal{E}_3 - \Lambda_{123}\mathcal{E}_3}{(2n_+)\sqrt{\tfrac{1}{4}(g - \epsilon)^2 + d}}$$
$$\Delta n_- = n'_- - n''_- = \tag{21}$$
$$= \frac{G_{123}\mathcal{E}_3}{2n_-} + \frac{\tfrac{1}{2}(g - \epsilon)\,G_{123}\mathcal{E}_3 - \Lambda_{123}\mathcal{E}_3}{(2n_-)\sqrt{\tfrac{1}{4}(g - \epsilon)^2 + d}}.$$

Introducing into Eq. (18) the mean index of refraction $\bar{n}_\pm$, it is easy to show that

$$\frac{n''_+ - \bar{n}_+}{n'_+ - \bar{n}_+} = -2,\quad \frac{n''_- - \bar{n}_-}{n'_- - \bar{n}_-} = -2. \tag{22}$$

From the solutions (17) and (20), it follows that the axis Oz along which the external electrical field is directed is at the same time the axis Oz of a three-axis ellipsoid, so that a crystal of cubic symmetry placed in a constant external electrical field becomes, in optical respects, bi-axial. When the effective mass of the exciton is positive, toward the red from the absorption region part of the spectrum, the indexes of refraction n'_+ and n''_+ have a physical sense (in this region n'^2_- and $n''^2_- < 0$);

---

* The sums of ϵ and G_{123} (16) with $\frac{d}{g}$ and $\frac{\Lambda_{123}}{g}$ respectively should be understood in ϵ and G_{123} here.

the waves with indexes of refraction n' and n'' exist in the crystal only for those frequencies which fulfill the condition

$$g > \frac{d + \Lambda_{123}\mathcal{E}_3}{\epsilon + G_{123}\mathcal{E}_3}.$$

When the effective mass of the exciton is negative near the region of strong absorption, by virtue of the peculiarities of the behavior of $\Gamma(q)$ [6], the value of double refraction will be determined by Eq. (19).

Crystals of Middle Symmetry (Trigonal, Tetragonal, Hexagonal).

We will now consider crystals of middle symmetry, assuming that the axis Oz (and therefore also the field $\mathcal{E}$) are directed along the axis of symmetry of highest order (C_3, C_4, C_6). Paying attention to the nature of the transformation of the components of the third rank tensor * h_{fkl} in transformations of symmetry, we may expect a linear Kerr effect in the crystallic classes S_4, C_4, D_{2d}, D_4, C_{4v}, C_3, D_3, C_{3h}, C_{3v}, D_{3h}, C_6, D_6, C_{6v}, while if we take into consideration the values of the components h_{fkl} [4], and the fact that the field is directed along Oz, then we may say at once that with a given direction of field $\mathcal{E}$, the linear Kerr effect will not be observed in crystal classes D_4, D_3, C_{3h}, D_{3h}, D_6, since all the components of the tensor which have the third subscript three, are zero, i. e., $h_{fk3} \equiv 0$, $f, k = 1, 2, 3$.

In the class D_{2d} only the components $h_{231} = h_{132} \neq h_{123}$ are not zero. Since only the component h_{123} enters into the equation for determining the values of the index of refraction, in the transition from the ground state to a state whose wave function is transformed according to the same irreducible presentation as are the x, y components of the polar vector ($\tau_0 \to \tau_{xy}$), Eqs. (20-22) hold good since [7] $d = d_1 \begin{pmatrix} 1&0&0\\0&1&0\\0&0&0 \end{pmatrix}$.

In the transition from the ground state to a state whose wave function is transformed according to the same irreducible presentation as is the z-component of the polar vector ($\tau_0 \to \tau_z$), we have

$$d = d_3 \begin{pmatrix} 0&0&0\\0&0&0\\0&0&1 \end{pmatrix},$$

therefore, in this case we use Eqs. (19a) and (19b).

In the remaining six crystal classes (except S_4), various components of the tensor differ from zero; however, inasmuch as in a given direction of field the optical behavior of the crystal is determined by the components h_{fk3}, and they differ from zero ($h_{113} = h_{223} \neq h_{333}$) for all these crystal classes, the optical properties of the crystals of all these classes will be identical in the given case.

We will consider the transition $\tau_0 \to \tau_z$. Since [7]:

$$d = d_3 \begin{pmatrix} 0&0&0\\0&0&0\\0&0&1 \end{pmatrix}, \quad \chi = \begin{pmatrix} 1&0&0\\0&1&0\\0&0&0 \end{pmatrix},$$

Eq. (14) is written as

$$(n^2 - \epsilon - G_{113}\mathcal{E}_3) D_1 = 0,$$

$$(n^2 - \epsilon - G_{113}\mathcal{E}_3) D_2 = 0,$$

$$E_3 = 0;$$

from which

$$n^2 = \epsilon + G_{113}\mathcal{E}_3, \quad D_1 \neq 0, \tag{23}$$

$$D_2 \neq 0, \; D_3 = 0, \; E_3 = 0.$$

For the transition $\tau_0 \to \tau_{xy}$

$$d = d_1 \begin{pmatrix} 1&0&0\\0&1&0\\0&0&0 \end{pmatrix}, \quad \chi = \begin{pmatrix} 1&0&0\\0&1&0\\0&0&0 \end{pmatrix},$$

and Eq. (14) takes the form

$$\left(n^2 - \epsilon - G_{113}\mathcal{E}_3 - \frac{d + \Lambda_{113}\mathcal{E}_3}{n^2 - g}\right) D_1 = 0,$$

$$\left(n^2 - \epsilon - G_{223}\mathcal{E}_3 - \frac{d + \Lambda_{223}\mathcal{E}_3}{n^2 - g}\right) D_2 = 0,$$

$$E_3 = 0;$$

and its solution is written as

$$n^2_{\pm} = \frac{g + \epsilon + G_{113}\mathcal{E}_3}{2} \pm \tag{24}$$

$$\pm \sqrt{\tfrac{1}{4}(g - \epsilon - G_{113}\mathcal{E}_3)^2 + d + \Lambda_{113}\mathcal{E}_3},$$

$$D_1^{\pm} \neq 0, \; D_2^{\pm} \neq 0, \; D_3 = 0, \; E_3 = 0.$$

From what has been stated above it follows that in an electric field directed along the axis of highest order, crystals of the classes C_4, C_{4v}, C_3, C_{3v}, C_6, C_{6v} remain uniaxial; the electric field causes only a change in the index of refraction, which is determined by Eqs. (23) and (24), depending on the value of $\mathcal{E}_3$.

In conclusion I thank A. S. Davydov for valuable discussions and interest in the work.

December 15, 1958

* By h_{fkl} we understand G_{fkl} and Λ_{fkl}.

References

1. A. S. DAVYDOV: Teoriia pogloshcheniia sveta v molekuliarnykh kristallakh. (Theory of light absorption in molecular crystals.) Kiev, 1951.
2. E. TITCHMARSH: Theory of Functions. In English from Oxford University Press, London, New York, 1939. (GITTL, Moscow, 1951).
3. W. G. CADY: Piezoelectricity. McGraw-Hill Book Company, New York, 1946.
4. W. P. MASON: Piezoelectric Crystals and Their Application to Ultrasonics. D. Van Nostrand Company, New York, 1950.
5. M. BORN: Optik. J. Springer, Berlin, 1933. (DNTVU Kharkov, 1937).
6. A. S. DAVYDOV, A. F. LUBCHENKO: ZETF, 36, 1499, (1958). (See Sov. Physics JETP).
7. A. F. LUBCHENKO: UFZ, 3, 575, (1958); 4, (1959).

ТОМ VII, Вып. 3 ОПТИКА И СПЕКТРОСКОПИЯ Sentiabr', 1959
VOL. VII, No. 3 OPTICS AND SPECTROSCOPY September, 1959

The Optical Properties of Sublimed Bismuth in the 3-15 Micron Spectral Region

M. N. MARKOV AND I. S. LINDSTREM

Abstract: The optical properties (refractive index coefficients of absorption, transmission and reflection) were investigated in sublimed bismuth in the region from 3-15 microns. A method, based on interference in the infrared region, was developed for measurement of the optical constants of sublimed bismuth.

An investigation of the optical properties of comparatively thick sublimed metallic layers ($d > 0.1$ microns) is of great interest not only from the point of view of studying their structural peculiarities and their effects on the characteristics of the metal itself (concentration of conduction electrons, etc.), but also because such layers are widely used in practice for reflecting coatings and filters, as well as for radiation detectors. The study of the structure of such layers using electron microscopes is difficult because of the fact that high energy electron beams exert a strong influence on the sample [1], and the information on the structure of the surface layers obtained by using replicas in the investigation does not allow one to obtain information on the presence of fine details in the structure (for example, spaces between crystals, etc.). This circumstance lends special value to indirect methods of studying the structures of layers, connected with the effect of the latter on their physical properties.

In the work presented here, the optical properties of sublimed layers of bismuth were investigated in the 0.1 – 1.0 micron thickness range. Sublimed metallic bismuth layers are notable for a negative temperature coefficient of resistivity for any layer thickness practically obtainable, and also for substantial changes in its electrical properties in the presence of very small (~ 0.1-1%) metallic impurities. This indicates that, in some respects, the layers are analogous to semiconductors, even though their conductivity is higher than that of the majority of semiconducting materials. The selected interval of thickness was interesting since the density of such layers is almost equal to the density of bulk bismuth, and the value of the resistivity, even though larger than in the bulk metal, does not depend on the layer thickness in this region. [2]. The value of the temperature coefficient of resistivity also almost does not depend on the thickness, [3].

METHOD OF MEASUREMENT

The investigated bismuth layers were obtained by vacuum evaporation on glass, rock salt, and nitrocellulose substrates. The evaporation was made with tantalum ribbons positioned at a distance of 15 cm. from the samples. The evaporation temperature was maintained at about 700° C, which ensured an average rate of evaporation of 2-3 Å per second, at a vacuum of $1 - 2 \times 10^{-5}$ mm Hg. The material evaporated was bismuth containing impurities (according to the certificate) of less than 0.01% by weight. A spectral analysis made of the bismuth in the sublimed layers showed that in the process of evaporation the bismuth was purified and the amount of impurities decreased to approximately 10^{-3} %.

Preliminary investigations showed that the layers which were studied were sufficiently transparent in the infrared region of the spectrum and, in addition, distinct interference patterns were obtained, with transmitted, as well as reflected, rays, and were analysed with the help of a double beam infrared spectrometer. The amplitude of the interference maxima in the 3-15 μ region was quite large, which points to a large value of the refractive index n and a small value of the absorption coefficient κ. This circumstance was used to determine the optical constants. In our method, the value of n is determined from the position of the interference maxima and an independent measurement of the thickness of the layers. The quantity κ is calculated from the value of n and the measured reflection or transmission coefficient for a given wave length.

A multibeam interferometer method was used for measurement of the thickness. For this purpose, an arrangement, similar to that described in reference [4] was constructed. Bismuth was sublimed onto two rows of plates, one of which served for measurement of the thickness, and the other for obtaining reflection and transmission spectra. On one half of the plates, intended for measurements of the thickness, bismuth was deposited, and then a thin layer of silver was deposited on the whole plate (also by an evaporation method). This plate was then used as one of the plates of a multibeam interferometer . Control experiments, carried out with this apparatus, showed that, by taking necessary precautions, namely, assuring sufficient homogeneity of the bismuth layers, as well as of the silver layers, the precision of the thickness measurement was of the order of 3-5% for thicknesses of 0.1-1.0 microns.

The transmission spectra (on rock-salt substrates) and reflection spectra (on rock-salt, glass, and nitrocellulose substrates) were obtained with the help of an AIKS-F4 double beam infrared spectrometer [5], a block diagram of which is shown in figure 1.

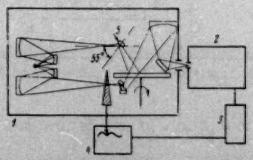

Figure 1. Block diagram of the double beam AIKS-F4 infrared spectrometer.

1- Double beam illuminator. 2- Monochromator. 3- Receiver-amplifier setup. 4- Recording arrangement. 5- Mirror on which are placed samples for recording the reflection spectra.

The refractive index was determined from these spectra by a study of the positions of the interference maxima and minima. Indeed, to the first approximation (neglecting absorption)

$$n = \frac{m\lambda}{2d}, \qquad (1)$$

where m is the order of the interference band, and λ is the wave length, which corresponds to the maximum (or minimum) of a given band.

The absorption coefficient κ was calculated from the measured quantities n and d and also the coefficient of reflection R or transmission T. The expression for the reflection coefficient R in the case of an absorbing layer with optical constants n and κ, situated on a transparent substrate with an index of refraction n_1, has the form

$$R = \frac{r_1^2 + 2r_1r_2\cos\frac{4\pi nd}{\lambda}\exp[-\frac{4\pi\kappa d}{\lambda}] + r_2^2\exp[-\frac{8\pi\kappa d}{\lambda}]}{1 + 2r_1r_2\cos\frac{4\pi nd}{\lambda}\exp[-\frac{4\pi\kappa d}{\lambda}] + r_1^2r_2^2\exp[-\frac{8\pi\kappa d}{\lambda}]}, \quad (2)$$

where r_1 and r_2 are the Fresnel coefficients for reflection from the first and second surfaces of the sublimed layer. Correspondingly for transmission

$$T = \frac{n_1t_1^2t_2^2\exp[-\frac{4\pi\kappa d}{\lambda}]}{1 + 2r_1r_2\cos\frac{4\pi nd}{\lambda}\exp[-\frac{4\pi\kappa d}{\lambda}] + r_1^2r_2^2\exp[-\frac{8\pi\kappa d}{\lambda}]}, \quad (3)$$

where t_1 and t_2 are the Fresnel coefficients for transmission. Formulas (2) and (3) are easily obtained directly from the expressions for the amplitudes of reflected or transmitted waves (compare, (for example, reference [6]):

$$R = \frac{r_1 + r_2\exp[-2i\delta]}{1 + r_1r_2\exp[-2i\delta]}, \quad (4)$$

$$T = \frac{t_1t_2\exp[-i\delta]}{1 + r_1r_2\exp[-2i\delta]}, \quad (5)$$

where $\delta = \frac{2\pi d}{\lambda}(n - i\kappa)\cos\varphi$.

However, since the value of n for bismuth is very large, one may consider that $\cos\varphi \sim 1$.

From (2) and (3) one can obtain the value of κ, using for the calculations the coefficients r_1, r_2, t_1, and t_2 which were obtained from the value of n obtained earlier.

Measurements of the transmission were made with light normally incident on the sample. Reflection measurements were made by substituting a plate of sublimed bismuth for one of the aluminized mirrors of the illuminator. The angle of incidence here was 55°, and therefore the reflected beam was elliptically polarized. Taking into account the polarizing action of the monochromator (the apparatus was an IKS-11 with an NaCl prism) was done on the basis of a calculation according to the Fresnel formula. A comparison of values of κ obtained from the expressions for R and T (where the angle of incidence was normal) showed that, when the polarizing effect of the monochromator was considered, the differences between them lie within the limits of experimental error. An estimate of the effect of the absorption on the value of n for the least satisfactory case, when κ is large, and n is small (for example, for layers with d = 0.69 μ and m = 1, λ = 11.61 μ, n = 8.38, and κ = 1.07) showed that the deviation of the value of n, determined in the first approximation, from the more precise value was only 2-3%. Consequently, the first approximation is sufficient for the determination of n and κ for sublimed bismuth in the 3-15 micron region. Thus in our case, the precision of the determination of the refractive index was ~ 6-8% which arose from errors in the determination of the wave length (~ 1%), errors due to the absorption of the layers (~ 2-3%), and errors in the thickness measurements (~3-5%). The precision of the determination of κ is significantly lower and depends basically on the precision of the measurements of the reflection and transmission coefficients. For us, the latter is 2-5%. As is seen from formulas (2) and (3), such errors allow one to obtain the value of κ with a precision of ~20%. If, however, one considers the errors in the determination of n, then it turns out that the value of κ is measured with an error of ~ 30%.

RESULTS OF THE MEASUREMENTS

A comparison of the values of n and α for layers sublimed onto different substrates, showed that the results for glass, rock salt, and nitrocellulose substrates are essentially the same. Therefore, in the future we shall present data which has been obtained for layers sublimed onto polished rock salt, since in this case both reflection and transmission spectra can be made. In figure 2, reflection and transmission spectra are shown for samples of three thicknesses — 0.22 μ, 0.56 μ, and 0.69 μ, characterizing the three regions of thickness for which the dependence n = f (λ) differed. From these and analogous spectra for other thicknesses, the values of n and κ in the 3-15 μ region were obtained for sublimed bismuth by the method described above. In figure 3, the dependence of the index of refraction n on wave length for sublimed bismuth is shown for layers 0.22, 0.69, and 0.89 μ thick. For the first layer, the dependence was obtained for the 3-8 μ region, and for the latter two, in the 3-15 μ region.

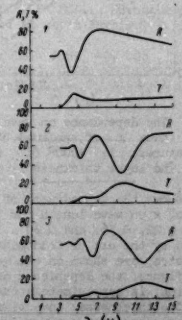

Figure 2. Spectra of the reflection R and the transmission T of bismuth, sublimed onto rock salt. Layer thickness in microns: 1— 0.22; 2— 0.56; 3— 0.69.

As is seen in figure 3, the value of n for layers in the first thickness range increases with decreasing λ, for thicker layers it has a maximum at about 7 μ and for thicknesses of 0.5 - 0.7 μ, it has an intermediate position.

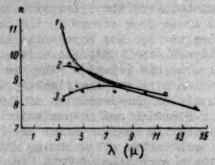

Figure 3. The dependence of the refractive index n of sublimed bismuth on wave length. Layer thickness in microns: 1- 0.22; 2- 0.69; 3- 0.89.

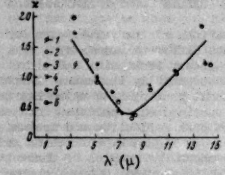

Figure 4. The dependence of the absorption coefficient κ of sublimed bismuth on wave length. The thickness of the layers in microns and the methods of determination are: (R - Reflection, T - Transmission): 1- 0.22 (R); 2- 0.22 (T); 3- 0.56 (R); 4- 0.56 (T); 5- 0.69 (R); 6- 0.69 (T).

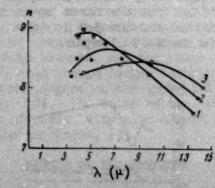

Figure 5. The dependence on wave length of the refractive index n of sublimed bismuth for various temperatures. 1- +200° C; 2- +20° C; 3- (-90° C). The layer thickness is 0.9 μ.

Figure 4 shows the dependence of the absorption coefficient κ on wave length for layers with thicknesses of 0.22, 0.56, and 0.69 μ. The points for κ, obtained by the use of transmission and reflection spectra, are shown on the graph. As is seen from the figure, the dependence of κ on λ in the 3-15 μ region, is approximately the same for layers of all the thicknesses investigated. In addition, the presence of a minimum in the 7.5 μ region is characteristic of the dependence of κ on wave length. It is possible that small displacements of this minimum in the transition from layers of one thickness to those of another (if they occur), were not distinguished due to the low precision of the determination of κ. However, the presence of a minimum in this region was established beyond doubt.

An investigation of the temperature dependence of the refractive index of sublimed bismuth was also carried out. In this case a sample ~ 0.9 μ thick was placed in a special vacuum cylinder with NaCl windows. In this cylinder, the sample could be cooled to -100° C and heated to + 200° C, without oxidation or condensation of water vapor. The measurements showed that a displacement of the interference maximum was observed along the wavelength axis with an increase or decrease of temperature, which indicated a change in the refractive index since the experimental conditions were not changed here, and the value of the thickness change lies within the limits of the precision of the experiment. It is necessary to point out that these changes in the refractive index are small (at the extreme points ~ 10%); however, they lead to a displacement of the interference maximum of 0.5 - 1.0 μ, which, with the precision of the measurements of the position of the maximum (~0.05 ~ 0.1 μ), is quite easily observed. The results of the temperature measurements are shown in figure 5. As is seen in the figure, the maximum of the curve for n is displaced to the longer wavelength region, with a decrease in the sample temperature, and the maximum value of the refractive index decreases. It would be desirable to obtain the temperature dependence for the quantity also. However, the experimental difficulties connected with the determination of precise values of the reflection and transmission coefficients at different sample temperatures prevented these data from being obtained.

DISCUSSION OF THE RESULTS

It is well known that thin sublimed metallic layers are formations consisting of an accumulation of fine crystals separated by gaps. These gaps frequently play a decisive role in the optical and electrical properties of such layers. It could be assumed that there are also such gaps which influence the electrical and optical properties in thicker (d > 0.1 μ) bismuth layers. Therefore, using data on the temperature coefficient of resistance [3] and the specific resistance [2] of sublimed bismuth layers, we made an attempt to evaluate the dimensions of the intercrystalline gaps, proceeding from an idea developed by Frenkel' [7, 8]. The value in our case turned out to be 0.1 Å, which hardly makes sense physically. Therefore it is obvious that in thick sublimed bismuth layers, the mechanism of conductivity does not correspond to a model in which crystals are separated by gaps. Apparently more probable is the influence of defects which are formed in the crystalline lattice of the sublimed bismuth. It is well known that such defects are formed not only in the sublimed layers but also in the bulk metal by mechanical treatment, the addition of impurities, the formation of alloys, and so on. In this connection it is interesting to compare our data with data obtained for bulk bismuth (poured on glass) by Hodgson [9], and also with data for bulk bismuth obtained by Alekseevskii and Potapov by calorimetric measurements at liquid helium temperature [10]. Hodgson's dependence of n and κ on wavelength resembles our data for thick layers (d > 0.8 μ); however, the maximum n and corresponding minimum κ are situated in another region

($\lambda \sim 4\ \mu$). At the same time, the maximum value of n coincides (~0.5) but the value of κ somewhat exceeds (~ 0.8) the values we obtained. On the other hand, our data, as well as Hodgson's data, greatly differ from the results of Alekseevskii and Potapov who obtained values of n and κ in the 7 micron region equal to 2 and 2.5. Analyzing his own results, Hodgson assumed that the position of the maximum n (minimum κ) determines the width of the forbidden band of bismuth, whose value in this case turned out to be 0.3 eV, which is in agreement with the calculations for the band model of bismuth [11]. A determination of the width of the forbidden band from our data gives a value of 0.18 eV. The deviation in the position of the maximum n and the related deviation in the width of the forbidden band could have been caused by the structural peculiarities of sublimed bismuth. Unfortunately, it is impossible to express this assumption in more definite form because of the absence, in Hodgson's data, of information on the chemical purity of the bismuth he investigated. It is well known that an extremely small amount of impurities (0. 1 to 1%) has a substantial effect on the properties of bismuth.

Our temperature measurements also allow one to determine the temperature dependence of the width of the forbidden band, namely:

$$\frac{\partial E}{\partial T} = +\ 4.8 \cdot 10^{-4}\ \text{eV/deg.}$$

The value obtained is close to the values which are observed in the majority of semiconductors ($3\text{-}5 \times 10^{-4}$ eV/degree), and the sign is analogous to the sign of the group of semiconductors of the type PbS ($+\ 4 \times 10^{-4}$ eV/degree) [12].

As regards the differences between our data and that of Alekseevskii and Potapov, it is possible that it may be connected with the influence of temperature. It is necessary to point out that the increase in the refractive index with decreasing wavelength (Fig. 3) for comparatively thin sublimed layers apparently points to the substantial effects already described, not only of defects in the crystalline lattice but also in the structural peculiarities of the sublimed layers (gaps, etc.). These peculiarities possibly have a stronger influence on the optical properties than on the electrical properties. Actually for still thinner layers (from 0.035 up to 0.12 μ) Schulz found that the value of the refractive index has a maximum in the 2 micron region where it reaches 20 [13]. Therefore, it is possible that in the case of our thin samples, the value of n also has a maximum which is situated in the shorter wave length region of the spectrum. With regard to the use of values of n and κ that were obtained for determining the concentration of conduction electrons N in bismuth, (compare for example reference [14]) it is necessary to be cautious here. The dependences of n and κ on wavelength in the 3-15 micron region are such (the presence of a maximum and minimum at about 7-8 microns) that the formula usually used for calculation of N from n and α [14] is apparently applicable at wavelengths longer than 12-15 microns. Therefore for its correct use it is necessary to measure n and κ at longer wavelengths than has been done in the present work.

In conclusion the authors consider it their duty to express thanks to V. I. Malyshev and S. G. Rautian for their valuable advice and consideration of the work.

December 20, 1958

References

1. L. HOWARD: J. Appl. Phys., 25, 125 (1954)
2. M. N. MARKOV, I. S. LINDSTREM: FTT, 1, 827, (1959) (See: Sov. Phys., Solid State Phys.)
3. M. N. MARKOV: DAN USSR, 108, 428, (1956) (See: Sov. Phys., Doklady)
4. G. D. SCOTT, T. A. McLAUCHLAN, F. SENNET: J. Appl. Phys., 21, 843, (1950)
5. V. I. MALYSHEV, M. N. MARKOV, A. A. SHUBIN: DAN USSR, 86, 273, (1952)
6. O. S. HEAVENS: Optical properties of thin solid films, London (1955)
7. P. SIMPSON: Nature, 160, 791 (1947)
8. J. A. FRENKEL: Phys. Rev., 36, 1604 (1930)
9. J. N. HODGSON: Proc. Phys. Soc., 67B, 267 (1954)
10. N. E. ALEKSEEVSKII, E. V. POTAPOV: ZETF, 33, 283 (1957) (See: Sov. Phys. JETP)
11. A. WILSON: Quantum Theory of Metals, GITTL (1941)
12. E. BURSTEIN, P. EGLI: Advances in Electronics and Electron Physics, 7, 1-77, New York (1955)
13. L. G. SCHULZ: JOSA, 43, 406 (1953)
14. V. L. GINZBURG, G. P. MOTULEVICH: UFN, 55, 469 (1955)

TOM VII, Vyp. 3 OPTIKA I SPEKTROSKOPIIA Sentiabr', 1959
VOL. VII, No. 3 OPTICS AND SPECTROSCOPY September, 1959

On the Use of an Additive-Statistical Method to Study Absorption and Fluorescence Spectra

P. G. MASLOV

Abstract: This paper considers the possibility of using an additive-statistical method to study the electronic absorption and fluorescence spectra of organic molecules.

Relations are obtained which permit the various characteristics of the electronic spectra of molecules (position, intensity, quantum yield, etc.) to be calculated by assuming the additivity of the effects of various substituents on these characteristics. Data obtained from a large group of aromatic compounds show that the relations mentioned are in satisfactory agreement with experimental results.

Knowledge of the ultraviolet absorption and fluorescence spectra is of considerable practical importance [1, 2, 13]. The experimental measurement of the spectra is often fraught with great difficulties, however, and is sometimes impossible [1]. Consequently, it is of interest to develop a theoretical method of finding the absorption and luminescence (particularly, the fluorescence) spectra of various compounds and their solutions.

The present paper demonstrates the possibility of using the additive-statistical method of IU. P. Maslov and the author [3-5] to study the absorption and luminescence spectra of chemical compounds.

As is known [3], the frequencies of the fundamental, composite and torsional vibrations, as well as a number of other physico-chemical properties of families of related compounds "i" are calculated by means of their values for simpler models "j". The following kind of formula is used for this purpose [3;5]

$$B_i = \frac{1}{s_o}\sum_j \delta_j B_j \qquad (1)$$

where B is the value of the frequency or other characteristic of the substance (for convenience, here, the compound of interest $A\Pi X^{(i)}_{n_i}$ and the original compound $A\Pi X^{(i)}_{m_j}$ are denoted, respectively, by the subscripts i and j); $s_o = \sum_j \delta_j$ is the valency of the coordinating group A which is common to all the members of the selected family of compounds [3,4]; δ_j is a numerical coefficient for B_j.

Among the characteristics subject to (1) are, particularly, the dissociation energy, the anharmonicity constant, the internal energy, the heat content etc. [3-10].

Taking the Born-Haber cycle into account, it can be stated that (1) is valid for the molecular ionization energy also (Table 1). This is also verified by earlier literature sources [1, 6, 11-21].

Up to the present, however, no attempt has been made to generalize or to lay a theoretical foundation for the abovementioned fact, which is related basically to the impossibility of solving the Schroedinger equation for such complex molecular systems. Under the conditions at hand, it is reasonable to use indirect means, including semi-empirical methods and even qualitative considerations. One such device is the Born-Haber cycle, which we use herein. In this connection, the question of the coupling between the vibrations of the molecular nucleus and its electric field acquires particular significance. The properties of the electron shell of the molecule determine the nature of its vibrations, and conversely, the properties of the electronic spectra can be estimated by means of the vibrational spectra.

However, the foundation for the additivity of electronic levels results most clearly from the quantum mechanical explanation of the origin of Raman spectra. If a molecule, having absorbed a quantum of energy $h\nu_o$ makes the transition from the electronic ground state with energy E_1 to another state with energy $E_2 > E_1$ and then emits the energy $h\nu' < h\nu_o$ by making the transition to one of the vibrational levels with energy E_k corresponding to the electronic ground state, then the energy of the vibration thus excited is written as:

$$\epsilon_k = h\nu_k = h\nu_o - h\nu' = (E_2 - E_1) - (E_2 - E_k) = E_k - E_1 \qquad (2)$$

Since the frequencies of the molecular vibrations [3] are subject to condition (1) [3], then writing (2) for our compounds and the original compounds "i" and "j" and applying (1), it is easy to obtain expressions of the form

$$h\nu_{ki} = \frac{h}{s_o}\sum_j \delta_j \nu_j, \qquad (3)$$

$$h\nu_{oi} - h\nu'_i = \frac{h}{s_o}\sum_j \delta_j \nu_{oj} - \frac{h}{s_o}\sum_j \delta_j \nu'_j, \qquad (3^I)$$

or

$$E_{ki} - E_{1i} = \frac{1}{s_o}\sum_j \delta_j E_{kj} - \frac{1}{s_o}\sum_j \delta_j E_{1j}. \qquad (3^{II})$$

Taking into account the effects of a Born-Haber cycle on the applicability of (1) to the ionization energy, and the other considerations presented above, we have for the family of related compounds from (3^I) and (3^{II}):

$$h\nu_{oi} \cong \frac{h}{s_o}\sum_j \delta_j \nu_{oj}, \quad h\nu'_f \cong \frac{h}{s_o}\sum_j \delta_j \nu'_j, \qquad (4)$$

and, in general,

Table 1

Comparison of Ionization Potentials and Dipole Moments of Certain Compounds, Calculated Using (1), with Experimental Data [26,27]

Substance	Formula	Ionization Potential	
		Computation Using (1)	Experiment [26]
Methane	CH_4	–	13.1 *
Tetramethyl Methane	$C(CH_3)_4$	8.3*	–
n-Propane	C_3H_8	11.4	11.3
	$C_2(CH_3)_6$	8.9*	–
Ethane	C_2H_6	–	11.6*
n-Butane	C_4H_{10}	10.7	10.34
Isobutane	C_4H_{10}	10.27	10.34
Ethylene	C_2H_4	–	10.5*
Tetramethyl Ethylene	$C_2(CH_3)_4$	7.81*	8.3
Propylene	$C_2H_3CH_3$	9.82	9.70
Isobutene	$C_2H_2(CH_3)_2$	9.16	8.95
Trimethyl Ethylene	$C_2H(CH_3)_3$	8.48	8.80
Methylamine	NH_2CH_3	9.8	9.8
Dimethylamine	$NH(CH_3)_2$	9.6	9.6
Benzene	C_6H_6	–	9.24*
Hexamethyl-benzene	$C_6(CH_3)_6$	6.87*	–
Toluene	$C_6H_5CH_3$	8.85	8.92
o-Xylene	$C_6H_4(CH_3)_2$	8.45	8.3
m-xylene	$C_6H_4(CH_3)_2$	8.45	8.3
p-Xylene	$C_6H_4(CH_3)_2$	8.45	8.3
Methyl Alcohol	CH_3OH	10.7	10.8
Ethyl Alcohol	CH_3O_5OH	10.75	10.7
Propylene Alcohol	C_3H_7OH	10.6	10.7
Ethylene Dichloride	C_2Cl_4	8.91	–
Vinyl Chloride	C_2H_3Cl	10.1	10.0
Cis-Ethylene Dichloride	$C_2H_2Cl_2$	9.70	9.66
Trans-Ethylene Dichloride	$C_2H_2Cl_2$	9.70	9.66
Trimethylamine	$N(CH_3)_3$	9.4	9.4*

T^oK	$ClH_2C \cdot CH_2Br$ Dipole Moment (in D)		
	Computation In [27]	Computation Using (1)	Experiment [27]
	Solution in Heptane		
243	1.01	0.995	0.99
263	1.05	1.095	1.06
283	1.10	1.14	1.12
303	1.15	1.19	1.21
323	1.19	1.20	1.20
	Solution in Hexane		
273	1.08	1.04	1.04
298	1.14	1.14	1.14
323	1.19	1.17	1.21
	Gaseous State		
339	1.08	1.08	1.08
368	1.14	1.14	1.12
405.2	1.20	1.20	1.19
435.7	1.25	1.26	1.27
	$BrH_2C \cdot CH_2Br$ Dipole Moment (in D)		
	Solution in Hexane		
298	0.90	0.90	0.91
323	0.94	0.98	0.92

Substance	Dipole Moment (in D) –	
	Calculated by Formula (1)	Experiment [28]
CH_3Cl	—	1.83
$C(CH_3)_3Cl$	—	2.14
$C(CH_3)_2HCl$	2.05	2.10
$C(CH_3)H_2Cl$	1.95	2.03
HCl	1.04	1.35
H Br	0.79	0.71
HJ	0.54	0.39

* Experimental data taken as initial data in the computation.

$$(5)\quad E_{nf} \cong \frac{1}{s_o} \sum_j \delta_j E_{nj} \quad (n = 1, 2, 3 \ldots \infty).$$

Hence, additivity in the sense of the authors' conception [3, 4, 5] should, to a first approximation, be demonstrated not only by the energy and frequency of the vibrations but also by the electronic energy levels E_n of the stationary states of the molecules and, therefore, by the energy and frequency of the electronic transitions. Hence, having solved the quantum-mechanical problem of finding the stationary states and energy levels for the simplest molecular models, these quantities can be calculated for the remaining members of the family of compounds by using (1), bypassing the difficult, and not always possible, quantum-mechanical solution of the problem. This in itself is of theoretical interest.

The abovementioned considerations thus lead to the conclusion that the positions of the maxima and minima of the absorption and luminescence bands of a family of related compounds can be calculated to a first approximation by using a relation such as (1). Analysis of an enormous amount of material on ultraviolet absorption and luminescence spectra, [1, 2, 11-22], completely confirms and supplements our conclusions.

Relying on the most trustworthy results from [20, 21] and using the method proposed above, we obtained the following approximate general formula for predicting the positions of the maxima or minima of the absorption and fluorescence bands of various benzene, naphthalene or anthracene derivatives and their solutions:

$$(6)\quad \lambda_i = B_{oi}\left(n - \sum_j \delta_j\right) + \sum_j \delta_j B_j + b_1 \alpha_o + b_2 \alpha_m + b_3 \alpha_p$$

α_o is the number of substituent pairs in ortho-positions. α_p is the number of substituent pairs in meso or para-positions, with respect to each other; α_m is the number of substituent pairs in meta or 3, 10; 2, 9; 6, 10; or, 7, 9; etc. positions in the case of anthracene type derivatives, etc.; δ_j is the number of substituents of a specific type which have displaced hydrogen which was on the main ring (i. e. at A); n is the valency of the main ring or group A in the compound ($n = 6$ in benzene, $n = 8$ in naphthalene, $n = 10$ in anthracene, etc.). The meanings of the remaining symbols are given in Table 2.

The last three terms on the right side of (6) which take into account the influence of the relative locations of the substituent groups on λ_i, are usually small. They are somewhat larger in the case of alkyl groups, but even in this case make only a small contribution (on the order of 0-7 mμ) to the total λ_i. This quantity is only very slightly outside the limits of the experimental results presented by various investigators [1, 2, 11-21]. As is seen from tables 3-5, formulas (1) and (6) yield results which are in satisfactory agreement with experiment.

Without doubt, the additive-statistical method and, in particular, formulas (6) or (1) combined with the initial data (Table 2), permit a prediction of the positions of the absorption and fluorescence spectra for many anthracene derivatives.

Equally good agreement is obtained in all the rest of the cases [17, 20].

On the basis of the data of table 2, the positions of the fluorescence spectra of solutions of anthracene derivatives in benzene are also calculated directly by using (1) or (6) (without taking α_o, α_m, and α_p into account).

The results of the computation are in satisfactory agreement with experiment [17, 16, 21].

Using the additive-statistical method, i. e., actually, formula (1) and the experimental data from [23-25] as initial data, approximate relationships were also obtained for calculating the positions of absorption maxima of solutions of methyl derivatives of naphthalene in petroleum ether. Here, the initial data for naphthalene were borrowed from [23] and taken as the average values of a number of authors for solutions of naphthalene in isooctane, petroleum ether and pentane. The computational equations have the following form:

For the first group of maxima

$$(7)\quad \lambda_1 = [(8 - n_1)40.12 + 50 \cdot 68 \cdot n_1]$$

For the Second group

$$(7^{I})\quad \lambda_1 = [(8 - n_1)38.88 + 43.29 \cdot n_1]$$

$$(7^{II})\quad \lambda_2 = [(8 - n_1)38.25 + 41.99 \cdot n_1]$$

$$(7^{III})\quad \lambda_3 = [(8 - n_1)37.75 + 41.25 \cdot n_1]$$

and for the third group

$$(7^{IV})\quad \lambda_1 = [(8 - n_1)35.75 + 39.78 \cdot n_1]$$

$$(7^{V})\quad \lambda_2 = [(8 - n_1)35.50 + 36.55 \cdot n_1]$$

$$(7^{VI})\quad \lambda_3 = [(8 - n_1)34.38 + 35.51 \cdot n_1]$$

$$(7^{VII})\quad \lambda_4 = [(8 - n_1)33.25 + 34.02 \cdot n_1]$$

respectively. Formulas (7) - (7^{VII}) were derived on the basis of data obtained from [23].

Finally, starting out with data obtained from [25] for the absorption spectra of solutions of benzene, methyl benzene, 1, 2-, 1,3- and 1,4-dimethyl benzene in 2,2,4- trimethyl benzene, the proposed method easily yields approximate formulas for estimating $\lambda_{1\,max}$, $\lambda_{2\,min}$ and $\lambda_{3\,max}$ of methyl derivatives of benzene; namely:

$$(8)\quad \lambda_{1\,max} = [(6 - n_1)\,44.63 + 46.58 \cdot n_1]$$

$$(9)\quad \lambda_{2\,min} = [(6 - n_1)\,44.42 + 46.13 \cdot n_1]$$

$$(10)\quad \lambda_{3\,max} = [(6 - n_1)\,43.4 + 46.88 \cdot n_1]$$

respectively. The positions of the maxima and minima, calculated by using (7) and (10), are in good

Table 2

Contribution of various substituents to the values of the wavelengths of the absorption and fluorescence band maxima and magnitude of the oscillator strength and luminescence quantum yields of solutions of anthracene derivatives

Substance		Substituents																		
		Bj																		
		B_{of}	C_nH_{2n+1}	C_6H_5	$C\equiv N$	NH_2	NO_2	$C(=O)H$	$C(=O)CH_3$	$C(=O)C_6H_5$	$C(=O)OH$	$O\text{-}C(=O)OH_3$	Br	Cl	$O\text{-}C(=O)C_6H_5$	OCH_3	Naph-thyl	b_1	b_2	b_3
Solution of Anthracene Derivatives in Alcohol	λ_f(mμ)	Fraction contributed by substituents to the value of absorption maximum wavelength																		
	λ_1	37.54	46.96+0.4·z	45.38	65.22	72.16	44.13	83.21	44.69	46.19	43.29	45.80	51.82	51.82	46.19	50.40	47.20	5.2	-7.3	3.4
	λ_2	35.64	44.21+0.4·z	42.02	61.23	32.74	42.24	77.18	42.15	43.45	41.14	42.92	48.48	48.48	43.45	47.32	45.00	5.2	-7.3	3.4
	λ_3	33.93	41.77+0.4·z	40.68	58.10	30.17	41.58	67.18	40.90	41.50	40.10	40. 68	46.12	45.82	40.9	44.68	41.91	5.2	-7.3	3.4
	λ_4	32.37	39.85+0.4·z	38.49	54.67	28.14	39.66	63.61	37.99	39.09	37.99	38.12	43.66	43.66	38.49	42.02	40.05	3.11	-2.23	1.1
	λ_7	25.20	28.77+0.4·z	31.77	23.43	35.41	25.44	35.41	26.47	26.63	26.67	26.57	30.07	29.07	26.47	27.67	26.73	3.11	-2.33	1.1
		Fraction contributed by substituents to the value of fluorescence maxima wavelengths																		
	λ_1	37.88	48.84	51.64	–	–	–	–	–	–	47.4	46.20	55.94	54.18	–	54.30	49.3	5.2	-7.3	3.4
	λ_2	39.96	52.51	53.81	–	–	–	–	–	–	51.06	49.36	60.40	58.01	–	56.61	53.91	–	–	–
	λ_3	42.37	55.30	55.67	–	–	–	–	–	–	54.37	52.62	61.67	60.92	–	60.04	54.77	–	–	–
	λ_4	45.04	60.01	60.56	–	–	–	–	–	–	57.64	55.06	~ 69	~ 65	–	63.04	62.22	–	–	–
	λ_7	–	–	–	–	–	–	–	–	–	–	–	–	–	–	–	–	–	–	–
		Fraction contributed by substituents to magnitude of oscillator strengths [20, 21]																		
	λ_1	0.01	0.02+0.005·z	0.055	–	–	–	–	0.03	0.04	0.04	0.03	0.04	0.04	0.03	0.035	–	–	–	–
	λ_2	0.168	-0.032·z	0.046	–	–	–	–	-0.03	0.37	0.27	-0.03	0.07	0.07	0.17	-0.25	–	–	–	–
		Fraction contributed by substituents to magnitude of relative luminescence quantum yields [20, 21]																		
	–	0.1	0.42+0.1·z	1.36	–	–	–	–	–	–	–	–	–	–	–	–	–	–	–	–
		Fraction contributed by substituents in magnitude of absolute luminescence quantum yield																		
	–	0.022	0.1+0.02·z	0.297	–	–	–	–	-0.198	-0.198	+0.158	0.10	-0.2	-0.21	-0.19	0.08	–	–	–	–

Substance		B_{of}	CH_3	C_2H_5	$n\text{-}C_3H_7$	$n\text{-}C_4H_9$	$C_6H_5\text{-}CH_2$	CH_2	b_1	b_2	b_3
Solution of Anthracene derivatives in Heptane	λ_f(mμ)	Fraction contributed by substituents into value of absorption maxima wavelengths									
	λ_1	37.5	45.6	52.37	52.53	53.0	53.0	47.57	1.81	-6.4	6.4-2·z
	λ_2	35.55	42.82	49.70	49.80	50.3	49.3	44.8	1.81	-6.4	6.4-2·z
	λ_3	33.85	40.62	46.08	46.3	46.59	45.57	42.34	1.81	-6.4	6.4-2·z
	λ_4	32.25	40.26	41.74	42.54	42.64	41.74	37.5	1.81	-2.23	+1.3
	λ_7	25.20	28.56	30.33	30.43	30.60	31.33	28.33	1.81	-2.23	+1.3

Substance		B_{of}	CH_3	C_2H_5	$n\text{-}C_3H_7$	$\beta\text{-}(CH_2)_2OH$	iso-C_4H_9	iso-C_5H_{11}	Cl	Br	J	$\beta\text{-}C_3H_6OH$
Solution of Anthracene derivatives in Benzene	λ_f(mμ)	Fraction contributed by substituents into value of fluorescence maxima wavelengths										
	λ_1	38.50	51.5	51.5	52.0	49.3	52.25	53.50	52.30	55.37	~58.1	52.0
	λ_2	40.50	53.0	53.0	53.5	53.0	54.25	55.0	54.20	55.50	~56.8	53.5
	λ_3	42.75	56.5	56.5	56.5	54.68	57.00	57.0	55.65	58.32	~61.0	~56.5

Table 3

Comparison of Calculated and Experimental Wavelengths of Absorption and Fluorescence Band Maxima of Solutions of Certain Anthracene Derivatives in Alcohol

Substance	Position of Maximum λ(mμ)				Substance	Position of Maximum λ(mμ)			
	Absorption		Fluorescence			Absorption		Fluorescence	
	Calculation	Experiment [20,21]	Calculation	Experiment [20,21]		Calculation	Experiment [20,21]	Calculation	Experiment [20,21]
9-Anthracene carboxylic acid	381.2	381.0	388.3	388.3	9-Bromoanthracene, 10-Carboxylic acid	395.4	393.7	406.4	407.3
	361.9	362.0	410.7	410.7		374.7	373.8	431.1	431.0
	345.5	345.2	435.7	435.7		357.4	354.9	455.0	456.6
	329.3	329.5	463.0	463.0		340.1	339.0	~487	487.6
	253.5	253.2	–	–		258.3	259.1	–	–
9-Acetyoxyanthracene	383.7	383.5	387.1	386.8	9, 10-Diacetyoxy-anthracene	391.9	391.8	395.4	396.0
	363.7	363.6	409.0	409.0		371.0	371.4	418.4	418.4
	346.0	345.7	434.0	433.8		352.8	352.7	444.2	443.5
	329.4	329.5	460.4	459.8		335.2	335.6	470.4	471.5
	253.4	252.8	–	–		254.7	255.6	–	–
9-Metoxyanthracene	388.3	388.0	395.2	395.2	9,10-Dimethoxy-anthracene	401.2	401.2	411.6	411.5
	368.1	368.0	416.2	415.8		379.8	380.2	332.9	433.8
	350.0	349.7	441.4	440.5		360.8	360.7	459.0	460.8
	333.4	333.3	468.4	465.1		~343.0	~343.6	–	–
	254.5	253.2	–	–		256.9	258.7	–	–
9-Chloroanthracene-10-Carboxylic acid	395.4	392.9	404.6	405.7	9-Methyl-10-Methoxy-anthracene	401.1	400.0	406.2	409.0
	374.7	372.4	428.0	428.3		380.3	378.8	428.8	431.5
	357.4	354.0	454.2	454.5		361.2	359.4	454.3	455.6
	340.1	339.0	~ 483	483.1		342.3	342.2	483.4	478.5
	257.3	259.0	–	–		259.1	259.1	–	–
9-Chloro, 10-Metoxyanthracene	402.5	402.4	411.5	411.5	9-Bromine-10-methoxyanthracene	402.5	402.4	413.3	414.9
	380.9	381.0	434.3	436.7		380.9	381.0	436.7	435.7
	361.9	361.7	459.9	459.8		362.2	362.0	460.7	460.8
	344.6	344.8	–	–		344.6	344.8	–	–
	258.3	258.1	–	–		259.3	259.1	–	–
9, 10-Dimethyl-anthracene	397.6	398.0	400.7	402.0	9,10-Diphenyl anthracene	391.1	392.5	406.3	406.9
	376.9	377.0	424.7	426.0		369.2	372.1	427.3	427.8
	358.4	358.1	449.6	453.0		352.8	354.0	450.3	449.9
	339.7	341.0	480.3	481.9		335.9	337.8	481.4	483.1
	260.2	259.7	–	–		265.1	258.1	–	–
9,-10-n-dipropyl-anthracene	399.2	399.2	400.7	402.8	9-Phenyl, 10-α-naphthylanthracene	392.7	392.7	404.0	404.0
	378.5	377.7	424.7	427.3		372.1	372.1	427.4	427.4
	359.9	358.4	449.6	454.0		354.0	354.0	449.4	449.4
	341.4	341.0	480.3	482.5		337.0	337.5	483.1	483.1
	262.1	260.4	–	–		260.1	260.1	–	–

Table 4

Comparison of Calculated and Experimental Values of Oscillator Strengths and Absolute Fluorescence Quantum Yields of Solutions of Certain Anthracene Derivatives in Alcohol

Substance	Absolute Quantum Yield		Oscillator Strength			
			First Band		Second Band	
	Calc.	Exp. [20,21]	Calc.	Exp. [20,21]	Calc.	Exp. [20,21]
9-Acetylanthracene	0	0	0.12	0.12	1.48	1.5
9-Benzoylanthracene	0	0	0.13	0.13	1.88	1.9
9-Anthracene carboxylic acid	0.36	0.04	0.13	0.13	1.78	1.8
9-Acetyoxyanthracene	0.10	0.15	0.12	0.11	1.48	1.3
9-Benzoxyanthracene	0.01	—	0.12	0.12	1.68	1.7
9-Methoxyanthracene	0.12	0.17	0.12	0.11	1.42	1.3
9-Chloroanthracene, 10-Carboxylic acid	0.12	0.33	0.16	0.14	1.70	1.8
9-Bromoanthracene, 10-Carboxylic acid	0.13	0.11	0.16	0.17	1.68	1.7
9,10-Diacetyoxyanthracene	0.38	0.44	0.14	0.13	1.28	1.7
9,10-Dimethoxyanthracene	0.34	0.41	0.15	0.14	1.20	1.6
9-Methyl, 10-Methoxyanthracene	0.36	0.24	0.14	0.12	1.23	1.4
9-Chloro, 10-Methoxyanthracene	0.05	0.05	0.16	0.13	1.33	1.6
9-Bromo, 10-Methoxyanthracene	0.06	0.06	0.16	0.13	1.33	1.6
9,10-Dimethylanthracene	0.40	0.63	0.12	0.12	1.28	1.22
9,10-Di-n-propylanthracene	0.46	0.76	0.14	0.14	1.15	1.19
9,10-Diphenylanthracene	0.77	0.86	0.19	0.18	1.44	1.35

Table 5

Comparison of Computed and Experimental Wavelengths of Ultraviolet Absorption Band Maxima of Solutions of Anthracene Derivatives

Type of Maximum λ_i (mμ) *	9-Methylanthracene						9,10-Dimethylanthracene						9-Methyl, 10-Ethyl-anthracene			2,3,9,10-Tetramethyl-anthracene		
	In n-Heptane			In Alcohol			In n-Heptane			In Alcohol			In n-Heptane			In n-Heptane		
	Calculation by (1)-(7) without correction	Experiment [17]	Calculation with correction	Calculation by (1)-(7) without correction	Experiment [17]	Calculation with correction	Calculation by (1)-(7) without correction	Experiment [17]	Calculation with correction	Calculation by (1)-(7) without correction	Experiment [17]	Calculation with correction	Calculation by (1)-(7) without correction	Experiment [17]	Calculation with correction	Calculation by (1)-(7) without correction	Experiment [17]	Calculation with correction
λ_1	383.1	385.5	383.1	384.8	386.2	384.8	391.2	397.4	397.6	394.2	397.9	397.6	398.0	397.9	402.2	407.4	–	402.8
λ_2	362.8	365.5	362.8	365.0	366.0	365.0	370.0	376.5	376.4	373.5	376.9	376.9	376.9	376.9	381.3	384.6	–	380.0
λ_3	345.3	347.5	345.3	347.2	348.3	347.2	352.0	357.0	358.4	355.0	358.0	358.4	358.0	357.5	361.9	365.6	–	361.0
λ_4	330.5	331.4	330.5	331.2	332.0	331.2	338.5	340.0	339.8	338.7	339.9	339.8	340.0	340.0	341.2	354.5	–	353.2
λ_7	255.4	256.0	255.4	255.6	255.2	255.6	258.7	260.0	260.0	259.1	260.0	260.2	260.5	260.5	261.8	265.4	265.96	264.0

Type of Maximum λ_i (mμ)	2,3,9,10-Tetramethyl-anthracene			1, 3-Dimethylanthracene						2, 9, 10-Trimethylanthracene					
	In Alcohol			In n-Heptane			In Alcohol			In n-Heptane			In Alcohol		
	Calculation by (1)-(7) without correction	Experiment [17]	Calculation with correction	Calculation by (1)-(7) without correction	Experiment [17]	Calculation with correction	Calculation by (1)-(7) without correction	Experiment [17]	Calculation with correction	Calculation by (1)-(7) without correction	Experiment [17]	Calculation with correction	Calculation by (1)-(7) without correction	Experiment [17]	Calculation with correction
λ_1	413.1	406.0	407.1	391.2	380.5	384.2	259.0	–	256.8	399.3	398.6	399.3	403.7	399.0	399.8
λ_2	390.7	385.0	384.7	370.0	258.0	363.6	338.7	–	336.4	377.3	377.5	377.3	382.1	377.9	378.2
λ_3	370.7	365.0	364.7	352.0	342.9	345.6	355.0	–	347.7	358.8	358.6	358.8	362.8	358.9	358.9
κ_4	353.6	–	353.6	338.5	–	336.3	373.5	–	366.2	346.5	341.4	345.5	346.0	342.0	345.0
λ_7	266.3	266.0	265.8	258.7	256.5	256.5	394.2	–	386.9	262.1	262.0	262.1	262.7	261.5	261.6

* Subscripts 1, 2, 3, 4 and 7 correspond to H, G, F, E and B in [17].

agreement with experimental results [23-25].

Furthermore, the following expressions (λ in mμ) can be proposed for an approximate estimate of the positions of the first, second (a and b), third (a, b and c) and fourth (a, b and c) maxima of the fluorescence bands of solutions of diphenyl polyenes in xylene [15] at - 196° C:

$$\lambda_I = (248.78 + 50.84 \cdot z) \quad (z \geq 2), \tag{11}$$

$$\lambda_{IIa} = (279.2 + 50.84 \cdot z) \quad (z \geq 2), \tag{12}$$

$$\lambda_{IIb} = (245.2 + 59.97 \cdot z) \quad (z \geq 2), \tag{13}$$

$$\lambda_{IIIa} = (243.8 + 65 \cdot z) \quad (z \geq 2), \tag{14}$$

$$\lambda_{IIIb} = (242.7 + 67.88 \cdot z) \quad (z \geq 2), \tag{15}$$

$$\lambda_{IIIc} = (232.1 + 72.78 \cdot z) \quad (z \geq 2), \tag{16}$$

$$\lambda_{IVa} = (231.9 + 78.53 \cdot z) \quad (z \geq 2), \tag{17}$$

$$\lambda_{IVb} = (234.8 + 80.98 \cdot z) \quad (z \geq 2), \tag{18}$$

$$\lambda_{IVc} = (231.16 + 84.96 \cdot z) \quad (z \geq 2), \tag{19}$$

where z is the number of repetitive groups in the polyene chain. A summary of the computation using (11) - (19) is in satisfactory agreement with experiments [1, 14, 15]. A similar picture is observed at 20° C.

Numerous checks of the method on other compounds completely confirm its applicability both to the prediction of the positions of electronic levels and to the calculation of the positions of the absorption and fluorescence band maxima of various substances.

Hence, the additivity of a number of properties of the absorption bands, which had been noted previously by a number of authors [1, 14-21], reduces to the additivity (in our conception) of electronic levels of molecules and is verified and explained on the basis of the additive-statistical method.

Moreover, the approximate additivity of the intensities of vibrational spectra [3] and also of the electronic absorption and fluorescence spectra was noted earlier [1, 14, 15].

We state in this report that oscillator strengths, to a first approximation, have similar additivity

$$f[21] \quad (f = 4.32 \cdot 10^{-9} \int \epsilon_\nu d\nu), \tag{20}$$

as do apparently the fluorescence quantum yields and the molar absorption coefficients ϵ_ν as well.

Formula (1) or (6) in conjunction with the data of table 2 can be used for the calculation.

As is seen from table 4, the calculated values of the oscillator strengths and absolute quantum yields of the fluorescence of anthracene derivatives are generally in satisfactory agreement with experiment [20, 21].

We suggest that the additive-statistical method may be useful for the study of absorption and fluorescence spectra of compounds not yet investigated. Its accuracy depends on the accuracy and quantity of the initial data. The error expected in the computation of the position of the maximum is from 0 - 3 mμ on the average (it can be of the order of 5 - 7 mμ in rare cases).

December 22, 1958

References

1. V. L. LEVSHIN: Fotoluminestsentsiia zhidkikh i tverdikh veshchestv. (Photo-luminescence of liquid and solid substances) GITTL, Moscow-Leningrad, 1951
2. P. P. PRINGSHEIM, M. VOGEL: Luminescence of liquids and solids. (GIIL, Moscow, 1948)
3. IU. P. MASLOV, P. G. MASLOV: OiS, 3, 38, (1957)
4. IU. P. MASLOV, P. G. MASLOV: ZFKh., 32, 1715, (1958)
5. P. G. MASLOV, IU. P. MASLOV: Chim. i Tekhn. Topliva, 10, 50, (1958)
6. P. G. MASLOV: Dissertation, Moscow, 1953
7. P. G. MASLOV: Usp. Khim., 25, 1069, (1956)
8. P. G. MASLOV: ZNKh, 3, 2618, (1958)
9. P. G. MASLOV, IU. P. MASLOV: Tr. Vsesoiuzn. konfer. "Khimiia i prakticheskoe primenenie kremneorganicheskikh soedinenii" (Trans. All-Union Conf. "Chemistry and practical use of silico-organic compounds") No. 6, Lensovnarkhoz Press, 1959
10. P. G. MASLOV, IU. P. MASLOV: DAN USSR, (1959) (In press)
11. LANDOLT-BORNSTEIN: Physikalisch-chemische Tafelen. Berlin, 1935-1956
12. W. C. PRICE: Chem. Rev., 41, 257, (1947)
13. P. P. FEOFILOV: ZETF, 12, 64; 275; 328; (1942) DAN USSR, 44, 159, (1944); 45, 387 (1944) 55, 407, (1947); 57, 343, 447 (1947); 71, 29, (1950)
14. K.W. HAUSSER, R. KUHN, G. SEITZ: Zs. phys. Chem., 29, 391 (1935)
15. K. W. HAUSSER, R. KUHN: Zs. phys. Chem., 29, 417, (1935)
16. G. N. LEWIS: JACS, 67, 770, (1945)
17. R. N. JONES: Chem. Rev., 41, 353, (1947)
18. E. V. SHPOL'SKII, A. A. IL'INA, V. V. BAZILEVICH: IAN USSR FS, 12, 519, (1948)
19. A. A. IL'INA, V. V. BAZILEVICH: IAN, USSR, FS, 12, 527, (1948)
20. A. S. CHERKASOV: ZFKh, 29, 2209, (1955)
21. A. S. CHERKASOV, T. M. VEMBER: OiS, 1, 663, (1956)
22. M. V. VOL'KENSHTEIN, M. A. EL'IASHEVICH, B. I. STEPANOV: Kolebaniia molekul (Vibrations of molecules) 1, GITTL, 1949
23. E. HEILBRONNER, U. PROHLICHER, P. A. PLATTNER: Helv. Chim. Acta, 32, 2479, (1949)
24. A. S. BAILEY, K. C. BRYANT, R. A. HANCOCK, S. H. MORRELL, J. C. SMITH: J. Inst. Petrol., 33, 503, (1947)
25. Fiziko-Khimicheskie svoistva individual'nykh uglervodorodov (Physical chemical properties of individual hydrocarbons) No. 4, 375, 1953
26. W. C. PRICE: Chem. Rev., 41, 257, (1947)
27. S. MIZUSHIMA: Structure of molecules and internal rotation, IIL, Moscow, 1957
28. M. V. VOL'KENSHTEIN: Stroenie i fizicheskie svoistva molekul (structure and physical properties of molecules) Akad. Nauk Press, Moscow, 1955
29. G. M. KOSOLAPOFF: JACS, 67, 1182, (1945)
30. A. L. HENNE, J. B. HINKAMP: JACS, 67, 1194, (1945)

TOM VII, Vyp. 3 OPTIKA I SPEKTROSKOPIIA Sentiabr', 1959
VOL. VII, No. 3 OPTICS AND SPECTROSCOPY September, 1959

Plastic Scintillators with Additions of Aryl Derivatives of 1,3,4-Oxadiazole

N. P. SHIMANSKAIA, A. P. KILIMOV, A. P. GREKOV, L. M. EGUPOVA AND R. S. AZEN

Abstract: The scintillation efficiency and luminescence and absorption spectra of solutions of eight 2,5-aryl derivatives of oxadiazole in polystyrene were measured. The data obtained were compared with that measured earlier for eight derivatives of oxadiazole. It was shown that, among the substituents examined, the biphenyl and 1-naphthyl groups have the most favorable effect on the scintillation efficiency.

Estimation of the scintillation efficiency of polystyrene solutions, carried out by the method of Swank and Buck, shows that this characteristic of plastic scintillators is determined basically by the optical properties (absorption and luminescence spectra) of the monomer and additive used.

Among the organic luminescent materials used as additives in the manufacture of liquid and plastic scintillators, aryl derivatives of oxazole and oxadiazole are the most promising classes of materials.

Their scintillation properties in liquid solutions have been studied particularly intensively [1], but significantly less attention has been given solutions of these materials in polystyrene.

In the present paper we present data on the spectral properties and scintillation efficiencies of solutions of a series of 2,5-diaryl derivatives of oxadiazole in polystyrene and a comparison is made of these properties with the structural characteristics of materials of this class.

EXPERIMENTAL

The following derivatives of 1,3,4-oxadiazole were investigated: 2-(4-biphenyl)-1,3,4-oxadiazole (BD); 2,5-di-(4-methoxyphenyl)-1,3,4-oxadiazole (MtPMtPD); 2-phenyl-5-(4-biphenyl)-1,3,4-oxadiazole (PBD); 2-phenyl-5-(1-naphthyl)-1,3,4-oxadiazole (αNPD); 2-phenyl-5-(2-naphthyl)-1,3,4-oxadiazole (βNPD); 2-(1-naphthyl)-50(2-naphthyl)-1,3,4-oxadiazole (αNβND).

The compound BD was obtained using a known method [2], by heating 4-biphenylhydrazide with the ethyl ester of o-formic acid. Compounds MtPMtPD, PBD, αNPD, βNPD, BBD, βNBD, αNβND were synthesized, using the general method for obtaining 2,5-diaryl-1,3,4-oxadiazoles [3], by cyclizing the corresponding dihydrazides by heating with $POCl_3$.

All the materials were purified by recrystallization and chromatography until constancy of the luminescence spectra of the crystalline samples was obtained.

The samples of the plastic scintillators were 20 mm in diameter and 12 mm high; they were obtained by high temperature polymerization in a nitrogen atmosphere [4].

The absorption spectra were measured on an SF-4 spectrophotometer. The luminescence spectra were measured on the same apparatus, which was used as a monochromator and was supplemented by a special photoelectric attachment.

The heptane and styrene used in this work were purified by the usual methods [5,6].

The scintillation efficiencies were estimated on an FEU-19 phototube.

As source of excitation, a Ag^{110} standard with intensity of approximately 0.1 microcurie was used.

RESULTS AND DISCUSSION

The absorption spectra of compounds are shown in figures 1 and 2, as is also the luminescence spectrum of polystyrene. It is seen that all the materials with 1-naphthyl substituents, i. e. the compounds αNPD, αNβND and αNBD, are notable for having the greatest overlap of their absorption spectra with the luminescence spectrum of polystyrene. The absorption spectra of the remaining compounds are toward the shorter wavelength region.

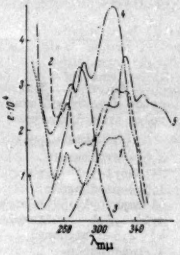

Figure 1. Absorption spectra of oxadiazoles in heptane. 1) 2-phenyl-5-(1-naphthyl)-1,3,4-oxadiazole. 3) 2-(4-biphenyl)-1,3,4- oxadiazole. 4) 2-(4-biphenyl-5-(2-naphthyl)-1, 3,4-oxadiazole. 5) luminescence spectrum of polystyrene.

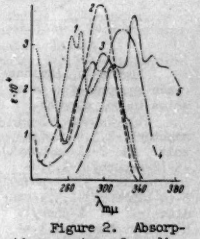

Figure 2. Absorption spectra of oxadiazoles in heptane. 1) 2-phenyl-5-(2-naphthyl)-1,3,4-oxadiazole. 2) 2,5-di(4-methoxyphenyl)-1,3,4-oxadiazole. 3) 2-phenyl-5-(4-biphenyl)-1,3,4-oxadiazole. 4) 2-(biphenyl)-5-(1-naphthyl)-1,3,4-oxadiazole. 5) luminescence spectrum of polysterene.

In figures 3 and 4 are presented the photoluminescence* spectra of the scintillators obtained. The best coincidence of the spectra with the region of maximum sensitivity of the FEU-19 occurs with those compounds which contain at least one 1-naphthyl group.

As is evident from the curves of the dependence of the scintillation efficiency on the concentration of the luminescent additive (Fig. 7), these same compounds -- αNPD, αNβND, αNBD -- are the most effective. 2, 5-di-(4-biphenyl)-1,3,4-oxadiazole also has a very high scintillation efficiency, which, evidently, may be explained by the more favorable conditions for transmission of energy from the host to the luminescent additive, just as is found in liquid scintillators [1].

In the table, along with data related to the materials enumerated, are presented the results of an earlier investigation of the following compounds which we synthesized and studied: 2-phenyl-1,3,4-oxadiazole (PD), 2-(4-methylphenyl-1,3,4-oxadiazole (MtPD), 2-(4-methoxyphenyl)-1,3,4-oxadiazole (MtPD), 2,5-diphenyl-1,3,4-oxadiazole (PPD), 2-phenyl-5-(4-methoxyphenyl)-1,3,4-oxadiazole (MtPPD),

*Excitation by the mercury lines at 253 and 313 mμ, thickness of the sample 12 mm.

2,5-di-(2-naphthyl)-1,3,4-oxadiazole (ββND), and, 2,5-di-(1-naphthyl)-1,3,4-oxadiazole (αααND).

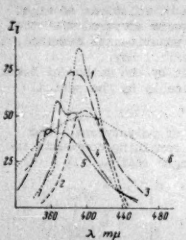

Figure 3. Luminescence spectra of oxadiazoles in polystyrene. 1) 2-phenyl-5-(1-naphthyl)-1,3,4-oxadiazole. 2) 2-(1-naphthyl)-5-(2-naphthyl)-1,3,4-oxadiazole. 3) 2-phenyl-5-(4-biphenyl)-1,3,4-oxadiazole. 4) 2-phenyl. 5) (2-naphthyl)-1,3,4-oxadiazole. 5) 2,5-di-(4-methoxyphenyl)-1,3,4-oxadiazole. 6) Spectral sensitivity curve of the FEU-19 phototube.

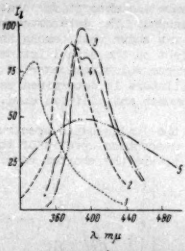

Figure 4. Luminescence spectra of oxadiazoles in polystyrene. 1) 2-(4-biphenyl)-1,3,4-oxadiazole. 2) 2-phenyl-5-(4-biphenyl)-1,3,4-oxadiazole. 3) 2-(1-naphthyl)-5-(4-biphenyl)-1,3,4--oxadiazole. 4) 2,5-dibiphenyl-1,3,4,-oxadiazole. 5) Spectral sensitivity curve of FEU-19 Phototube.

Examination of the table allows us to draw some preliminary conclusions about the influence of features of chemical structure on the luminescence and scintillation properties of derivatives of oxadiazole.

The first thing noted is the low technical scintillation efficiencies and energy yield of the photoluminescence of monoaryl substituents of oxadiazole. The maxima in the absorption and luminescence spectra of these compounds are situated in a comparatively short wavelength region of the spectrum, which coincides poorly with the luminescence spectrum of polystyrene and with the region of maximum sensitivity of the FEU-19 phototube.

Introduction of substituents CH_3, OCH_3, and C_6H_5 in the para position of the phenyl group leads to increased scintillation efficiency and luminescence yield, where the introduction of a phenyl group gives the best results. Regarding the diaryl substituents of oxadiazole, we must note that derivatives which contain the 1-naphthyl group have better properties than their 2-naphthyl analogs. Evidently the biphenyl in general is somewhat inferior to the 1-naphthyl group with respect to intensification of the scintillation efficiency; however, the 2, 5-dibiphenyl derivative gives the greatest scintillation effectiveness. It is possible that this circumstance is connected with better conditions for transfer of the excitation energy from the long chains of polystyrene to the additive molecules stretched along the chain.

Just as A. S. Cherkasov and his coworkers [7] did for plastic scintillators containing anthracene derivative additives, so we tried to compare the yield of photo-luminescence of oxadiazole derivatives with their scintillation efficiencies.

Scintillation efficiency, $I_{scint.}$; concentration of additive, C; and position of the maxima of absorption and luminescence spectra of plastic scintillators with addition of derivatives of 1,3,4-oxadiazoles.

No.	Compound	λ_{max} abs. (mμ)	λ_{max} lum. (mμ)	C(%)	$I_{scint.}$ (%)
1	2-phenyl-1,3,4-oxadiazole	245	335	1.5	4.4
2	2-(4-methoxyphenyl)-1,3,4-oxadiazole	263	335	0.7	13.9
3	2-(4-methylphenyl)-1,3,4-oxadiazole	253	335	0.5	15.8
4	2-(4-biphenyl)-1,3,4-oxadiazole	280	325	0.8	48.5
5	2,5-diphenyl-1,3,4-oxadiazole	285	350	1.0	72.2
6	2-phenyl-5-(4-methoxyphenyl)-1,3,4-oxadiazole	293	370	1.6	134
7	2,5-di(4-methoxyphenyl)-1,3,4-oxadiazole	295	375	0.3	88.5
8	2-phenyl-5-biphenyl-1.3.4-oxadiazole	300	380	1.0	109
9	2-phenyl-5-(1-naphthyl)-1,3,4-oxadiazole	325	390	1.5	121
10	2-phenyl-5-(2-naphthyl)-1,3,4-oxadiazole	300	370	1.5	99
11	2-(4-biphenyl)-5-(1-naphthyl)-1,3,4-oxadiazole	320	395	0.45	119
12	2-(4-biphenyl)-5-(2-naphthyl)-1,3,4-oxadiazole	317	395	1.5	122
13	2,5-di-(1-naphthyl)-1,3,4-oxadiazole	295	405	1.6	139
14	2-(1-naphthyl)-5-(2-naphthyl)-1,3,4-oxadiazole	330	400	1.5	113
15	2,5-di-(2-naphthyl)-1,3,4-oxadiazole	265	390	2.0	99.6
16	2,5-di-(4-biphenyl)-1,3,4-oxadiazole	325	395	2.0	162

In figure 5 are shown the relative energy yields of photoluminescence R of polystyrene solutions of the materials, corrected for the sensitivity of the FEU-19 phototube.

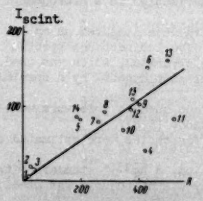

Figure 5. Comparison of the relative energy yield R with the value of $I_{scint.}$ Numbering of points corresponds to numbering of materials in the table.

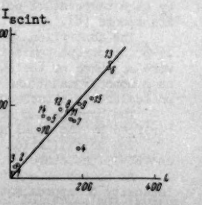

Figure 6. Comparison of the parameter L with the value of R and $I_{scint.}$ Numbering of points corresponds to numbering of materials in the table.

Although a linear relation between these values is not found, nevertheless we may note that, as a rule, a high value of R corresponds to a high scintillation efficiency of the sample. It is very likely that the absence of a linear relation between $I_{scint.}$ and R is caused by the following circumstance: on photoexcitation, which takes place in the surface layer of the sample, a reabsorption mechanism plays an important role in the process of excitation energy transfer, while in γ-ray excitation which is uniform at all depths of the sample, radiationless transfer is basic. We must take into account the fact that, in the case studied, self-extinction of the samples was not calculated.

In the treatments of the data obtained by the method of Swank and Buck [8], a proportional relation was found between $I_{scint.}$ and the value L, calculated according to a formula

$$L = R\left(\frac{q_o + \sqrt{I}C_M}{1 + \sqrt{I}C_M}\right) \cdot k,$$

where q_o is the quantum yield of photoluminescence of polystyrene, equal to 0.16; C_M is the molar concentration of the additive; k is the coefficient of proportionality, which depends on the type of mounting used for the measurement and kind of polymer. The value of R depends on the yield of photoluminescence, and may be calculated by the formula

$$R = \int_0^\infty I_l(\nu)\, k_{FEU}(\nu) d\nu,$$

where I_l is the intensity of luminescence of the additive in the sample; k_{FEU} is the sensitivity of the photocathode of the photomultiplier.

According to the data of Forster [9], the quantity $\sqrt{I}$ characterizes the effectiveness of the energy transfer and is equal to the square root of the integral of the overlapping of the absorption spectra of the additive and the luminescence spectra of the polystyrene. It is calculated by the formula:

$$I = \int_0^\infty f_o(\nu)\, \epsilon_g(\nu) \frac{d\nu}{\nu^4}.$$

A comparison of L and R with $I_{scint.}$ for the same sample blocks, carried out in the region of low concentration of the additive, where calculation for self-extinction is unnecessary, is shown in figure 6. As is evident, the scatter of points is not too great for so approximate a method of estimating the scintillation efficiency. Finally, figure 7 allows us to conclude that, for the materials investigated, the optimal concentration, c, of solution is of the order of 1-2%.

CONCLUSIONS

1. Among derivatives of oxadiazole, the most suitable as scintillation additives in plastic scintillators are the following: BBD, ONOND, MtPPD, ONBD, ONPD.

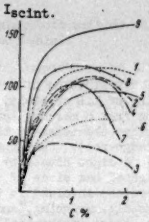

Figure 7. Concentration dependence of the scintillation efficiency $I_{scint.}$

1) 2-phenyl-5-(1-naphthyl)-1,3,4-oxadiazole.
2) 2-(1-naphthyl)-5-(2-naphthyl)-1,3,4-oxadiazole.
3) 2-(4-biphenyl)-1,3,4-oxadiazole.
4) 2-(4-biphenyl)-5-(2-naphthyl)-1,3,4-oxadiazole.
5) 2-phenyl-5-(2-naphthyl)-1,3,4-oxadiazole.
6) 2,5-di-(4-methoxyphenyl)-1,3,4-oxadiazole.
7) 2-phenyl-5-(4-biphenyl)-1,3,4-oxadiazole.
8) 2-(1-naphthyl)-5(4-biphenyl)-1,3,4-oxadiazole.
9) 2,5-dibiphenyl-1,3,4-oxadiazole.

2. In the diarylsubstituted oxadiazole series, the derivatives with the best scintillation properties are those which contain 1-naphthyl or biphenyl groups.

3. Scintillation efficiency may be estimated (in relative units) for low concentrations on the basis of a method of Swank and Buck, in which calculation the overlapping of the luminescent spectrum of the host and the absorption spectrum of the additive is taken into account, as well as the yield of photoluminescence of the additive and the sensitivity of the FEU phototube to the luminescence of the additive.

4. Scintillation efficiency of organic materials in plastic solutions is determined basically by three characteristics: a) absorption spectrum, b) luminescence spectrum, c) luminescence yield.

December 26, 1958

References

1. F. N. HAYES, D. G. OTT, V. N. KERR, B. S. ROGERS: Nucleonics, 13, (12), 38, (1955)
2. C. AINSWORTH: JACS, 77, 1148, (1955)
3. F. N. HAYES, B. S. ROGERS, D. G. OTT: JACS, 77, 1850, (1955)
4. E. AI. ANDREISHCHEV, E. E. BARONI, K. A. KOVYRZINA, I. E. PANI, I. I. ROZMAN, V. M. SHONIIA: PTE, NO. 1, 32, (1956)
5. A. WEISSBERGER: Physical Methods of Organic Chemistry, 4, 60, Interscience Publ., N. Y. (1951), (IL.,M.,(1955))
6. W. W. KORSHAK: (Monomers) 155, (IL, M., 1951).
7. A. S. CHERKASOV, G. A. TISHCHENKO, K. G. VAILDAIKINA: OIS, 4, (3), 344, (1958)
8. R. K. SWANK, W. L. BUCK: Phys. Rev., 91, 927, (1953)
9. T. FÖRSTER: Ann. Phys., 2, 55, (1948)

TOM VII, Vyp. 3 OPTIKA I SPEKTROSKOPIIA Sentiabr', 1959
VOL. VII, No. 3 OPTICS AND SPECTROSCOPY September, 1959

The Luminescence of Lithium Hydride

F. F. GAVRILOV

During an investigation of additive and photochemical coloring of LiH crystals, we discovered that under excitation from a mercury lamp these crystals luminesce brightly (the color of the luminescence is primarily orange-red). Only those crystals luminesce which have a light blue-gray color. The samples investigated had sizes of the order 2-5mm. All of the operations involved in the choice of the luminescent crystals, weighing, and irradiation took place in an atmosphere of chemically pure argon.

The luminescence of LiH has not been described in the literature.

THE SPECTRA OF THE LUMINESCENCE

The luminescence spectra were photographed in the visible and infrared regions with the help of an ISP-51 spectrograph (focal length 120mm., slit width 0.1 mm). The excitation source was a mercury lamp PRK-4 (3650 Å). The photographs were made using "Panchrom" film sensitized by number 103a dye (for the red luminescence), or else on photographic plates "infra-760" (for the infra-red luminescence). The spectral sensitivity of the film and plates was determined using a standard lamp whose filament was heated to a known temperature.

The luminescence spectra of LiH consist of three bands with maxima around 5970, 6550, and 7180 Å (Fig. 1).

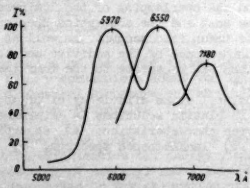

Figure 1. Luminescence spectra of colored crystals of LiH.

The short wavelength maximum is most pronounced in the crystals which luminesce with red-orange color. Crystals which luminesce with bright red color have a maximum around 6550 Å. The infra-red luminescence is of very high intensity especially in crystals luminescing with a dark red color. All three bands are present to a larger or smaller degree in the spectra of crystals luminescing with an orange color as well as those with a red color.

THE TEMPERATURE QUENCHING OF THE RED BAND

The temperature quenching of the luminescing of LiH was investigated using powders which were fixed to the outer surface of a tube which was soldered into a wide pipe connected to vacuum apparatus. Before pumping the apparatus out it was filled with argon. The phosphor was cooled by filling the tube with liquid nitrogen; it was heated by inserting a small electric heater in the tube. Visual photometry was used to measure the quenching curves with the help of a Pul'frikh photometer (the light filter was selected with a transmission band near 6550 Å). The same mercury lamp which had been used to excite the color of the luminescence was used for purposes of comparison.

The temperature quenching of the luminescence of crystal phosphors, whose emission is related to processes of a monomolecular type may be described by a formula first proposed by Gurney and Mott in 1938 [1]; it has the form

$$\eta = \frac{1}{1 + C \cdot \exp[-U/kT]}. \qquad (1)$$

Since then a formula of the same type has been used to describe the temperature quenching of infra-red luminescence in copper oxide [2], the luminescence of zinc sulphide phosphors [3], zinc oxide, and several other crystal phosphors [4].

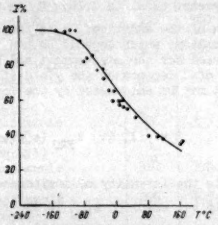

Figure 2. Temperature dependence of the luminescence intensity of LiH.

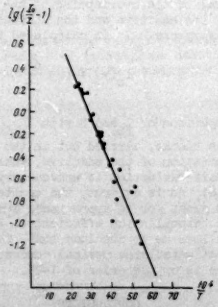

Figure 3. Same as Figure 2, in transformed coordinates.

With the goal of determining the applicability of this formula to the description of the temperature quenching of lithium-hydride luminescence, we have measured the dependence not only of I on T (Fig. 2)

but also of log $(\frac{I_0}{I} - 1)$ on $\frac{1}{T}$ (Fig. 3). In the event that the following law holds

$$I = \frac{I_0}{1 + C \cdot \exp[-U/kT]} \quad (2)$$

where I is the intensity of luminescence, the dependence of log $(\frac{I_0}{I} - 1)$ on $\frac{1}{T}$ should be a straight line As may be seen from figure 3 this dependence obtains. From the slope of the line and its intercept on the vertical axis, values were found for the activation energy U and the constant C equal respectively to 0.088 eV and 22.5.

THE CHEMICAL COMPOSITION OF THE LUMINESCENT CRYSTALS

The quantitative impurity content in luminescent and non-luminescent LiH crystals is different. Determination of the impurities in the crystals was made by spectrum analysis (the crystals of lithium hydride were converted into lithium sulphate before the analysis). The impurity content is shown in figure 4. In this figure the vertical axis represents the ratio of impurity concentrations in luminescent and non-luminescent crystals $\left(\frac{C_{lum.}}{C_{nonlum.}}\right)$.

The data given in the figure represent an average of the results of analyses of twenty different batches of samples. It follows from figure 4 that the luminescent crystals have a higher content of certain impurities.

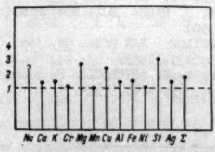

Figure 4. Impurity content in luminescent crystals. (Σ – the total of all impurities).

The stoichiometric composition of LiH was investigated by two methods. The first method was based on a volumetric determination of the amount of hydrogen produced in the decomposition of batches of lithium hydride by water, and on the determination of the amount of lithium by titration. In this way the amount of impurities was accounted for. The second method was based on the thermal decomposition of lithium hydride in a molybdenum retort with a continuous circulation of gas in a vessel, whose volume was known. The amount of gas liberated was determined by its pressure in this volume and also by a spectrographic method. Both methods are used in practical analytic studies.

The stoichiometric composition of lithium hydride was determined not only for a series of crystals of average weight 0.7 grams but also for small crystals weighing 2-5 mg. The results of the investigations using both methods turned out to be identical (see the table).

Stoichiometric Composition of LiH (atom %)

No.	Characteristic	Excess of Hydrogen	Excess of Lithium
1	Luminescent crystal	–	0.54
2	" "	–	0.50
3	" "	–	0.30
4	" "	–	0.80
5	" "	–	0.20
6	" "	–	0.20
7	Non-luminescent crystal	0.4	–
8	" "	–	–
9	" "	0.4	–

As may be seen from the table, in distinction to the non-luminescent crystals, the luminescent crystals of lithium hydride contain an excess of lithium (around 0.4% on the average).

THE RELATIONSHIP BETWEEN THE PHOTOCHEMICAL AND THERMAL PROCESSES AND THE LUMINESCENCE AND COLOR OF LiH CRYSTALS

Crystals of lithium hydride should be colorless and transparent. However, under the influence of light and heat the crystals take on either a dark blue or a light blue-gray coloration. Most frequently of all, the crystals become colored during preparation ("additive") coloring.

By analogy with F-centers, which have been well studied in crystals of the alkali-halide salts, the coloration of lithium hydride crystals might be connected with the stoichiometric excess of lithium [5] or with the presence of atoms of some other impurity.

We were interested in the coloration of LiH crystals from the point of view of its relationship to the luminescence [6]. With the aim of determining this relationship, colorless transparent, non-luminescent LiH crystals of high chemical purity were irradiated with ultra-violet light. The crystals were first reduced to powder.

Illumination was by means of unfiltered light from a PRK-4 mercury lamp, placed far enough away so as not to heat the powder directly. The crystalline powder was placed in a quartz tube in a vacuum of order 10^{-2} mm Hg. Within several minutes after the beginning of the illumination the crystals took on a dark blue color, different from the light blue-gray color of the luminescent crystals. During illumination several of the thinnest crystals exploded, indicating that the formation of F-centers takes place with the liberation of neutral hydrogen atoms, which, in trying to penetrate the lattice, destroy the crystals. The process of coloration of the crystals was observed continuously by visual observation through various colored light filters. The apparatus allowed one to change the wavelength of the exciting light rapidly by using various filters to select lines from the mercury spectrum.

Repeated experiments made to detect a visible luminescence during the formation of F-centers were unsuccessful. This seems to indicate that the photo coloration centers are not luminescent centers.

During illumination of the luminescent crystals, those which had been colored light blue-gray turned a noticeably darker blue and then gradually became

dark brown in color. At the same time the brightness of the luminescence decreased without any visible change in its color. The presence of two sorts of color centers in LiH crystals, one of which does not luminesce, might be established from analysis of the absorption spectrum of LiH and from the spectrum of the excitation of luminescence; however these spectra have not been investigated.

After heating the luminescent LiH crystals in a vacuum (10^{-2} mmHg.) at a temperature of 500° C for 30 minutes, the luminescence became less intense without any visible change in its color. Heating the non-luminescent crystals to 600° C for 30 minutes gave rise to a very weak luminescence, purplish-black in color, and the crystals became colored. When the crystals having a red luminescence were heated in the form of a powder in an atmosphere of hydrogen under 1.2 atm. pressure, the crystals are bleached, and the color of the luminescence changed from red to orange (500° C.) and then to bright yellow (600° C.)

ACTIVATION OF LiH USING GOLD AND MAGNESIUM

With the aim of determining the role of impurities in the processes of luminescence in LiH, preliminary experiments were carried out on the activation of pure crystals by gold and magnesium.

In the majority of cases of activation by gold, the crystals of LiH took on a gray and sometimes a somewhat yellowish color. For rated concentrations of gold of from 0.5 to 5% (by weight) the crystals luminesced with either an orange or a red color. Magnesium in rated concentrations of from 0.2 to 1% gave rise to a bright yellow luminescence. A particularly bright luminescence was observed for a magnesium concentration of 0.2%. The LiH crystals activated with magnesium, were always colorless and transparent. The LiH luminescence activated by magnesium differs from the red luminescence not only in its color but also, probably, in its mechanism. The absence of coloration in the crystals indicates that magnesium forms a solid solution with lithium hydride. One may suppose that the LiH luminescence activated by magnesium is due to magnesium ions and not to an excess of lithium atoms.

CONCLUSIONS

The data presented allow one to make certain preliminary qualitative conclusions. They show that the formation of luminescent centers in lithium hydride occurs because of a stoichiometric excess of lithium. In addition, impurities seem to play a role. It is possible that impurities take part only in the formation of lithium light-emission centers, i. e. the impurities promote the dissociation of the compound and provide the phosphor with activator atoms or with ions of the host metal [7].

The construction of models describing the processes of luminescence in lithium hydride is at present premature. In order to discover the mechanism of luminescence in lithium hydride it is necessary first of all to investigate the absorption spectra, emission kinetics, the photoconductivity, and the dependence of the luminescence on the intensity of excitation and the polarization of the luminescence.

The author extends his thanks to M. I. FEDEROVSKAIA and N. K. IAKHIMOVICH for help in carrying out the experiments.

December 11, 1958

References

1. R.W.GURNEY, N. F. MOTT: Trans. Farad. Soc., 35, (1939)
2. V. E. LASHKAREV, K. M. KOSONOGOVA: DAN USSR, 54, 125, (1946)
3. V. A. LASTREBOV: Tr., FIAN, USSR, 3, 123, (1954)
4. F. I. VERGUNAS, F. F. GAVRILOV: DAN, USSR, 57, 31, (1947); Tr. SFTI., 24, 196, (1947), ZETF, 20, 224, (1950)
5. PH. ALBER, J. MAHE: Bull.Soc.Chim.France, 1165, (1950)
6. P. P. FEOFILOV: DAN USSR, 92, 545, (1953); 92, 743, (1953)
7. W. PRIMAK, R. K. OSTERHOLD, R. WARD: Amer.Chem. Soc., 69, 1283, (1947)

TOM VII, Vyp. 3 OPTIKA I SPEKTROSKOPIIA Sentiabr', 1959
VOL. VII, No. 3 OPTICS AND SPECTROSCOPY September, 1959

Initial Stages of the Decay of Phosphors with Levels of Several Kinds

V. V. ANTONOV-ROMANOVSKII

Abstract: For phosphors with levels of several kinds when the probability of repeated capture of the free charges exceeds the probability of their recombination with the localized charges and saturation is absent, the decay curve in the initial stages can be represented as the sum of exponentials under certain conditions.

The problem of the decay of phosphorescence in the presence of levels of several kinds is very complex because of the nonlinearity of the appropriate kinetic equations. Actually, upon taking into account the motion of the electrons and holes and neglecting the free charge concentration in comparison with the localized charge concentration, the decay kinetics can be described by the following system of equations

$$\frac{dn_i^+}{dt} = -\frac{\sigma_{oi}^- n_i^+}{\sum_1^{m^+}\sigma_{ok}^- n_k^+ + \sum_1^{m^-}\sigma_k^-(\nu_k^- - n_k^-)}\sum_1^{m^-} w_k^- n_k^- - w_i^+ n_i^+ +$$

$$+\frac{\sigma_i^+(\nu_i^+ - n_i^+)}{\sum_1^{m^-}\sigma_{ok}^- n_k^- + \sum_1^{m^+}\sigma_k^+(\nu_k^+ - n_k^+)}\sum_1^{m^+} w_k^+ n_k^+, \qquad (1)$$

$$\frac{dn_i^-}{dt} = -\frac{\sigma_{oi}^+ n_i^-}{\sum_1^{m^-}\sigma_{ok}^+ n_k^- + \sum_1^{m^+}\sigma_k^+(\nu_k^+ - n_k^+)}\sum_1^{m^+} w_k^+ n_k^+ - w_i^- n_i^- +$$

$$+\frac{\sigma_i^-(\nu_i^- - n_i^-)}{\sum_1^{m^+}\sigma_{ok}^- n_k^+ + \sum_1^{m^-}\sigma_k^-(\nu_k^- - n_k^-)}\sum_1^{m^-} w_k^- n_k^-, \qquad (2)$$

where m^- and m^+ are the number of kinds of electron and hole traps, n_i^- and n_i^+ the localized charge concentrations, ν_i^- and ν_i^+ the trap concentration, w_i^- and w_i^+ the probability of liberating localized charges per unit time, σ_{oi}^- and σ_i^-, σ_{oi}^+ and σ_i^+ the effective cross-sections of free charge recombination and capture. The quantities with the minus sign refer to electrons and those with the plus to holes. The term "recombination" refers to the process of the reunion of separate charges and the term "capture" to all the rest of the free charge transition processes. The deeper the trap, the higher its ordinal number.

Since the phosphor as a whole is neutral then

$$\sum_1^{m^-} n_k^- - \sum_1^{m^+} n_k^+ = 0. \qquad (3)$$

This equality does not follow directly from the system of equations (1) and (2) because, combining them after first multiplying all the equations of (2) by -1 and remarking that all the terms of the right side of the equality cancel, we obtain just $\sum_1^{m^-} n_k^- - \sum_1^{m^+} n_k^+ = \text{const}$, which agrees with (3) only in the particular case that the constant is zero. One of the equations in (1) or (2) appears to be superfluous in the presence of (3).

Although the system of equations (1) and (2) is completely symmetric with respect to electrons and holes, we shall consider that luminescence can arise only because of recombination of the free charge with the localized holes (ionized luminescence centers). The luminescence intensity due to the ionized luminescence centers of the i-th kind will be

$$I_i = q_i\frac{\sigma_{oi}^- n_i^+}{\sum_1^{m^+}\sigma_{ok}^- n_k^+ + \sum_1^{m^-}\sigma_k^-(\nu_k^- - n_k^-)}\sum_1^{m^-} w_k^- n_k^-, \quad q_i \leqslant 1, \qquad (4)$$

where q_i is the probability of radiation during recombination. The quantity $\frac{I_i}{q_i}$ is none other than the first term in the right side of (1).

Despite the nonlinearity of the basic decay equations (1) and (2), the initial stages of quenching can appear to be quasi-linear in conformance with experimental results. This can be given a foundation on the basis of the following:

1. Even upon very intense and prolonged excitation, the traps are only partially filled. The shallow traps, because of the high probability of the thermal excursion of localized charge from them and the deep traps because of the quenching effect of the exciting light which consists of the exciting light itself being able to liberate localized charge [1]. Consequently, it is very probable that usually

$$n_i^- \ll \nu_i^- \text{ and } n_i^+ \ll \nu_i^+. \qquad (5)$$

2. It can be assumed that the probability of recombination is considerably less than the probability of repeated capture, i. e.,

$$\sigma_{oi}^- n_i^+ \ll \sigma_i^-(\nu_i^- - n_i^-) \approx \sigma_i^-\nu_i^- \text{ and}$$
$$\sigma_{oi}^+ n_i^- \ll \sigma_i^+(\nu_i^+ - n_i^+) \approx \sigma_i^+\nu_i^+, \qquad (6)$$

since even for such phosphors as SrS-Eu, Sm [2] and ZnS-Cu, Co [3], which store enormous light sums, these probabilities, appear to be just commensurable even in the very initial stages.

3. The thermal quenching curves of excited phosphors when uniformly heated have a number of maxima in the majority of cases especially for excitation at low temperatures. Usually they are separated well, which indicates a definite sequence in the effect of the filled traps. It is natural to relate this to

(7) $w_i^- \gg w_{i+1}^-$ and $w_i^+ \gg w_{i+1}^+$,

where w_i^- and w_i^+ are the probabilities of thermal liberation of localized charge and, consequently

(8) $w_i^- = w_{i,o}^- \exp\left[\frac{-\epsilon_i^-}{kT}\right]$ and $w_i^+ = w_{i,o}^+ \exp\left[\frac{-\epsilon_i^+}{kT}\right]$,

where ϵ_i^- and ϵ_i^+ are the energy depths of the traps, T the absolute temperature, k the Boltzmann constant, and $w_{i,o}^- \approx$ const and $w_{i,o}^+ \approx$ const.

4. Under short-time excitation the charge distribution in the traps will be sharply out of equilibrium temperature-wise since the charge localization will occur corresponding to the effective capture cross-sections of the traps. The pattern will also be similar under lengthy excitation since the exciting light, when its effect is long, will hinder filling of the traps (the fluorescing and quenching effect of the exciting light), particularly the deep traps. Consequently, it can be assumed that at the initial instant

(9) $\frac{n_{o'i}^-}{n_{o,i+1}^-} \gg \frac{n_{p,i}^-}{n_{p,i+1}^-} \ll 1$ and $\frac{n_{o,i}^+}{n_{o,i+1}^+} \gg \frac{n_{p,i}^+}{n_{p,i+1}^+} \ll 1$,

where the subscripts p and 0 denote, respectively, thermally equilibrium and unequilibrium concentrations of the localized charges.

The process of charge redistribution over the traps will be basic during any initial period of time for an initial sharply unequilibrium charge distribution over the traps and compliance with inequalities (5) and (6) because the decrease in charge of both kinds due to recombination will only be a correction. Consequently, the motion of the electrons and holes will proceed almost independently, which permits the investigation to be limited to the motion of charges of any one sign (let these charges be electrons for definiteness).

From (1), taking (5) and (6) into account and neglecting the recombination term in the right side of the equation, we obtain a linear system of equations (for simplicity, we omit the superscripts + and - everywhere)

(10) $\frac{dn_i}{dt} = -w_i n_i + \frac{\sigma_i \nu_i}{S_1^m} T_1^m$,

where

(11) $S_p^q = \sum_p^q \sigma_k \nu_k$ and $T_p^q = \sum_p^q w_k n_k$

(evidently $S_p^r + S_r^q = S_p^q$ and $T_p^r + T_r^q = T_p^q$). Under these conditions, we obtain from (4)

(12) $I_i = q_i \frac{\sigma_{oi} n_i}{S_1^m} T_1^m$.

Although the solution of the system (10) in general form is not difficult, it is visibly most laborious. However, a completely graphic picture of the decay (initial stages) and an approximate solution of (10) adequate to this picture can be given upon compliance with inequalities (7) and (9).

Because of (7) and (9), at the first instant of decay the majority of electrons will leave the shallowest traps and the free electron concentration will basically be determined thereby as will, moreover, the change in all the I_i also if only the holes do not succeed in leaving from certain kinds of traps (luminescence centers) during this time. As the shallowest traps become empty, the role of the next deeper traps gradually increases, then the role of the next, etc.

Because the traps become empty in succession, either one or (in the transition region) two kinds of traps of similar depth play an essential part at each given instant, for example, the (j - 1)st and the j-th traps. Thus, the electrons in the shallower traps will already be in equilibrium with the free electrons because the latter relax in a time larger than τ_i ($i < j - 1$). Consequently, the electron concentration in the shallower traps succeeds in "following" the free electron concentration due to the traps of the (j - 1)st and j - th kinds. On the other hand, the deeper traps ($i > j$) capture basically just electrons and, consequently, the electron concentration thus increases.

In conformance with the above, we obtain for the time interval

(13) $\tau_{j-2} \ll t \ll \tau_{j+1}$. ($i \leqslant 1$)

the following equations from the system (10)

(14) $\frac{dn_i}{dt} = -w_i n_i + \frac{\sigma_i \nu_i}{S_1^m} T_1^j \approx 0$, ($i < j - 1$),

(15) $\frac{dn_i}{dt} = -w_i n_i + \frac{\sigma_i \nu_i}{S_1^m} T_1^j$, ($i = j - 1, j$).

The definition of I, the upper limit of j, will be given later. The equation for $i > j$ will not be written because in practice all the deeper levels capture only electrons for $t \ll \tau_{j+1}$, giving nothing in exchange. For this reason the summation of $w_k n_k$ is made not over all levels but only (in order of increasing magnitude) up to the j-th kind ($T_1^m \approx T_1^j$). The summation of the $\sigma_k \nu_k$ is made over over all traps because they all capture electrons.

If all the equations in (14) are added, we can obtain

(16) $T_1^j = \frac{S_1^m}{S_{j-1}^m}(w_{j-1} n_{j-1} + w_j n_j)$.

Then substituting the expression found for T_1^j in (15) and (12), we obtain

(17) $\frac{dn_{j-1}}{dt} = -w_{j-1} n_{j-1} + \frac{\sigma_{j-1} \nu_{j-1}}{S_{j-1}^m}(w_{j-1} n_{j-1} + w_j n_j)$,

(18) $\frac{dn_j}{dt} = -w_j n_j + \frac{\sigma_j \nu_j}{S_{j-1}^m}(w_{j-1} n_{j-1} + w_j n_j)$,

$$I_i = q_i \frac{\sigma_{oi} n_i}{S^m_{j-1}} (w_{j-1} n_{j-1} + w_j n_j) \tag{19}$$

These equations are interesting. They are completely independent of the shallower traps for which $i < j-1$, i. e., the shallow traps seem to drop out.

As has already been remarked above, this is due to their population being in equilibrium with the free electron concentration.

The solution of (17) and (18) taking into account that $w_{j-1} \gg w_j$ is

$$n_{j-1} = n_{j-1,o} \exp[-\lambda_{j-1} t] + \tag{20}$$

$$+ \frac{w_j}{w_{j-1}} \delta_{j-1} (n_{j,o} + \delta_j n_{j-1,o}) \exp[-\lambda_j t] \quad \delta_{j-1} = \frac{\sigma_{j-1} \nu_{j-1}}{S^m_j},$$

$$n_j = -\delta_j n_{j-1,o} \exp[-\lambda_{j-1} t] + \tag{21}$$

$$+ (n_{j,o} + \delta_j n_{j-1,o}) \exp[-\lambda_j t], \quad \delta_j = \frac{\sigma_j \nu_j}{S^m_j},$$

where

$$\lambda_{j-1} = w_{j-1} \left(1 - \frac{\sigma_{j-1} \nu_{j-1}}{S^m_{j-1}}\right) + w_j \frac{\sigma_{j-1} \nu_{j-1}}{S^m_{j-1}} \frac{\sigma_j \nu_j}{S^m_j} + \tag{22}$$

$$+ \ldots \approx w_{j-1} \left(1 - \frac{\sigma_{j-1} \nu_{j-1}}{S^m_{j-1}}\right),$$

$$\lambda_j = w_j \left(1 - \frac{\sigma_j \nu_j}{S^m_{j-1}}\right) + \ldots \approx w_j \left(1 - \frac{\sigma_j \nu_j}{S^m_j}\right). \tag{23}$$

It is impossible to neglect the second term in (20) in comparison with the first since it decreases so very much more slowly than the first as t increases $\lambda_{j-1} \gg \lambda_j$, according to (22) and (23). This second term is due to the influence of levels of the j-th kind. The first term in (21) is negative and decreases rapidly with time t although the second term can be considered almost constant, i. e., n_j first increases. This is easily understood because the levels of the j-th kind do not succeed in delivering electrons at the beginning but electrons from levels of the (j-1)st kind "pour" into them through the band. After this, n_{j-1} and n_j diminish at the same rate. Hence, a computation of the decay made for two kinds of levels confirms the qualitative picture of the decay given above for a phosphor with several kinds of traps.

Using (20) and (21), we obtain from (19)

$$I_i = q_i \sigma_{oi} n_i \left[\frac{w_{j-1} n_{j-1}}{S^m_{j-1}} \exp[-\lambda_{j-1} t] + \right. \tag{24}$$

$$\left. + \frac{w_j}{S^m_j} \left(n_{j,o} + \frac{\sigma_j \nu_j}{S^m_j} n_{j-1,o}\right) \exp[-\lambda_j t] \right].$$

Attention is focussed in (24) on the fact that the coefficients of the exponentials are of different form. The fact is that at the moment when levels of the j-th kind play the principal role, the electron concentration therein increases with $n_{j,o}$ by an amount $\frac{\sigma_j \nu_j}{S^m_j} n_{j-1,o}$ because of electron liberation from levels of the (j-1)st kind (the electron concentration therein was $n_{j-1,o}$ but it drops by the fraction $\frac{\sigma_j \nu_j}{S^m_j}$ as electrons are liberated into levels of the j-th kind).

For fixed j (formula (24)) is valid not for all initial stages of decay but only within the time interval defined by (13). For another interval it will be valid for some other value of j. However, making use of the rapid decrease in the function $\exp[-\lambda_j t]$ with time, the following approximate formula can be written for I_i:

$$I_i = q_i \sigma_{oi} n_i \sum_1^l \frac{w_j}{S^m_j} n'_{j,o} \exp[-\lambda_j t], \tag{25}$$

where

$$n'_{j,o} = n_{j,o} + \frac{\sigma_j \nu_j}{S^m_j} \sum_1^{j-1} n_{k,o}, \tag{26}$$

which is valid for the whole initial period of decay

$$0 \leqslant t \leqslant \tau_{l+1} \tag{27}$$

obtained by summing the overlapping time intervals (13).

Formula (26) for $n'_{j,o}$ has been obtained by starting from the same simple considerations as for (24). At the instant levels of the j-th kind start to play a principal part, their electron concentration is increased over $n_{j,o}$ by the quantity $\frac{\sigma_j \nu_j}{S^m_j} \sum_1^{j-1} n_{k,o}$, obtained under the assumption that all the shallower levels appear in practice to be completely destroyed at this instant, i. e., almost all the electrons thereon make the transition to deeper traps and only an insignificant part are recombined. The sequence of the effect of the exponentials in (25) follows from the sequence of the effect of traps of different kinds.

The small changes (diminutions) in n_i^- and n_l^+ due to recombination can be taken into account thus. Let us carry out the computation for charges of any one sign, for example for holes.

Let us denote the changes in n_i^+ caused by recombinations with free electrons by Δn_i^+. Taking into account (5) and (6) and then expanding all the terms in (1) in power series in n_i^- and n_l^+, discarding linear terms and being limited only to quadratic terms, we obtain the following system of equations

$$\frac{d\Delta n_l^+}{dt} = -\frac{\sigma_{oi}^- n_i^+}{S^{m-}_l} n_l^{m-} - \frac{\sigma_l^+ \nu_i^+}{S^{m+}_l} \cdot \frac{\sum_o^m \sigma_{ok}^- n_k^-}{S^{m+}_l} n_l^{m+} \tag{28}$$

The first term on the right side of (28) determines the diminution in n_i^+ because of recombination of free electrons with holes localized on levels of the i-th kind; the second term is the diminution because of free hole recombination with all the localized electrons (the fact is that no matter what this recombination, whose quantity is defined by $\frac{1}{S_1^{m^+}} \sum^{m^-} \sigma_{ok}^+ n_k^-$, the fraction $\frac{\sigma_i^+ \nu_i^+}{S_1^{m^+}}$ of this quantity would still seem to be magnified by n_i^+).

Equation (28) only has meaning in the time interval

$$0 \leqslant t \lesssim \sim \tau_1^+, \tag{29}$$

because there will already be practically no holes on levels of the i-th kind for $t \gg \tau_i^+$.

Let us consider separately the diminution defined by the first and second terms on the right side of (28). Let

$$\Delta n_i^+ = \Delta_1 n_i^+ + \Delta_2 n_i^+, \tag{30}$$

so that

$$\frac{d\Delta_1 n_i^+}{dt} = -\frac{\sigma_{oi}^- n_i^+}{S_1^{m^-}} \tau_1^{m^-}, \tag{31}$$

$$\frac{d\Delta_2 n_i^+}{dt} = -\frac{\sigma_i^+ \nu_i^+}{S_1^{m^+}} \cdot \frac{\sum^{m^-} \sigma_{ok}^+ n_k^-}{S_1^{m^+}} \tau_1^{m^+}. \tag{32}$$

Because of the successive effect of the traps, we obtain for the time interval

$$\tau_{j-1}^- \ll t \ll \tau_{j+1}^- < \tau_i^+ \tag{33}$$

the following more simple formula in place of (31)

$$\frac{d\Delta_1 n_{i\tau_j^-}^+}{dt} = -\frac{\sigma_{oi}^- n_i^+}{S_1^{m^-}} w_j^- n_j^-, \tag{34}$$

because the traps with $i < j$ are in equilibrium with the band and, consequently, have been eliminated from the considerations while only electrons are captured for $i > j$. It can be assumed that

$$n_j^- = n_{j,o}^- \exp[-\lambda_j^- t], \tag{35}$$

since the basic change in n_j^- in the time interval (33) proceeds precisely according to this law [see the derivation of formula (25) above].

We obtain from (34) and (35) after taking (23) and (33) into account

$$\Delta_1 n_{i\tau_j^-}^+ = -\frac{\sigma_{oi}^- n_i^+}{S_j^{m^-}} w_j^- n_{j,o}' \int_{t \ll \tau_j^-}^{t \gg \tau_j'} \exp[-\lambda_j^- t]\, dt \approx -\frac{\sigma_{oi}^- n_i^+}{S_{j+1}^{m^-}} n_{j,o}^{1-}. \tag{36}$$

The computation of the quantity $\Delta_2 n_i^+$ is somewhat more complicated because of the presence of the $\sum^{m^-} \sigma_{ok}^+ n_k^-$ in (32) instead of the factor $\sigma_{oi}^- n_i^+$ in (31).

There will be another condition here instead of the time condition (33), which will refer not to electrons but to holes

$$\tau_{j-1}^+ \ll t \ll \tau_{j+1}^+, \ (j \leqslant i). \tag{37}$$

Again taking into account the sequence of the effect of the traps for this time interval, we obtain the following more simple formula in place of (32)

$$\frac{d\Delta_2 n_{i\tau_j^+}^+}{dt} = -\frac{\sigma_i^+ \nu_i^+}{S_j^{m^+}} \frac{\sum^{m^-} \sigma_{ok}^+ n_k^-}{S_j^{m^+}} w_j^+ n_j^+, \tag{38}$$

where j' in $\sum_{j'}^{m^-} \sigma_{ok}^+ n_k^-$ shows that electron traps in equilibrium with their band are excluded from the summation when hole traps of the j-th kind are most effective, hence the quantity n_k^- can be considered constant ($n_k^- \approx n_{k,o}^-$) for $k \geqslant j$. Then, taking (23) and (37) into account, we obtain from (35) and (38)

$$\Delta_2 n_{i\tau_j^+}^+ = -\frac{\sigma_i^+ \nu_i^+}{S_j^{m^+}} \frac{\sum^{m^-} \sigma_{ok}^+ n_{k,o}^-}{S_j^{m^+}} w_j^+ n_j'^+ + \int_{t \ll \tau_j^+}^{t \gg \tau_j^+} \exp[-\lambda_j^+ t]\, dt \approx -\frac{\sigma_i^+ \nu_i^+}{S_j^{m^+}} \frac{\sum_{j'}^{m^-} \sigma_{ok}^+ n_{j,o}^-}{S_j^{m^+}} n_{j,o}^+. \tag{39}$$

Having calculated $\Delta_1 n_{i\tau_j^-}^+$ and $\Delta_2 n_{i\tau_j^+}^+$ for various time intervals starting from the very beginning and ending with that after which external quenching approaches (departure of holes from levels of the i-th kind), the total losses after the whole initial decay period can be estimated, i. e., the quantity

$$\Delta n_i^+ = \sum \Delta_1 n_{i\tau_j^-}^+ + \sum \Delta_2 n_{i\tau_j^+}^+.$$

The mentioned method of estimating Δn_i^+ is sufficiently exact if

$$\frac{\Delta n_i^+}{n_i^+} \ll 1. \tag{40}$$

However, for $\frac{\Delta n_i^+}{n_i^+} \sim 1$, the following method can be used if only

$$(41)\qquad \frac{\Delta_1 n^+_{i\tau_j}}{n^+_j} \ll 1 \quad \text{and} \quad \frac{\Delta_2 n^+_{i\tau_j}}{n^+_j} \ll 1.$$

Condition (41) means that the quantity of separated charges decreases by a small quantity because of recombination during the time in which the basic bulk of the charge leaves traps of any one kind. However, the total losses can be great. In order to take them into account, it is necessary to introduce corrections into n^+_1 and n^-_1 (the computation for n^-_i is exactly the same as for n^+_i) each time that destruction of any kind of traps would occur.

Evidently such an operation will not violate the linearity of the equations considered above and, therefore, the "exponentiality" of the luminescence process is conserved. In particular, the form of the formula (25) for I_i is also conserved but the constants $n'_{j,o}$, which play the part of "initial" concentrations should be 'discounted'. These constants will be diminished corresponding to the recombination losses at the different stages of decay.

The question of the limiting value of l still remains open above in writing condition (13). That is, the value of l over the depth of the kind of levels from which the departure of the basic bulk of the charge is subject to a quasilinear law. According to the definition of l, condition (41) should already appear to be violated for levels of the $(l+1)$-st kind, and consequently, further decay will be "nonlinear".

The following cases are possible here. It can appear that there remain: 1) Only one kind of traps of either sign; 2) one kind of electron and several kinds of hole traps; 3) one kind of hole and several kinds of electron traps; 4) several kinds of traps of either sign.

The first case is very simple and its solution is not difficult even without conditions (5) and (6). The second and third can be considered (mathematically) to be identical because of the symmetry in the behavior of electrons and holes. Certain particular examples have already been analyzed in the literature. The fourth, very complex, case has still not been investigated.

In conclusion, it can be noted that a very general case of the initial stages of decay has been analyzed herein, when the kinetics of luminescence can be considered as quasilinear under certain conditions which are often justified by experiment. The remaining ' linear ' cases are specific in nature and have partially been examined in the literature. A special examination and comparison of all the "linear" cases with experiment is absolutely necessary.

December 26, 1958

References

1. V. V. ANTONOV-ROMANOVSKII: IAN USSR SF, 15,637, (1951)
2. L. I. ANIKINA: Dissertation, Tr. FIAN, 7, 5, (1956)
3. HSUI HSUI-YUN: DAN USSR, 106, 818, (1956) (See Soviet Physics, Doklady)

TOM VII, Vyp. 3 OPTIKA I SPEKTROSKOPIIA Sentiabr', 1959
Vol. VII, No. 3 OPTICS AND SPECTROSCOPY September, 1959

Investigation of Light Sums in the Phosphor SrS-Eu, Sm

(Communication I)

I. B. KEIRIM-MARKUS

Abstract: The light sums in the crystalophosphor SrS-Eu, Sm were investigated in detail by the method of thermal de-excitation. A number of new data were obtained pertaining to the storing of the electrons, their distribution among the traps and the parameters of the traps in the phosphor.

The investigation of light sums in crystallophosphors has recently acquired new practical significance, inasmuch as scintillating and thermoluminescent phosphors are finding application in the dosimetry of ionizing radiations [1-4]. The scintillating phosphor SrS-Eu,Sm is used in the method of dosimetry of the IIK [1,2]. Similar phosphors have been studied in detail by Soviet and foreign authors [5,6].

In the present work, the storing of electrons, their distribution among the traps and the parameters of the traps in the phosphor have been studied in more detail. The thermal de-excitation (TD) method was used for the investigation.

For complete de-excitation, the screens were heated to a temperature of above 400°C. Repeated measurements of the TD curve showed that under these conditions no light remained in the phosphors. The phosphors also failed to give flashes under the action of infrared rays.

The excitation of the phosphors was performed with the aid of a SF-4 spectrophotometer, which was used as a monochromator. The γ-radiation was furnished by cobalt-60 sources.

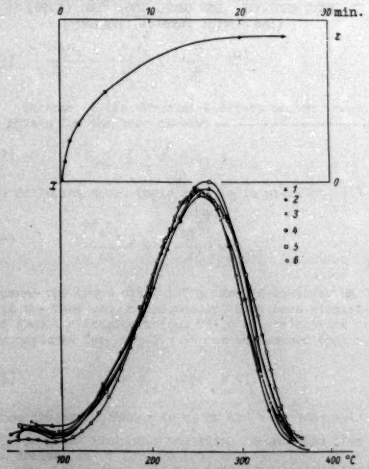

Figure 1. TD curves of a phosphor (dosimeter no.399), excited by 440 mμ light for various periods (after the sign X is the scale multiplier).

1- Exposure of 20 min. (curve 89)x 0.62; 2- 5 min. (100)x 1; 3- 2 min. (101)x 1.6; 4- 1 min. (102)x 2.2; 5- 0.5 min. (108)x 4.7; 6- γ-excitation (104)x 1.66.

Above - dependence of the light sum I on the exposure.

The TD curves of the phosphor, excited by light of wavelength of 440 mμ are presented in figure 1. The ordinate scales have been adjusted to make the curves coincide; the multiplication factors of the scales are indicated in the caption of the figure.

The form of the high temperature peak with a maximum of 260°C is analogous to the curve obtained by Urbach [6]. According to [6], however, the maximum of the curve proves to be at 377°C, apparently because of the high rate of heating (140degree/min., as compared to 5 degrees/min. in our experiments).

The limiting light sum is reached after 20 minutes. The accumulation of the light proceeds nonlinearly, as is evident from the upper part of figure 1. The form of the TD curve is practically unaffected by a fifty-fold change in exposure, i.e., it does not depend on the stored light sum right up to its limiting value.

The same thing is true for γ-excitation. This follows from figure 2 and will be demonstrated below in more detail.

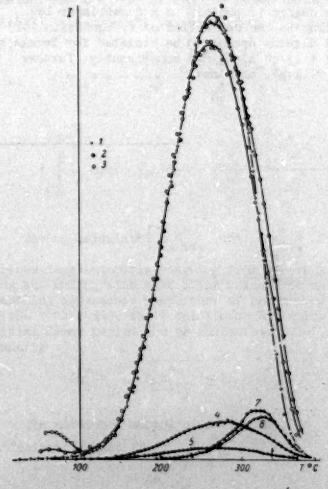

Figure 2. TD curves of a phosphor (dosimeter No. 371), excited with Co^{60} γ rays; various doses (after the sign X is the scale multiplier).

1- dose 1200 r (curve 54); 2- 100 r (37)x12; 3- 33 r (40)x36; 4- 100 r (37); 5- 33 r (40); 6- 1200 r after 2 minutes at 336° C (45); 7- the same (51).

As the experiment shows, the TD curves obtained immediately after excitation practically coincide with those obtained 11 days later, with the exception of the low temperature peak, which comparatively rapidly disappears.

Investigation of the TD curves obtained under various conditions of excitation has shown that they differ slightly in form. This, along with the great width of the peak, indicates the complexity of the composition of the main peak of the TD curve. On the other hand, when the degree of excitation of the phosphor is varied, the entire curve changes as a whole.

With the object of further analysis of the TD curves, the phosphor screen was excited by 440 mμ light for 20 minutes, and after 20 minutes the TD curve was determined. Then the same screen was excited by 440 mμ light for 20 minutes, irradiated with de-exciting light for 20 minutes, and the TD curve again measured. The difference between the first and second curves showed which electron traps were emptied under the action of the de-exciting light. The results of the experiment (Fig. 3) indicate that there is a whole system of traps of various depths [7,8] in the phosphor.

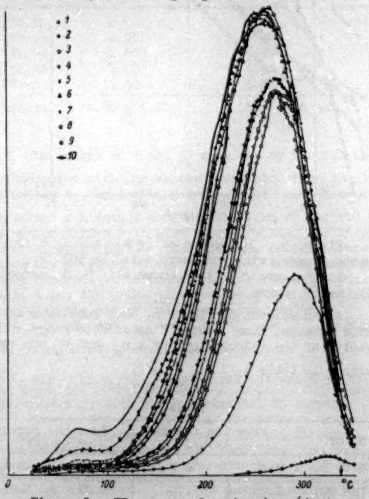

Figure 3. TD curves of a phosphor (dosimeter No.399), excited by 440 mμ light (20min.), after the action of light of wavelength λ during time t.
1- λ = 1400 mμ, t = 20 min. (curves 80, 87);
2- 1200 mμ, 20 min. (86,75); 3- 1000 mμ, 20 min. (59, 72, 82); 4- 900-100 mμ, 20 min. (92); 5- 900 mμ, 20 min. (85); 6- 800 mμ, 20 min. (58, 81); 7- 770 mμ, 20 min. (88); 8- 630 mμ, 60 min.(122); 9- 630 mμ, 15 min. (53); 10- heating to 338° C and exposure for 2 min. (105).

Over the entire range investigated (630-1400 mμ), the de-exciting light acts more strongly on the shallower levels, and has little effect on the deepest traps. This confirms the observation of Urbach [6], who noted the absence of any connection between the depth of the levels and the wavelength of the de-exciting light in the alkaline earth sulfides.

The maximal de-exciting action is possessed by light with a wavelength of around 100 mμ, which coincides with the maximum flash sensitivity of the SrS phosphors activated with samarium. Light with a wavelength of 630 mμ acts on levels which give luminescence at temperatures above 130° C in the same way that longer wavelength radiation does. At the same time, the shallower levels are emptied more rapidly by such light. Thus, the spectral sensitivity toward de-exciting action among the shallower levels has a second maximum with λ ⟨ 630 mμ, lying in the region of the exciting light. This is in agreement with the fact that when the wavelength of the exciting light is in the 600 mμ region, the shallow levels are filled to a lesser extent.

Let us note here the fact that the luminescence spectrum of the SrS-Eu,Sm phosphor overlaps the excitation spectrum – in the region of wavelengths shorter than 620 mμ – and the spectrum of sensitivity toward scintillation – in the longer wavelength region. In other words, the irradiation of the phosphor has a self-exciting and self-de-exciting action.

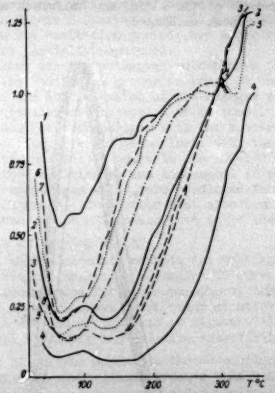

Figure 4. De-exciting action of light of varying wavelengths λ at traps of various depths.

Along the ordinate axis – ratio of the brightness of the thermoluminescence of the phosphor after 20 min. 440 mμ + 20 min. de-exciting light to the brightness after 20 min. of 440 mμ light.
1- λ = 1400 mμ; 2- 1200 mμ; 3- 100 mμ; 4- 900-100 mμ; 5- 900 mμ; 6- 800 mμ; 7- 630 (15 min.); 8- 630 (1 hour).

Figure 4 shows curves plotted according to the data of figure 3 and representing the ratio of brightness of thermoluminescence of the excited phosphor irradiated with de-exciting light to the brightness of luminescence of the phosphor not subjected to de-excitation. The shape of the curves permits one to determine roughly the location of the individual component peaks.

Actually, it follows from the theory of the TD method that in the case of first order kinetics (in

the coordinates of Fig. 4), the elementary peak of the TD curve should be depicted by a horizontal line. If the phosphor contains traps with different sensitivities toward the de-exciting light, the curve should have a step-like form, with the plateaus on the curve occurring at the locations of the individual peaks.

As is evident from the figure, the curves actually exhibit little steps, which can be ascribed to component peaks with maxima at approximately 60, 100, 130, 160, 200, 250, 300 and 320°C.

A second series of experiments set up for the analysis of the TD curves consisted in investigations with excited screens after they had been heated to high temperatures.

Figure 5 depicts TD curves of a phosphor, excited with a dose of 1200 r, heated to high temperature 5-6 minutes, held at this temperature for 2-3 minutes, and then quickly cooled to room temperature. As is evident on the figure, the maxima of the curves are displaced up to temperatures above 300°C; the halfwidth of the curves is diminished. Increasing the temperature of heating from 305°C, i.e., below the maximum, to 338°C, i.e., above the maximum, does not cause any substantial displacement of the curve; the halfwidth of the peaks is almost unchanged.

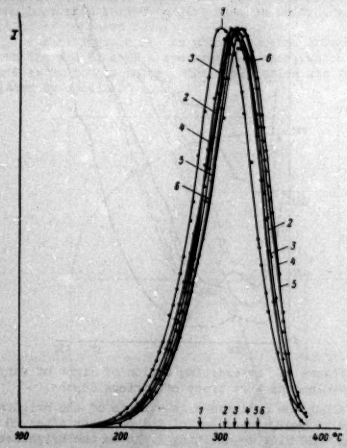

Figure 5. TD curves of a phosphor (dosimeter No. 371), excited by a dose of 1200 r of γ-rays of Cobalt-60, after heating to a temperature T and exposure for a period of time t.

1- T = 280° C, t = 3 min. after 23 hours at 20° C (curve 29); 2- 305° C, 3 min., (38, 24); 3- 214°C, 2 min. (39); 4- 327° C, 2 min. (41); 5- 338° C, 2 min. (45); 6- 338° C, 2 min. after 51 days at 20° C (51).

It also follows from these experiments [7-9] that in the SrS-Eu,Sm phosphor there is a complex spectrum of traps, so that when the phosphor is heated, levels of one type remain occupied. Consequently, the curves in figure 5 represent elementary TD curves.

If this is true, then by using the data of figure 5 one can determine the parameters of the traps by constructing curves showing $\lg(n/I)$ or $\lg(n^2/I)$ as a function of the quantity $5030/T°K$[7-9]*.

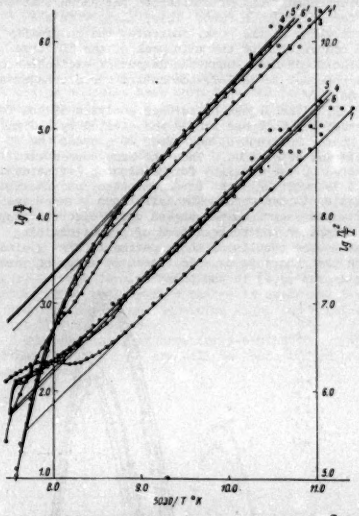

Figure 6. Dependence of $\lg n/I$ and $\lg n^2/I$ (upper curves, right ordinate axis) on 5030/T.

1, 1' curve 29; 4, 4' curve 41; 5, 5' curve 45; 6, 6', curve 51.

As is evident on figure 6, both functions approximate straight lines over a considerable range. The results of the calculations of ϵ, p_o and s_o are summarized in table 1.

Table 1

No. of curve on Figure 5	From the curves of lg n/I		From the curves of lg n^2/I	
	ε ev	lg p_o	ε ev	lg s_o
1 (No. 29)	0.98	5.99	1.02	1.01
4 (No. 41)	1.00	5.78	1.07	1.21
5 (No. 45)	1.01	5.81	1.06	1.12
6 (No. 51)	0.99	5.68	1.02	1.01
Average	1.00±0.01	5.82±0.15 $p_o = 6.6 \cdot 10^5$	1.04±0.02	1.02±0.20 $s_o = 10.5$

*When first order kinetics apply, i.e., the brightness of luminescence I = pn, where n is the light sum, $\lg \frac{n}{I} = \frac{5030\epsilon}{T} - \lg p_o$. For second order kinetics $I = sn^2$ and $\lg \frac{n^2}{I} = \frac{5030\epsilon}{T} - \lg s_o$.

An attempt was made to determine ϵ by another method, justified for the case in which the TD curve obeys second order kinetics. For this, the dependence of lg I on 1/T was plotted along the descending branch of the TD curve [7]. However, this method did not give satisfactory results.

The following method is based on knowing the value of the quantity $\delta_2 = T_2 - T_m$, where T_m is the temperature in °K of the maximum of the TD curve and T_2 is the temperature at which the brightness of luminescence on the descending branch of the curve has diminished by half. In the case of first order kinetics, $\epsilon = kT_m^2/\delta_2$, $p_o = (\beta/\delta_2)\exp[T_m/\delta_2]$. If the luminescence obeys second order kinetics, then $\epsilon = 2kT_m^2/\delta_2$ [8]. The results of the calculation are presented in table 2.

Table 2

No. of curve on Figure 5	$\frac{kT_m^2}{\delta_2}$	$\lg p_o = \lg\left(\frac{\beta}{\delta_2}\exp\left[\frac{T_m}{\delta_2}\right]\right)$
1 (No. 29)	0.92	5.49
2 (No. 24)	0.95	5.59
4 (No. 41)	1.00	5.84
5 (No. 45)	1.08	6.50
0 (No. 51)	1.00	5.88
Average	0.99 ± 0.07	5.86 ± 0.40

The values of ϵ and p_o obtained by the first method agree with the values calculated from the parameter δ_2, by starting from the assumption that first order kinetics obtain. The form of the TD curves on figure 5 is also characteristic for first order kinetics [8,9]. Thus, for the deepest traps which are detected by the TD method, thermoluminescence proceeds in accordance with first order kinetics; i.e., the probability of recapture is small.

With the aid of the experimental values $\epsilon = 1.00$ eV and $p_o = 6.6 \times 10^5$ sec.$^{-1}$ a curve was constructed according to the formula $I = I_o \exp[-\epsilon/kT\ p_o/\beta] \int_{T_o}^{T} \exp[-\epsilon/kT]\, dT$ which coincided satisfactorily with the experimental TD curves.

Knowing the parameters of the deepest traps, we attempted to decompose the experimental TD curves into elemental curves, at the same time, the somewhat arbitrary assumption was made that p_o is identical for all traps. The experimental curves were corrected with account taken of the diminution of the yield and changes in the sensitivity of the recording apparatus as the temperature of the phosphor increased. Then a calculated curve with $\epsilon_1 = 1.00$ eV was constructed on such a scale as to coincide as well as possible with the descending branch of the experimental curve. It was on the basis of the steeply descending high temperature branch of the curve, which represented the difference between the experimental and the calculated curves, that the energetic depth ϵ_2 of the following group of traps was determined, inasmuch as ϵ is approximately equal to T, etc.

The results obtained are presented in figures 7-10. One can estimate the distribution of electrons in the traps according to these figures. If one takes into account the fact that the luminosity P of the TD method $P = I_m/n \sim 1/\epsilon$ [8], then $n_1 \sim \epsilon_1 I_{m_1}$ and the fraction of electrons captured by the traps of the given depth ϵ_i is expressed as $n_{0i} = \epsilon_i I_{m_i} / \sum_i \epsilon_i I_{m_i}$. The values of n_{0i} are depicted on the figures in the form of vertical lines whose heights are proportional to n_{0i}. In the captions, along with the values of n_{0i}, the value of the ratio of the magnitude of the light sum at the traps after optical de-excitation to the light sum before de-excitation (in percent) is indicated in brackets.

Comparison of the curves obtained by γ-excitation and photoexcitation shows that in γ-excitation, the deepest traps with $\epsilon = 1$ eV are filled to a relatively greater extent, while the levels with $\epsilon = 0.72$ eV are hardly filled at all. The absence of electrons at the shallowest levels with $\epsilon \sim 0.56$ eV is associated with losses at the time of excitation. In figure 2 (curves 2 and 3) it is evident that when the excitation periods are shorter, these levels are partially populated.

We have already attempted to evaluate the position of the individual groups of traps on the TD curve via the investigation of the changes occurring in the curves after the action of de-exciting light on the phosphor. Comparison with the spectrum of the traps (Fig. 7 - 10) shows that, with the exclusion of the unresolved peaks in the 100-130°C region, the remaining maxima correspond in position to the temperatures which were predicted from the data of figure 4. The latter fact also confirms correctness of the assumption that p_o is identical for traps of varying depth.

The above described methods for testing elementariness and analyzing a complex TD curve can also be recommended for other phosphors, the luminescence of which obeys first order kinetics.

With the aid of the data of figures 7-10, one can roughly evaluate the relative sensitivity q_i of traps of various depths to the de-exciting light. For light with a wavelength greater than 900 mμ, $q_1:q_2:q_3:q_4:q_5:q_6:q_7:q_8 \simeq 0:0.3:4:10:20:45:70:100$. The relative sensitivities of the traps to light from the 630 mμ region are $q_1:q_2:q_3:q_4:q_5:q_6:q_7:q_8 \simeq$ $\simeq 0:0:0:7:21:52:70:100$.

Thus, the de-exciting action of long wavelength light falls off monotonically in proportion to the increase in the depth of the electron traps, and differs by a factor of hundreds for various traps in one and the same phosphor.

These experiments confirm the correctness of the assumptions to the effect that non-single-valued dependence of the brightness of the flash on the light sum is determined by a set of centers with differing sensitivities to the de-exciting light [6, 10].

Judging on the basis of the curves of figures 8-10, the optical de-excitation of a phosphor in certain cases involves repeated captures of electrons. Evaluation of the probability of repeated capture shows, that this probability is small.

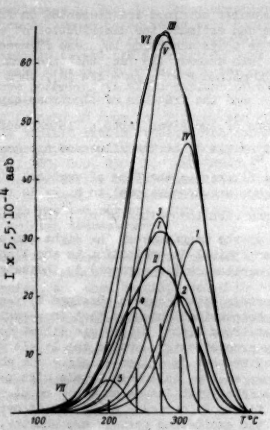

Figure 7. Analysis of the TD curve of a phosphor (dosimeter No. 270), excited with 260 r of γ-rays of Cobalt-60. — I. Experimental curve (No. 95); II. Corrected for change of the spectrum; III. Corrected for change of the spectrum and for quenching of the luminescence. — 1. Calculated curve (ϵ_1 = 1.0 eV, p_o = 6.6 x 10^5 sec^{-1}, n_{o1} = = 0.293); 2. The same (ϵ_2 = 0.96 eV, n_{o2} = 0.200); 3. The same (ϵ_3 = 0.91 eV, n_{o3} = 0.305); 4. The same (ϵ_4 = 0.85 eV, n_{o4} = 0.155); 5. The same (ϵ_5 = = 0.78 eV, n_{o5} = 0.044). — IV = 1 + 2; V = IV + + 3; VI = V + 4; VII = VI + 5.

Let us calculate the probability of thermal liberation of captured electrons and compare it with the change in the magnitude of the flash of the phosphor when it is stored after excitation (Fig. 11).

The initial decrease in the readings was caused by the departure of electrons from the ~0.56 eV and 0.68 eV levels. At 20° C the average lifetime of the electrons in these traps is

$$\frac{1}{p} = \frac{10^{-5}}{6.6} \frac{0.56 \cdot 11 \cdot 606}{293} = 6{,}500 \text{ sec.}, \sim 2 \text{ hours}$$

and approximately 9 days, respectively.

At 40° C these times are equal to 25 minutes and 1.5 days; at 60 ° C, to 7 minutes and 8 hours. At a temperature of 80° C the light sum at the traps with ϵ_7 ~ 0.68 eV is diminished by a factor of e after 2 hours. The initial diminution of the readings of dosimeters is well described by these figures.

Levels with a depth of 0.72 eV are hardly filled at all by γ-excitation (Fig. 7). An e-fold diminution of the light sum at the traps with ϵ_5 = 0.78 eV occurs after 460, 60, 11, and 2.5 days at

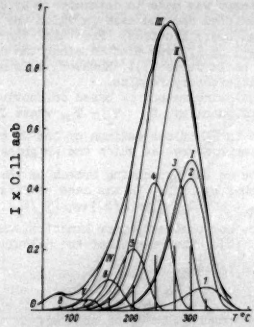

Figure 8. Analysis of the TD curve of a phosphor (dosimeter No. 399), excited before saturation with 440 mμ light. — 1. Calculated curve (ϵ = 1.0 eV, p_o = 6.6 x 10^5 sec^{-1}, n_{o5} = 0.05); 2. The same (ϵ_3 = 0.96 eV, n_{o2} = 0.27); 3. The same (ϵ_3 = 0.91 eV, n_{o3} = 0.27); 4. The same (ϵ_4 = 0.85 eV, n_{o4} = 0.23); 5. The same (ϵ_5 = 0.79 eV, n_{o5} = 0.10); 6. The same (ϵ_6 = 0.72 eV, n_{o6} = 0.05); 7,8. Group of fine levels (ϵ_7 ≈ 0.68 eV , n_{o7} ≈ 0.01 and ϵ_8 ≈ ≈ 0.56 eV, n_{o8} ≈ 0.02): — I = 1 + 2; II = 1 + 3; III = II + 4; IV = II +5; V = IV + 6.

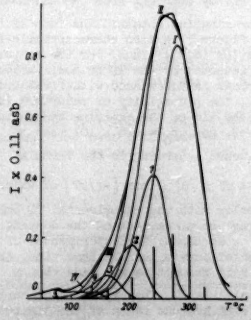

Figure 9. Analysis of the TD curve after exposure to 1400 mμ light. — I. Sum of the calculated curves with parameters ϵ_1 = 1.0 eV, p_o = 6.6 x 10^5 sec^{-1}, n_{o1} = 0.05; ϵ_2 = 0.96 eV, n_{o2} = 0.27; ϵ_3 = 0.91 eV, n_{o3} = 0.27. — 1. Calculated curve ϵ_4 = 0.85 eV, n_{o4} = 0.22 (96%); 2. The same, ϵ_5 = 0.79 eV, n_{o5} = 0.09 (90%); 3. The same, ϵ_6 = 0.72 eV, n_{o6} = 0.05 (80%); 4. The same, ϵ_7 ≈ 0.68 eV, n_{o7} ≈ 0.006 (≈ 60%); 5. The same, with ϵ_8 ≈ 0.56 eV, n_{o8} ≈ 0.01 (≈ 50%).—II=I+1; III=II+2; IV=III+3.

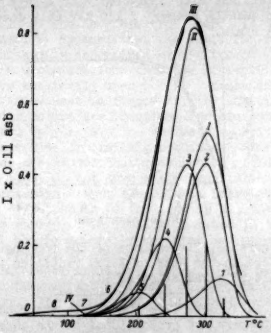

Figure 10. Analysis of the TD curve after the action of 1200 mμ light. — 1. Calculated curve with $\epsilon_1 = 1.0$ eV, $n_o = 0.07$ (140%); 2. The same, $\epsilon = 0.96$ eV, $n_{o2} = 0.27$ (100%); 3. The same, $\epsilon_3 = 0.91$ eV, $n_{o3} = 0.25$ (93%); 4. The same, $\epsilon_4 = 0.85$ eV, $n_{o4} = 0.12$ (52%); 5. The same, $\epsilon_5 = 1.79$ eV, $n_{o5} = 0.03$ (30%); 6. The same, $\epsilon_6 = 0.72$ eV, $n_{o6} \sim 0.02$ (~ 5%); 7. The same, $\epsilon_7 \sim 0.68$ eV, $n_{o7} \sim 0.003$ (~ 30%); 8. The same $\epsilon_8 \sim 0.56$ eV, $n_{o8} \sim 0.004$ (~ 20%). — I = 1 + 2; II = I + 3; III = II + 4; IV = III + 5.

20, 40, 60, and 80° C, respectively. It is evident that the changes which occur when the dosimeters are stored for a prolonged period are occasioned by these levels.

It appears that the readings of the dosimeters change in such a fashion, as to indicate that the levels below 0.78 eV are not filled (at 80° C, the lifetime of the electrons at the traps with $\epsilon_4 = 0.85$ eV is 20 days; the loss of these electrons would be depicted on the 80° curve of figure 11 by an almost horizontal line). Apparently, the long wavelength light exerts a quenching action on the deep traps.

As follows from figure 11, the readings taken directly after excitation are lower at higher temperatures. This is associated with quenching of the flash. Temperature quenching of luminescence also takes place at the time of excitation [6]; this is evident in figure 12. The activation energy of the radiationless transition ϵ, calculated using the formula [11] $\frac{I_o}{I} = 1 + \exp[-\epsilon/kT]$, proved to be 2.1 ± 0.2 eV.

As is evident on figure 11, the readings of dosimeters transferred from a lower to a higher temperature (for example, from 0°C to 20°C, or from 20°C to 60°C), diminished rapidly, and reached the same values as those of dosimeters which had been held the whole time at the higher temperature. At first glance such behavior can be explained by losses of the light sum from the shallower traps; however, as calculations show, such serious losses cannot be explained by this single cause. Actually, when the phosphor is cooled, the readings of the dosimeters are increased, and the magnitude of the flash increases by a factor equal to the ratio of the initial readings of the dosimeters at the two different temperatures. Thus the increase in the readings of the dosimeters at lower temperatures is associated with an increase in the yield of the flash, while the decrease in readings at higher temperatures is associated with quenching.

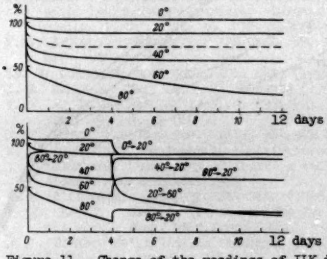

Figure 11. Change of the readings of IIK dosimeters depending on the length of storage (in days) at various temperatures (figures on the curves in °C. The reading taken directly after excitation with γ-rays at 30°C (dose 0.2 r) was taken as 100%. The dotted line is a dose of 1000 r, 20°C.

Previous explanations [1] of these results must be considered erroneous.

When the phosphor is excited with γ-rays, it is not difficult to determine the quantity of energy absorbed and, consequently, also the energetic yield of the light sum, i. e., the fraction of the energy of the exciting radiation transmitted to the phosphor, which is stored in the form of light.

For a dose of one roentgen, 88 ergs are absorbed per gram of phosphor (the mass coefficient of electron transformation of the γ-rays of Co^{60} is practically identical in air and in SrS [12]). The energy of γ-radiation absorbed per cm^2 of surface of the phosphor is $E = 88 \cdot d \cdot D = 40\ D$ erg/cm^2, where D is the dose in roentgens, d = 0.45 g/cm^2 is the thickness of the phosphor screen.

Inasmuch as the visual effectiveness of the luminescence of the phosphor is equal to 0.25 [13], 1 asb minute corresponds to 780 erg/sec. cm^2 [14]. If one takes into account that about 70% of the light emerges from the phosphor layer*, then 1 asb minute corresponds to 1100 erg/cm^2. Consequently, the energy yield

$$\eta = \frac{L}{E} = \frac{1100\Sigma}{40\ D} = 28\frac{\Sigma}{D},$$

where L & Σ is the light sum, expressed in erg/cm^2 and in asb. minute respectively.

For a dose of 260 r, 0.85 asb. minute of energy is stored in the phosphor, (Fig. 7). Consequently, the energy yield $\eta = 0.09$, for γ-excitation. The

*Determined in experiments with screens of varying thickness.

quantum yield, or the number of photons emitted per absorbed γ-quantum, reaches 20-25 thousand.

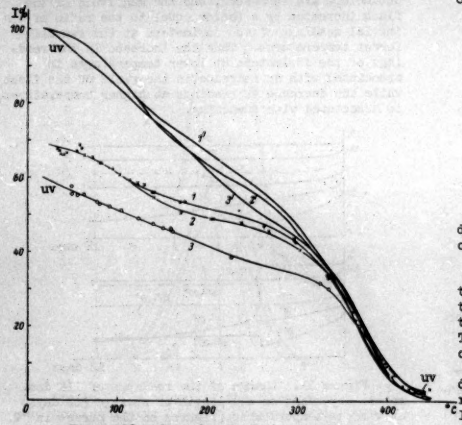

Figure 12. Dependence of the steady-state brightness of luminescence on the temperature of the phosphor.

1,2 – for excitation with blue light; 3 – excitation with ultraviolet light. 1' and 3': curves corrected for the change of the luminescence spectrum (brightness of the luminescence at 20° C taken as 100%).

Ours is apparently the first measurement of the energy yield of the light sum of scintillation phosphors excited by γ-radiation. The yield is apparently high. Among the scintillators the highest yield is possessed by the zinc sulfide phosphors: $\eta_{sc.} = 0.20 - 0.28$ [15]. In the alkali halide and tungstate phosphers $\eta_{sc.} = 0.01$ or 0.10 [15].

In scintillation phosphors, a part of the energy of the γ-rays is also transformed into luminescence at the time of excitation. Inasmuch as the total energy yield of luminescence in SrS cannot be much higher than in the zinc sulfide phosphors, one must recognize that in SrS the processes of accumulation and liberation of the light sum are accompanied by small losses of energy.

In further investigations, the dependence of the light sum on exposure (dose) was studied. It follows from figures 1 and 2 that the distribution of the electrons among the traps is not changed even when the light sum approaches the limiting value. As the limit is approached, however (in photoexcitation) the yield of the light sum gradually diminishes.

For γ-excitation, the yield remains constant over a wide range. The light sum is still proportional to the dose at 1200 r. This dependence was investigated in more detail in terms of the influence of the dose on the readings of IIK dosimeters (Fig. 13).

The readings did not depend on the dose rate between 0.35 and 900 r/min. The irradiation of the dosimeters was also conducted with X-rays with an average quantum energy of 110 keV at a dose rate of 20.3 r/min.

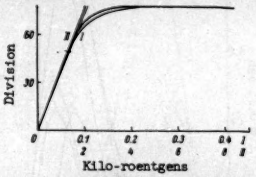

Figure 13. Dependence of the readings of IIK dosimeters on the dose of X-ray radiation (I) and of Cobalt-60 γ-radiation of (II).

As is evident from the figure the readings of the dosimeters are proportional to the dose right up to 1300 r of γ-radiation. In the small dose range, the linear dependence was traced down to 5×10^{-3} r. Thus, the proportionality is retained over a range of five orders of magnitude.

Since the light sum is also proportional to the dose (Fig.2), up to 1200 r, it follows that the readings of the dosimeters are proportional to the light sum over this range. One can assume that this dependence is also retained for large doses, when the readings of the dosimeters rapidly reach saturation.

On this assumption, the limiting reading corresponds to the light sum, which would be accumulated in a phosphor for a dose of 2000 r, if the light sum continued to be stored in proportion to the dose. The magnitude of the limiting light sum is 6.5 asb. min.; for a dose of 1200 r, 3.9 asb·min. is stored.

In the literature, values of the limiting light sum of the order of 10 asb·min. are encountered [16]. The light sum has similar or somewhat greater values in the best of the screens which are at our disposal. Inasmuch as the average energy of a light photon of the luminescence of SrS-Eu,Sm is 1.93 eV = 3.1×10^{-12} erg, 1 asb·min. corresponds to 3.6×10^{14} photons/cm^2, while the limiting light sum is 2.3×10^{15} photons/cm^2, i.e., 1.6×10^{16} photons/cm^3 or 5.2×10^{15} photons/g.

The limiting concentrations of the captured electrons and ionized centers have similar or even greater values. One can compare them with the total number of traps (and centers of luminescence) in a crystal, inasmuch as they are associated with concentrations of the activators in the phosphor equal to 5×10^{16} (or $5 \cdot 10^{17}$) atoms of Sm (or Eu) per gram of SrS (in the mixture).

If one assumes that all Eu atoms introduced into the mixture, form centers of luminescence in the phosphor, then it turns out that the limiting light sum corresponds to ionization of more than 1% of the total number of Eu luminescence centers. If one assumes that deep traps are formed near the Sm ions (one trap per ion), one finds that more than 10% of the deep traps are filled (according to the data of [6], around 1/3).

Inasmuch as apparently more than one Sm ion enters into the composition of a capture center, while some of the Sm ions do not form deep traps, and since the limiting light sum in individual screens proved to be 2-2.5 times greater than that

assumed in calculations, one can infer that under complete excitation by γ-rays, a significant part, if not all of the deep electron traps, is populated.

Hence, it appears that the limit for storage of the light sum is determined by filling of the deep traps. One can conclude that the de-exciting action of γ-rays apparently does not play an essential role.

As is evident in figure 13, the limiting readings of the dosimeters are identical for excitation by X-rays and by γ-rays. The dosimeters excited by daylight gave similar limiting readings. Starting from this, one can assume that penetrating radiation and visible light do not have any de-excitation effect on electrons in traps, since it is improbable that such an effect would be the same in all these cases.

The energy of excitation absorbed in the host material should generally speaking be transmitted not only to centers of luminescence, but also to the captured electrons. Actually, Lushchik [17] has detected a de-exciting effect of X-rays on certain alkali-halide phosphors. The absence of this effect evidently is a peculiarity of the alkaline-earth phosphors [18], thanks to which they store very great light sums.

The author expresses profound gratitude to the director of the work V. V. Antonov-Romanovskii, and also to E. A. Trapeznikova, M. V. Fok, N. A. Sergeeva, and E. E. Bukke.

September 26, 1958

References

1. V. V. ANTONOV-ROMANOVSKII, I. B. KEIRIM-MARKUS, M. S. POROSHINA, Z. A. TRAPEZNIKOVA: Sessiia AN SSSR po mirnomu ispol'zovaniiu atomnoi energii [Session of the Academy of Sciences USSR on the Peaceful Use of Atomic Energy], Akad. NAUK Press, 1955
2. I. P. BELOV, K. S. KALUGIN, I. B. KEIRIM-MARKUS, V. I. NIKIFOROV, M. S. POROSHINA: PiTE (in press)
3. B. M. NOSENKO, L. A. REVZIN, V. IA. IASKOLKO: ZTF, 26, 2046-2048 (1956) (See Sov.Phys., Tech.Phys.), OiS, 3, 345, (1957)
4. V. A. ARKHANGEL'SKAIA, B. I. VEINBERG, T. K. RAZUMOVA: OiS, 1, 1018-1020 (1956), 4, 681-683 (1958)
5. V. L. LEVSHIN, V. V. ANTONOV-ROMANOVSKII, Z. L. MORGENSHTERN, Z. A. TRAPEZNIKOVA: DAN SSSR, 54, 19-22 (1946) [in English]; ZETF, 17, 949-963, (1947)
6. F. URBACH: Preparation and characteristics of solid luminescent materials. Cornell symposium, 1948; JOSA, 36, 372-38, (1946)
7. V. V. ANTONOV-ROMANOVSKII: IAN USSR, SF, 10, 477 (1946)
8. CH. B. LUSHCHIK: DAN SSSR, 101, 641, (1955)
9. I. A. PARFIANOVICH: ZETF, 26, 696-703 (1954)
10. V. V. ANTONOV-ROMANOVSKII, E. S. KRYLOVA: ZETF, 19, 63-73 (1949)
11. N. F. MOTT: Proc.Roy.Soc., A167, 384-391 (1938)
12. K. K. AGLINTSEV: Dozimetriia ioniziruiushchikh izluchenii [Dosimetry of ionizing radiations], Gostekhizdat 1957
13. R. T. ELLICKSON: JOSA, 36, 261-264, (1946)
14. S. V. KRAVKOV: Glaz i ego rabota [The Eye and its work], Akad. NAUK Press 1950
15. J. B. BIRKS: Scintillation Counters, N.Y., (1953); (IL, Moscow, 1955)
16. R. T. ELLICKSON: JOSA, 36, 264-269, (1946)
17. CH. B. LUSHCHIK, G.G.LIID'IA: Tr.IFA AN ESSR No. 7, 193-226 (1958); CH. B. LUSHCHIK, F.N. ZAITOV: Tr.IFA AN ESSR, No. 7, 276-310, (1958)
18. B. O.BRIEN: Preparation and characteristics of solid luminescent materials, Cornell Symposium, (1948)

TOM VII, Vyp. 3 OPTIKA I SPEKTROSKOPIIA Sentiabr', 1959
Vol. VII, No. 3 OPTICS AND SPECTROSCOPY September, 1959

The Influence of the Electric Prehistory of the Electroluminophore on the Characteristics of its Luminescence Excited by Short Voltage Pulses

I. IA. LIAMICHEV AND I. N. ORLOV

Abstract: Experimental data are presented pertaining to the excitation of electroluminescence by rectangular voltage pulses, which show the influence of preliminary excitation of an electroluminophore on the character of its luminescence. The relation of the luminescence to the preliminary excitation of the phosphor by an electric field was studied by applying three independently variable series of voltage pulses to an electroluminescing layer, in a controlled time sequence. A qualitative explanation is presented for the mechanism of production of two peaks in each pulse of luminescence of the electroluminophore.

It has been noted repeatedly in works on electroluminescence [1-3], that the polarization of phosphors which arises in them due to the action of an applied electric field, exerts an influence on the character of the "luminous flash", obtained by subsequent excitation of the electroluminescence. The prolonged maintenance of such an influence ("frozen polarization"), even after removal of the preliminarily applied voltage, has been explained as the accumulation of electrons, drawn off by the field from the excited region at the trapping levels in the bulk of the crystal, where the applied field is small [4-8]. These polarization phenomena have ordinarily been studied during the excitation of electroluminescence by sinusoidal fields, and in only one case was work [1]* carried out with excitation by prolonged voltage "pulses" of a single polarity.

The experimental results of a study of the luminescence characteristics of electroluminophores as a function of the parameters of an electrical field, which was acting on the luminophore before the moment of time being considered, are presented below. Such a study proved to be possible thanks to the application of a special method of investigation by pulsed excitation of the electroluminescence.

APPARATUS AND METHOD OF MEASUREMENTS

A specially made generator of voltage pulses (Fig. 1), consisting of four parallel circuits and having two outputs, permitted the electrodes of the luminescent capacitors to be supplied with pulses of five independently controlled series, the relative timing of which could be arbitrarily changed. Pulses of opposite polarity were applied simultaneously to the capacitor electrodes, to insure excitation of the electroluminophore.

An FEU-19 multiplier connected to an oscilloscope served as a receptor of the radiation from the electroluminophores. The amplifier following the photomultiplier had a bandwidth of about 6.5 Mc/s to insure distortion-free amplification of the electrical signal generated by the light pulse. To investigate the connection between the luminescence pulses and the voltage pulses supplied at the capacitor, we used two wide-band oscilloscopes: on the screen of one were fixed values of the voltage pulses; on the screen of the other the corresponding pulses of luminescence.

We studied electroluminophores of the ZnS-Cu (Pb, Cl) and ZnS-Cu, Cl type with a blue and green radiation color. The luminescing capacitor consisted of an electroluminescing layer (luminophore + solid organic dielectric) from 30 to 100 microns thick placed between a transparent glass and a film of metallic aluminum. The capacity of the layer amounted to about 100 pf/cm^2.

In the remainder of the article, the magnitude of the electric signal from the photomultiplier proportional to the light flux striking the FEU photocathode will be designated by the term "luminosity".

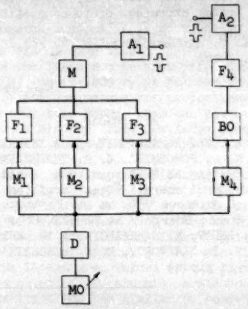

Figure 1. Block diagram of the pulse generator. — MO - master oscillator; D - voltage divider; M_{1-4} - driving multivibrators; F_{1-4} - shaping stages; M - mixer; BO - blocking oscillator; A_{1-2} - amplifer.

EXCITATION OF ELECTROLUMINESCENCE BY PULSES OF A SINGLE SERIES

In simple pulse excitation, when single pulses of voltage are applied to a luminophore, each produces a pulse of luminescence from the capacitor, if the exciting pulses follow each other continuously (with a definite repetition rate), and are identical in amplitude and polarity [10, 11].

When such excitation is steady state, each luminescence pulse consists of two peaks: a "first", coinciding in time with the growth of the voltage pulse, and a "second", corresponding to the drop off of the voltage pulse (Fig. 2). As it turned out, the ratio of the heights of both peaks depends strongly on the repetition rate of the exciting pulses and the temperature of the electroluminescing layer. With an increase of the period of repetition T, the height of the first peak gradually diminishes and for periods of the order of 10 seconds, this peak disappears almost completely (comparable in magnitude with the noise). The second peak is only slightly

*Many new works have recently been published on electroluminescence, including one [9], directly touching upon the impulse excitation of electroluminophores.

changed under these conditions: its height slowly grows up to the time when the first peak of the luminescence pulse disappears.

Figure 2. Pulse of the exciting voltage (below) and the corresponding luminescence pulse of the electroluminescing capacitor for a single pulse excitation. — Photo made from the screen of a double beam oscilloscope.

a b

Figure 3. Luminescence pulses of an electroluminophore for repetition rates of the exciting pulses of 10 millisecond (a) and 1 second (b).

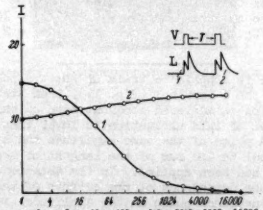

Figure 4. Dependence of the heights of the first (1) and second (2) peaks of the luminescence pulse (L) on the period T of the repetition of the exciting voltage pulses (V). — Along the ordinate — instantaneous luminosity (in relative units).

In figures 3 and 4 is shown such a change in the form of the pulse of luminescence depending on the period of repetition of the exciting pulses, which are constant in amplitude and duration. It is evident from figure 5, that the character of the change of the first peak, depending on the period of repetition, remains the same for various amplitudes and durations of the exciting pulses — these two parameters change only the absolute magnitudes of the peaks of the luminescence pulse, but scarcely influence the ratio of the two peaks (increase of the duration of the pulses changes this ratio because of preferential growth of the first peak, although by an insignificant amount).

A rise in the temperature of the electroluminophore leads to a similar change in the form of the luminescence pulse, as does also an increase in the time between exciting pulses. The disappearance of the first peak is observed at temperatures of 70-100° C (Fig. 6). The higher the temperature of the luminophore, the more rapidly the first peak is diminished as the period of repetition increases. (Fig. 7).

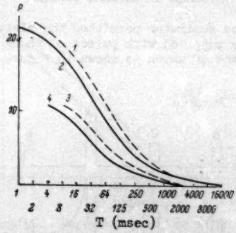

Figure 5. Dependence of the height of the first peak P (in relative units) on the repetition rate of voltage pulses of different amplitude and duration. — 1- amplitude 550 V lasting 20 microseconds; 2- 550 V, 4 microseconds; 3- 300 V, 20 microseconds; 4- 300 V, 10 microseconds.

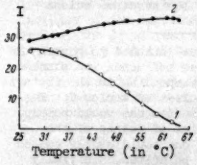

Figure 6. Dependence of the height of the first (1) and second (2) peaks of the luminescence pulse on the temperature of the electroluminescing layer. — Repetition rate of the voltage pulses 250 millisecond. Along the ordinate axis - instantaneous luminosity (in relative units).

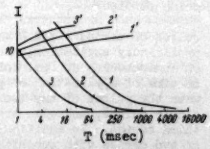

Figure 7. Dependence of the heights of the first (1, 2, and 3) and second (1', 2', and 3') peaks on the repetition rate of the voltage pulses for different temperatures of the electroluminophore. — 1 and 1'- 26° C; 2 and 2'- 65° C; 3 and 3'- 100° C. Along the ordinate axis — instantaneous luminosity (in relative units).

If one takes account also of the fact that in the excitation of electroluminescence by a series of identical pulses, the first peak of the luminescence pulse does not appear immediately at the instant of application of the first pulse of the train, but only after the supply of 5-7 pulses (see below Fig. 13a), then the hypothesis suggests itself, that the first peak arises only because of the generation of a certain "residual" excited state in the grains of the luminophore by the effect of the preceding voltage pulses. If this state is destroyed by a rise in the temperature, or by an increase in the repetition rate of the voltage pulses, then the first peak of the luminescence pulses also disappears. In order to have the

possibility of regulating the magnitude of the "residual" excitation and to study the nature of the luminescence pulse in more detail, a study of electroluminescence using several independent series of voltage pulses was undertaken.

EXCITATION OF ELECTROLUMINESCENCE BY PULSES OF SEVERAL SERIES

A pulse generator permitted the electroluminophore to be supplied with pulses of three series, the time sequence of which is shown in figure 8.

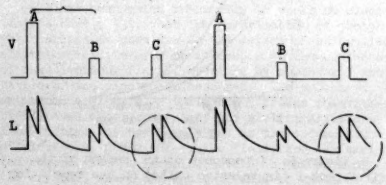

Figure 8. Sequence of supply of voltage pulses of different series at the electroluminescing capacitors. — V- voltage pulse; L- luminescence pulse; A,B- preliminary excitation; C- observation pulse. The dashed circles note the luminescence pulses being studied.

Pulses of series A and B were intended to govern the preliminary excitation, whose influence was studied on luminescence pulses, corresponding to the instants of time of application of pulses of series C. Between the pulses of any two series one could supply single pulses, and also trains of pulses of the third series. In addition, one could supply pulses of two series with opposite polarites. Initially the interaction of pulses of only two series, A and C was studied.

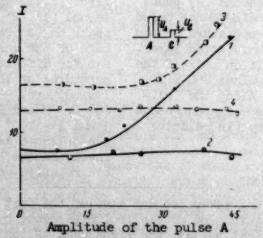

Figure 9. Dependence of the heights of the first (1 and 3) and second (2 and 4) peaks on the amplitude of the voltage pulses of series A. 1 and 2-U_C = 20 units; U_B = 0; 3 and 4-U_C = 34 units; U_B = 0. — Along the abscissa axis – the amplitude of the pulse A (in relative units); along the ordinate axis — instantaneous luminosity (in relative units).

It is evident from figure 9, that the A pulses begin to exert an influence on the luminescence from the C pulses only after their amplitude begins to be greater than the amplitude of the C pulses: in this case the height of the first peak in the luminescence pulse being observed grows linearly with the growth of pulse A. The second peak, here, depends hardly at all on the amplitude of pulse A. An increase in the duration of the A pulses or in their number between the neighboring C pulses leads to the growth of the first peak, continuing until a magnitude of the first peak is achieved, which corresponds to the given amplitude of the exciting pulses. Figure 10 shows that the preliminary excitation, which can generate A pulses of given amplitude, is reached after a time of the order of 10-20 microseconds.

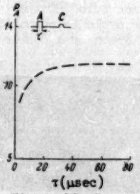

Figure 10. Dependence of the height of the first peak P_A (in relative units) on the duration τ of the voltage pulse of series A. – $U_A/U_C \cong 3.5$; U_B = 0.

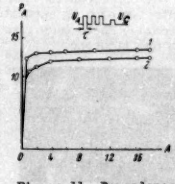

Figure 11. Dependence of height of the first peak P_A (in relative units) on the number n of series A voltage pulses, supplied between two C pulses. – $U_A/U_C \cong 3.5$; U_B = 0; 1- τ_A = 10 microseconds; 2- τ_A = 2 microseconds.

If there is supplied a train of short A pulses between the C impulses (Fig. 11), then stable preexcitation is achieved somewhat more quickly, but the level of this excitation is lower than if a single A pulse of the same amplitude and of a duration equal to the sum of the lengths of the short A pulses, had been applied. In the absence of A pulses the dependence of the heights of the peaks of the luminescence pulse on the amplitude of the C pulses is expressed by the power function $E = U_C^n$, where E is the height of the peaks of the luminescence pulse, while U_C is the amplitude of the C pulses (see Fig. 12, curves 3 and 4). The introduction of A pulses changes this dependence: the exponent n is diminished (curves 1 and 2 of Fig. 12.). In the case of the first peak the diminution of n is the more significant, the smaller the C pulses are in relation to the A pulses.

If there is supplied not just a single but a train of C pulses between A pulses, then as is evident from figure 13, b and c, the height of the first peak for each subsequent C pulse will be less than for the preceding one. The C pulses in this case "cancel out" the excitation produced by the A pulses, leading the luminophore into a new state of residual excitation of a lower level. The degree of this "canceling out" is determined by the number of C pulses in the train and by their amplitude (Fig. 14).

In the case of differing polarity of the A and C pulses, all the phenomena indicated above are retained without changes, but the canceling out of

the excitation by a train of C pulses proceeds somewhat more rapidly (Fig. 13, c, and curve 2 of Fig.14).

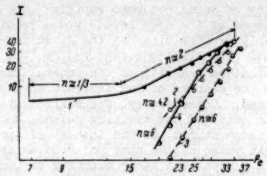

Figure 12. Dependence of the height I of the first (1 and 3) and second (2 and 4) peaks on the amplitude (P_C)(in relative units) of the series C pulses in a logarithmic scale. — 1 and 2- $U_A = 42$ units; 3 and 4 for $U_A = 0$.

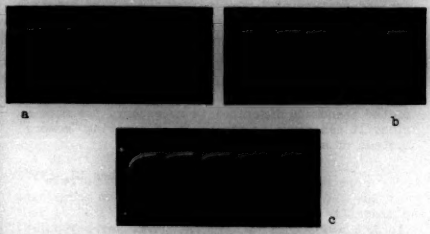

Figure 13. Luminescence pulses from a train of pulses of series C. — a- in the absence of A and B pulses; b- A pulses supplied with a polarity identical with that of C; c- A and C pulses of opposite polarity.

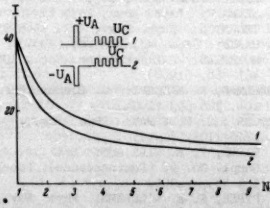

Figure 14. Dependence of the heights I of the first peak on the number of pulses N_C of series C in the train. — $U_A/U_C \cong 3.5$; 1- A and C pulses of the same polarity; 2- A and C pulses of opposite polarity.

An increase of the time between A and C pulses (Fig. 15) leads to a diminution of the first peak. This dependence can be approximated over a wide interval of time by the equation

$$E_n = 1g \frac{K}{T},$$

in which E_n is the height of the first peak, T is the time between A and C pulses, and K is a constant. The region of small T, where character of the change of the first peak with T depends on the polarity of the A and C pulses, constitutes an exception, as is evident from the figure: when their polarities are identical, there is observed a short horizontal segment, which is absent when the pulses differ in polarity.

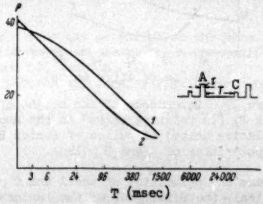

Figure 15. Dependence of the first peak p (in relative units) on the time shift (T) between pulses of series A and C. — $U_A/U_C \cong 3$; 1- $U_A = +40$ units; 2- $U_A = -40$ units.

The phenomenon of canceling out the pre-excitation described above is more conveniently observed when independently controlled pulses of series B are introduced between the A and C pulses. With an increase of the amplitude of the pulses of this series, the first peak of the pulse of luminescence is initially little changed, and then it drops sharply.

For a definite amplitude of the B pulses, the first peak reaches a minimum value, after which it again begins to grow (Fig. 16).

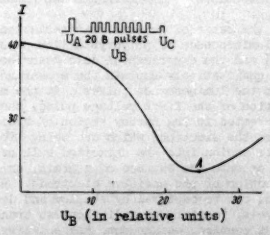

Figure 16. Dependence of the height (in relative units) of the first peak on the amplitude U_B (in relative units) of pulses of series B. — The combination of pulses indicated at the top of the figure was applied to the capacitor. — $U_A/U_C \cong 3.5$.

Thus, the B pulses can be sufficiently large in amplitude to cancel out completely the excitation from the A pulses, and to create a new excited state of the luminophore, determined only by their amplitude. The complete change of the first peak under the action of the B pulses is achieved when their train consists of not less than 5-7 pulses. If the polarities of the A and B pulses are opposite, then the character of the phenomenon of canceling out is determined by the polarity of the C pulses in relation to the A pulses (Fig. 17).

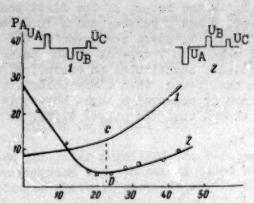

Figure 17. Dependence of the height of the first peak P_A (in relative units) on the amplitude U_B (in relative units) of pulses of series B for opposite polarities of A and B pulses.

In case the polarities of the A and C pulses are identical, the first peak of the luminescence pulse is approximately equal to the sum of the heights of the peaks obtained from the separate actions of the A and B pulses. If the polarities of the A and C pulses are different, then the first peak is approximately equal to the difference of the heights obtained from the separate actions of the A and B pulses (this applies to small B pulses). In figure 17 at the points C and D a combination of A and B pulses of equal amplitudes is applied; however, the first peaks are different. Consequently, the excited state created by the differently polarized A and B pulses, can not unequivocally determine the luminescence at the instant of application of the C pulses, since it depends on the polarity of the C pulses themselves.

DISCUSSIONS OF THE EXPERIMENTAL RESULTS

On the basis of general representations of the electroluminescence of polycrystalline phosphors [12, 13] and the experimental data described above, one can qualitatively explain the appearance of two peaks in the luminescence pulses. At the moment of application of the first voltage pulse, the strong field, created in the narrow region of excitation, transfers the electrons which are being liberated from this region into the unexcited bulk of the crystal or onto the surface of a grain, oriented in the direction of the positive electrode. Here the electrons can be captured by shallow and deep trapping levels, "centers of radiationless transitions" and, at a contact, escape onto the positive electrode. Where the electrons do not "stick", they cannot return to the region of ionized centers of luminescence until the external field is removed or its direction changed. At the moment of removal of the field (the trailing edge of the pulse) a field is set up in the crystal which is created by the positive space charge in the excitation region. The electrons which are at this instant in the conduction band are rapidly returned to the excited region under the action of this field and recombine with the ionized centers of luminescence. There arises a "second" peak of the pulse of luminescence. But not all of the electrons liberated in the excitation have the opportunity of being returned rapidly: the electrons trapped at the deep levels would require a considerably greater time, at the given temperature conditions. The electrons captured by "the centers of radiationless transitions" in general cannot return to the centers of luminescence through a conduction band. Consequently, for sufficiently low repetition rates of the exciting pulses, and for moderate temperatures, at the instant of application of the next pulse of the same polarity as the first there will always be a large quantity of ionized centers of luminescence in the region of excitation with which those electrons can recombine, which have been just liberated by the new pulse. Such recombination can occur until the new pulse propagates over the entire "old" region of excitation, i.e., achieves full amplitude. As a result of recombination of the newly liberated electrons with the previously created ionized centers of luminescence, there also occurs a "first" peak of the luminescence pulse.

The greater part of the phenomena described above, it seems to us, can be explained on the basis of the assumptions just advanced. Certain difficulties arise in the attempt to explain the experiments with oppositely polarized pulses. A more detailed study of the phenomena described is necessary, the more so since it can serve as the basis of creating "memory" systems of a new type [14].

November 12, 1958

References

1. J. F. WAYMOUTH: F. BITTER. Phys. Rev., 95, 941 (1954)
2. F. MATOSSI: Phys. Rev., 98, 434-437, (1955)
3. J. DESTRIAU, H. F. IVEY: Proc. IRE, 43, 1911-1940 (1955)
4. P. ZAIM: Philips Res. Rep., 11, 417-451, (1956)
5. P. D. JOHNSON, W. W. PIPER, F.E. WILLIAMS: J. Electrochem. Soc., 103, 221-224, (1956)
6. G. F. NEUMARK: Phys. Rev., 103, 41-46, (1956)
7. W. A. THORNTON: Phys. Rev., 103, 1585-1586 (1956)
8. C. H. HAAKE: JOSA, 47, 881-887 (1957)
9. F. F. MOREHEAD: J.Electrochem. Soc., 105, 461-468, (1958)
10. S. NUDELMAN, F. MATOSSI: J. Electrochem. Soc., 101, 546-553 (1954)
11. F. MATOSSI, S. NUDELMAN: Phys. Rev., 99, 1100-1103, (1955)
12. W. W. PIPER, F. E. WILLIAMS: Brit. J. Appl. Phys. Suppl. No. 4, (Luminescence), Paper 7, 539-549, (1955)
13. W. W. PIPER, F. E. WILLIAMS: Phys. Rev., 98, 1809-1813 (1955)
14. I. N. ORLOV, I. IA. LIAMICHEV: Tr. NII MRTP, No. 9, 3, (1957), of the Scientific Research Institute of the Ministry of the Radio-Engineering Industry

TOM VII, VYP. 3 OPTIKA I SPEKTROSCOPIIA Sentiabr', 1959
VOL. VII, NO. 3 OPTICS AND SPECTROSCOPY September, 1959

Luminous State in the Interior of a Medium with Rayleigh Scattering

G. V. ROZENBERG

Abstract: The basic characteristics of the luminous state in the interior of a medium with Rayleigh scattering as a function of the properties of the medium, the specific absorption and depolarization have been considered theoretically. Various methods of calculation have been compared and the errors arising from neglect of polarization effects pointed out. The possibility of utilizing the relations found for spectroscopic purposes is discussed.

In a previous report [1], we elucidated the general characteristics of the luminous state in the interior of a scattering medium having a small specific absorption. Here these regularities will be illustrated by a specific example of a medium with Rayleigh scattering, for which the form of the scattering matrices is known. The atmospheres of stars are practically the only places we meet with great thicknesses of Rayleigh scattering media. In some circumstances, however, as shown by this specific example, it is also germane and essential for understanding the picture, presented by the propagation of light in any dispersing medium. Having in mind a calculation of the polarization effect, we will as usual use the terminology and mathematical apparatus appropriate to the description of the state of polarization of the light rays by means of the Stokes vector parameter (See ref [2].). At the same time we will use the results of reference [1], some of which, for convenience, are reproduced below.

1. BASIC RELATIONS

Let us assume that a homogeneous isotropic scattering medium fills the half space $z > 0$ and that it is illuminated from outside. We will characterize the medium by its specific absorption $\beta = \frac{\alpha}{\sigma}$ (where α and σ are the volume absorption and dispersion coefficients) and the scattering matrix $\frac{1}{4\pi} f_{ik}(\mu, \mu', \varphi - \varphi')\, d\omega$ $(i = 1, 2, 3, 4)$. Here $\mu = \cos\vartheta$, ϑ and φ are the polar and azimuthal angles, defining the direction of the light rays (the polar axis was chosen along z); $d\omega$ is the element of the solid angle occupied by the light ray; the primed quantities relate to the incoming radiation, and the unprimed to those scattered by the light rays.

At sufficiently large depths a luminous stationary state is established which is determined by the properties of the medium and is independent (to a certain approximation) of the condition of irradiation of the surface [1]:

$$S_i(\mu, z) = s_i(\mu) \exp[-k\gamma(z - z_0)]. \tag{1.1}$$

Here S_i is the ith component of the Stokes vector parameter, $k = \alpha + \sigma$ is the extinction coefficient, z_0 is a constant which depends on the boundary conditions, and $s_i(\mu)$ is determined by the equation

$$(1+\beta)(1-\gamma\mu)s_i(\mu) = \frac{1}{2}\sum_{k=1}^{4}\int_{-1}^{+1} F_{ik}(\mu,\mu')s_k(\mu')d\mu' \tag{1.2}$$

in which

$$F_{ik}(\mu, \mu') = \frac{1}{2}\int_0^{2\pi} f_{ik}(\mu, \mu', \varphi-\varphi')d(\varphi - \varphi') \tag{1.3}$$

and γ is a constant depending on the properties of the medium and determinable from the condition for a solution of equation (1.2).

In particular, when $\gamma \ll 1$ one may set

$$s_i(\mu) = j_0[\delta_{i1} + \gamma a_i(\mu) + \gamma^2 b_i(\mu) + \gamma^3 c_i(\mu) + \ldots] \tag{1.4}$$

where j_0 is a constant, depending on γ and the boundary conditions and

$$\beta = p\gamma + q\gamma^2 + r\gamma^3 \ldots, \tag{1.5}$$

from which we obtain [1]

$$\begin{cases} p = 0, \\ q = \frac{1}{2}\int_{-1}^{+1} \mu a_1(\mu)d\mu, \\ r = -q\frac{1}{2}\int_{-1}^{+1} a_1(\mu)d\mu + \frac{1}{2}\int_{-1}^{+1} \mu b_1(\mu)d\mu, \end{cases} \tag{1.6}$$

and

$$\begin{cases} a_i(\mu) = \mu\delta_{i1} + \frac{1}{2}\sum_k \int_{-1}^{+1} F_{ik}(\mu,\mu')a_k(\mu')d\mu', \\ b_i(\mu) = -q\delta_{i1} + \mu a_1(\mu) + \frac{1}{2}\sum_k \int_{-1}^{+1} F_{ik}(\mu,\mu')b_k(\mu')d\mu'; \\ c_i(\mu) = (q\mu - r)\delta_{i1} - qa_1(\mu) + \mu b_1(\mu) + \\ \quad + \frac{1}{2}\sum_k \int_{-1}^{+1} F_{ik}(\mu,\mu')c_k(\mu')d\mu'. \end{cases} \tag{1.7}$$

The equations which have been presented allow one to find the basic characteristics of the luminous state completely, if $\beta \ll 1$ and the properties of the scattering medium itself are known.

If as a plane of reference for the scattered light rays and for those which are to be scattered the plane of scattering is chosen, then in the case of Rayleigh scattering the scattering matrix has the form [2]:

$$f(\vartheta) = \frac{3}{4+3d}\begin{Vmatrix} (1+\cos^2\vartheta)+d & -\sin^2\vartheta & 0 & 0 \\ -\sin^2\vartheta & (1+\cos^2\vartheta) & 0 & 0 \\ 0 & 0 & 2\cos\vartheta & 0 \\ 0 & 0 & 0 & 2\cos\vartheta \end{Vmatrix}, \tag{1.8}$$

where ϑ is the scattering angle, $d = \frac{4\Delta}{1-\Delta}$ and Δ

is the depolarization. Correspondingly, using (1.3) and making the necessary transformations to the plane of reference (1), we obtain*

$$F(\mu,\mu')=\frac{3}{2(4+3d)}\begin{Vmatrix} (3-\mu'^2)-\mu^2 & (1-3\mu'^2)+d(1-\mu'^2)(1-3\mu^2) & 0 & 0 \\ (1-\mu^2) & (1-3\mu'^2) & 3(1-\mu^2)(1-\mu'^2) & 0 \\ 0 & 0 & 0 & 0 \\ 0 & 0 & 0 & 2\mu\mu' \end{Vmatrix} \tag{1.9}$$

2. THE DIRECT SOLUTION FOR $\gamma \ll 1$

From the form of the matrix (1.9) it is obvious that the system of equations (1.2) for $S_1(\mu)$ and $S_2(\mu)$ is independent of the equations for $S_3(\mu)$ and $S_4(\mu)$ and that $S_3(\mu) \equiv 0$. The comparative simplicity of the matrix (1.9) also allows one to solve the system of equations (1.2) directly, without resorting to the approximate method [equations (1.4)-(1.7)] developed in [1]. Indeed, from the form of (1.9) it is obvious that the solution of the system is:

$$S_{1=1,2}(\mu) = \frac{A_i + B_i\mu^2}{(1+\beta)(1-\gamma\mu)}, \tag{2.1}$$

$$S_4(\mu) = \frac{C_1}{(1+\beta)(1-\gamma\mu)}, \tag{2.2}$$

where A_1, B_i, and C are constants. For A_1, B_1, A_2, and B_2 a system of four linear equations is obtained, the coefficients of which contain, besides β and d, the quantities

$$I_{2p} = \frac{1}{2\gamma^{2p+1}} \int_{1-\gamma}^{1+\gamma} \frac{(1-z)^{2p}}{z}\, dz = \sum_{n=0}^{\infty} \frac{\gamma^{2n}}{2n+p+1}. \tag{2.3}$$

Assuming that $\gamma \ll 1$, and limiting ourselves to terms up to γ^4, we obtain the condition for solvability of the system as

$$\beta = \frac{\gamma^2}{3}\left(1 + \frac{\gamma^2}{2}\cdot\frac{1 - 7.8d + 3.24d^2}{1 + 3.26d + 1.88\,d^2}\right), \tag{2.4}$$

which (with the same precision) corresponds to the solution

$$S_1(\mu) = \frac{J_0}{(1+\beta)(1-\gamma\mu)}\left(1 + \frac{\gamma^2\mu^2}{3}\chi \frac{(1+\frac{2}{7}\gamma^2)}{(1+2.5d)+(0.54+\frac{d}{3})\gamma^2}\right), \tag{2.5}$$

$$S_2(\mu) = -\frac{J_0(1-\mu^2)}{(1+\beta)(1-\gamma\mu)}\cdot\frac{\gamma^2}{3}\chi \frac{(1+\frac{2}{7}\gamma^2)}{(1+2.5d)+(0.54+\frac{d}{3})\gamma^2}. \tag{2.6}$$

*The integration was done by O.A. Germogenova.

For the degree of polarization of the most scattered light we obtain [2]:

$$P(\mu) \equiv \frac{S_1(\mu)}{S_2(\mu)} = -\frac{\gamma^2}{3}\chi \frac{(1-\mu^2)(1+\frac{2}{7}\gamma^2)}{(1+2.5d)+(0.54+\frac{d}{3})\gamma^2+\frac{\gamma^2\mu^2}{3}}. \tag{2.7}$$

The condition for solvability of the homogeneous linear equation for C, which is obtained by substitution of (2.2) in the corresponding equations (1.2), is the requirement

$$1 + \beta = 2I_2, \tag{2.8}$$

which is incompatible with (2.4), as a consequence of which C becomes zero.

Below we will discuss the results obtained. First we turn to the solution of the same equations by the method of successive approximations, presented in reference [1].

3. SOLUTION BY THE METHOD OF SUCCESSIVE APPROXIMATIONS

Assuming in (1.7)

$$a_i(\mu) = \sum A_i^j \mu^j \tag{3.1}$$

and considering the form of the matrix (1.9) we obtain:

$$a_1 = A_1^0 + \mu, \qquad a_{i\neq 1} = 0, \tag{3.2}$$

where A_1^0 is an arbitrary number; then, in accord with (1.6),

$$q = \frac{1}{3}, \tag{3.3}$$

Assuming further

$$b_i(\mu) = \sum B_i^j \mu^j, \tag{3.4}$$

we find

$$\begin{cases} b_1(\mu) = B_1^0 + A_1^0\mu + \mu^2 + \frac{1}{3}\frac{\mu^2}{1+2.5d}, \\ b_2(\mu) = -\frac{1}{3}\frac{(1-\mu^2)}{1+2.5d}, \\ b_3(\mu) = b_4(\mu) = 0. \end{cases} \tag{3.5}$$

where B_1^0 is an arbitrary number, from which, in accord with (1.6), $r = 0$.

Thus, (to fourth order in γ^4) $\beta = \frac{\gamma^2}{3}$, in accord with (2.4).

Analogously, assuming

$$c_i(\mu) = \sum C_i^j \mu^j, \tag{3.6}$$

we find

$$(3.7)\quad \begin{cases} c_1(\mu)=C_1^0+B_1^0\mu+(A_1^0+\mu)\mu^2+\frac{1}{3}\cdot\dfrac{(A_1^0+\mu)}{1+2.5\,d}\mu^2, \\ c_2(\mu)=-(A_1^0+\mu)\dfrac{(1-\mu^2)}{3(1-2.5d)}, \\ c_3(\mu)=c_4(\mu)=0, \end{cases}$$

where C_1^0 is an arbitrary number.

Substituting the expressions obtained in (1.4) and collecting terms, we obtain

$$(3.8)\quad S_1(\mu)=J_0\,[(1+\mu\gamma+\mu^2\gamma^2)+$$

$$(1+\mu\gamma+\mu\gamma^2)\,A_1^0\gamma+(1+\mu\gamma)\,B_1^0\gamma^2+$$

$$+C_1^0\gamma^3+(1+\mu\gamma+\mu\gamma^2)\frac{\gamma^2}{3}\cdot\frac{\mu^2}{1+2.5d}+\ldots],$$

$$S_2(\mu)=-J_0\cdot\frac{\gamma^2}{3}\cdot\frac{(1-\mu^2)}{(1+2.5d)}[(1+\mu\beta+A_1^0\gamma+\ldots],$$

$$S_3(\mu)=S_4(\mu)=0.$$

It is not difficult to see that expanding (2.5) and (2.6) in a power series in γ and limiting the terms to the third order, we obtain (3.8) with the difference that the multiplier $\frac{1}{1+\beta(\gamma)}$ is replaced by some unknown function $A(\gamma)=1+A_1^0\gamma+B_1^0\gamma^2+C_1^0\gamma^3+\ldots$.

The latter does not change the solution, since the solution itself is determined with the accuracy of an unknown multiplier J_0 which depends on γ. The appearance of the arbitrary constants A_1^0, B_1^0, C_1^0, and so on, in the solution by the method of successive approximations, and also the arbitrary multiplier which depends on γ, is connected with the general properties of the F_{ik} matrix for an isotropic medium pointed out in [1], namely:

$$(3.9)\quad \frac{1}{2}\int_{-1}^{+1}F_{11}(\mu,\mu')\,d\mu'=1,$$

$$\frac{1}{2}\int_{-1}^{+1}F_{21}(\mu,\mu')\,d\mu'=\frac{1}{2}\int_{-1}^{+1}F_{31}(\mu,\mu')\,d\mu'=$$

$$=\frac{1}{2}\int_{-1}^{+1}F_{41}(\mu,\mu')\,d\mu'=0.$$

Thus, the method of successive approximations presented in [1] gives solutions which agree with the direct solution of equations (1.2) to within an arbitrary multiplier depending on γ, that is, it appears correct within the limits of the given problem. Besides, from the point of view of the calculation it is incomparably simpler than the direct solution.

4. ELIMINATION OF POLARIZATION EFFECTS FROM THE CALCULATION

We have already pointed out (compare, for example [3]) that ignoring the polarization of light, which is done in the overwhelming majority of work on the transport of light in scattering media, is equivalent to cutting off terms of the same order of magnitude as those which are retained in the transport equations. Of course, such a method is permitted only in those cases where specific conditions of the problem fully ensure the smallness of the corresponding terms of the equation. In particular, this occurs when it is possible to consider only single scattering of unpolarized light, but it is not permissible, generally speaking, if multiple scattering plays a significant role, or if the irradiation light flux is polarized. A second example of the possibility of reducing the transport equations is in the deep region, where it is as though the "complete scrambling" and the highly symmetric conditions prevented polarization effects from playing any role. In reality, as we saw, in the presence of even weak specific absorption, significant polarization of the "limiting scattered light" will be observed and the polarization effect will turn out to be very substantial. We illustrate the above by a direct calculation.

If in the matrix (1.9) all F_{ik} except F_{11} are put equal to zero, and $d=0$ is assumed for simplicity, then the condition for solvability of the equations for A_1 and B_1 [compare (2.1)] has the form:

$$(4.1)\quad \beta=\frac{\gamma}{3}(1+0.63\gamma^2)$$

and the solution is obtained in the form:

$$(4.2)\quad S_1(\mu)=J_0\,\frac{1+\frac{\gamma^2\mu^2}{3}\,\frac{(1+0.12\gamma^2)}{(1+0.57\gamma^2)}}{(1+\beta)\,(1-\gamma\mu)}.$$

Analogously the solution by the method of successive approximations gives $S_1(\mu)=J_0\,1+\gamma\mu)(1+\frac{10}{3}\gamma^2\mu^2)$, which agrees exactly with (4.2) up to terms of order γ^4. Comparing (4.1) and (4.2) with (2.4) and (2.5), into which $d=0$ is substituted, we find that the relative errors arising from neglect of the polarization effect are approximately (for given γ)

$$(4.3)\quad \frac{\Delta\beta}{\beta}\cong 0.4\beta,\quad \frac{\Delta S_1(\mu)}{S_1(\mu)}\cong -\frac{2}{3}\beta\mu^2,$$

that is, by no means small. Hence, neglect of the polarization effects involves (for a given mass attenuation coefficient $k\gamma$) an exaggeration of the attenuation resulting in the absorption $\alpha=\sigma\beta\cong k\beta$ (since $\alpha\ll\sigma$) and a distortion of the form of the luminous region in the direction of rounding it off.

5. THE DATA WHICH ARE EXPLAINED AND DISCUSSION OF THE RESULTS

The formulas presented above permit one to obtain quantitative characteristics of the luminous state in the interior of a medium with Rayleigh scattering and their dependence on the parameters of the medium.

Figure 1 shows the dependence on γ of the quantity

$$(5.1)\quad J(\gamma,\mu)=\frac{(1+\beta)\,S_1(\mu)}{J_0},$$

which characterizes the shape of the bright region of scattered light for various μ under the assumption that $d=0$. The dependences of the same quantity $J(\gamma,\mu)$ on μ, that is, of the cross section of

the bright region of scattered light for different γ are presented in the vector diagrams (figure 2). From these figures it is seen that an increase of γ (that is, specific absorption) involves (as follows from general considerations [1]) an increase of elongation of the brightness axis. Hence, the degree of elongation is extremely sensitive to even small changes of γ.

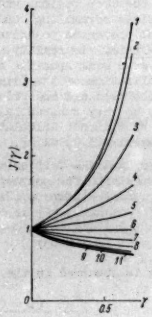

Figure 1. Dependence of J on γ with d = 0 for different values of μ: 1- 1.00; 2- 0.95; 3- 0.75; 4- 0.50; 5- 0.25; 6- 0.00; 7- (-0.25); 8- (0.50); 9- (-0.75); 10- (-0.95); 11- (-1.00).

The degree of elongation of the bright body is conveniently characterized by the parameter $\bar{\mu}$, which is defined by the expression:

$$\bar{\mu} = \frac{\int_{-1}^{+1} \mu S_1(\mu)\, d\mu}{\int_{-1}^{+1} S_1(\mu) d\mu}. \qquad (5.2)$$

The dependence of this parameter on γ for d = 0 is shown in figure 3. We point out that the numerator of expression (5.2) is proportional to the radiation flux through a horizontal section, but the denominator is the flux which shines on the spherical surface surrounding the point of observation. Thus, both these quantities, and therefore also $\bar{\mu}$, may be measured directly with the use of an appropriate system of photocells.

In reference [1] it was shown that in any medium the absorption coefficient α is connected with $\bar{\mu}$ by the relation

$$\alpha = k' \bar{\mu}, \qquad (5.3)$$

where $k' = k\gamma$ is the mass coefficient of attenuation, also directly measurable by experiment. Dividing (5.3) by $k = \alpha + \sigma$, we obtain

$$\frac{\beta}{1+\beta} \cong \beta = \gamma\bar{\mu} \qquad (5.4)$$

or, considering that with small β, we have $\beta^2 \cong q\gamma^2$ [compare (1.5)], we find

$$\bar{\mu} \cong q\gamma. \qquad (5.5)$$

Thus with small β the quantity $\bar{\mu}$ is approximately proportional to γ which is illustrated by the curve of figure 3, almost linear over all its length (with Rayleigh scattering, as we saw, $q = \frac{1}{3}$). Further, as has been shown in [1] the coefficient of attenuation is

$$k' = \left(\frac{\alpha_k}{q}\right)^t, \qquad (5.6)$$

where at small β the exponent is of degree $t = \frac{1}{2}$. The dependence of the exponent t on γ for d = 0 and d = 4, obtained from the relation $3\beta = \gamma^{1/t}$, is shown in figure 4. As seen, the deviation of t from $\frac{1}{2}$ becomes noticeable starting approximately with $\gamma = 0.5$, and has a different sign depending on the amount of depolarization Δ since, depending on the value of d, the sign may change before terms in γ^4 in expression (2.4).

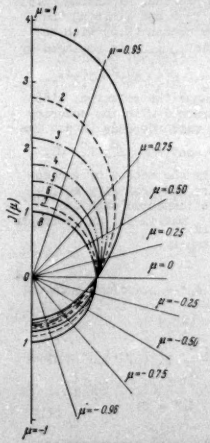

Figure 2. The dependence of J on μ with d = 0 for different values of γ. The values of γ: 1- 0.7; 2- 0.6; 3- 0.5; 4- 0.4; 5- 0.3; 6- 0.2; 7- 0.1; 8- 0.0.

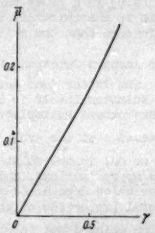

Figure 3. The dependence of $\bar{\mu}$ on γ with d = 0.

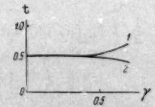

Figure 4. The dependence of t on γ with d = 0 (1) and d = 0.4 (2).

Insofar as both quantities which are on the right hand side of relation (5.3) may be measured directly by experiment, the relation (5,3) allows one to carry out measurements of the absorbing power α of the medium independently of its scattering power σ. Therefore it is of interest to estimate the degree of reliability of similar experiments. From (5.3) it follows that the relative error is

$$\delta \ln \alpha = \delta \ln k' + \delta \ln \bar{\mu}. \qquad (5.7)$$

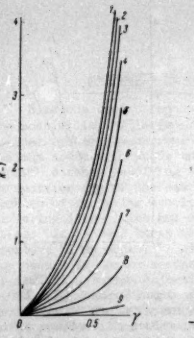

Figure 5. The dependence of R-1 on γ for different values of μ. The values of μ: 1- (-1.00); 2- (-0.75); 3- (-0.50); 4- (-0.25); 5- 0.00; 6- 0.25; 7- 0.50; 8- 0.75; 9- 0.95. For $\mu = 1.00$, we have R-1 = 0.

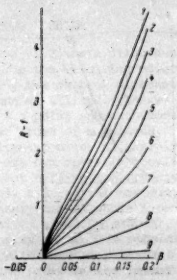

Figure 6. The dependence of R-1 on β for different values of μ. The values of μ: 1- (-1.00); 2- (0.75); 3- (0.50); 4- (-0.25); 5- 0.00; 6- 0.25; 7- 0.50; 8- 0.75; 9-0.95. For $\mu = 1.00$, we have $R - 1 = 0$.

In accord with (5.2) $\bar{\mu}$ is determined as the ratio of the difference of the descending and the ascending fluxes to the spherical flux, as a consequence of which $\delta \ln \mu = 3\delta$, where δ is the relative error in the determination of the amount of each of the fluxes.

The coefficient of attenuation k' is determined from relation (1.1), which we may rewrite in the form:

$$k' = \frac{\Delta \ln \Phi}{\Delta z}, \tag{5.8}$$

where we shall call Φ the descending light flux. Correspondingly the relative error in the determination of k' is

$$\delta \ln k' = \frac{2\delta}{k'\Delta z}, \tag{5.9}$$

where Δz is the depth interval, which is included in the measurement. Thus,

$$\delta \ln \alpha = \left(3 + \frac{2}{k'\Delta z}\right)\delta \tag{5.10}$$

In practice, sufficient precision of the electro-photometric measurements is conveniently assured if, in the measured interval of depth, the amount of light flux changes approximately by an order of magnitude, that is, if $k'\Delta z \cong 2 \div 3$. Thus, it is easy to assure a relative error of about $\delta = 0.02$ for the separate measurements. Consequently, without special experimental devices it is possible to determine the true absorption in a strongly scattering medium with errors not exceeding 8%. We point out that the initial premises in the estimate which was made correspond to an error of $100\,\frac{2\delta}{k\Delta z} \cong 2\%$ of the absorption of transparent substances determined by standard methods. Here, however, as already pointed out in [1], the interval accessible for measurement of the value of α is displaced approximately two orders of magnitude (at the same values of Δz) in the direction of weak absorption.

In the works of Timofeeva [4], the quantity

$$R(\gamma,\mu) = \frac{J(\gamma,\mu = 1)}{J(\gamma,\ \mu)}\ . \tag{5.11}$$

instead of the quantity $J(\gamma,\mu)$ was used.

The corresponding curve of the dependence of R-1 on γ with different μ is presented in figure 5. In figure 6 the same curves are presented as a function of β. It is not difficult to show that in the latter case they have a rather well defined linear region, but at small β they suddenly curve, approaching zero according to the law $(R-1)^2 \sim \beta$. But if the linear portions of the curves of figure 6 are extrapolated to zero, then they all converge to $\beta = 0.05$ rather well (see the dotted lines in figure 6). We present these data in connection with the fact that an exactly analogous method of extrapolating to zero the linear portion of the experimental curves of R-1 as a function of $\alpha - \alpha_0$ (that is $\beta - \beta_0$) was used by Timofeeva [4] for the determination of the absorption α_0 of clear water in the visible region of the spectrum. From figure 6 it appears that the value of α_0 obtained by such a method is not correct and that the only well-founded method for finding α in a scattering medium is the utilization of the relation (5.3).

Simultaneously with the increase of $\bar{\mu}$, that is, elongation of the bright body, the polarization of the scattered light also increases. In correspondence with (2.7) the degree of polarization P is approximately proportional to γ^2 (that is β), which is connected with the form of the scattering index. With indices of other forms one can expect a proportionality of P to the first power of γ. From (2.7), also follows an approximate proportionality of the degree of polarization to the quantity $1-\mu^2 = \sin^2\theta$. In other words, the degree of polarization must be a maximum at $\mu = 0$, and diminish proportionally to $\sin^2\theta$, on approaching vertical lines of observation. An increase in the depolarization Δ also must lead to a decrease in the degree of polarization of the most scattered light (approximately double at $d = 0.4$). In view of what has been said, figure 7 shows the dependence of $P(\gamma)$ only for the case $\mu = 0$, $d = 0$. As is seen in the figure, for small γ the degree of polarization is insignificant, but then rapidly increases and for $\gamma \cong 0.56$ (that is $\bar{\mu} \cong 0.2$) has already reached a very significant value of the order of one-tenth. Nevertheless, considering the complexity of the polarization measurements, the use of the dependence of $P(\gamma)$ for spectroanalytic purposes may scarcely be recommended, especially if the difficulties connected with the deciphering of this dependence as a consequence of the unknown form of the scattering indicatrix are considered.

We have already mentioned that despite the comparatively small degree of polarization, ignoring the polarization effects involves a substantial distortion of the form of the bright body, as well as of the dependence of γ on β (that is, the value of the depth coefficient of attenuation k'). This is

illustrated in figures 8 and 9. In the first of these is presented the dependence of $J(\gamma)$ for different μ, calculated by neglecting the polarization effect. The character of the distortion is clearly set forth by comparison with figure 1. In figure 9 the dependence of β on γ is shown for different values of d found by considering the polarization effect (Δ = 0.05, for d = 0.2, Δ = 0.09 for d = 0.4), without considering the polarization effect for d = 0 and by the simplified formula $\beta = \frac{\gamma^2}{3}$ (that is, t = 0.5).

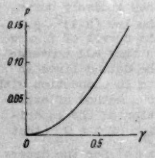

Figure 7. The dependence of the degree of polarization P on γ with μ = 0, d = 0.

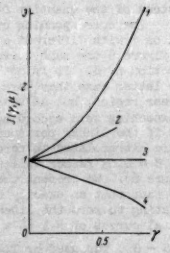

Figure 8. The dependence of J on γ for different values of μ. Calculated without considering polarization with d = 0. The values of μ: 1- 1.0; 2- +0.5; 3- 0.0; 4-(1.0)

As is seen, with $\gamma \geqslant 0.3$ or 0.4 the calculation of terms of higher powers of γ becomes essential and a dependence on the amount of depolarization abruptly appears. One must also consider the polarization effect. The same conclusions follow from figure 10, which shows the dependence of $J(\gamma)$ for μ = 1 with different d, also neglecting the polarization effect and calculated according to the formula $J = \frac{1}{1-\gamma\mu}$.

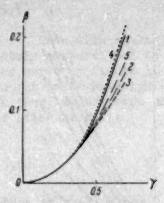

Figure 9. The dependence of β on γ for different values of d. Taking account of polarization: 1- d = 0; 2- d = 0.2; 3- d = 0.4; 4- without taking account of polarization: for d = 0; 5- by the simplified formula $\beta = \frac{\gamma^2}{3}$

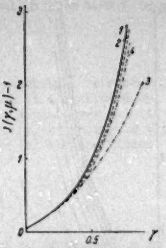

Figure 10. The dependence of $(J - 1)$ on γ for different values of d with μ = 1. Taking account of polarization: 1- d = 0; 2- d = 0.4; 3- without taking account of polarization with d = 0; 4- by the simplified formula $J = \frac{1}{1-\gamma}$.

In conclusion, we point out that some of the results presented above were obtained by other methods and in more limited form, but without the assumption of small γ, by Sobolev [5] and Lenoble [6].

December 2, 1958

References

1. G. V. ROZENBERG: OIS, 5, 440, (1958)
2. G. V. ROZENBERG: UFN, 56, 77, (1955)
3. G. V. ROZENBERG: Candidate's dissertation 1946: IAN USSR SF, 21, 1473, (1957) (See CIT, Bulletin)
4. V. A. TIMOFEEVA: IAN USSR geophy. ser., (2), 265, (1957)
5. V. V. SOBOLEV: Transport of radiant energy in the atmospheres of stars and planets. Moscow-Leningrad, 1956
6. J. LENOBLE: C.R., 246, 924, (1958)

TOM VII, Vyp. 3 OPTIKA I SPEKTROSKOPIIA Sentiabr', 1959
VOL. VII, No. 3 OPTICS AND SPECTROSCOPY September, 1959

On the Possibilty of Resolving Two Light Sources of Sharply Differing Intensities

A. N. RIAZANOV

STATEMENT OF THE PROBLEM

Numerous recent reports [1,2] have discussed the possibility of increasing the resolving power of optical systems by narrowing the central diffraction maximum and moving aside the satellites. These reports discuss resolving two point sources whose intensities are of the same order of magnitude. The problem of resolving two light sources of sharply differing intensities has its own specific peculiarities. It is well known that diffraction from the aperture of an objective gives a central maximum, surrounded by weaker secondary maxima whose intensities, with a slit objective, are 0.047, 0.017, 0.008 etc. times the intensity of the central maximum. If the difference in intensity of two point sources is of the same order as the intensity difference between the zero and first order maxima, then such sources are impossible to resolve with the use of the usual uniform objective, even if the angular distance between them is somewhat larger than is required by the Rayleigh criterion. Consequently, for the resolution of two such light sources it is necessary to reduce the background around the zero order maximum. It is possible to achieve this at the price of some broadening of the central maximum.

For our investigations we chose a slit objective, which simplified both the calculations and the experimental verification. Since the angular distance between the light sources was small, it could be assumed that the light beams from both sources fell normally on the objective ($\cos\varphi \approx 1$, φ is the angle of incidence) and that the diffraction patterns of both were identical.

The method of calculation is the same as in a preceding report [2]. For an objective consisting of three pairs of slits with a common axis of symmetry and distances between corresponding slit pairs equal to 2d, $\frac{2}{3}$ 2d and $\frac{1}{3}$ 2d, the resultant amplitude is given by the expression

$$(*) \qquad A(x) = A_1 u\left(\tfrac{1}{3}x\right) + A_2 u\left(\tfrac{2}{3}x\right) + A_3 u(x),$$

where $u(x) = \cos x$, and $x = \kappa d$ ($\kappa = \frac{2\pi}{\lambda}\sin\theta$, θ is the diffraction angle, 2d is the entire width of the objective).

The expression (*) is correct for very narrow slits. Taking into account their widths leads only to the appearance of a common factor dependent on the diffraction angle, which in practice gives rise to a weakening of the intensity at the maxima, the weakening of intensity is insignificant.

We set the amplitude value at the zero order maximum as $A(0) = 1$. We also set the position of the two zero amplitudes $A(x) = 0$ at $x = \frac{2}{3}\pi$ and $x = 2\pi$, that is where $\sin\theta = \frac{3}{4}\frac{\lambda}{d}$ and $\frac{\lambda}{d}$. These conditions give 3 equations for the determination of the unknown quantities A_i, which turn out to be $A_1 = 0.667$, $A_2 = 0$, and $A_3 = 0.334$, respectively. The distribution of intensity corresponding to this case is presented in figure 1 (curve a). The central maximum in this case has the same half-width as in the case of the uniform objective. The first satellite maximum with a uniform objective (intensity 0.047) is found at $\sin\theta = \frac{3}{4}\frac{\lambda}{d}$. In our case, the intensity of the background around the zero order maximum (approximately up to the value $\sin\theta = \frac{\lambda}{d}$) is about 0.001, but at $\sin\theta = 1.5\frac{\lambda}{d}$ the intensity increases to 1.

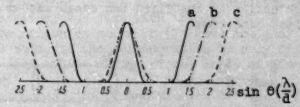

Figure 1

Separating four pairs of slits by distances of 2d, $\frac{3}{4}$ 2d, $\frac{2}{4}$ 2d, and $\frac{1}{4}$ 2d, we assume that $A(0) = 1$ and that $A(x) = 0$ at $x = \frac{3}{2}\pi$, 2π, $\frac{5}{2}\pi$, or $\sin\theta = \frac{3}{4}\frac{\lambda}{d}$, $\frac{\lambda}{d}$, $\frac{5}{4}\frac{\lambda}{d}$. The solution of the corresponding equations gives $A_1 = 0.707$; $A_2 = 0$, $A_3 = 0.293$ and $A_4 = 0$. The intensity distribution curve is given in figure 1 (curve b). The zero order became somewhat broader than in the preceding case, but the surrounding region of reduced background intensity broadened significantly with, in this case, a value on the order of 0.0005.

Figure 2

For five pairs of slits, we set the values $A(0) = 1$ and $A(x) = 0$ at $x = \frac{3}{2}\pi$, 2π, $\frac{5}{2}\pi$, $\frac{6}{2}\pi$ or $\sin\theta = \frac{3}{4}\frac{\lambda}{d}$, $\frac{\lambda}{d}$, $\frac{5}{4}\frac{\lambda}{d}$, $\frac{6}{4}\frac{\lambda}{d}$. Solving the equations, we obtain $A_1 = 0.552$, $A_2 = 0$, $A_3 = 0.342$, $A_4 = 0$ and $A_5 = 0.106$. The corresponding intensity distribution is shown in figure 1 (curve c). We see that the region of reduced background intensity becomes still broader. In it the intensity level is on the order of 0.00001. The half-width of the central maximum is almost the same as in the preceding case (they coincide on the graph).

The position of the centers of the slits corresponding to the cases a, b, and c are depicted in figure 2. The solid and dotted lines show the initial positions of the slits. In calculating the above intensity distributions, zero intensity was obtained for the slits shown as dotted; i. e. they do not exist in the diaphragm.

SOME RESULTS OF THE EXPERIMENTAL TEST

For the purpose of checking the results described above, the setup shown schematically in figure 3,

was assembled. S is the light source (an incandescent or mercury lamp), f is a green filter, L_1 is a lens which focuses an image of the light source on the slit, diaphragm D, whose width is approximately 0.03 mm. Lens L_2 sends parellel light rays onto the investigated objective P, which is set up directly in front of the objective of camera C (focal length f≈130 cm). In the focal plane of the latter, an image of the source (slit D) was obtained, consisting of a diffraction pattern of the aperture P of the objective, this aperture being a system of slits. The objective aperture P was made in the form of a high quality plane parallel glass plate coated with an opaque layer of aluminum, in which a ruling engine scratched the corresponding slits. The intensity relationships needed for calculation were given by the different slit widths. The width 2d of the objective in the first two cases was 4mm, and in the last case, 8mm.

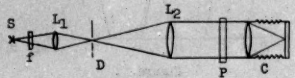

Figure 3

Figure 4 (curves a, b, and c) shows the experimental intensity distributions which are in sufficiently good agreement with the corresponding theoretical curves.

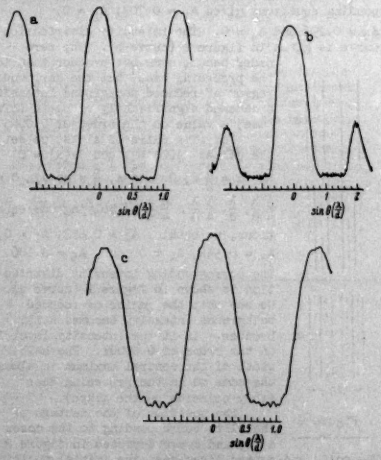

Figure 4

The curves were made on an MF-4 recording microphotometer. We point out that for the attainment of a significant lowering of the background intensity about the zero maximum, a strict maintenance of the same phase values in all pairs of slits is necessary. This is not always possible in practice, since when the slit-scratch is ruled, a thin layer of metal sometimes remains stuck to the glass, as a result of which the background was somewhat greater than its theoretical intensity.

Placing a Wollaston prism between lens L_2 and diaphragm D, and a Polaroid between lens L_1 and diaphragm D, we obtain two images of the slit in the focal plane of the camera. By rotation of the Wollaston prism one can make sure that one of the images will be found in the region of the first or second maximum of the second image. By further rotation of the Polaroid we make sure that with a uniform objective one of the images almost merges with the background of the second (fig. 5,a). By the use of an objective, whose intensity distribution is given by curve (fig. 4,b) one may obtain a perfectly distinct resolution of the two images (fig. 5,b). A scale is included in figure 5 to show the distribution of intensity. In our case the relative intensity of the two sources was 10:1.

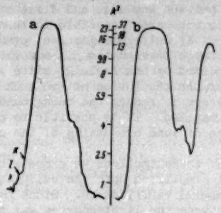

Figure 5

We point out that the microphotograms of figure 5 do not illustrate in full measure the advantage of a complex objective as a consequence of the strong fogging of the weak image by the more intense one. Therefore, for resolution of sources with still more sharply different intensities it is necessary to use a photoelectric method of recording. We note in passing that figure 5 graphically illustrates the suppression of the satellite maxima k and ℓ on the left hand slope of the zero order maximum with the use of a complex objective (the disappearance of the ℓ maximum is particularly evident). The drop-off of intensity on the flank of the zero order maximum is sharper because of this.

In practice, we may encounter a similar case of two light sources of sharply differing intensities in the resolution of close spectral lines.

As far as intensity of illumination is concerned, it is reduced several fold in this case, but not several orders of magnitude, as in the previous case [2].

In conclusion I take this opportunity to express sincere thanks to my instructor Prof. K.D.Sinel'nikov for valuable advice, constant attention and interest in the work, and also Asst. Prof. I. N.Shkliarevskii for constant interest in the work and valuable discussion.

November 25, 1958

References

1. TORALDO di FRANCIA: Nuovo Cimento, 9, 426 (1952)
2. K. D. SIDEL'NIKOV, A. N. RIAZANOV: OiS, 5, 184 (1958)

TOM VII, Vyp.3 OPTIKA I SPEKTROSKOPIIA Sentiabr', 1959
VOL. VII, No.3 OPTICS AND SPECTROSCOPY September, 1959

On the Use of the Integrating Sphere in Differential Spectrophotometric Methods

ZH. L. BROUN

Abstract: The possibility of using an integrating sphere for the determination of scattered light in differential spectrophotometric methods of measuring the absorption spectra of photographic emulsions was investigated. Comparison of the results of spectrophotometric measurements obtained with the aid of the integrating sphere and by the usual spectrophotometric equipment allows one to conclude that the types of curves are the same.

The use of the integrating sphere is necessary when the scattering emulsion layer changes during the course of the investigation.

With the help of specially developed spectrophotometric methods of great accuracy Kirillov with his collaborators [1] found that the absorption spectra of exposed polycrystalline silver halide and Lippmann emulsions have a fine structure of equally spaced maxima of narrow bands.

In work on the study of chemical sensitization we developed a spectrophotometric method similar to that indicated in so far as the nature of results based on infrared experimental data allowed direct observation of the formation and change of silver grains. The value of the method consists, moreover, of permitting the recording not only of the formation of new centers but of the disintegration of those primitive centers which are present in the emulsion before processing.

Spectrophotometric equipment allows the measurement of the transmitted light intensities I_N and I_o through respectively the unprocessed and processed halves of a sample of the substance being studied, with a deposited emulsion layer. In the case that $I_N/I_o > 1$, the resulting curve is the normal spectrum indicating the formation of new centers; if this ratio is smaller than unity, it produces a curve of the "inverted spectrum" indicative of the disintegration of the primitive centers.

In the papers [2-6] on the investigation of reducing agents and sulfur compounds on the optical properties of photographic emulsions it was indicated that in the measurement of real layers of low scattering emulsions by spectrophotometric methods the formation of broad bands with large oscillations of I_N/I_o was observed. In this connection the idea was expressed that such a picture is the result of the influence of light scattering superimposed on the impurity absorption spectrum.

In the investigation of sulfur sensitization reactions on Lippmann emulsions, in certain experiments was found (concurrently with the normal spectrum, an essentially relatively smooth curve) the appearance of broader bands with large oscillations in I_N/I_o. This phenomenon is explained by the increased light scattering dependent on the separating out of the difficult-to-dissolve products of the topochemical reactions near the surface of the solid phase of the emulsion.

Following from this is the very essential problem of measuring only the impurity spectrum of a photographic emulsion and taking into consideration light scattering (particularly in the presence of physical ripening when as it proceeds there occurs a change of the dispersion in the solid phase). However, up to the present time spectrophotometric methods have not afforded the possibility of taking into account light scattering.

Chief among these is the work of Nechaeva and Kirillov [7] in which they succeeded by very refined methods in separating the light absorption from the light scattering, and they demonstrated conclusively that the fine structure in the spectrum of photochemically stained silver halide is associated not with scattering, but just with absorption. Scattering in the medium as shown in [7] does not play an essential role, if the consideration is only of the spectrum loci of the maxima of the bands of fine structure.

For the solution of the problem of taking light scattering into account we used the integrating sphere of Ulbricht [8].

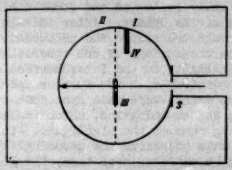

Figure 1. Plan of integrating sphere of Ulbricht type.

The interior of the integrating sphere of 200 mm diameter (Fig. 1) was coated with magnesium oxide and it was constructed in two halves. The first half (I), in which was cut a rectangular window of dimensions 3x10 mm, was fastened securely onto a special frame near the exit slit of a monochromator; the second (II) was located on a movable adapter and could move freely on an optical bench, for the introduction of samples into the sphere. It could then be returned to its original position engaging securely with the first by means of special thumb screws fastened to the drum. In the lower part of the sphere a slot was cut on which an adapter carriage for the sample could slide freely (III). In the upper part of the sphere was securely fastened a photocell (IV, FESS-13) aimed at the uniformly illuminated surface of the sphere.

Since it was not possible in the construction of the integrating sphere to satisfy completely the requirements imposed by theory, it was necessary to determine how much of the total light (both transmitted and scattered by one part or another of the measured sample) was received by the photocell. A ground glass with two windows of unequal diffusion was used for this purpose [7]. In the photocell measurement of the total reflected light the ratio I/I' of the luminous flux through the two windows, as well as the ratio of their scattered light, should be practically equal to unity.

The ground glass with two windows of unequal diffusion was measured twice in the range 410-770 mμ,

where a second measurement was made when the windows were interchanged. The results of the measurements (average values) appear in figure 2. On the basis of these data it was possible to conclude that the equipment was working satisfactorily.

The sample to be measured was placed at a distance of 10 cm from the plane of the exit slit of a monochromator. There was thus formed on the surface of the sample a luminous spot having the dimensions 10x30 mm. Such a relatively large field of measurement is very useful, since the influence of inhomogeneities of the separate parts of the emulsion layer on the measurements is hence diminished.

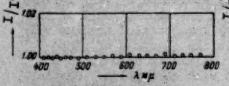

Figure 2. Equipment check: ground glass with two windows of unlike diffusion.

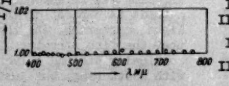

Figure 3. Equipment check: verification of the uniformity of the ground glass.

In our measurements the monochromatic luminous flux falls first on the glass portion of the sample, and is partially reflected and forms a highlight on the surface of the sphere. After this it passes further through the sample and produces a second highlight on the surface of the sphere. The presence of highlights on the inner surface of the sphere is undesirable, hence further spectrophotometric measurements were made upon contact of the sample with the ground glass, which in consequence of scattering removes the highlights. In the carrying out of this objective the ground glass was first verified to be uniform. For this, the glass was measured in the range 410-770 mμ three times: in the violet, in the red, and again in the violet end of the spectrum. After this the measured parts of the ground glass were interchanged and the same measurement operations were repeated. Averaged values of six measurements are presented in figure 3, from which it is seen that the selected ground glass is practically uniform.

The control sample spectrophotometric test of a photochemically stained silver bromide Lippmann emulsion on the new apparatus showed that the fine structure impurity spectrum has maxima coincident within the limits of measurement error with the maxima observed in the same sample measured on the usual spectrophotometric equipment (fig. 4).

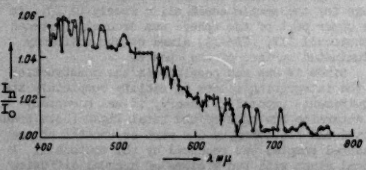

Figure 4. Fine structure of the absorption spectrum of a photochemically stained layer of Lippmann emulsion.

In this figure the observed mean square error is indicated (the measurement accuracy attained 0.1%). In the table the positions of the maxima obtained from equipment with the integrating sphere and from the customary equipment are compared.

Location of the maxima in the impurity absorption spectrum of photochemically stained silver bromide Lippmann emulsions obtained with the help of the integrating sphere (I), and by the usual spectrophotometric equipment (II)

Equip. type	Wave length (in mμ)								
I	417.5	425.0	432.5	438.0	447.5	455.0	467.5	482.5	
II	416.0	422.0	431.0	440.0	450.0 565.0	461.0	470.0	480.0	
I	510.0	–	–	555.0	575.0	602.5	617.5	630.0	
II	–	519.5	541.0	556.0	570.0	596.0	617.0	635.0	
I	645.0	667.5 682.5	–	710.0	725.0	740.0	–	–	767 772
II	650.0	670.0	695.0	710.0	720.0	–	750.0	–	770.0

The principal results of previous work were carefully verified in the new apparatus. This verification was necessary for the reason that in work on the study of chemical sensitization conclusions were found on the basis of a comparison of the absorption intensities in the impurity spectra, which resulted from the influence of different chemical agents. Repeated spectrophotometric measurements were made of samples of silver bromide Lippmann emulsions (photochemically stained, treated with a solution of thiourea in different concentrations c at its own pH value and at pH = 10.17 [3], processed with a solution of sodium thiosulfate at a pH = 10.17 [5], treated with a solution of potassium bromide [5] and subjected to accelerated aging in an oven [3] as well as of the internal latent image centers [1]. Sensitometric tests of the layers were made in parallel with the spectrophotometric measurements, the results of which agreed with the data obtained earlier.

Results of spectrophotometric measurements of the indicated samples are shown in figures 5 to 7. The measurements were made in the range 400-800 mμ at comparatively large intervals (10-20 mμ). For the purpose of comparing the spectrophotometric measurements made with the help of the integrating sphere with the data obtained from the usual spectrophotometric equipment, in each figure are inserted supplementary curves marked with the letter K (standard). These curves are taken from the pertinent literature sources [1, 5, 6].

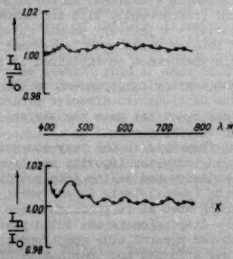

Figure 5. Accelerated "aging" of photo layers (seasoned in an oven at 52° C.)

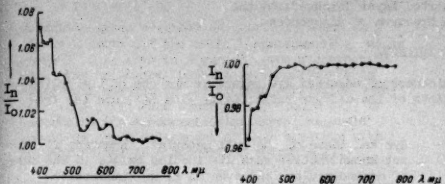

Figure 6. Absorption spectrum on treating with a solution of thiourea (c = 0.3x10-5 mole/liter, natural pH = 10.17).

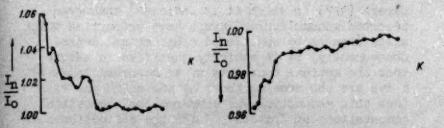

Figure 7. Absorption spectrum on treating with a solution of thiourea (c = 0.3 x 10-1 mole/liter, natural pH).

The results of the experiments lead to the following conclusions.

1. The type of curve obtained by using the integrating sphere, and consequently free from the influence of light scattering, is the same as that obtained in the previous experiments with the use of the usual spectrophotometric equipment.

2. As is seen from the data presented, the influence of light scattering results in a more or less parallel displacement of the curves, as was also shown in the work of Nechaeva and Kirillov [7]. This displacement does not change the qualitative picture of any chemical agent.

3. The use of the integrating sphere may be completely justified in those cases where the problem is the isolation of the pure effect of the scattering centers. This is especially important in those cases where in the course of an experiment the scattering changes appreciably (for example, in the case of the investigation of the processes of physical maturing of photographic emulsions).

In conclusion, the author feels it his duty to thank E. A. Kirillov and K. V. Chibisov for their valuable advice and interest in the work.

December 1, 1958

References

1. E. A. KIRILLOV: Fine structure in the absorption spectrum of photochemically stained silver halide.(Russian) Akad. Nauk Press.USSR,1954.
2. E. A. KIRILLOV, Zh. L. BROUN, K.V.CHIBISOV: DAN USSR, 98, 427, (1954)
3. E. A. KIRILLOV, ZH. L. BROUN, K.V. CHIBISOV: DAN USSR, 102, 1159, (1955)
4. E. A. KIRILLOV, ZH. L. BROUN, K. V. CHIBISOV: IAN USSR, SF, 18, 689, (1954)(See CTT, Bulletin)
5. ZH. L. BROUN, E. A. KIRILLOV, K.V. CHIBISOV: Zh. Nauchn. i Priklad Foto i Kinem., 1, 982, (1956)
6. A. A. MIKHAILOVA, ZH. L. BROUN, K. V. CHIBISOV: Zh. Nauchn. i Priklad. Foto. i Kinem., 1, 342, (1956)
7. T. A. NECHAEVA, E. A. KIRILLOV: Zh. Nauchn. Priklad. Foto., Kinem., 2, 404, (1957)
8. K. ULBRICHT: Das Kügelphotometer, Berlin, 1920

TOM VII, VYP. 3 OPTIKA I SPEKTROSKOPIIA Sentiabr', 1959
VOL. VII, NO. 3 OPTICS AND SPECTROSCOPY September, 1959

The Influence of the Adsorbed Layer Thickness on the Diffuse Reflection Spectrum of Adsorbates

Z. V. ZHIDKOVA

Abstract: It is shown in the paper that the thickness of adsorbed dye layers is not one of the optical factors which lead to differences between spectral plots of the diffuse reflectivity -log R(λ) and the true absorption kl.

Any attempt to explain the influence of the thickness of an adsorbed layer of a substance on its diffuse reflection spectrum raises the question of whether it is actually possible to use these spectra for the qualitative and quantitative characterization of strongly absorbing adsorbed substances such as dyes. Actually, as is known [1], dyes in the solid phase possess high values of the absorption index κ; the values of the refractive index, and hence the reflectivity, of such substances depend strongly on the wavelength (see Fig. 1, curve 1)*

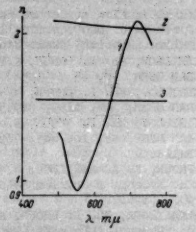

Figure 1. Dispersion curves of malachite green (1), AgCl (2), and quartz (3).

If such a substance forms an infinitely thick layer, then as pointed out in references [2, 3], the spectrum of the quantity -log R(λ)** (where R is the diffuse reflection coefficient) does not even approximately characterize the true absorption spectrum k(λ), in contrast to a substance of small index (for example, powdered glass).

However, we are interested in layers in which the dye (or optical substance of similar type) forms a thin layer of adsorbed film.

In this case, will the diffuse reflection spectra of different film thicknesses of adsorbate qualitatively agree with the true absorption spectrum of these films?

For a direct answer it would be necessary to determine the dependence of absorption and refractive index on wavelength for different thicknesses of adsorbed films. But this is impracticable because of the extremely small thicknesses of the films.

There is an obvious distinction between the optical constants of single adsorbed molecules of a dye and those of the bulk material. However, it is not known whether such distinction exists in the case of monomolecular, and even more, multimolecular adsorbed layers. Actually, there are a number of papers [4-7] in which it is indicated that even adsorbed monomolecular layers have properties which allow them to be considered coherent and dense. Consequently, it is entirely justified to assume that the optical constants of an adsorbed layer of a dye are the same as those of the solid phase. To test this assumption, we compared the theoretical computations of Kravets [8] for the reflection coefficient of systems analogous to adsorbates with our experimental data.

The calculation of Kravets was made under the assumption that the optical constants of a dye in adsorbed layers are similar to those obtained in the solid phase; after all permissible simplifications had been made the following expression for the reflection coefficient was obtained

$$(1)\qquad r = \left(\frac{n_1 - n_3}{n_1 + n_3}\right)^2 \left[1 - \frac{2k l 2n}{n_1^2 - n_3^2}\right] = r_o(1 - \Delta), \ldots$$

where n is the real part of the complex index of refraction of the dye n' = (n − iκ); k is the coefficient of absorption of the adsorbed dye film ($k = \frac{4\pi\kappa}{\lambda}$); n_1 is the index of refraction of air; n_3 is the index of refraction of the adsorbate; l is the thickness of the adsorbed film.

From (1) it follows that r depends on three refractive indices. Since n_1 and n_3 depend weakly on the wavelength (the values of n_3 for quartz and AgCl are shown in figure 1), their variation can cause only quantitative differences in the diffuse reflection spectra. But the value of n depends strongly on the wavelength (as is seen from curve 1, figure 1) and this may lead to distortion of the diffuse reflection spectrum.

From formula (1) it follows also that the extent of the influence of n depends on the thickness of the adsorbed layer.

Actually, when l is of the order of a layer one molecule thick, then the correction term

$$(2)\qquad \Delta = \frac{2k l 2n}{n_1^2 - n_3^2} \ldots$$

already amounts to several percent. On the absorption spectrum of each adsorbed dye layer (we denote it by kl = -log τ) shown in figure 2, curve 1, is superimposed the spectrum of the quantity [+log (1-r_o) -log (1-r_o-$r_o\Delta$)] specified [formula (1)] by the influence of the correction term (2)***.

* The value of the index of refraction for the dye is taken from the work [1].

** The quantity -log R (λ) was formerly called the "conditioned optical density" because for substances with small values of the absorption index κ this quantity qualitatively characterizes the absorption spectrum k(λ).

*** The pure adsorbent was chosen as the comparison sample.

A plot of $[+\log (1 - r_o) - \log (1-r_o-r_o\Delta)]$ for malachite green adsorbed on quartz is shown in figure 2 curve 1,* the overall spectrum is shown in curve 1". As seen in figure 2, even a correction amounting to several percent is insufficient to cause such changes in the diffuse reflection spectrum -log r (λ) [and consequently -log R (λ)] of adsorbates (in a monomolecular layer) as would result in the displacement of this spectrum with respect to the true absorption spectrum kl.

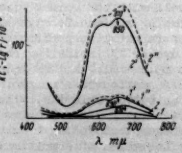

Figure 2. Variation of the quantities kl and -log r(λ) with wavelength. In a monomolecular layer: 1, the correction term; 1', the quantity k; 1", the quantity -log r. In a multimolecular layer: 2, the correction term; 2', the quantity kl; 2", the quantity -log r.

In adsorbed layer thicknesses greater than one molecule, the correction term (2) must increase rapidly (curve 2, Fig. 2), which must not only cause a distortion of the contour of the spectrum -log r(λ) [and consequently -log R(λ)], but also cause its displacement (curve 2", Fig. 2] with reference to the true absorption spectrum kl (curve 2'), and likewise with reference to the spectrum -log r (λ) for a monomolecular layer (curve 1"). With increasing thickness of adsorbed layer, the spectrum of the quantity -log R(λ), ** must approach the position and form of the dye absorption spectrum in the solid phase [2, 3].

Thus if the computations of T. P. Kravets for the adsorbed layers of a dye are used under the assumption that the layers possess the same values of the optical constants as the dye does in the solid phase, then it is found that the spectrum of the quantity -log R(λ) in the case of an adsorbed dye film of thickness greater than one molecule is altered in form and displaced in position relative to the true absorption spectrum of this film because of the effect of optical factors. Consequently, it is impossible in this case to make use of the diffuse reflection spectrum to characterize the true absorption.

The absence of such distortion would indicate the incorrectness of the assumption that the optical constants of the dye in the solid phase are the same as those in the adsorbed condition.

* n and κ have values of the same order for all dyes. Consequently all that is said here regarding malachite green also applies to other dyes.

** The diffuse reflectivity R (and consequently -log R) is built up in a complex manner from elementary reflections by each particle of adsorbate r(u - log r (λ)), as a result of multiple reflection in the diffusing medium [3].

METHODOLOGICAL SECTION

The principal problem consisted of obtaining adsorbed dye layers of different thicknesses. The thickness of a layer was determined with the help of the adsorption isotherms for the investigated dye on selected adsorbents.

The following dyes were investigated by us: phenosafranine, dye No. 3 (3, 1'diethyl-5,6 dimethyl-8' chlorothia-4'-quinocarbocyanine iodide), dye No. 4 (1' 3-diethylthia-2'-cyanine iodide), and dye No. 6 (5, 5'-dichloro-3, 3', 9-triethyl carbocyanine bromide***.

The absorption spectrum of alcoholic solutions of dye No. 3 is shown in Figure 3.

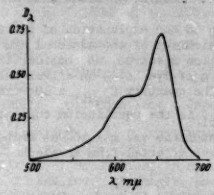

Figure 3. Absorption spectrum of alcohol solution of dye No. 3 in concentrations from 0.0005 to 0.2 mg/cm-3.

The size of the molecules was taken from data in the literature [9, 10]. The molecules of dye No. 3 have a length of 18.2 Å, a thickness of 4 Å, and a width 10.2 Å. The length of the dye molecule No. 4 is 14 Å, its thickness 4 Å. The molecules of dye No. 6 have the following dimensions: length 20. 7 Å, thickness 4 Å.

Powdered fused glass TF-5 was used as adsorbent; its preparation has been reported previously [1]. Powdered silver chloride (AgCl) was also used.

In the preparation of silver chloride we strove for a powder that was pure with particles which were of uniform size, but not too small (which is necessary for rapid settling). The first two requirements were met by recrystallizing the silver chloride from a saturated solution of ammonium chloride, the last by heating.

The specific surface of the glass spheres was determined by the method of Deriagin and by computation of the geometrical surface.

The choice of adsorbent has very important consequences in the determination of the specific surface of an adsorbent by adsorption of one substance or another. It is known [13] that the specific surface of even non-porous adsorbent has different values when determined by the adsorption of different substances; that is, we always determine actually the adsorption capacity of a adsorbent by comparison with a known substance. For us it was essential to determine the specific adsorptive capacity of silver

***The identifications Nos. 3, 4, 6, are applicable only in our papers. These dyes were kindly donated by E. L. Petrushkin, to whom the author expresses his sincere appreciation.

chloride relative to some dye giving a distinct plateau in the adsorption isotherm on forming a monomolecular layer. We decided on dye No. 4, which furthermore belongs to the same class as dyes No. 3 and 6.

The area (more accurately, the adsorptive capacity) of 1 gram of the adsorbent AgCl was computed from the formula.

$$S = \frac{m}{M} 6.03 \cdot 10^{23} lh..., \quad (3)$$

where M is the molecular weight of the dye, l the length of the dye molecule, h the spacing between the centers of the molecules, m the quantity of dye in grams adsorbed on one gram of adsorbent.

By computation in this way the surface of silver chloride was found to be S=784 cm^2.

RESULTS AND DISCUSSION

Passing to the explanation of the influence of the layer thickness of the adsorbed dye on the diffuse reflection spectrum, we consider the adsorption isotherm of dye No. 3 on silver chloride (Fig. 4). The quantity $C_{equil} \times 10^{-6}$ in moles/liter (where C_{equil} is the equilibrium concentration) is plotted as abcissae vs. $m \times 10^6$ as ordinates. The adsorption was effected from an alcohol-water solution.

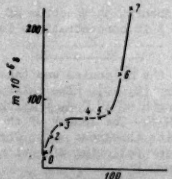

$C_{equil} 10^6$ (moles/liter)

Figure 4. Adsorption isotherm of Dye No. 3 adsorbed on AgCl from alcohol-water solution (λ = 652.5 mμ). Original concentrations (in mg/cm^3: 1- 0.005; 2- 0.01; 3- 0.02; 4- 0.04; 5- 0.05; 6- 0.07; 7- 0.08.

As is evident from Figure 4, the isotherm has an S shape* with a small plateau in the range of equilibrium concentrations 63.5×10^{-6}–81.8×10^{-6} moles/liter. In order to make sure that this section corresponds to the filling up of a monomolecular adsorbed layer, we first of all verified whether the isotherm complied with the equation of Langmuir in this region. This was done quantitatively determining the dependence of C_{equil}/m on C_{equil}. If this dependence is linear, then the isotherm in the straight-line section conforms to the equation of Langmuir [14-17], that is, in this region of concentration we are dealing with monomolecular adsorbent. The correctness of our statement, insofar as it applies to our case over the specified interval of equilibrium concentration, may be seen from Figure 5.

In the second place, knowing the dimensions of the molecules and the value of m in the above indicated interval of equilibrium concentrations and assuming that the molecules of dye No. 3 are adsorbed on edge during the formation of monomolecular layers on silver chloride**, we may compute the adsorbing surface which that adsorbent must have in order to form a monomolecular layer in the concentration range $63.5 - 81.8 \times 10^{-6}$ moles/liter. Calculation by formula (3) gives a surface area of S = 766 cm^2. This agrees well with the values given above for the computed adsorbing surface for dye No. 4.

Thus the straight line portion of the adsorption isotherm for dye No. 3 in the region of equilibrium concentration $63.5 - 81.8 \times 10^{-6}$ moles/liter actually indicates the formation of a monomolecular layer of dye adsorbed on silver chloride, with distances between the centers of the molecules equal to about 5 Å. The subsequent ascending branch of the isotherm indicates the formation of a multimolecular layer. Thus the position of the system on the isotherm plotted as point 7 corresponds to the formation of an adsorbed layer with a thickness of about three molecules.

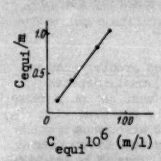

$C_{equil} 10^6$ (m/l)

Figure 5. Graph of dependence of C_{equil}/m on C_{equil} for dye No. 3 adsorbed on AgCl (λ = 652.5 mμ).

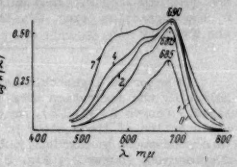

Figure 6. Diffuse adsorption spectrum of dye No. 3 adsorbed on AgCl for various thicknesses of adsorbed layer. The numbers of the curves correspond to the points in Figure 4.

Figure 6 shows diffuse reflection spectra of dye No. 3 adsorbed on powdered silver chloride in different layer thicknesses. The numbers of the curves in figure 6 match the appropriate points of the adsorbate marked on the adsorption isotherm (see Fig. 4.). Thus, curve 4 presents the diffuse reflection spectrum from an adsorbate on filling up the adsorbent surface with a monomolecular layer, and curves 0 and 1 the development of a monomolecular layer.

Thus as is seen in Figure 6, the position of the fundamental absorption band maximum in curves 0 and 1 is somewhat displaced with regard to its position on curve 4.

This difference in the position of the fundamental maxima for individual adsorbed molecules and the layers they produce is well known in the literature [14, 15]; it is caused not by the optical conditions of reflection (according to equation (1'), it should not be observed), but by purely physicochemical conditions, that is, by another arrangement

*A similar form of isotherm for dyes on adsorption from solutions onto silver chloride was obtained by many authors [9, 14-16].

**Our assumption is based on the widely known experimental data concerning the adsorption of sensitizing dyes [10, 15, 16].

of adsorbed molecules on the surface of the adsorbent (maximum surface), involving molecular polarizabilities which are different from the polarizabilities obtained when the molecules are adsorbed edgewise.

Curve 7 represents the diffuse reflection spectrum of a layer of dye No. 3, approximately three molecules thick. According to formula (1), curve 7 should be altered in form and the position of its primary absorption band displaced with respect to curve 4. However, we see from figure 6 that the diffuse reflection spectrum expressed in curve 7 is distinguished from curve 4 only quantitatively: in the redistribution of maxima and the appearance of new ones because of changes in the physico-chemical condition of the dye in the initial solution, and consequently in the adsorbed film of dye. No changes occur which are associated with the displacement of the fundamental absorption bands with varying layer thickness (from one molecule to many), as should follow from formula (1). This circumstance compels a review of the fundamental assumptions underlying the abovementioned basic computations: it follows that the identification of the optical properties of a dye in the adsorbed state with those of the solid phase is incorrect. This conclusion is corroborated by the fact that the absorption spectra of dyes in the adsorbed state, as a rule, always differ from the absorption spectra of dyes in a solid film.

The conflict between the optical properties of dyes in adsorbed layers and in the solid phase is reminiscent of the discrepancy between the optical constants of thin metal films and the constants in the bulk state [18, 19]. However, the constancy of location of principal absorption maxima of adsorbed dye layers with increasing thickness (from monomolecular dimensions to greater) sharply distinguishes these layers from thin metal films, in which the optical properties vary continuously with changing of thickness [up to 1000 Å].

The positions of the principal absorption maxima for layers of adsorbed dyes of specified thicknesses agree with the positions of these dye maxima in any solvent (assuming the solvents' intermolecular forces to be the same) [20, 21]. This circumstance suggests that the optical constants of an adsorbed dye layer are similar to (or close to) the values of these constants in solution.

CONCLUSION

The diffuse reflection spectra of dye adsorbates of various layer thicknesses are not altered because of the influence of the optical constants. Consequently, they may be used for a qualitative determination of the true absorption spectrum k (λ) of these layers.

In conclusion I wish to express my sincere appreciation to Professor M. V. Savost'ianova for interest in the work and for valuable advice.

August 20, 1958

References

1. N. N. PRIBYTKOVA, L. S. AGROSKIN: OIS, 3, 628, (1957)
2. Z. V. ZHIDKOVA: ZETF, 26, 458, (1954)
3. O. P. GIRIN, B. I. STEPANOV: ZETF, 27, 467, (1954)
4. A. CAMERON, C. H. GILES: J. Chem. Soc., 7, 3140, (1957)
5. P. DUBOULOZ, R. RINALDI: C. R., 238, 2506, (1954)
6. M. MURAMATSI: Bull. Chem. Soc., Japan, 31, 871, (1958)
7. M. V. SAVOST'IANOVA, L. G. MATSINOVA: DAN USSR, 125, 1294, (1959)
8. T. P. KRAVETS: 3rd Session, in memoriam to S. I. VAVILOV. Oborongiz, Moscow, 1953
9. Z. L. PETRUSHKINA: Nauch. i. Priklad. Photog. i Kinematog., 1, 414, (1956)
10. W. WEST, B. H. CARROLL, D. H. WHITCOMB: J. Phys. Chem., 56, 1054, 1952
11. Z. V. ZHIDKOVA: Use of Spectroscopic Methods in the Consumer's Goods Industries and Agriculture. Publisher LGU, 241, 1956
12. B. V. DERIAGIN, V. I. KRYLOVA, R. M. FRIDLIAND: ZFKh, 24, 137, (1950)
13. M. M. DUBININ: Physico-Chemical Foundations of sorption techniques. ONTI, Moscow, 1935
14. B. H. CARROLL, W. WEST: Photog. Sci., 162, (1951)
15. S. E. SHEPPARD, H. CROUCH: J. Phys. Chem., 32, 751 (1928)
16. A. I. RABINOVICH, S. V. NATANSON: ZFKh, 11, 434, (1938)
17. S. BRUNAUER: Adsorption of Gases and Vapors, IL, MOSCOW 1, 1948
18. G. V. ROSENBERG: UFN, 47, 3, (1952)
19. G. V. ROSENBERG: UFN, 58, 487, (1956)
20. Z. V. ZHIDKOVA, IU. M. SUSS: Zh. Nauch i Priklad. Photog. i Kinemat., 3, 25, (1958)
21. Z. V. ZHIDKOVA: Zh. Nauch. i Priklad. Photog. i Kinemat. (in press)

TOM VII, Vyp. 3 OPTIKA I SPEKTROSKOPIIA Sentiabr', 1959
VOL. VII, No. 3 OPTICS AND SPECTROSCOPY September, 1959

On the Threshold Sensitivity of an Optical-Acoustic Radiation Detector

III. The General Case of a Selective Detector with a Non-Cylindrical Light-Receiving Chamber. Sample Calculations.

A. O. SALL'

Abstract: Formulas are deduced for defining the numerical value of the threshold sensitivity of a selective optical-acoustic radiation detector, the light-receiving chamber of which has a complex shape. Sample calculations of chamber depth are presented.

1. As we saw in Part II. of the present work [1], the concentration of the radiation-absorbing component in the chamber can be chosen in such a way that the absorption of radiation by the gas will be approximately uniform. In this case the formula for the heat conductivity of a planar ($l \ll r$) or a cylindrical ($l \gg r$) light-receiving chamber [1], may be generalized for chambers of irregular shape

$$(1) \qquad G_{fl.;\ l.f.} \simeq G_{sel.;\ l.f.} = \left(1 + \frac{2}{n}\right)\left(\frac{\lambda S^2}{V}\right),$$

where S is the sum of the areas of the walls and the window of the light-receiving chamber.

We denote the depth of the chamber by h; i.e. the maximum distance from the point farthest from the window in the reflecting surface of the chamber wall to the interior window surface. The numerical value of the parameter n, introduced in the first part of the work, depends on the ratio hr^{-1} (r is the radius of the window) and varies from 1 (for a planar chamber with $h \ll r$) to 3 (when h is commensurate with r). If $r < h < 10r$, then the error in using formula (1)(for n = 3) does not exceed 20%. If $h \gg r$, then $n \simeq 2$. In any case for approximate calculations we may take n 2.

Utilizing Eq. (14) of part I [1], for the threshold sensitivity, we obtain

$$(2) \qquad (\Delta J) = NB^{-1}(p\tau)^{-1}\sqrt{1 + (\omega\tau)^2}\sqrt{4kT^2\Delta f\left\{G + \frac{[G^2 + (\omega C)^2]}{G'}\right\}},$$

where $G' = (PE)^2 (TR')^{-1}$ is a numerical coefficient which has the dimensions of heat conductivity; R' is the effective noise resistance of the input series amplifier taking into account the noise of the grid resistance and the shot effect of the electron tube.

Using Eq. (2) it may be shown that for $\delta \gg r$, the optimum value of the volume V of the light-receiving chamber corresponding to maximum sensitivity of the detector is equal to

$$(3) \qquad V = \xi \delta S_o,$$

where S_o is the area of the window. The numerical coefficient ξ depends on G', on the passive premicrophone volume V_p [2] and on the surface S_p of the walls of the passive volume and on Ω the ratio of the acoustic resistance of the passive volume to the acoustic resistance of the microphone [2].

Formula (3) for defining V is applicable only in the case of such large values of δ and absorption coefficient k, that one of the conditions – (7), or (17), or (18) [1] – is fulfilled. In the opposite case it follows that the depth of the chamber increases.

If $G' \ll G$ (the sensitivity of the detector is limited by the noise at the input of the series amplifier) then, as shown by calculation, the dependence of the numerical value of ξ on the quantity $(\delta S_o)^{-1}(1 + \Omega) V_p$ for a cylindrical light-receiving chamber is expressed in the following manner:

$(\delta S_o)^{-1}(1 + \Omega)V_p$	0	1	10	10^2	10^3	10^4	10^5
ξ	2.5	2.7	4	6	9	14	23

It is necessary to note that when substituting into Eq. (3) to calculate the volume of the chamber, the value of δ depends on ξ: for comparatively small values of ξ presented at the left it is necessary to employ C_v, the specific heat of the gas at constant volume to calculate δ while for large values of ξ, presented on the right, it is necessary to use C_p the specific heat at constant pressure.

As V_p increases, ξ increases. If one uses $\xi = 2.5$ (corresponding to the case $V_p = 0$), for $V_p \neq 0$, instead of the corresponding value of ξ from the table, then the sensitivity will be smaller. However, if we assume $\xi = 2.5$ even for a large V_p then the sensitivity will be at least half of the maximum possible value, which would occur for the value for ξ in the table. For $\xi = 5$ the sensitivity is at least 80% of the maximum possible.

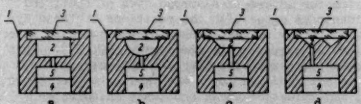

Figure 1. Selective optical-acoustic detectors. 1- body of chamber; 2- light-receiving chamber; 3- transparent window; 4- microphone; 5- passive premicrophone volume.

If the numerical value $V_p(1 + \Omega)$ is unknown, then we may assume approximately that $\xi \simeq 3.5$. This value is equally well suited for the case of $V_p(1 + \Omega) \ll \delta S_o$, as for the case $V_p(1+\Omega) \gg \delta S_o$. The detector sensitivity here differs from the maximum by not more than 20-30%. If the detector is used in an optico-acoustic gas analyzer then $\xi > 5$-10 usually is reasonable only in those cases when this is necessary to decrease the error of the gas analyzer (by means of increasing h).

We have examined the cases for which $G' \ll G$. In the other limiting case, when the detector sensitivity is limited by the fluctuations of the gas temperature in the chamber ($G' \gg G$), the numerical

value of the coefficient ξ increases with increasing V_p.

2. Let us examine the question of the optimum form of the light-receiving chamber. First we check the case of such low modulation frequencies that $\delta \gg r$. As a first approximation we can consider $V_p = 0$ and $\Omega \ll 1$. Then the optimum form of the light-receiving chamber will be such that the thermal conductivity is a minimum (i.e. the relation $S^2 v^{-1}$ is a minimum). We limit the comparison to only those forms of light-receiving chambers whose construction is not difficult.

We compare the sensitivity thresholds of three basic chamber forms: cylindrical (Fig. 1,a), hemispherical (Fig. 1,b) and conical with a vertex angle of 90° (in Fig. 1,c, we show a truncated cone). As the calculations indicate, the thermal conductivity of the hemispherical chamber ($h = r$) is smaller than that of the cylindrical one ($h = l = 1$, $2r$) by about 20% and is almost 30% smaller than the conductivity of the coneshaped chamber ($h = r$).

We now examine the case where the modulation frequency is so great that $\delta \ll r$ and $\delta \ll h$. We compare different forms of light-receiving chambers, assuming $V_p(1 + \Omega) < \delta S_o$ and $G' \ll G$. Let the length of the light path in the light-receiving chamber of the radiation detector of the gas analyser be equal to 1 cm, for example, as calculated from the condition for minimum error. Then for a cylindrical chamber with reflecting base $h = l = 5$ mm. We compare the sensitivity of such a cylindrical chamber (Fig. 1,a) with that of one with a truncated cone (Fig. 1,c), and one formed with a circular trihedral groove (Fig. 1,d). Two sides of the groove are polished reflecting surfaces and the third is the plane of the window. In other words, the size of such a chamber is determined by the surface of rotation of an equilateral triangle about an axis, passing through one of its vertices perpendicular to the base and lying in the plane of the triangle. The axis of rotation coincides with the axis of the chamber. The depth of the two latter chambers will also be taken equal to 5 mm, with $r = 1$ cm (this corresponds almost exactly to the path length of the light in the chambers compared). The most sensitive chamber must possess the smallest volume. Among the indicated simplest chambers the one with the trihedral reflecting grooves will possess the greatest sensitivity. The sensitivity of this chamber is twice that of the cylindrical one.

If $G' \gg G$ and $\delta \ll r$, the best chamber will be the one with the smallest surface. In the specific case cited, ($r = 1$ cm, $h = 5$ mm) the sensitivity of the chamber in the form of a truncated cone will be 13% higher, and that of the chamber with the trihedral groove 11.5% higher than the sensitivity of the cylindrical chamber. The chamber in the form of a spherical segment ($h = 5$ mm) is 14% more sensitive than the cylindrical one.

If h is commensurate with δ, then for $G' \ll G$ the chamber with the smallest value of $\sqrt{\alpha^2 + (\omega C_v)^2}$. has the maximum sensitivity. If, for example, the cylindrical chamber is filled with carbon monoxide, with $h = 5$ mm; $r = 1$ cm; $f = 5$ cps; $V_p(1 + \Omega) \ll \delta S_o$ and is replaced by the spherical segment, the truncated cone or the trihedral circular groove, then the amplitude of the signal increases by approximately the same value (40% - 50%). To use the chamber in the form of a concentric groove in this case is unreasonable; it is very complicated to prepare. The indicated increase of sensitivity, upon replacement of the cylindrical chamber by the complex one, takes place only if $V_p \ll \delta S_o (1 + \Omega)^{-1} < 0.3$ cm^3. Such a passive volume can be realized only by means of an alternate overlapping by the modulator of the working and comparison fluxes directed into one and the same light-receiving chamber [3].

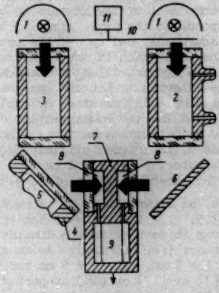

Figure 2. Optical-acoustic gas analyser with gas compensation.

1 - radiation source; 2 - working chamber; 3 - comparison chamber; 4 - compensating device; 5 - radiation reflector; 6 - mirror; 7 - detector; 8 - light receiving chamber; 9 - microphone; 10 - chopper; 11 - motor.

3. To clarify the presentation above we pause to give some example of calculating the depth of the light-receiving chamber of a selective optical-acoustic radiation detector.

Example 1. Let us calculate the chamber depth so that the detector will have maximum sensitivity. Let the radiation absorption coefficient of the gas be $k \simeq 0.03$ (mm %)$^{-1}$ in the band of wave numbers used. Using Eq. (7) of part II supposing $\psi = 0$, and taking into account that the concentration of absorbing gas $C \leqslant 100\%$, we get $l \geqslant 1.8\ (k\mathrm{C})^{-1} \simeq 1.8\ (0.03 \cdot 100)^{-1}$ mm $\simeq 0.06$ mm. Eq. (3) for a cylindrical chamber takes the form $V = S_o l = \xi \delta S_o$, from which $l = \xi\delta$. Considering $G' \ll G$; $\delta \simeq 1$ mm; $V_p(1+\Omega) < \delta S_o$, we obtain $l = \xi\delta = 2.5$ mm. From the two resulting values of l, we take the maximum (2.5 mm). The chamber is accordingly not filled with a purely absorbing gas, but with a mixture containing a non-absorbing component.

Example 2. The width of the spectral region in which the detector sensitivity is different from zero is determined by the absorption spectrum of the gas filling the chamber and by the chamber depth. We allow the necessary spectral sensitivity of the detector to be obtained by a product of cylindrical chamber depth and absorbing gas concentration equal to 500 mm%. Then when the chamber is filled with a pure component ($C = 100\%$) we obtain $l = 5$ mm for the chamber depth. Such a chamber depth is used for sufficiently high modulation frequencies that calculation according to the formula $l = \xi\delta$ gives

a value smaller than 5 mm. If however $\xi\delta > 5$ mm (which occurs for sufficiently low frequencies), then the value $l = \xi\delta$ is used. In the second case the chamber is filled with a mixture of absorbing and nonabsorbing gas.

Example 3. Let us calculate the chamber depth of a selective detector used in an optical-acoustic gas analyser. We denote by u the product of the working chamber's length and the concentration of the particular component of the mixture to be analyzed that corresponds to the upper limit of the gas analyser measurement, and by v the product of the length of the light path in the light-receiving chamber and the concentration of the component to be determined therein. Let the gas analyser use a continuous double differential optical system of measurement, and let the concentration of the component to be determined be found directly from the amplitude of the signal originating in the radiation detector. Let r = 1 cm; f = 5 cps; $G' \ll G$. The numerical value of $(1 + \Omega) V_p$ is not known. Thus, as shown above, it is necessary to assume $\xi = 3.5$. For the value of the cylinder depth we obtain from three (for carbon dioxide) to about four millimeters (for methane). As an approximation we may take $l = 5$ mm. For $l = 5$ mm and $u \leq 100$ mm %, conditions (7) or (17) or (18) of part II are usually fulfilled. If we want the scale of the gas analyser to be approximately uniform [2] then at $u \simeq 100$ mm %, the depth of the cylindrical light-receiving chamber increases usually to 20-30 mm.

Example 4. In the gas analyser with gas compensation [2, 4, 5] (see Fig. 2) the radiation emanating from source 1 is directed into two channels one of which contains the working chamber 2, filled with the gas mixture being analysed, and the other the comparison chamber 3. The compensating apparatus 4 acts upon fluctuntions of the amount of the gaseous mixture in the path of the comparison radiation flux. Variations in the amount of the compensating mixture in the path of the radiation flux are brought about by means of varying the distance between the reflecting surface 5 and the window (shifting a movable rod, the end of which is connected to the reflecting surface). The reflecting surface of plate 6 is used to change the direction of the working flux in the righthand light-receiving cylinder of the detector. The detector 7 consists of a housing and cover. The light-receiving cylinders 8, filled with the gaseous mixture are located directly in the chamber housing. The microphone 9 is connected with the cylinders through connecting channels. Chopping of the radiation flux is accomplished by the chopper 10, mounted on the shaft of a synchronous motor 11.

We calculate the depth of the light-receiving cylinder in such a way that the scale of the gas analyser approaches maximum uniformity. The deviation of the gas analyser's scale from uniformity can be quantitatively estimated in the following manner: the beginning and end of the nonuniform scale which actually occurs, coincide with the beginning and end of the uniform scale. We denote by C the concentration of the particular component of the analysed mixture that corresponds to the upper limit of the gas analyser's measurement. Let ΔC be the maximum value of the absolute magnitude of the difference of readings on these scales (for the same concentration). Then the deviation of the gas analyser scale from uniformity may be calculated from the expression

$$(4) \quad \left(\frac{\Delta C}{C}\right)_{\text{scale}} \simeq 0.5\sqrt{\eta}(1 + 0.75\sqrt{\eta}F) + 0.15r'F + \frac{0.3F_n}{F},$$

where η is the ratio of the minimum gap between the movable reflecting surface and the window of the compensating chamber located at the reflecting surface (which corresponds to the beginning of the gas analyser scale), to the length of the full shift of the reflecting surface; r' is the reflection coefficient of the radiation from the window of the compensating chamber in the direction of the radiation detector; F_n is the residual relative nonselective variation of compensating radiation flux occuring for the full shift of the reflecting surface [5] (in the derivation of Eq. (4) we consider that the nonselective variation of the compensating radiation flux is proportional to the size of the shift of the reflecting surface);

$F \simeq \sqrt{\frac{u}{v}} + 1 - \sqrt{1 + \frac{u}{v}} \simeq \sqrt{\frac{u}{v}}$ is the ratio of the signal due to variation of the concentration of the given component of the analysed mixture from zero to its maximum value, to the signal at full radiation flux [2] (obtained by assuming the absence of passive layers at the window of the light-receiving chamber, and fulfillment of the square-root law upon absorption by the given component).

Having assumed n = 0.05; r' = 0.05; F_n = 0.01; we find the optimum value of F, which corresponds to the least value of the error $\left(\frac{\Delta C}{C}\right)_{\text{scale}}$.

$$F \simeq \sqrt{F_n(0.5r' + 1.25\eta)^{-1}} \simeq 0.3;$$

having taken $u \leq 100$ mm %, we obtain $l \simeq 5$ mm. Figure 2 shows the differential optical-acoustic detector with two gas-filled cavities separated by the microphone. Each cavity comprises a light-receiving cylinder and a passive premicrophone space. The numerical value of Ω in this case is equal to the ratio of the resistance of the passive volume to the sum of the acoustic resistances of the microphone and the cavity. For sufficiently high modulation frequencies the volume of the light-receiving cylinder is smaller than the passive volume. In this case $0 < \Omega < 1$. We obtain $\Omega = 0.5$. Assuming that the chamber is filled with carbon monoxide, with r = 1 cm; f = 5 cps; $V_p = 4$ cm^3; $G' \ll G$ we obtain $\xi \simeq 4.2$. From this $l = \xi\delta \simeq 5$ mm. The resulting value was the one taken for the depth of the light-receiving chamber. An automatic self-recording industrial gas analyser has been developed, based on the optical system of figure 2. In the industrial models, in contrast with the optical scheme of figure 2, the reflecting surface of the compensating chamber moves perpendicularly to the window of the light-receiving chamber. Nevertheless, the depth of the light-receiving chamber remains as before (5 mm).

The gap between the reflecting surface and the

window of the compensating chamber introduces a considerable deviation of the scale from uniformity when zero is the lower limit of measurement of the gas analyser (absence of the given component from the mixture analysed). If the lower limit of the gas analyser measurement is different from zero, then the distance from the window to the movable reflecting surface at the position corresponding to the beginning of the scale can be chosen in such a way that the influence of the gap on the scale is considerably decreased. The influence of the zero gap on the scale can also be decreased by adding the given component to a filter chamber in the working channel. The error component dependent on the radiation reflected from the window of the compensating chamber in the direction of the detector (in the absence of such a reflection from the window of the working chamber in the other channel) may be decreased by making use of reflection working and compensating chambers [5]. Thus, those error components which increase with increasing F may be considerably reduced. This optimum value of F is thus increased. However, the depth of the light-receiving cylinder must necessarily remain equal to 5 mm (because the thermal and acoustic parameters defining the operation of the detector do not change).

May 9, 1958

References

1. A. O. SALL': OiS, 6, 219, (1959); 6, 557, (1959)
2. A. O. SALL': ZTF, 29, 324, (1959); 29, 330, (1959) (See Sov. Phys. Tech. Phys.)
3. M. L. VEINGEROV: DAN USSR, 19, 687, (1938), 46, 200, (1945); ZL, (4), 426, (1947)
4. A. O. SALL': Priborostroenie, (6). 14, (1956)
5. A. O. SALL': OiS, 5, 316, (1958)

ABBREVIATIONS OFTEN ENCOUNTERED AND USED HEREIN

DAN USSR	Doklady Akademii Nauk	(Reports of the Academy of Sciences of the USSR)
DAN UkrSSR	Dopovidi Akademii Nauk UkrSSR	(Reports of the Academy of Sciences of the Ukraine SSR)
DAN ArmSSR	Doklady Akademii Nauk ArmSSR	(Reports of the Academy of Sciences of the Armenia SSR)
IAN USSR	Izvestiia Akademii Nauk USSR	(Bulletin of the Academy of Sciences of the USSR)
	SF Seriia fizika	(Physics series)
	SM Seriia matematika	(Mathematics series)
	OKhN Otdelenie khimicheskikh	(Section of Chemical sciences)
OiS	Optika i Spektroskopiia	(Optics and Spectroscopy)
PiTE	Pribory i Tekhnika Eksperimenta	(Instruments and Techniques of Experiment)
AE	Atomnaia Energiia	(Atomic Energy)
AZ	Astronomicheskii Zhurnal	(Astronomy Journal)
FMM	Fizika Metallov i Metallovedenie	(Physics of Metals and Metallography)
Radiotekh.	Radiotekhnika	(Radio Engineering)
RiE	Radiotekhnika i Elektronika	(Radio Engineering and Electronics)
UK	Uspekhi Khimii	(Progress in Chemistry)
UFN	Uspekhi Fizicheskikh Nauk	(Progress in Physical Sciences)
UFZ	Ukraninskii Fizichni Zhurnal	(Ukraine Physical Journal)
ZETF	Zhurnal Eksperimental'noi Teoreticheskoi Fiziki	(Journal of Experimental Theoretical Physics - JETP)
ZTF	Zhurnal Tekhnicheskoi Fiziki	(Journal of Technical Physics)
FTT	Fizika Tverkogo Tel	(Solid State Physics)
ZFKh	Zhurnal Fizicheskoi Khimii	(Journal of Physical Chemistry)
ZOKh	Zhurnal Obshchee Khimii	(Journal of General Chemistry)
ZNKh	Zhurnal Neorganicheskoi Khimii	(Journal of Inorganic Chemistry)
ZPKh	Zhurnal Prikladnoi Khimii	(Journal of Applied Chemistry)
Tr.	Trudy	(Transactions, as for instance, Tr. FIAN)
FIAN	Fizicheskii Institut Akademii Nauk USSR	(P.N.Lebedev Physical Institute of the Academy of Sciences USSR)
Sb.	Sbornik	(Collection, as for instance, Fizich. sb. L'vovskogo Universitet) Fizich. sb. Fizicheskaia sbornik (Physics Collection)
Uch. Zap.	Uchenye Zapiskii	(Scientific Records)
Vestn.	Vestnik	(Herald or Messenger)
FTIAN	Fiziko-Tekhnicheskii Institut A Akademii Nauk	(Physical-Technical Institute of the Academy of Sciences)
GOI	Gosudarstvennyi Opticheskii Institut	(State Optical Institute)
VEI	Vsesoiuznyi Elektrotechnicheskii Institut	(All-Union Electrotechnical Journal)
MFTI	Moskovskaia Fiziko-Tekhnicheskii Institut	(Moscow Institute of Physics and Technology)
NIIZMIR	Nauchno-Issledovatel'skii Institut Zemnogo Magnetizma, Ionosfery i Rasprostraneniia	(Research Institute of Terrestrial Magnetism and Ionospheric Propagation)
GIFTI	Gor'kovskii Issledovatel'skii Fiziko-Tekhnicheskii Institut	(Gor'kii Research Institute of Physics and Technology)
NIFI	Nauchno-Issledovatel'skii Fizicheskii Institut	(Scientific Research Institute of Physics, Leningrad Univ.)
NIRFI	Nauchno-Issledovatel'skii Radio-fizicheskii Institut	(Scientific Research Institute of Radiophysics, Gor'kii Univ.)
GITTL	Gostekhizdat-Gosudarstvennoe Izdatel'stvo Tekhniko-Teoreticheskoi Literatury	(State Publishers of Technical-Theoretical Literature)
GIFML	Fizmatgizdat-Gosudarstvennoe Izdatel'stvo Fiziko-Matematicheskoi Literatury	(State Publishers of Physical-Mathematical Literature) formerly Gostekhizdat)
IL or IIL	Izdatel'stvo Inostrannoi Literature	(Publishers of Foreign Literature)
Izd. AN USSR	Izdatel'stvo Akademiia Nauk USSR	(Academy of Sciences Press)
ZL	Zavodskaia Laboratoriia	(Factory Laboratory)
GOST	Gosudarstvennyi Obshchesoiuznyi Standart	(All-Union State Standard)
LIPAN USSR	Laboratoriia izmeritel'nykh priborov AN USSR	(Laboratory of Measuring Instruments)
IFAN UkrSSR	Institut Fiziki AN UkrSSR, Kiev	(Physics Institute AN UkrSSR)
SFTI	Sibirskii Fiziko-Tekhnicheskii Institut, Tomsk	(Siberia Physical-Technical Institute)
IFAAN ESSR	Institut Fiziki i Astronomii AN ESSR, Tartu	(Institute of Physics and Astronomy)
IFA AN USSR	Institut Fiziki atmosfery AN USSR	(Institute of the Physics of the Atmosphere)

SYMBOLS FOR SOURCES OF TRANSLATIONS

AIP
American Institute of Physics
335 East 45th Street
New York 17, New York

ATS
Associated Technical Services Inc.
P. O. Box 271
East Orange, New Jersey

CB
Consultants Bureau, Inc.
227 West 17th Street
New York 11, New York

CCT
Consultants Custom Translations, Inc.
227 West 17th Street
New York 11, New York

CTT
Columbia Technical Translations
5 Vermont Avenue
White Plains, New York

HB
Henry Brutcher
P. O. Box 157
Altadena, California

LC
Photoduplication Service
Publication Board Project
Library of Congress
Washington 25, D. C.

MDF
Morris D. Friedman, Inc.
P. O. Box 35
West Newton 65, Mass.

NRCC
National Research Council Library
Ottawa 2, Canada

OTS
Office of Technical Services
Department of Commerce
Washington 25, D. C.

PS
Primary Sources
11 Bleecker Street
New York 12, New York

RIS
Research Information Service
40 East 23rd Street
New York 10, New York

SLA
SLA Translation Center
The John Crerar Library
86 East Randolph Street
Chicago 1, Illinois

ZH. L. BROUN O primenenii svetomernogo shara v differentsial'nom spektrofotometricheskom metode	421	On the Use of a Light-Measuring Sphere in the Differential Spectrophotometric Method	271
Z. V. ZHILKOVA O vliianii tolshchiny adsorbirovannogo sloia na spektr diffusnogo otrazheniia ot adsorbatov	426	On the Influence of the Thickness of the Adsorbed Layer on the Diffuse Reflection Spectrum From Adsorbates	274
A. O. SALL' O poroge chuvstvitel'nosti optiko-akusticheskogo priemnika radiatsii. III. Obshchii sluchae netsilindricheskoi luchepriemnoi kamery selektivnogo priemnika. Primery rascheta	432	On the Threshold Sensitivity of an Optico-Acoustic Radiation Detector. III. General Case of a Non-Cylindrical Ray-Receiving Chamber of a Selective Detector. Examples of Computations	278
		Abbreviations Often Encountered and Used Herein	282
		Symbols for Sources of Translations	283

TOM VII, Vyp. 3
Vol. VII, No. 3

Sentiabr', 1959
September, 1959

SODERZHANIE

F. F. GAVRILOV
Spektral'nyi metod izotopnogo analiza litiia 285

V. P. MOROZOV
Partsial'nye chastoty trekhatomnykh gidridov i deiteridov simmetrii C_{2v} 289

IU. IA. GOTLIB
Teoriia kolebatel'nykh spektrov polimerov. I 294

KH. KESLER, IU. A. PENIN, E. G. TRESHCHOVA, V. M. TATEVSKII
Issledovanie infrakrasnykh spektrov pogloshcheniia uglevodorodov pri raslichnykh temperaturakh v zhidkoi i tverdoi faze 301

L. D. KISLOVSKII
Opticheskie kharakteristiki vody i l'da v infrakrasnoi i radiovolnovoi oblasti spektra 311

A. S. CHERKASOV, T. M. VEMBER
O vliianii n-toluidina na kvantovye vykhody fotookisleniia i fotodimerizatsii nekotorykh proizvodnykh antratsena 321

A. S. CHERKASOV
Spektry pogloshcheniia, spektry fluorestsentsii i kvantovye vykhody fluorestsentsii nekotorykh metil- i metilmezoarilantratsenov 326

A. F. LUBCHENKO
Teoriia iavleniia Faradeia v oblasti eksitonnogo pogloshcheniia sveta molekuliarnymi kristallami 332

A. F. LUBCHENKO
Teoriia lineinogo iavleniia Kerra v oblasti eksitonnogo pogloshcheniia sveta molekuliarnymi kristallami 341

M. N. MARKOV, I. S. LINDSTREM
Opticheskie svoistva napylennogo bismuta v oblasti spektra 3-15 μ 349

P. G. MASLOV
O primenenii additivno-statisticheskogo metoda k izucheniiu spektrov pogloshcheniia i fluorestsentsii 355

N. P. SHIMANSKAIA, A. P. KILIMOV, A. P. GREKOV, L. M. EGUPOVA, R. S. AZEN
Plastmassovye stsintilliatory s dobavkami arilproizvodnykh 1, 3, 4-oksadiazola 366

F. F. GAVRILOV
Liuminestsentsiia gidrida litiia 371

V. V. ANTONOV-ROMANOVSKII
Nachal'nye stadii zatukhaniia fosforov s urovniami neskol'kikh sortov 376

I. B. KEIRIM-MARKUS
Issledovanie svetovykh summ v fosfore SrS-Eu, Sm. I. 384

I. IA. LIAMICHEV, I. N. ORLOV
Vliianie elektricheskoi predystorii elektroliuminofora na kharakteristiki ego svecheniia pri vozbuzhdenii korotkimi impul'sami napriazheniia 398

G. V. ROZENBERG
Svetovoi rezhim v glubine sredy s releevskim rasseianiem 405

A. N. RIAZANOV
O vozmozhnosti razresheniia dvukh istochnikov sveta rezko razlichnoi intensivnosti 417

CONTENTS

Spectral Method of Isotopic Analysis of Lithium 185

Partial Frequencies (Modes) of Triatomic Hydrides and Deuterides of C_{2v} Symmetry 188

Theory of the Vibrational Spectra of Polymers. I 191

Investigation of Infrared Absorption Spectra of Hydrocarbons at Various Temperatures in the Liquid and Solid Phase 195

Optical Characteristics of Water and Ice in the Infrared and Radiowave Region of the Spectrum 201

On the Influence of p-Toluidine on the Quantum Yields of Photo-Oxidation and Photo-Dimerization of Some Anthracene Derivatives 207

Absorption and Fluorescence Spectra and the Fluorescence Quantum Yield of Certain Methyl- and Methylmesoaryl Anthracenes 211

Theory of the Faraday Effect in the Region of Exciton Absorption of Light by Molecular Crystals 215

Theory of the Linear Kerr Effect in the Region of Exciton Light Absorption by Molecular Crystals 221

Optical Properties of Sublimed Bismuth in the 3-15 μ Spectral Range 228

On the Use of the Additive-Statistical Method to the Study of Adsorption and Fluorescence Spectra 232

Plastic Scintillators with Admixtures of 1, 3, 4-Oxadiazol Arylderivatives 239

Luminescence of Lithium Hydride 242

Initial Stages of Decay of Phosphors with Levels of Several Kinds 245

Investigation of Light Sums in an SrS-Eu,Sm Phosphor. I 250

Influence of the Electrical Prehistory of an Electroluminophor on its Luminescence Characteristics Under Excitation by Short Voltage Pulses 258

Luminous State in the Interior of a Medium with Rayleigh Scattering 263

On the Possibility of Resolving Two Light Sources of Sharply Differing Intensities 269